The computer-aided design of rectangular microstrip antennas

by

Noel Maxwell Martin,

M.Sc., B.Eng., C.Eng.

A thesis submitted to the Department of Electrical and Electronic Engineering, the University of Adelaide, to meet the requirements for the award of the degree of Doctor of Philosophy

December, 1984

SUMMARY

A computer-aided design program has been developed for use with probe or transmission line fed rectangular microstrip antennas and arrays. The antenna is modelled using both a single mode leaky resonant cavity and a transmission line with radiating apertures at each end, where in both cases a series reactance is used to represent the effects of the feed probe. The cavity model is used to specifically define and calculate the resonant frequencies to within 2% of measurements, where the effective electrical dimensions of the antenna are empirically determined. The accuracy of the transmission line model in determining input impedances is greatly improved through the use of empirical equations for the effective admittances located at each end of the antenna. Typical errors of 17% and 2% are obtained for the resonant resistances and impedance resonant frequencies respectively. In the case of probe fed antennas, the success of both the resonant frequency and input impedance calculations depends on the accurate determination of the equivalent series reactance of the probe. Here a coaxial transmission line with an empirical taper is used as a model. The resultant reactances are within $\pm 3\Omega$ of the transformations in the measured input impedance loci. The near field distributions of the two apertures at each end of the antenna are examined using a liquid crystal film, and leads to the conclusion that the respective far field patterns are tilted off the broadside direction and emanating at different power levels. The far field radiation pattern is calculated to within 2dB of measurements using an array of two uniformly illuminated apertures, where the separation takes into account the effective length to which the fields fringe at each end of the antenna. A space radiation model for the power transfer between two apertures is used to calculate the mutual coupling to within 3dB of measurements, where the antennas are separated by at least $0.75\lambda_o$. The definition of bandwidth used for resonant cavities is proposed as a more appropriate quantity for comparative studies between microstrip antennas whether they are

matched or not; and is used in an investigation into the bandwidth performance of a novel hexagonal element, which is shown to exhibit wider bandwidth and greater gain performance than a rectangular antenna. All of the models are tested on typical geometries operating up to a frequency of 5GHz, and are shown to provide results of sufficient accuracy for most design purposes without requiring extensive computations.

STATEMENT

This thesis contains no material which has been accepted for the award of any other degree or diploma in any University and to the best of the candidate's knowledge and belief, contains no material previously published or written by another person, except where due reference is made in the text.

Also the author consents to the thesis being made available for photocopying and loan if accepted for the award of the degree.

Noel Martin

ACKNOWLEDGEMENTS

The guidance of the author's supervisor, Dr.D.W.Griffin, is gratefully acknowledged. His balanced practical and theoretical approach to problems in electromagnetics has been invaluable to this research programme.

The author's wife, Kathleen, is also thanked for her constant support and encouragement, for without it this candidature would have never started. She is also thanked for typing the thesis. The author is also grateful for the regular encouragement of Mr. and Mrs. P. Budimir.

Messrs G.W.Pook and G.L.Allison are thanked for their skilled technical assistance.

The author also acknowledges the financial support from the University of Adelaide through a URG scholarship.

LIST OF PRINCIPAL SYMBOLS

a radius of a circular patch or the inner conductor of a coaxial transmission line.

a_e effective radius of a circular patch.

A_l length of a rectangular aperture.

A_s separation between two apertures in a broadside array.

A_w width of a rectangular aperture.

b radius of the outer conductor of a coaxial transmission line.

B_a input susceptance of a radiating aperture.

B_s input susceptance of a slot antenna.

BW bandwidth.

c velocity of electromagnetic waves in free space.

d diameter of the feed probe.

D inset distance: distance between the feed probe and the nearest end of a rectangular patch antenna.

$\underline{E}$ electric field intensity vector.

$\underline{u}_\rho E_\rho, \underline{u}_\theta E_\theta, \underline{u}_\phi E_\phi$ spherical components of $\underline{E}$.

f frequency in hertz.

f_o resonant frequency.

$f_{m,n}$ resonant frequency of the m, n mode.

f_{oc} resonant frequency of an ideal unloaded cavity.

f_{oz} frequency at which the input impedance of an antenna is real.

G_a input conductance of a radiating aperture.

G_{rad} radiation conductance.

h thickness of a dielectrically filled substrate.

$J_o(x), J_n(x)$ Bessel functions.

$k_{m,n}$ wave number of the m, n mode.

l_e electrical length.

l_{ph} physical length.

L length of a transmission line or a rectangular patch antenna.

Q_{cu} quality factor due to ohmic losses.

Q_{die} quality factor due to dielectric losses.

Q_{ext} quality factor that includes only the external load.

Q_L quality factor that includes internal and external losses.

Q_o quality factor of an ideal unloaded cavity.

Q_{rad} quality factor due to radiation losses.

r aspect ratio W/L.

R_o resonant resistance: input resistance at f_{oz}.

R_{cu} equivalent resistance due to ohmic losses.

R_{die} equivalent resistance due to losses in the dielectric.

R_{rad} radiation resistance.

$s_{11}, s_{21}, s_{12}, s_{22}$ scattering matrix parameters.

TEM transverse electromagnetic

t thickness of copper cladding.

$\tan\delta$ loss tangent of a dielectric material.

$\underline{u}_x$ unit vector in the x-direction; similarly $\underline{u}_y, \underline{u}_z, \underline{u}_\rho, \underline{u}_\theta, \underline{u}_\phi$.

v_{ph} phase velocity.

W width of a microstrip transmission line or a rectangular microstrip patch antenna.

W_e effective width of a microstrip transmission line or a rectangular microstrip patch antenna.

X_s series reactance used to model the antenna's feed probe ($= \omega L_s$).

Y_a input admittance of a radiating aperture.

Y_{om} characteristic admittance of a microstrip line.

Z_a input impedance of a radiating aperture.

Z_{in} input impedance of an antenna.

Z_{om} characteristic impedance of a microstrip line.

Z_o characteristic impedance of an air filled transmission line.

Z_r impedance located at the receiving end of a transmission line.

Z_a input impedance of slot or aperture A.

Z_b input impedance of slot or aperture B.

α attenuation constant.

β_o phase constant in free space.

β_s phase constant in the substrate.

δL edge extension.

δ_s skin depth.

ϵ_e effective relative dielectric constant.

ϵ_r relative dielectric constant of a dielectric substrate.

γ propagation constant.

η_o intrinsic impedance in a vacuum ($120\pi\Omega$).

η antenna efficiency.

η_s intrinsic impedance of a dielectrically filled medium.

λ_s wavelength in a dielectrically filled medium.

λ_o wavelength in free space.

σ conductivity.

Ω ohm.

$\mho$ mho.

ω angular frequency.

LIST OF TABLES

LIST OF PLATES

LIST OF FIGURES

TABLE OF CONTENTS

CHAPTER III

THE CALCULATION OF THE RESONANT FREQUENCY USING AN EMPIRICALLY DETERMINED EDGE EXTENSION PARAMETER

CHAPTER I

INTRODUCTION

1.1 General introduction

Microstrip antenna elements were originally proposed by Deschamps in 1953 [1]. However, eighteen years or more passed before the work was carried further by Howell [2,3], Munson [4] and Weinschel [5], after which numerous analytical and experimental studies into the operation of the antenna followed [6].The fundamental form of the antenna is an arbitrarily shaped thin uniform sheet of metal, called a patch, bonded to the surface of a thin dielectric substrate clad with a large metal sheet on the other surface to form a ground plane. The element is usually excited at a frequency such that the wavelength in the substrate is comparable with the dimensions of the patch. The relative dielectric constant of the substrate material is usually less than ten, resulting in significant fringing fields around the periphery of the patch. These fields give rise to electric currents on the patch and the ground plane, so the element's far field radiation may be regarded as being directly related to these electric currents or to the equivalent magnetic currents of the fringing fields.

This investigation is primarily concerned with the operation of antenna elements constructed using rectangular patches because they have been the most widely used

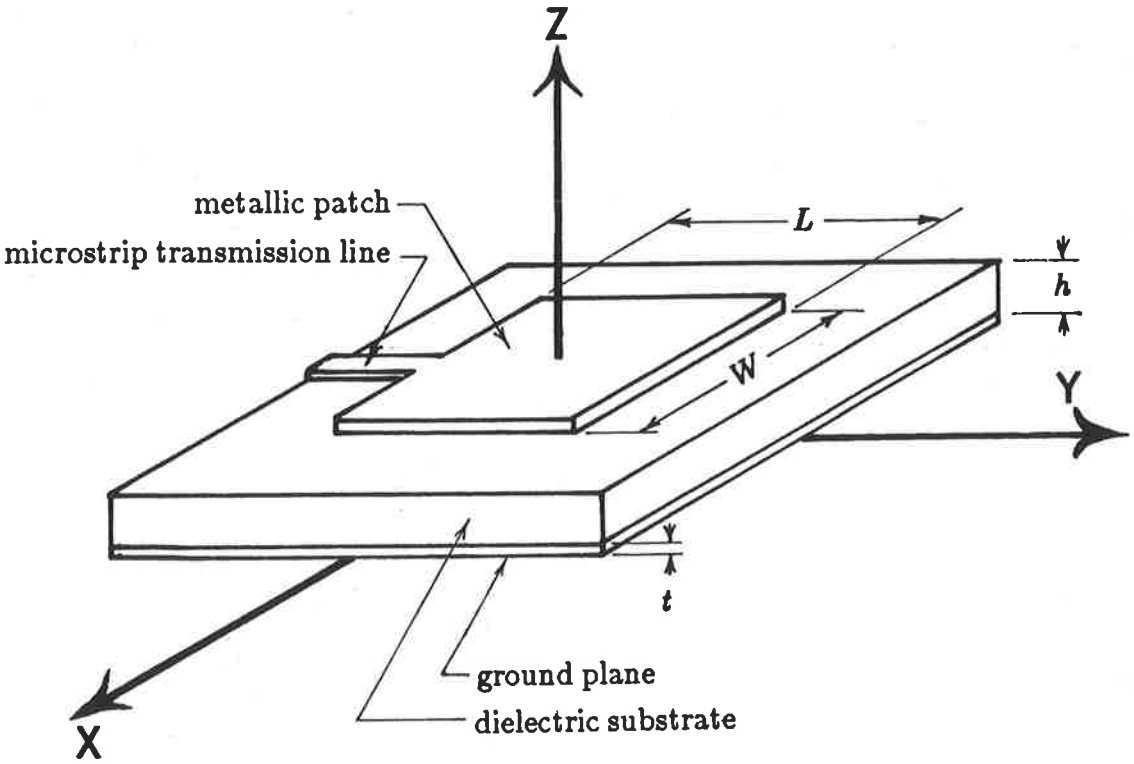

Figure 1.1: Rectangular microstrip antenna.

in industry, and lend themselves to analysis by simple models. Figure 1.1 shows a rectangular element fed by a microstrip transmission line.

To radiate as an antenna the rectangular element should be excited at a frequency such that the length of the side L is approximately equal to half of the wavelength in the dielectric. The electric field associated with this transmission line resonator fringes beyond the ends of the patch to create two main sources of radiation. Fringing also occurs along the two sides but the radiation from these sources does not contribute significantly to the main beam, is cross polarised, and creates side lobes in the element's radiation pattern.

There are three common excitation structures for the antenna. Figure 1.1 shows an element fed at its edge by a microstrip transmission line. Figure 1.2(a) illustrates a patch fed from behind the ground plane by the inner conductor of a coaxial transmission line that extends through the substrate to make connection with the metallic patch.

This extension of the coaxial line through the substrate is called a "probe," hence this configuration is referred to as probe feeding. In the third arrangement shown in figure 1.2(b), feeding is achieved by placing the patch in close proximity to some other source such as the microstrip transmission line shown, thereby permitting the excitation of the antenna element through electromagnetic coupling.

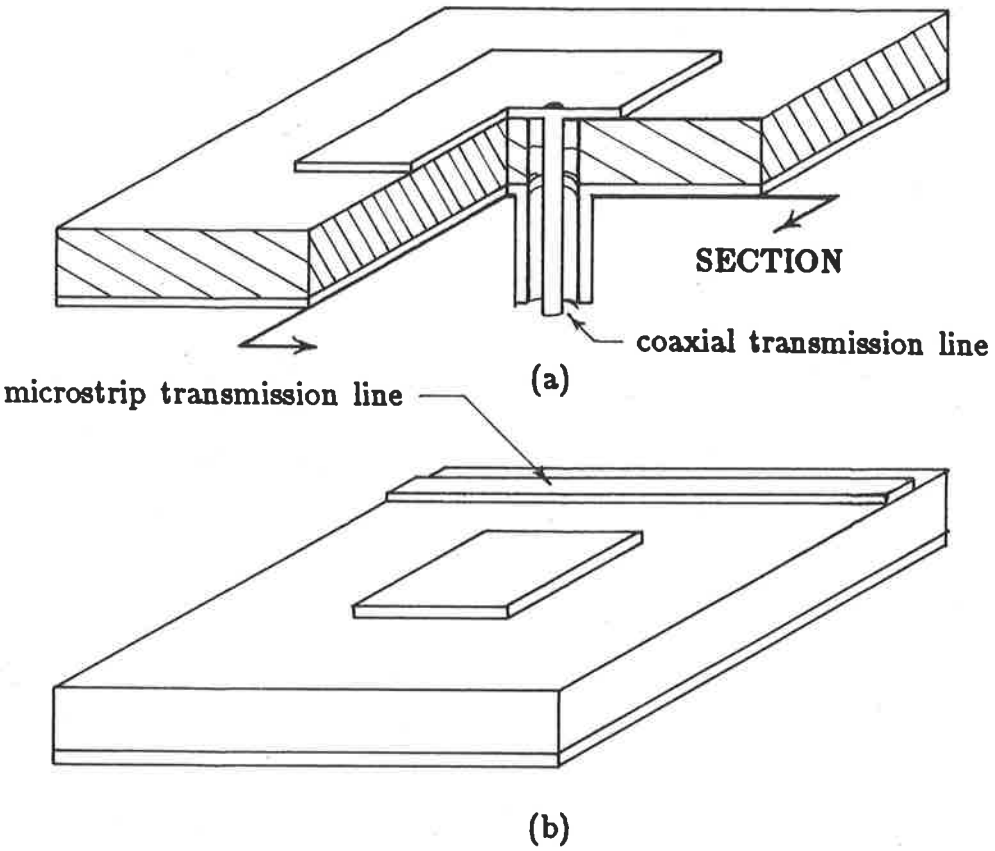

Figure 1.2: Feeding arrangements: (a) probe feeding and (b), electromagnetic coupling.

Probe fed elements have been used almost exclusively in this investigation because at microwave frequencies input impedances are most accurately measured by coaxial equipment. Also the ground plane provides a shield against interference between the measurements and the test equipment, and serves as a well defined reference plane for the measurement of the input impedance. Probe feeding also offers a degree of

design flexibility because the location of the probe can be used to select the impedance presented by the antenna, or the polarisation characteristics of its far field radiation pattern.

Rectangular and circular patches can be used to build up linear arrays to achieve fan shaped far field radiation patterns. Figure 1.3(a) shows an example [7] where the elements are arrayed in the E-plane. This arrangement is called a series fed array. Isolated elements can also be arrayed in the H-plane, or joined together to form one wide radiator [4]. This wide microstrip radiator together with its feed network, as shown in figure 1.3(b), is ideal for wrapping around the body of a satellite to provide an omni-directional radiation pattern. A pencil beam can also be formed by a two dimensional array of single elements [7], or by arraying wide microstrip radiators in the E-plane.

Microstrip antenna elements and arrays are finding many uses in the field of antenna engineering because they have many unique advantages over the costly and bulky mechanical structures which they have the potential to replace. They are conformal, low in profile, and best suited to applications requiring small size and light weight. They are also attractive because of the advantages of low production cost, high design flexibility and ruggedness.

The antenna's fabrication advantages are the result of the monolithic planar manufacturing technology which is used, and include: low cost because all of the advantages of printed circuit technology can be exploited, high reliability, because there are no registration problems, and technology compatibility with other circuit elements such as transmission lines, filters and active devices. Also where necessary a radome can be included as an integral part of the antenna structure. The mechanical advantages start with the antenna's flat and low profile, therefore there is minimum disturbance to the aerodynamic flow across the outside of a vehicle and minimum protrusion into the vehicle's interior. There is also good reliability due to the absence of high stress components and the need to assemble the antenna system. The electrical advantages of microstrip antenna technology include: reliability and general flexibility because there

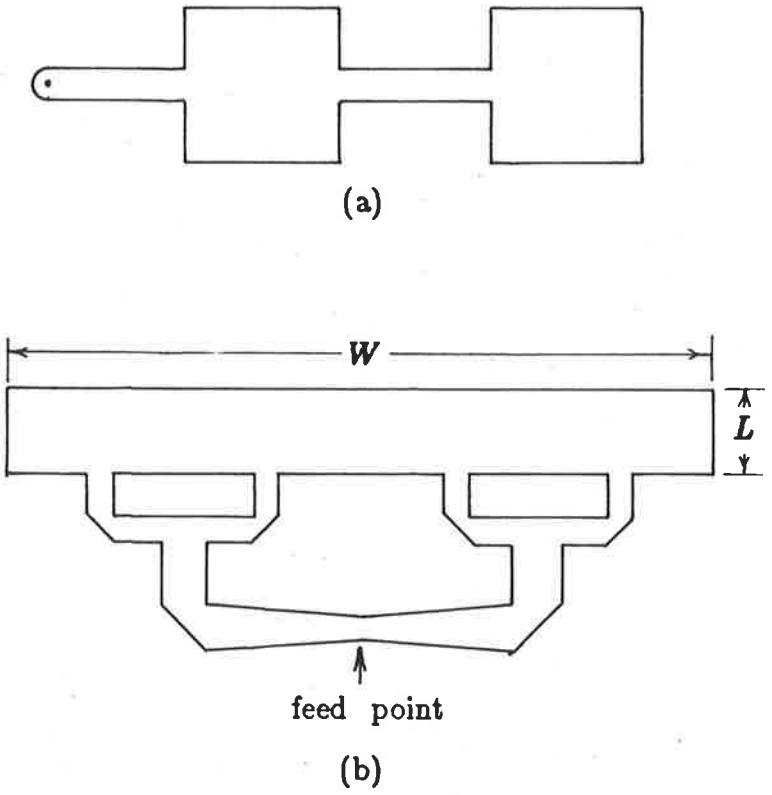

Figure 1.3: Microstrip antenna array configurations: (a) series fed array and (b), a wide radiator antenna.

is no restriction on the antenna's shape.

The antenna has also been found to have the following disadvantages. For operation on common substrates around 5GHz, the bandwidth is typically limited to about 3% and 4% for basic rectangular and circular elements respectively. The electrical characteristics of the antenna are very sensitive to the relative dielectric constant which is subject to variation during manufacture and thermal stress. Voltage breakdown can be a problem in high power transmitter applications because of the close proximity of the patch to the ground plane. In array applications spurious radiation from the feed network occurs when using microstrip lines to feed the antenna, particularly whenever there are bends or curves or simple perturbations in the characteristic impedance due to surface imperfections and material inhomogeneity. In array applications this problem

together with line attenuation raises the side-lobe level of the radiation pattern.

Even with the above limitations, microstrip antenna technology has many advantages over other antenna classes in a wide variety of applications. However the pace at which they have found application has been greatly hindered by the expensive cut-and-try design techniques that have been employed. The analytical models available to the designer are now reviewed.

1.2 Analytical Models

1.2.1 Introduction

This review of analytical models is concerned primarily with resonant frequency and input impedance because these characteristics are difficult to calculate because they are very sensitive to an accurate representation of the fields within the antenna. Conversely, the main lobe of the far field radiation pattern is insensitive to small errors that might occur in modelling the fields under the patch and is therefore regarded as a lesser challenge to analysts.

The analytical approaches that are accurate enough for some but not all design purposes are now discussed. In turn they are each shown to give agreement with measurements when applied to antennas operating in the lower microwave band. This review will also provide a foundation for the simple novel models that are proposed for the resonant frequency, input impedance, and radiation pattern, and demonstrated to be accurate up to mid-microwave frequencies in Chapters III, V, and VI respectively. The analytical models for the mutual coupling between rectangular patches are reviewed in Chapter VII.

1.2.2 Transmission Line Model

The transmission line model is the oldest and simplest model, being first applied to rectangular elements in 1974 by Munson [4]. For input impedance calculations the antenna shown in figure 1.1 is modelled by the equivalent transmission line circuit of

figure 1.4, which includes two radiating slot antennas in the $y = \pm L/2$ planes, both of area W by h and separated by a low characteristic impedance parallel plate transmission line.

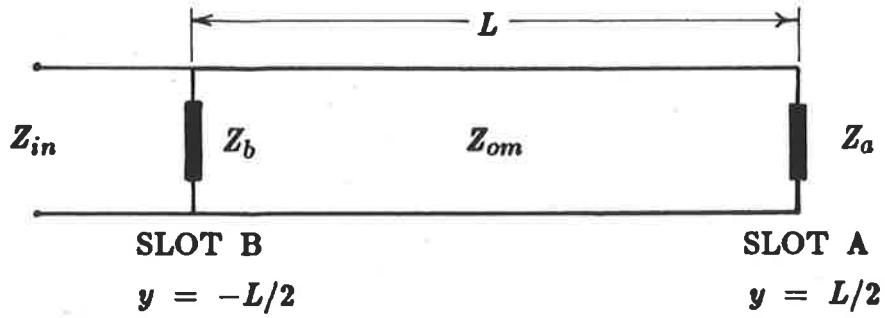

Figure 1.4: Transmission line model of a microstrip transmission line fed rectangular element.

The input impedance at the junction between the antenna and the transmission line, where $y = -L/2$, is calculated by transforming the input impedance of slot antenna A, Z_a, a distance L along a transmission line of characteristic impedance Z_{om}, to the reference plane at $y = -L/2$. If the transformed impedance is labelled Z_a', then the input impedance is obtained from the parallel combination of Z_a' and Z_b, hence

$$Z_{in} = \frac{Z_a' Z_b}{Z_a' + Z_b} \tag{1.1}$$

This equation can be used to show that the antenna is resonant when its length is slightly less than $\lambda_s/2$. Introducing the input resistance and reactance of the equivalent radiating aperture of the slot antenna, let

$$Z_a = Z_b = R_a + jX_a \tag{1.2}$$

then if the antenna's length is $\lambda_s/2$, the transmission line equation [8] can be used to show that the transformed slot impedance (Z_a') equals the original impedance(Z_a).

However if the slot impedance is transformed by $0.48\lambda_s$ to $0.49\lambda_s$, then

$$Z_a' = R_a - jX_a \tag{1.3}$$

Substituting equations (1.2) and (1.3) into (1.1) gives a real result called the resonant resistance, where

$$R_o = \frac{R_a}{2} \tag{1.4}$$

The expressions due to Harrington [9] for the conductance and susceptance of an aperture in a ground plane have been widely applied to microstrip antennas in the literature [4,10]. They are:

$$G_a = \frac{\pi(1-(\beta_o h)^2/24)}{\lambda_o \eta_o} \quad \text{mho/unit length} \tag{1.5}$$

$$B_s = \frac{3.135 - 2\log\beta_o h}{\lambda_o \eta_o} \quad \text{mho/unit length} \tag{1.6}$$

where the aperture is assumed to be thin, $h/\lambda_o < 0.1$. It is concluded in Chapter V, where the slot admittance is considered in detail, that expressions (1.5) and (1.6) are only useful for a very limited set of antenna electrical dimensions. In the literature on microstrip antennas the terms slot, aperture, and wall admittance are used interchangeably. Except for these introductory comments, the term aperture admittance is used throughout this thesis.

Early use of the transmission line model by Munson [4] was accompanied by a simple method of calculating the far field radiation pattern, where the antenna was represented by a uniformly illuminated metallic rectangle, or array of rectangles in the case of an antenna array. The radiation pattern is calculated by standard techniques [11]. Even though this rudimentary form of the model only gives fair agreement with experiments for cases where the antenna is fed at its edge [15], it is still used as a computational aid to the antenna designer working in the lower microwave band [4]. Milligan [10] used this simple form of the transmission line model to account for the

variation in the frequency bandwidth as other antenna parameters are changed. Chapter VIII continues with a review of the bandwidth characteristics of the antenna.

Derneryd [12] carried the transmission line model further when a TEM-mode field distribution was proposed as an approximation to the field in the cavity between the patch and the ground plane; where the TEM standing wave is the distribution resulting from the interference of two TEM travelling waves in the plus and minus y-directions. Refer to figure 1.5. This approximate field distribution has no x-directed components under the patch, and the same is assumed for the fringing fields at each end of the patch. Thus the two imaginary slot antennas are assumed to have electric field distributions that are constant in the z-direction and zero in the x-direction. Figure 1.5 also shows how the electric field vectors of the fringing field, E_θ, are decomposed into E_z and E_y components. Derneryd proposed that the E_y components should be used to represent the fields across the slot antennas, rather than the E_z-components that were previously used by Munson [4]. The input impedance and far field radiation pattern of the antenna element are modelled by an array of two slots in the $z = h$ plane.

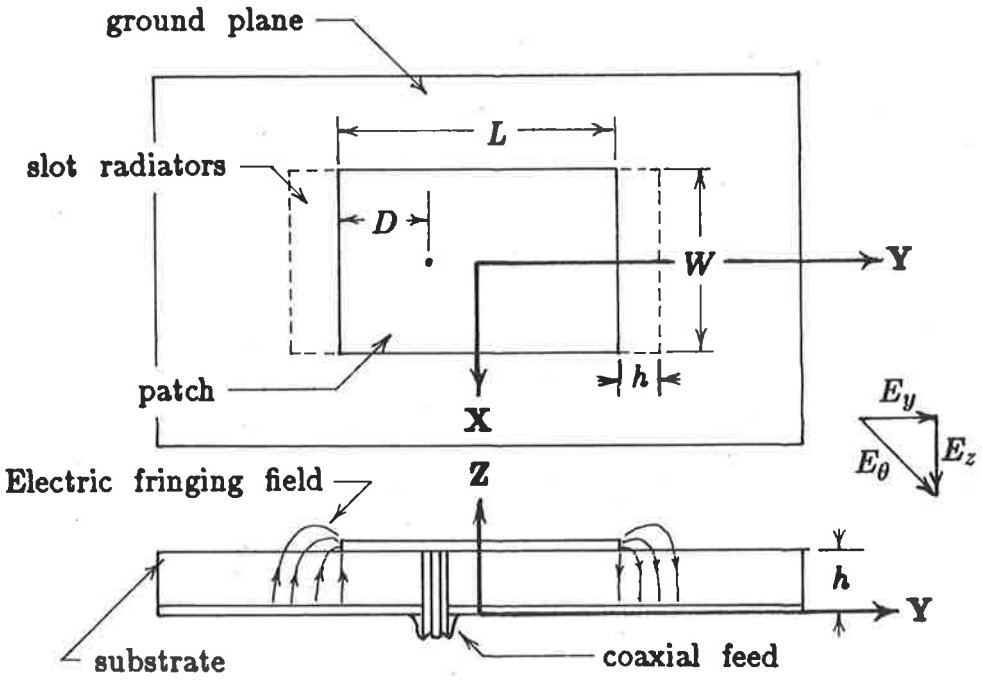

Figure 1.5: A rectangular microstrip patch antenna fed by a coaxial probe.

The transmission line equivalent network shown in figure 1.4 was used by Derneryd [12] to derive an expression for the antenna's input admittance referred to the $y = -L/2$ plane,

$$Y_{in} = G_a + jB_a + Y_{om}\frac{G_a + j(B_a + Y_{om}\tan\beta_e L)}{Y_{om} - B_a\tan\beta_e L + jG_a\tan\beta_e L} \tag{1.7}$$

The element is said to be resonant when the imaginary part of the input admittance equals zero, which occurs when the length of the patch satisfies

$$\tan\beta_e L = \frac{2Y_{om}B_a}{G_a^2 + B_a^2 - Y_{om}^2} \tag{1.8}$$

In developing new design methods new formulas for the slot admittance were proposed by Derneryd [12]. The conductance is calculated by integrating the real part of the Poynting vector over a hemisphere surrounding a magnetic dipole. The susceptance is represented by the static capacitance associated with the fringing fields of an open-circuited microstrip line. Detailed investigations of the methods for representing the admittance of the slot antennas will be given in Chapter V.

Derneryd [12] was the first worker to apply to microstrip antennas the approximate electrostatic expressions for the effective dielectric constant (ϵ_e) and edge extension (δL) proposed for use with microstrip lines by Schneider [13] and Hammerstad [14] respectively. They are

$$\epsilon_e = \frac{\epsilon_r + 1}{2} + \frac{\epsilon_r - 1}{2}(1 + \frac{10h}{W})^{-0.5} \tag{1.9}$$

$$\delta L = 0.412h\frac{\epsilon_e + 0.300}{\epsilon_e - 0.258}\frac{W/h + 0.262}{W/h + 0.813} \tag{1.10}$$

Derneryd also proposed treating the transmission line between the slot antennas as a microstrip line of characteristic impedance $Z_{om}(= Y_{om}^{-1})$. There have been three formulas used for Z_{om} in the analysis of microstrip antennas, and they are as follows.

Using a conformal mapping approach Schneider [13] developed an exact solution which was then approximated by a truncated series expansion,

$$Z_{om} = \frac{\eta_o}{\sqrt{\epsilon_e}(W/h + 2.42 - 0.44h/W + (1 - h/W)^6)} \quad \text{ohm} \tag{1.11}$$

where $W/h \geq 1$. Carver [15] suggested using Schneider's approximation to the above equation,

$$Z_{om} = \frac{h\eta_o}{W\sqrt{\epsilon_r}} \quad \text{ohm} \tag{1.12}$$

and Sengupta [16] suggested using an equation published by Hammerstad [14] that was a modification of Wheeler's result [17] for two parallel strips separated by a dielectric sheet, Hammerstad's equation is,

$$Z_{om} = \frac{h\eta_o}{\alpha W\sqrt{\epsilon_e}} \quad \text{ohm} \tag{1.13}$$

where

$$\alpha = 1 + 1.393\frac{h}{W} + 0.667\frac{h}{W}\ln(\frac{W}{h} + 1.444) \tag{1.14}$$

For typical antennas operating at 5GHz with widths roughly equal to $0.5\lambda_s$, there is only a 5% variation in the calculated characteristic impedances obtained from these three formulas.

As far as the radiated field in the normal direction is concerned, the components of the near field fringing beyond the ends of the patch parallel to the ground plane, E_y, add in phase to give a maximum radiated field normal to the element, while for this direction the radiation associated with the E_z components is out of phase and cancels. The far field radiation pattern can be determined by the classical methods [18] for a two element side by side array of slots in the x-y plane. This two element array is used in Chapter VI, where it is refined and used to calculate radiation patterns that are in good agreement with measurements.

Derneryd [12] also used this model to calculate the directivity and bandwidth, and to design linear arrays of rectangular patches interconnected with microstrip lines.

It has also been used by Newman et.al. [19] in conjunction with the moment method technique to calculate the input impedance of a rectangular element fed part way along its E-plane axis, as shown in figure 1.2(a). Here the moment method technique is used to determine the slot impedance, and the input admittance of the antenna is determined using the transmission line model shown in figure 1.6 as,

$$Y_{in} = Y_{om}\frac{Z_{om}C_1 + jZ_aS_1}{Z_aC_1 + jZ_{om}S_1} + Y_{om}\frac{Z_{om}C_2 + jZ_aS_2}{Z_aC_2 + jZ_{om}S_2} \tag{1.15}$$

where

$$C_1 = \cos\beta_s L_1 \tag{1.16a}$$

$$C_2 = \cos\beta_s L_2 \tag{1.16b}$$

$$S_1 = \sin\beta_s L_1 \tag{1.16c}$$

$$S_2 = \sin\beta_s L_2 \tag{1.16d}$$

At 600MHz this analytical approach was compared with measurements and shown to be within -1.6% and 32% for the resonant frequency and resonant resistance respectively.

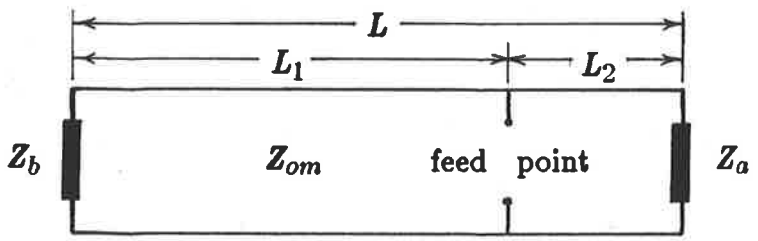

Figure 1.6: The transmission line model of a probe fed rectangular patch.

The transmission line model has been useful for studying rectangular elements operating at fundamental or simple higher order modes in the y-direction. Refer to figure 1.5. However like the more complicated models it depends on an accurate determination of a few key parameters, including: effective dielectric constant, effective

electrical dimensions and the admittance of the equivalent slot antennas that model each end of the element. Chapter V shows that the agreement between the calculated and measured input impedances falls off as the frequency is increased because the formulas used for the above parameters do not model the actual behaviour accurately enough. Chapter V also shows how the accuracy of the transmission line model is improved using an empirical approach to determine some of the key parameters, permitting the use of the model up to at least 5GHz.

1.2.3 Cavity model

Some of the limitations of the transmission line model have been overcome by various workers using a dielectrically loaded cavity analogy for the microstrip antenna. This analogy was used much earlier for the analysis of microstrip resonators [20,21,22], so its application to antennas has been a natural progression. In this method the antenna was initially modelled by Lo et.al. [23] as a cavity bounded by two short-circuited and four open-circuited walls; and because the cavity is thin, the following assumptions about the electromagnetic fields within it can be made:

i Only the E_z, H_x, H_y components exist within the cavity.

ii The above field components are independent of the z-coordinate over the frequency bandwidth of interest.

iii The electric current in the microstrip must have no component normal to the edge at any point on the edge, implying a negligible tangential component of the magnetic field intensity along the edge.

Initially only rectangular and circular cavities were considered. The rectangular cavity was treated as a section of a microstrip transmission line of length equal to half of the wavelength in the dielectric and supporting a TEM-mode standing wave. The circular cavity was treated as a thin section through a cylindrical cavity supporting a TM standing wave derived from propagation in the z-direction.

Howell [2,3] used the cavity model to calculate the fundamental resonant frequencies of both circular and rectangular elements. For a rectangular element; as was the case using the transmission line model, the fundamental resonance occurs when the distance, L, between the two radiating slots is equal to one half of the wavelength in the dielectric. Therefore,

$$f_o = \frac{c}{2L\sqrt{\epsilon_r}} \tag{1.17}$$

The lowest order resonant frequency for a circular element of radius a is

$$f_o = \frac{1.841c}{2\pi a\sqrt{\epsilon_r}} \tag{1.18}$$

However the measured resonant frequency was found to be 5% lower than that calculated, mainly because in practice the effective edge of the patch was extended slightly, due to the fringing fields around the patch. This means that the antenna's electrical length or radius is larger than the physical dimensions, hence lowering the resonant frequency. Therefore the physical length L in (1.17) is replaced by the electrical length of the patch $(L + 2\delta L)$ using the edge extension given in equation (1.10). The fringing around the edge of the circular patch is taken into account in equation (1.18) by using an effective radius [24], given by

$$a_e = a[1 + \frac{2h}{\pi a\epsilon_r}(\ln\frac{\pi a}{2h} + 1.7726)]^{0.5} \tag{1.19}$$

where $a/h >> 1$.

Further consideration of a cavity leads to the possibility of higher order resonant frequencies for microstrip patch antennas [3]. For a rectangular antenna these resonances occur when the distance in the dielectric between the slots is a multiple number of half wavelengths, therefore the resonant frequencies f_n are given by

$$f_n = \frac{c}{2n(L + 2\delta L)\sqrt{\epsilon_r}} \tag{1.20}$$

It has also been shown [25] that a series of modes exists for the circular element that is similar to those of a cylindrical cavity except for the boundary conditions at the

edges. Here the resonant frequencies are given by

$$f_{m,n} = \frac{cX_{mn'}}{2\pi a_e \sqrt{\epsilon_e}} \tag{1.21}$$

where $J_{m'}(X_{mn'}) = 0$, $J_{m'}$ being a Bessel Function. The lowest order of resonance occurs when $X_{n'} = 1.841$.

The cavity model has been extended to determine most of the electrical characteristics of microstrip disc antennas [26,27,28]. Here the cavity comprises the patch, the ground plane, and the open circuited walls around the periphery of the patch. The field internal to the cavity is approximated solely by a dominant mode. Because of the close proximity of the patch and the ground plane ($h < \lambda_s/10$), the antenna can be modelled as a thin resonant cavity with equivalent magnetic line currents along the perimeter of the patch. The source of the radiation field of the rectangular antenna is still modelled as a two element side-by-side array of uniformly illuminated slots.

The model has been used to calculate the stored, lost, and radiated energies, and also the input impedance, quality factor, radiation efficiency, and bandwidth. Figure 1.7 is a graph of the quality factor and radiation efficiency against the resonant frequency for rectangular and circular antennas on a 1.524mm thick substrate with ϵ_r= 2.55 and tanδ=0.0018. Because the quality factor is inversely proportional to bandwidth ($\%BW$=100/Q), the figure implies that bandwidth is an increasing function of frequency. The improved bandwidth can be attributed to the increasing electrical substrate thickness which in turn permits greater radiation from the element due to the increased fringing fields.

The cavity model has been very helpful in providing all of the electrical characteristics for microstrip antennas of a few simple shapes, as long as the antenna is thin compared with the wavelength. Both the transmission line and single-mode cavity models give results that are in agreement with measured radiation patterns. However, these models ignore the effects of the terminal region and therefore calculate the input

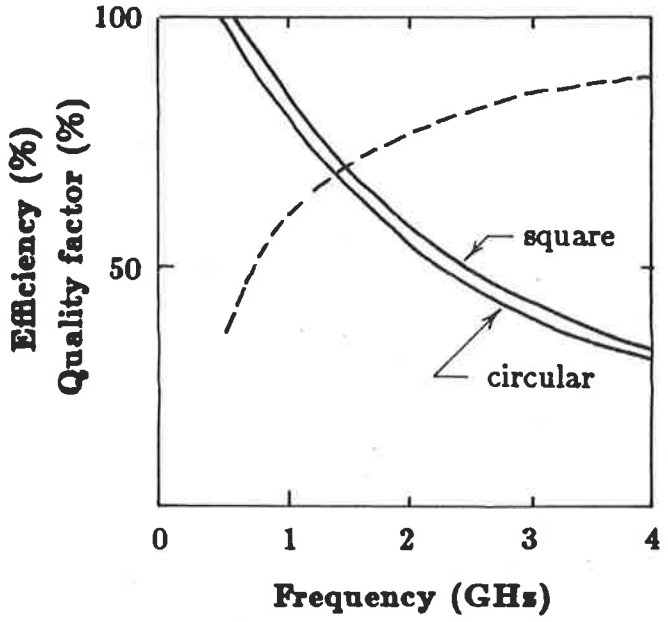

Figure 1.7: Quality factor (———) and efficiency (– – –) versus frequency [24].

impedance loci to be symmetrical about the real axis of the Smith chart, which is not the case with the experimental results. Hence good agreement between the calculated and measured input impedance loci only occurs when the feed point is located near the edge of the antenna, because when this is the case, the measured impedance locus is approximately symmetrical about the real axis anyway. The deficiencies of these simple models, as they have been presented in the literature, can be summarised:

i In the case of probe fed elements, they predict resonant frequencies that are a few percent lower than the measured resonant frequencies.

ii They cannot be easily adapted to account for structures that support transverse modes as may be caused by perturbations in the cavity's internal field due to the feed point.

iii They are only suitable for modelling rectangular or circular patches.

The modal-expansion cavity model is an extension of the cavity model already discussed. Again the antenna is viewed as a thin cavity with short circuit and open circuit walls, and the field within the cavity is expanded in terms of a series of discrete resonant modes. Initially the field distributions for the modes are established assuming

that the end and side walls are open-circuited, which implies that there is no radiation from the antenna. Richards et.al. [29] accounted for the radiation and other losses to the cavity by an artificially increased loss tangent, and Carver [15,30] replaced the open-circuited walls by an impedance boundary condition, or wall admittance. The accuracy of both approaches depends on the complex wave number for each mode, the real part of which is used to determine the resonant frequency.

The feed is then modelled as a z-directed current strip and a double summation of cosinusoidal terms is used to represent the cavity field distribution of the resonant modes, where the distribution of the fundamental mode is identical to that used with the transmission line model discussed earlier. A double summation expression is derived for the input impedance which is in effect a Foster [31] expansion of resonant sections. Figure 1.8(a) shows a general network representation of the input impedance. The (0,0) section includes the static capacitance and a resistor to represent losses in the substrate. The (0,1) section represents the dominant mode and is equivalent to the parallel RLC network where the R represents the radiation and losses in the metal cladding and dielectric substrate. The (m,n) section represents an unspecified higher order mode. The infinite number of higher order sections have negligible losses and sum to form a series inductance. The microstrip antenna is typically narrow band; therefore provided that the modes are well separated, the input impedance can be represented by the single (m,n) Foster section and a series inductance, as shown in figure 1.8(b).

The modal-expansion model incorporating the wall admittance gave good input impedance results when applied to circular and rectangular antennas operating at or near 2.2GHz [30]. The wall conductance was based on a parallel-plate TEM waveguide radiating into an open half space [9], and represents the effects of radiation and cavity losses. The susceptance of the walls represents the energy stored in the fringing fields, and is based on the static capacitance of an open ended microstrip line [14]. The method has been extended using a finite element approach to obtain the magnetic currents on the radiating walls of a general five-sided patch [30].

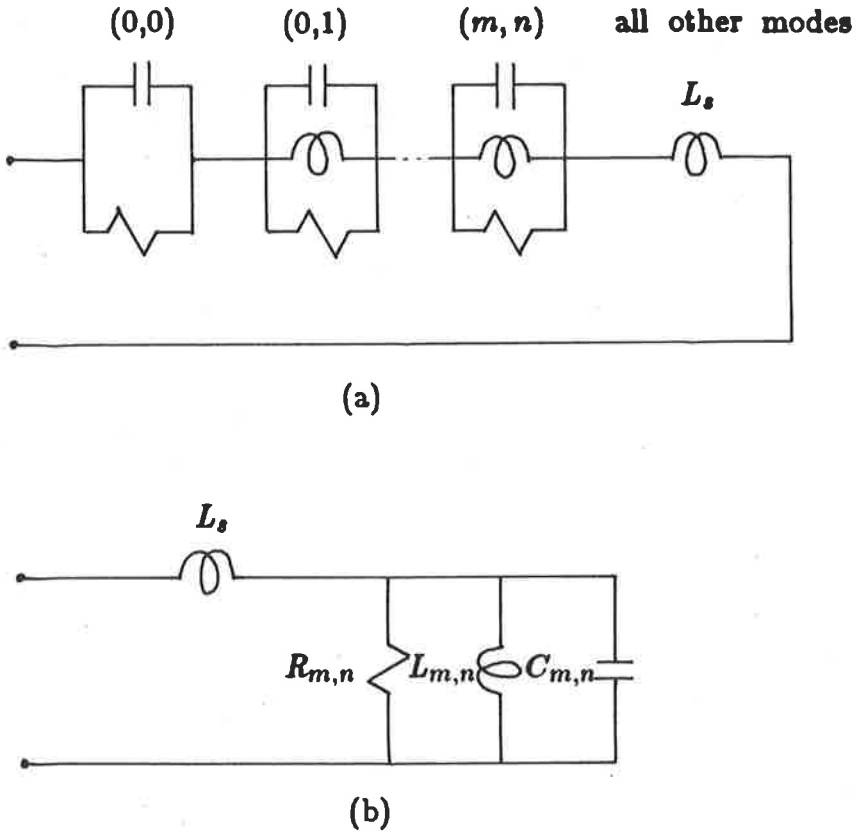

Figure 1.8: (a) Network model for a multi-mode cavity and (b) a simplified network model for operation around a dominant mode of resonant frequency, f_{mn}.

A similar investigation by Carver [32] followed where the field within the cavity was expanded into a Fourier series. Also proposed was an empirical modification to the aperture admittance equations that accounted for the aspect ratio of the metallic patch. At 1GHz the calculated and measured resonant frequency and resistance were within ±0.25% and ±5% respectively. This model was later tested against measurements at 2.2GHz [15], and showed a 0.5% error in resonant frequency and negligible error in resonant resistance. However as the frequency increased to +4.5% above the resonant frequency the error in the input impedance increased markedly. This approach was also shown [33] to give errors in the resonant frequency of 4% when used with rectangular antennas operating at 5GHz.

Carver [34] used the wall admittance approach in a detailed investigation of the equivalent series reactance of the feed probe. At S-band a comparison between the

calculated and measured series reactance revealed an error of 47%. This unacceptably high error led Carver to conclude that an effective probe diameter of five times the physical diameter should be used in the model. This was also suggested by Richards et.al. [35]. It was further recommended by Carver that the modal-expansion model not be used to determine the series reactance because the computation time is not rewarded by accuracy. Furthermore, as will be elaborated on in Chapter II, the modal-expansion model gives series reactance errors of the order of 250% for a 5GHz antenna on a 1.57mm thick substrate fed by a probe of 3.04mm diameter.

The second method of representing the radiation from the cavity in equivalent circuit terms is based on an effective loss tangent, which is determined using the quality factor of a non-radiating cavity of the same dimensions and resonant at a frequency slightly higher than the cavity under consideration [29,35]. This approach gives radiation pattern and input impedance results that are in good agreement with measurements for a number of different feed points, even when the dominant mode is not strongly excited. Typical agreement between the measured and calculated resonant frequency is within 0.3%, with negligible difference between the input impedance loci over a 7% frequency bandwidth around 1190MHz. However, once again the effective radius of the feed probe was used to ensure good agreement between the measured and calculated impedance loci.

Even though the modal-expansion cavity model gives good results for antenna elements that are simple in shape, its application is still limited to antennas mounted on electrically thin substrates because the accuracy of key parameters in the model falls off as the substrate thickness increases. Calculation of the aperture admittance parameter is based on an empirical modification to formulas that ignore radiation. This is a reasonable approach when dealing with electrically thin antennas with minimal fringing fields, but Chapter V shows that it leads to useless results at higher frequencies of the order of 5GHz. The same limitation applies to the accurate determination of the effective loss tangent because the quality factor of the cavity needs to be assumed

high enough to be insensitive to the frequency, which is the case for electrically thin substrates. Therefore the modal-expansion cavity model remains limited to the analysis of antennas on electrically thin substrates, unless new formulas for the key parameters are found that are applicable to cases where the substrate is not necessarily thin.

1.2.4 Models for numerical analysis.

Rectangular and circular shaped patch antennas have fulfilled most design requirements. However other shapes are occasionally used when particular electrical characteristics of the antenna require enhancement. In particular the pursuit of increased bandwidth performance has resulted in a number of shapes like the pentagon, triangle, and hexagon to be discussed in Chapter VIII. Also rectangular patches have been modified by removing corners or cutting holes or notches into the patch. The models hitherto discussed cannot be easily applied to these arbitrary shapes, therefore numerical techniques have been directly applied to evaluate the currents or the fields associated with these antenna structures.

A wire grid model has been proposed by Agrawal et.al. [36] for the patch and its electromagnetic image. Here the two metal surfaces are modelled by wire meshes of vee-dipoles and the current distribution solved numerically. The dielectric slab is taken into account using empirical frequency shift and impedance scaling information. The results of the analysis were compared with measurements, but it is difficult to establish the accuracy of the work because the authors have tended to minimize computing time at the expense of accuracy. For a 4.4GHz square patch antenna fed at its edge by a microstrip transmission line, comparisons with measurements show an error in the radiation pattern of 3dB, a resonant frequency error of 2.3%, and a resonant resistance error of 33%. The method appears to have possibilities as a design tool because it is potentially very general in its application. However it is more costly in computing time than most other methods and provides little physical insight into the operation of this class of antenna.

Carver et.al. [30] used a finite element approach was also used to find the interior fields within a general five-sided cavity. An equivalent aperture admittance was placed around the boundary of the patch in the same manner as was used with the modal-expansion cavity model, and therefore once again the accuracy of the results depends upon empirically modified formulas that are only useful at lower frequencies. The results of this work could not be found in the open literature so it is highly possible that it was never finished.

A general method of moments solution of the reaction integral equation was proposed by Newman et.al. [37] to determine the electric and magnetic surface currents associated with a strip dipole on a thin dielectric slab, where the volume equivalence theorem was used to replace the dielectric inhomogeneity by equivalent volume polarisation currents in free space. The work was later continued using a surface patch model for a patch antenna and a thin-wire model for the feed lines [38]. The image theory was used to account for the ground plane. Very good input impedance results were shown for rectangular and pentagonal shaped patches operating at frequencies up to 1200MHz. For the rectangular patch the agreement was within 0.08% and 15% for the resonant frequency and resonant resistance respectively. In fact at this frequency the accuracy of the model is no better than that obtained using the transmission line and cavity models. Even compared to the other numerical analysis techniques, the model requires excessive computing time because of the high precision needed for the computation of the impedance matrix.

Another method of moments solution was proposed by Pozar [39], and uses an exact Green's function to analytically account for the dielectric slab and ground plane. The earlier problem [38] of the sensitivity of the input impedance results to the numerical accuracy was overcome because the ground plane was included in the Green's function. Also the Green's function rigorously accounts for the surface waves launched into the dielectric. For rectangular patch antennas operating at 660MHz, this approach provides results that agree with measurements to within -0.08% and +23% for the reso-

nant frequency and resonant resistance respectively. Also the mutual coupling between rectangular antennas at 1410MHz was calculated to within ±1db of measurements. However, the excellent agreement with measurements was only arrived at after the adjustment of the dielectric constant.

1.3 Conclusions

The analytical models for the radiation pattern and input impedance of microstrip antennas fall into three main categories. In the first category the transmission line model is simple and provides results that are adequate for the design of microstrip transmission line fed rectangular antennas. The modal-expansion cavity model is in the second category, and can be applied to simple shaped antennas and their feed structures. The accuracy of both the transmission line model and the modal-expansion cavity model, incorporating the boundary condition, depends on the accuracy of the aperture admittance. The resonant frequency is a function of the aperture susceptance and the aperture conductance has a major effect on the resonant resistance. The aperture admittance that has been used in both of these models is based on the empirical adjustment of equations that were originally proposed for use with thin microstrip lines, or long thin slot radiators. Some of these equations for the key parameters of the models are based on electrostatic considerations, and ignore dispersion and radiation and the possible effect of evanescent modes on the field distribution around the patch periphery. Moreover they are demonstrated in the following chapters to give incorrect results as the frequency increases to 5GHz. Modelling the patch and its image by fine wire grids is representative of the third category of analytical models, and is applicable to the analysis of antenna structures of general shape. This approach could be carried out using one of the widely available wire grid computer-aided analysis programs. Although the results obtained using the wire grid model are in fair agreement with measurements, it is clear that the electromagnetic near fields of the antenna are not accurately represented. Firstly, the same current distribution is supported above and below each of the wire meshes, which is not the case for the patch and its image in an inhomogeneous medium. Secondly,

the image principle is widely applied to field problems involving electrostatic charges and isolated thin wires supporting electromagnetic fields above ground planes. However the application of this principle to meshes of wire antennas does not necessarily follow. Along with the other two classes of analytical models, this wire grid model requires the empirical adjustment of key parameters and has the disadvantage of demanding much more computer power than the models in the other two categories.

The analysis of the microstrip antenna element is made very difficult because the electromagnetic fields around the periphery of the patch exist in an inhomogeneous medium. Figure 1.1 shows that the half-space above the ground plane is partly filled with air and partly with a thin dielectric substrate of some non-unity dielectric constant. The problem is more clearly illustrated if the transmission line model is used, and the patch is treated as a section of microstrip transmission line comprising a plate above a ground plane. Firstly the image principle is used to replace the currents in the ground plane by another fictitious plate located a distance $2h$ from the first plate at $z = -h$ on figure 1.1. A length of parallel-plate transmission line is the result, comprising two plates separated by a dielectric substrate of thickness $2h$. If this structure was in a homogeneous uniform isotropic medium, then it could support two TEM waves propagating in the plus and minus y-directions, and the analysis would be relatively straight forward. But for the partially filled space under consideration the structure can only support a set of hybrid modes having non-zero E_y and H_y components. However at low frequencies the lowest-order hybrid mode resembles a TEM mode and is therefore referred to as a quasi-TEM mode, and because the antenna is a half wavelength long section of this transmission line, this quasi-TEM standing wave distribution can be used to approximate the field between the patch and the ground plane. This complexity in the mode structure has impeded the development of solutions sufficiently accurate for engineering purposes for even the simplest electrical parameters. Chapter VI describes an investigation into the fringing field distributions around the patch using a liquid crystal film. It is concluded that, for frequencies above 3GHz, the distribution under

the patch is much more complicated than a quasi-TEM mode would indicate.

In the absence of an exact electromagnetic treatment of the antenna element, various workers have used approximate solutions based on quasi-static or full-wave representations of the electromagnetic problem. Then part of their procedure appears to have been the empirical adjustment of results to account for the approximations in the field distribution under the patch, particularly those that occurred when radiation was ignored. These approaches have been very useful for the input impedances and radiation patterns of antennas operating at frequencies up to 3GHz, where the radiation efficiency of the structure is low. As the frequency is increased however, so does the effective electrical thickness of the substrate thereby permitting increased fringing and associated radiation, eventually rendering the previous refinements useless.

The aim of this investigation is to develop a computer-aided design program for rectangular elements operating at frequencies beyond those where the existing analytical models have been successfully applied. There are numerous examples in the open literature of analytical techniques that have been useful at frequencies below 3GHz. However, microstrip antennas are typically used up to 10GHz and to a lesser extent up to 30GHz. This investigation was carried out around 5GHz because of the extensive use of this band in radar, communication and biomedical applications, and because the models suggested in the literature are very inaccurate at 5GHz.

This investigation uses a lossy cavity model to determine the resonant frequency and the bandwidth, and a transmission line model for the input impedance, far field radiation pattern and mutual coupling. These models were chosen instead of the more complicated ones because:

i They have been shown to be quite adequate for design purposes at lower frequencies, giving useful results for resonant frequency, input impedance, radiation pattern, and mutual coupling.

ii They use the same field distribution under the patch as the fundamental mode

used in the cavity models, and the assumption that most of the energy is stored in the fundamental mode is reasonable because the antenna has such a narrow bandwidth. Also, the transmission line model will require no more empirical refinement than the modal-expansion cavity model because the accuracy of both models is dependent on knowledge of the aperture admittance.

iii Given a fundamental acceptance that modelling of the antenna at frequencies of about 5GHz will necessarily require a large empirical component in determining the key electrical parameters, it is then an advantage to use simple models where reasonably obvious account of the electromagnetic phenomenon taking place can be maintained. Another advantage is that the simple models will only require moderate computing facilities.

Novel models for the main electrical characteristics of rectangular microstrip antennas will now be developed for application in a computer-aided design program. The starting point is to model the equivalent series reactance of the coaxial feed probe because it must be known before the resonant frequency and input impedance can be calculated. Chapter II surveys the literature associated with modelling the feed probe and goes on to describe an extensive experimental investigation into the characteristics of the probe. A coaxial transmission line with an empirical taper is then developed as a model. The resonant frequency is discussed in Chapter III. Here a cavity model is used as the basis for the introduction of specific definitions for resonant frequency, and the development of an empirical model for the effective edge extension. The cavity model is also used in Chapter IV, where the definition of bandwidth usually applied to single port resonant cavities is put forward as a more appropriate definition of bandwidth for microstrip antennas, particularly when there is a need for bandwidth comparisons between antennas, as is the case in Chapter VIII. The models for the aperture admittance are reviewed in Chapter V, and then the transmission line model with empirical aperture admittances is used to calculate the input impedance. Chapter VI describes some of the properties of the effective apertures at each end of the antenna, and then

continues with the calculation of the radiation pattern using a two aperture side-by-side array. A far field radiation model is used to calculate the mutual coupling in Chapter VII. Finally Chapter VIII explores the bandwidth properties of the antenna and the efforts of other researchers to enhance the bandwidth of microstrip antennas generally. A novel hexagonally shaped patch is then proposed as a more suitable element than the rectangular patch because of its superior bandwidth and gain characteristics.

The new models for calculating many of the electrical characteristics of rectangular microstrip antennas and arrays operating up to 5GHz are incorporated into a computer-aided design program listed in Appendix C. The body of the thesis describes the development and testing of the models used in the program.

CHAPTER II

A TAPERED TRANSMISSION LINE MODEL FOR THE COAXIAL FEED PROBE

2.1 Introduction

This chapter describes an investigation into the characteristics of the feed point region of probe fed microstrip antennas. The study of the feed point precedes the chapters to come because the results of the resonant frequency and input impedance models must be transferred, using the feed point model, to the antenna terminals before they can be compared with measurements. So an accurate model for the feed point is required before the resonant frequency and input impedance of the antenna can be considered.

Lo et.al. [23] proposed modelling the microstrip antenna by a resonant cavity in series with an inductive reactance, called the series reactance. Figure 1.8(b) shows this network model where the series reactance represents the effects of the probe on the cavity resonant circuit, where $X_s = \omega L_s$.

Insight into the characteristics of the probe is obtained if the self-inductance of a short length of wire is used as a model. Basic physics suggests that the self-inductance of the wire is proportional to its length and inversely proportional to its diameter. This will be shown to be the case for the coaxial probe.

The series reactance has been measured in three independent investigations. In each case the probe is terminated in a different load with the aim of isolating the

effect of the connection region from the measured input impedance versus frequency characteristics of the overall apparatus. The first arrangement terminates the probe in a large cavity and the second in a short circuited, low characteristic impedance transmission line. In the third arrangement the probe is used to feed a rectangular patch antenna. The measured series reactances are used to show that the results of the analytical and empirical models proposed by other authors become increasingly inaccurate as the frequency increases, and in fact seriously incorrect at 5GHz.

A new model for deriving the series reactance of the probe is also proposed. A tapered transmission line is used to transform a short circuit termination down the length of the probe to the antenna's terminals at the ground plane, where the taper has been empirically determined to be a function of the dimensions of the probe and the aspect ratio of the patch. This model will be shown to give series reactances that agree with measurements for a variety of commonly used antenna and feed dimensions, and operating up to 5GHz.

2.2 Models for the series reactance

The need to determine the series reactance is illustrated by considering the Smith chart plot of the measured input impedance versus frequency characteristic of a rectangular microstrip antenna resonant at 5GHz, refer to figure 2.1. The locus can be closely approximated by a circle of best fit, which in turn can be approximated by the input impedance of the network shown in figure 1.8(b); that is, an RLC resonant circuit fed through a series inductive reactance. The plot of the input impedance of an RLC circuit, as seen from the detuned short position [41], is a circle placed symmetrically about the real axis of the chart. The effect of adding the series reactance, $+j\omega L_s$, to each point on the locus is to transform the circular locus around the chart in a clockwise direction. The problem is to model this transformation of the input impedance locus. The models to be described in the following sections use either a series inductance derived from the net reactance of a parallel combination of detuned RLC networks or a

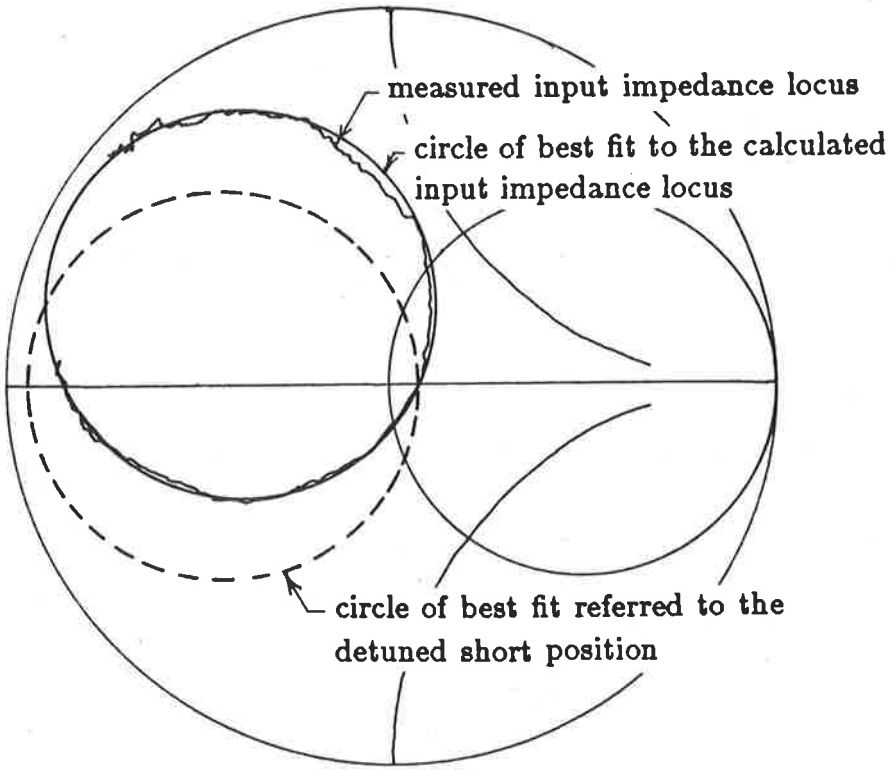

Figure 2.1: Transforming the measured input impedance versus frequency locus of a rectangular microstrip antenna, 16.93mm by 16mm by 1.57mm, D=5.5mm, ϵ_r=2.55: measured locus (~~~), circle of best fit to the measured locus (———), and the circle of best fit referred to the detuned short position (– – –).

transmission line analogy.

2.2.1 Modal-expansion cavity model

Richards et.al. [29] suggested that the transformation in the impedance locus is due to the energy stored in higher order mode resonances within the cavity. The antenna's input impedance is in affect a Foster [31] expansion and is represented by the network shown in figure 1.8(a). Notice that the series inductance, L_s, represents the net energy stored in all of the higher order Foster sections, and contributes to the calculated impedance locus of the Foster sections being displaced by $+jX_s$ to the inductive side of the Smith chart's real axis. Carver [34] expanded the fields within the cavity into a series of modes for a detailed investigation of the effects of both the coaxial and microstrip line type feed point structures. The narrow-band approximation to the resulting expression

for the input impedance describes the input impedance of the resonant network shown in figure 1.8(b), where the parallel RLC circuit represents resonance at the dominant TM mode frequency. The R represents the resistive losses and the radiation associated with the dominant mode, and L_s is the net series inductance of the higher order modes. This approach has been used to show the dependence of the series reactance on the probe diameter and feed point position, shown in figures 2.2 and 2.3 respectively [34].

The results graphed in figure 2.2 show that the series reactance is a decreasing function of the diameter of the probe. It also shows that the series reactance increases by 6Ω when W/λ_o increases from 0.304 to 0.503, which is equivalent to an increase in the aspect ratio (W/L) from 0.96 to 1.60. From figure 2.3 it is concluded that the series reactance is almost independent of the position of the feed point, except for $D/L \leq 0.1$. Figure 2.3 also presents the results of an experimental investigation carried out by Carver [34] which shows that the series reactance is independent of the position of the feed point for a $0.02W$ $(0.01\lambda_o)$ diameter probe. It is disappointing that the experimental technique was not described because these measurements disagree with the conclusion obtained when measured input impedances of Carver [30] are used to derive values of the series reactance. That is, it will be later shown in figure 2.21 that the position of the feed point does have an effect on the series reactance. However, the measurements shown in figure 2.3 can be used to verify the conclusion of Richards et.al. [29] that the probe diameter to be used with the modal-expansion model should be an effective diameter equal to five times the physical diameter of the probe. Carver [34] goes on to conclude that the computational time required by this method is not justified because the results are not accurate and in fact, require the probe diameter term to be altered in order to ensure good agreement with measured series inductances.

2.2.2 Transmission line models

Carver [34] proposed the use of the classical transmission line equation to calculate the inductance of the probe, where the equivalent inductance of the probe was

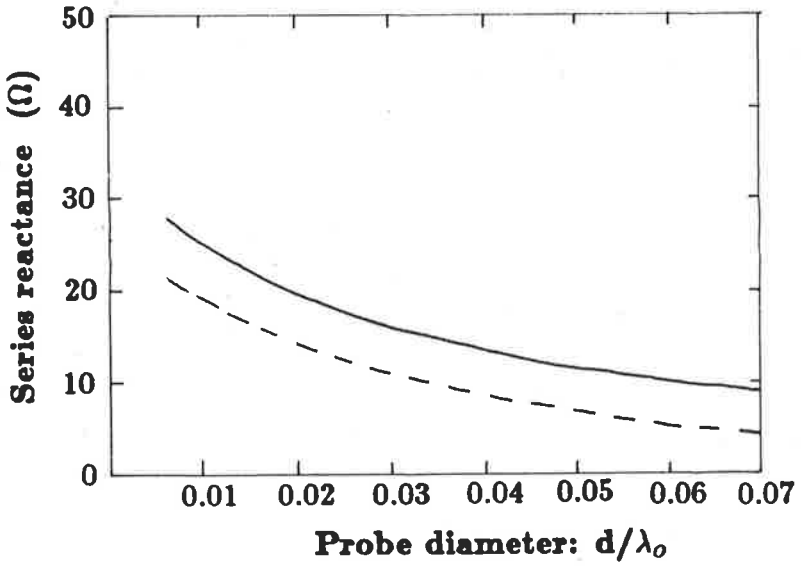

Figure 2.2: Series reactance calculated using the modal-expansion method versus probe diameter (d) for a rectangular element: $h = 0.0116\lambda_o, D = 0.05L, \epsilon_r = 2.5$, for $W = 0.503\lambda_o$(———) and $0.304\lambda_o$(— — —).

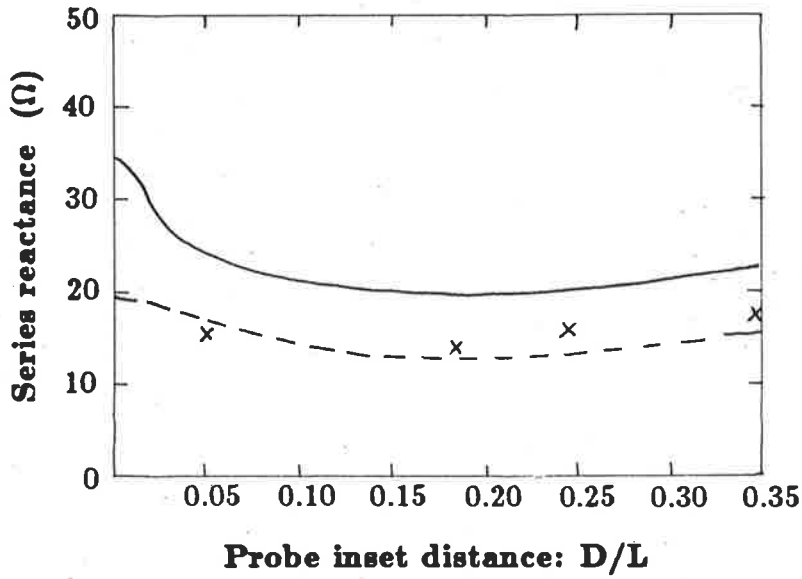

Figure 2.3: Series reactance calculated using the modal-expansion method versus probe inset distance (D) for a rectangular element: $h = 0.0116\lambda_o, \epsilon_r = 2.5, W = 0.503\lambda_o$, for $d = 0.02W$(———) and $0.1W$(— — —).The results of an experimental study are also shown where $d = 0.02W$(×).

obtained using a simple formulation that ignores the probe diameter and views the reactance as that of a coaxial transmission line of length h which is shorted by the top patch. There was no detailed explanation given by Carver, however his result can be obtained if a number of assumptions are made and his line of reasoning postulated.

The variation of input impedance with frequency shown in figure 2.1 gives rise to the notion that a microstrip antenna can be considered as a leaky resonant cavity in series with an inductance L_s. Figure 2.4 shows the development of this model schematically. Firstly consider the cross-section diagram of the antenna and feed shown in figure 2.4(a). Notice that the coaxial line feeding the antenna supports a transverse electromagnetic wave which extends into the region around the probe. Reference planes (1) and (2) respectively represent the antenna terminals, defined at the ground plane, and the point at which the feed probe contacts the metallic patch. The problem is then to model the self-inductance of the thin wire between the two planes (1) and (2). Figure 2.4(b) gives the network equivalent, where the effect of the probe is taken into account by the inductance L_s. Characteristic impedances Z_o and Z_{opp} are respectively that of the transmission line feeding the antenna and the equivalent wide parallel-plate transmission line that terminates the probe. Figure 2.4(c) shows the result of the parallel combination of the two low impedance microstrip transmission lines Z_r, and figure 2.4(d) the network after the parallel combination is approximated to zero. Finally in figure 2.4(e) the lumped inductance component is replaced by an equivalent coaxial transmission line terminated in a short circuit. Z_{ot} is the characteristic impedance of the coaxial transmission line between reference planes (1) and (2). Carver's [34] expression for the series reactance is that for the sending end impedance of a short circuited coaxial transmission line of length h, and is obtained using the transmission line equation [8],

$$Z_s = Z_{ot}\frac{Z_r + Z_{ot}\tanh(\gamma h)}{Z_{ot} + Z_r\tanh(\gamma h)} \tag{2.1}$$

This is used to derive an expression for the impedance at reference plane (1) in figure 2.4(e). That is, equation (2.1) is used to transform the approximate short circuit at

plane (2),

$$Z_r \approx 0 \tag{2.2}$$

through a distance h to the antenna terminals at plane (1). Assuming that the attenuation, α, is negligible, then

$$\gamma = j\beta_s \quad = \frac{2\pi}{\lambda_s} \quad = \frac{2\pi\sqrt{\epsilon_r}}{\lambda_o} \tag{2.3}$$

When equations (2.2) and (2.3) are substituted into (2.1), the resulting expression for the series reactance ($Z_s = jX_s$) is:

$$X_s = Z_{ol} \tan \frac{2\pi h}{\lambda_s} \tag{2.4}$$

In determining the characteristic impedance of the coaxial line Carver has chosen the special case of a line of dimensions such that its characteristic impedance is that of a dielectric filled free space. Thus

$$Z_{ol} = \frac{\eta_o}{\sqrt{\epsilon_r}} \tag{2.5}$$

However Carver [30,34] has been inconsistent in that the evacuated free space wavelength is used, rather than the wavelength in the substrate as shown in equation (2.4). Newman et.al. [19] uses the wavelength in the substrate.

Figure 2.5 shows the series reactance versus the substrate thickness for both of the above cases, together with the results obtained by the modal-expansion cavity model and a measured result [34]. At $h/\lambda_s = 0.018$, the error between the measured reactance and the reactance calculated using equation (2.5) and the free space wavelength is only 1.0Ω, or 6%. However it will be shown later that the results of experimental work carried out as part of this investigation at 5GHz indicate that the reactances calculated by the transmission line model, using either wavelength, become increasingly inaccurate as the substrate thickness increases.

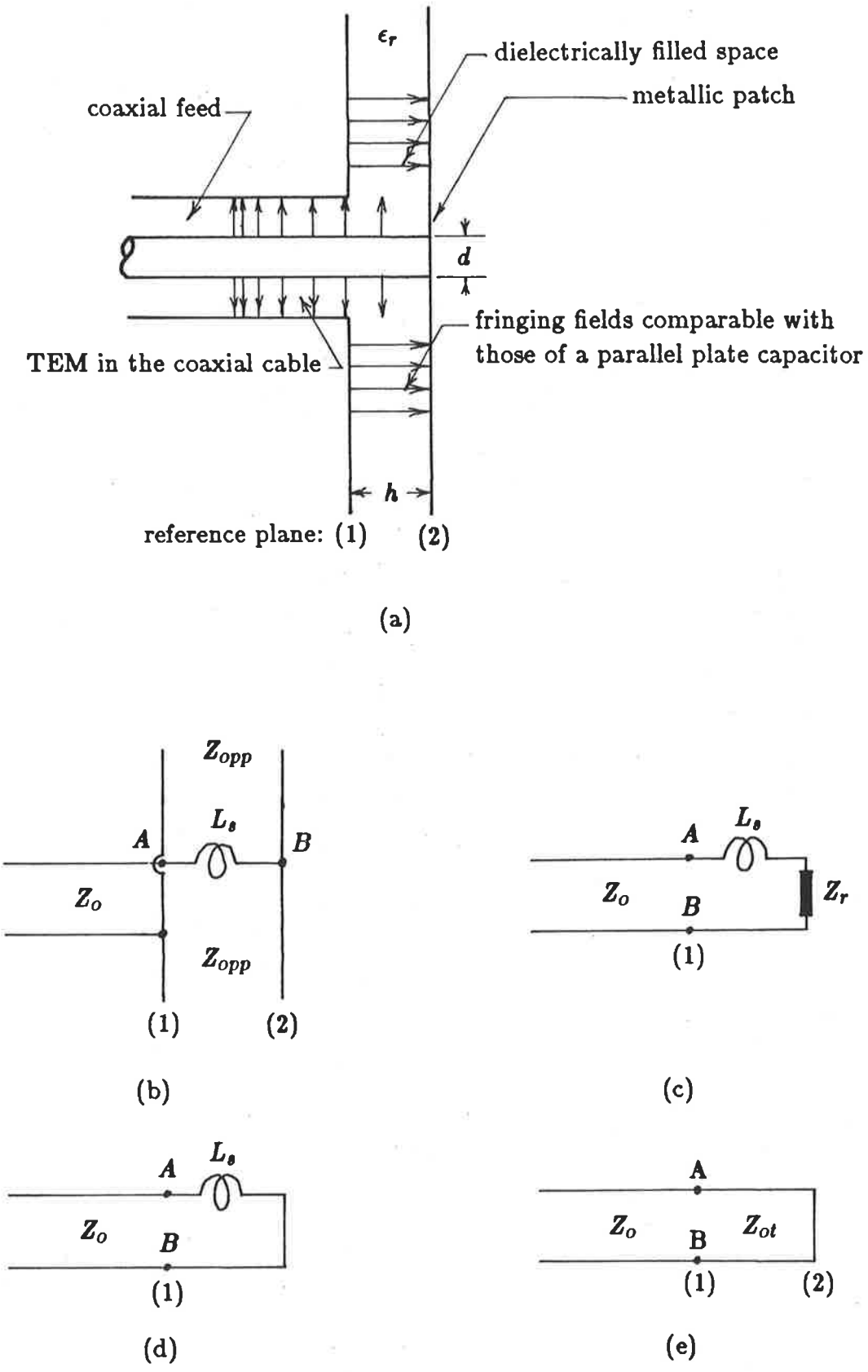

Figure 2.4: Schematic representation of the development of Carver's transmission line feed point model, (a) sketch of the electric field in the proximity of the probe and, (b),(c) and (d) lumped parameters models and (e), its transmission line equivalent.

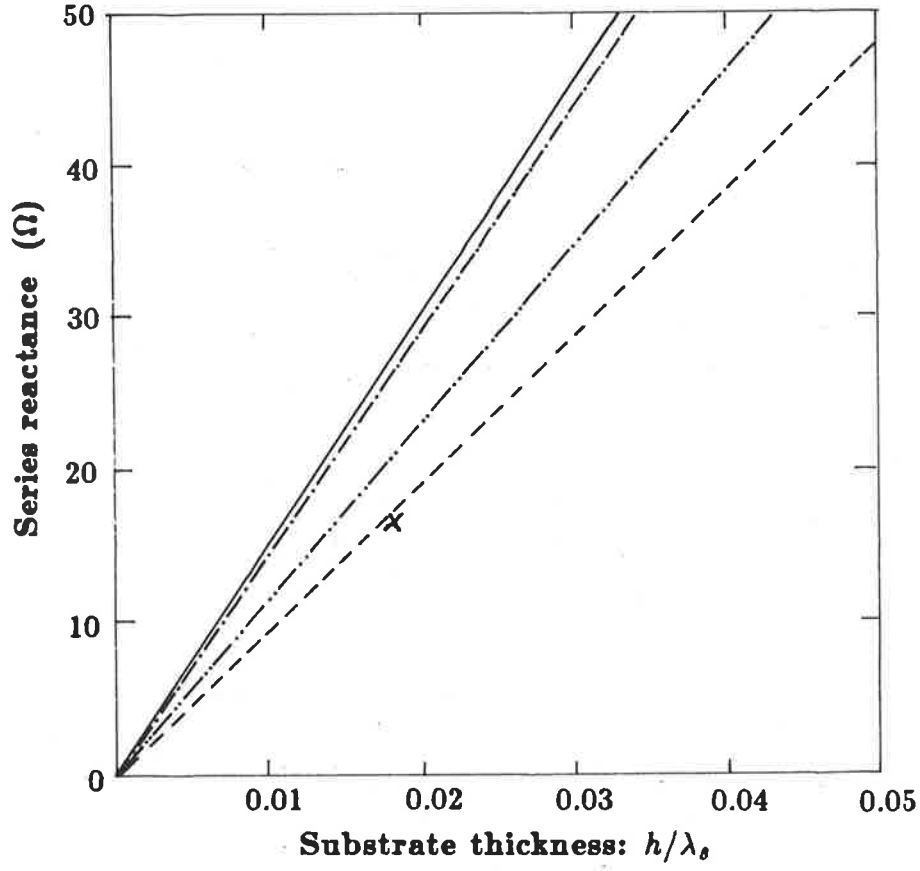

Figure 2.5: Series reactance calculated by the transmission line model using λ_o (– – –) and λ_s (———); and the modal-expansion model for $d = 0.016\lambda_s$ (–·–·–) and $d = 0.08\lambda_s$ (–··–··–). A measured result (×) is also shown.($\epsilon_r = 2.5$)

Griffin et.al. [43] proposed another transmission line model for the series reactance of the probe. The model was initially applied to probe fed disc antennas of radius a, fed through a probe of radius $d/2$. The radius of the outer conductor of the equivalent coaxial transmission line was assigned to the disc radius and the radius of the probe used for the inner conductor. The reactance is calculated by transforming an equivalent short circuit load at the patch, through the distance h, to the antenna terminals. The characteristic impedance of the of the coaxial line is

$$Z_{ol} = \frac{60}{\sqrt{\epsilon_r}} \ln \frac{2a}{d} \tag{2.6}$$

and the series reactance is then

$$X_s = Z_{ol} \tan \frac{2\pi h}{\lambda_s} \quad \text{ohm} \tag{2.7}$$

This approach has been applied to a rectangular patch, replacing the disc radius in (2.6) by the distance from the centre to the corner of the rectangle that forms the patch. The result of a test of the model is shown in figure 2.6, together with the transmission line model of Carver, using the free space wavelength, and the results of other models yet to be discussed.

2.2.3 Model based on the field solution of a coaxial feed probe located in a radial waveguide

Sengupta [16,44,45] proposed a model where the series reactance is a function of the probe diameter

$$X_s = \frac{Z_{om}\beta_s W \alpha}{2\pi} \ln\left(\frac{4}{\gamma\beta_s d}\right) \quad \text{ohm} \tag{2.8}$$

where α is a factor calculated by equation (1.14) and Euler's constant, $\gamma = 1.781$. This expression was obtained from considerations similar to those for the excitation of a parallel-plate guide supporting a dominant E-type radial mode. Figure 2.6 shows a test of this model.

2.2.4 Model that uses a parallel-plate transmission line to represent the transverse mode

A more detailed model that includes the aspect ratio of the patch has been proposed by Lier [46], where the series reactance is the series combination of two reactances X_f^t and X_q. Figure 2.7(a) shows a W_e wide rectangular patch resonant over the length L_e and fed at a general point (x_o, y_o). Lier uses X_f^t to represent the contribution towards the energy stored in the region of the feed point from a travelling wave propagating in the y-direction. Figure 2.7(b) is a circuit representation of the resonant antenna where Z_k^t is the characteristic impedance of the parallel-plate transmission line in the y-direction. The open circuit terminations at $y = 0$ and $y = W_e$ are transformed along the parallel-plate transmission line to the feed point where they are combined in

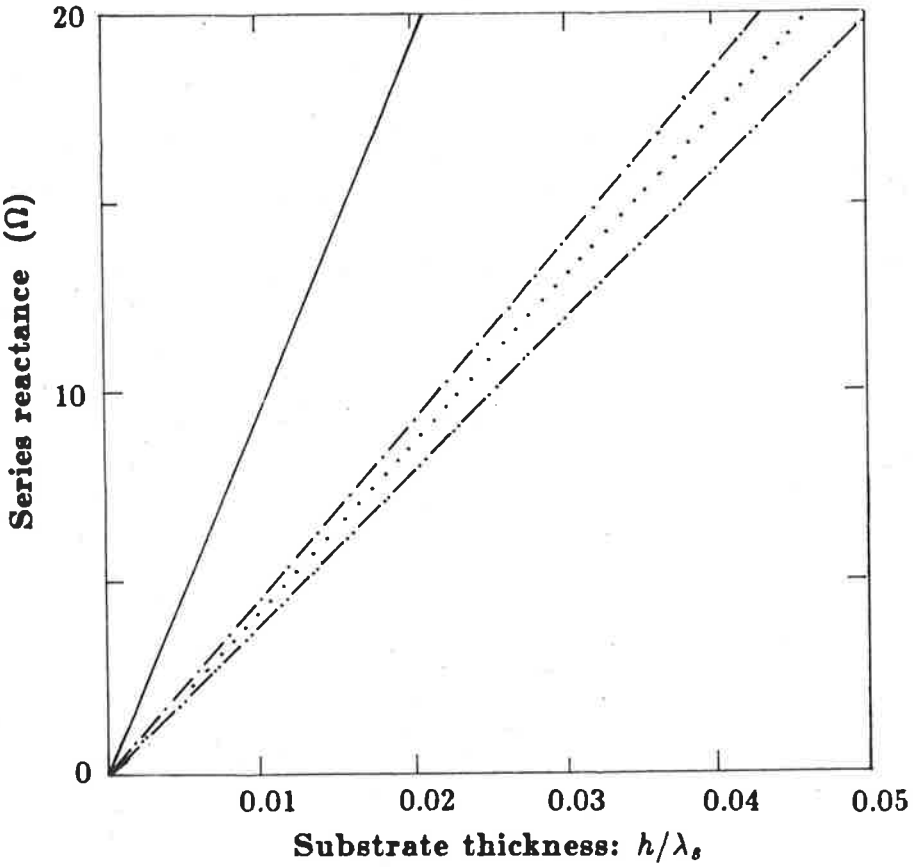

Figure 2.6: Calculated series reactance for the case of an APC-7 probe, where $d/\lambda_s = 0.08, h/\lambda_s = 0.04, \epsilon_r = 2.55$.*: calculated by Carver's transmission line model using* λ_o *(———), Griffin (–·–·–), Lier (·····), Sengupta (–··–··–).*

parallel to give

$$X_f^t = \frac{-Z_k^t}{\tan(\pi W_e'/L_e) + \tan(\pi W_e''/L_e)} \quad \text{ohm} \tag{2.9}$$

where the effective electrical lengths and widths are defined in figure 2.7(a).

The reactance X_q is representative of the energy stored in higher-order modes, and is obtained by a calculation of the input reactance of a square cavity excited at the resonant frequency through a coaxial probe located in the centre of the patch. The result is:

$$X_q = \mu_o h f_o \ln\left(\frac{2c}{\pi\gamma\sqrt{\epsilon_r} d f_o}\right) \quad \text{ohm} \tag{2.10}$$

where f_o is the frequency of the resonant mode and γ is Euler's constant. The total series reactance is then

$$X_s = X_q + X_f^t \tag{2.11}$$

This series reactance has been calculated for the previously considered antenna and plotted on figure 2.6. It can be seen that the reactances calculated using this model lie between those of Griffin and Sengupta. Lier [46] also presented the results of an experimental investigation which will be discussed in section 2.3.3.

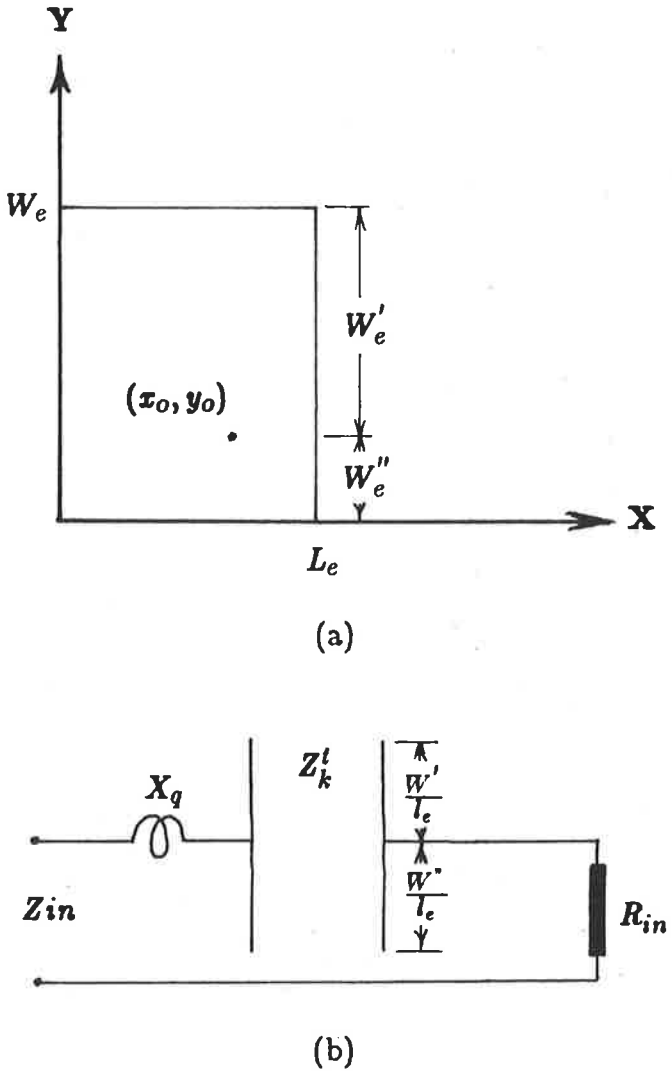

Figure 2.7: (a) The geometry for a rectangular element fed at a general point, and (b) the circuit representation of the antenna, where the transmission line is related to the transverse mode.

The apparent similarity between equations (2.10) and (2.8) can be better appreciated if both equations are simplified. If equation (1.13) is substituted into (2.8) the

resulting equation of Sengupta is

$$X_s = \frac{\eta_o h}{\lambda_o} \ln\left(\frac{2\lambda_o}{\gamma\pi\sqrt{\epsilon_r}d}\right) \tag{2.12}$$

Lier's equation can be simplified using

$$c = \frac{1}{\sqrt{\mu_o \epsilon_o}} \tag{2.13}$$

$$\eta_o = \sqrt{\frac{\mu_o}{\epsilon_o}} \tag{2.14}$$

to give

$$X_s = \frac{\eta_o h}{\lambda_o} \ln\left(\frac{2\lambda_o}{\gamma\pi\sqrt{\epsilon_r}d}\right) \tag{2.15}$$

Thus equations (2.12) and (2.15) are the same.

2.2.5 Conclusions

All of the models presented have been useful in studying the dependence of the series reactance upon the antenna geometry. However, the difference between the calculated and measured reactances will be shown, in the next section, to increase rapidly as the equivalent electrical thickness of the substrate increases. This problem will be clearly illustrated when the results of these models are compared with measurements made around 5GHz.

2.3 Experimental investigations

The series reactance has been measured by three methods, where in each case the probe is terminated in a different load with the aim of isolating the effect of the connection region from the measured input impedance versus frequency characteristics of the overall structure. The first arrangement terminates the probe in a large cavity and the second in a short circuited low characteristic impedance transmission line. In the third arrangement the probe is used to feed a rectangular patch antenna. The measured series reactances are used to show that the results of the analytical and empirical models

proposed by other authors become increasingly inaccurate as the frequency increases, and in fact become seriously incorrect as the frequency approaches 5GHz.

2.3.1 The large cavity method

In order to isolate the series reactance from the input impedance presented to the probe by the patch structure, the metallic patch associated with the antenna was removed and replaced by a large sheet of copper. In essence, the coaxial probe was then feeding a large sheet of double sided copper clad board, refer to figure 2.8(a). The network in figure 2.8(b) shows the coaxial probe represented by a series reactance, X_s, and the sheet as a large open cavity with input impedance Z_c, called the cavity impedance. Therefore a value for the series reactance can be determined from the measured input impedance of the overall structure, Z_{in}, as long as the value of Z_c is known or at least can be approximated. Moreover it is only the reactive component of the cavity impedance that needs to be known. The length and width of the cavity were chosen large while the substrate thickness was minimised in order that Z_c might approach a short circuit. The value of the imaginary component of the cavity impedance will be later shown to approximate zero over the frequency range of interest. Hence the measured input reactance of the structure can be equated to the series reactance of the probe.

Measurements of the input impedance were performed on four structures over a twenty percent frequency bandwidth, using the following combinations of connector type and substrate thickness: APC-7/1.57mm, APC-7/0.735mm, SMA/1.57mm and SMA/0.735mm. The relevant connector dimensions are listed in Appendix A, and the dimensions of the cavity were $10.8\lambda_s$ by $24.3\lambda_s$ by $0.04\lambda_s$ at 5GHz.

A typical result for the measured input impedance versus frequency is shown in figure 2.9 for the case of an APC-7 connector feeding a 1.57mm thick substrate. The figure shows a cluster of reflection coefficient points with significant real and imaginary components. This cluster is attributed to the reflection coefficient of the series com-

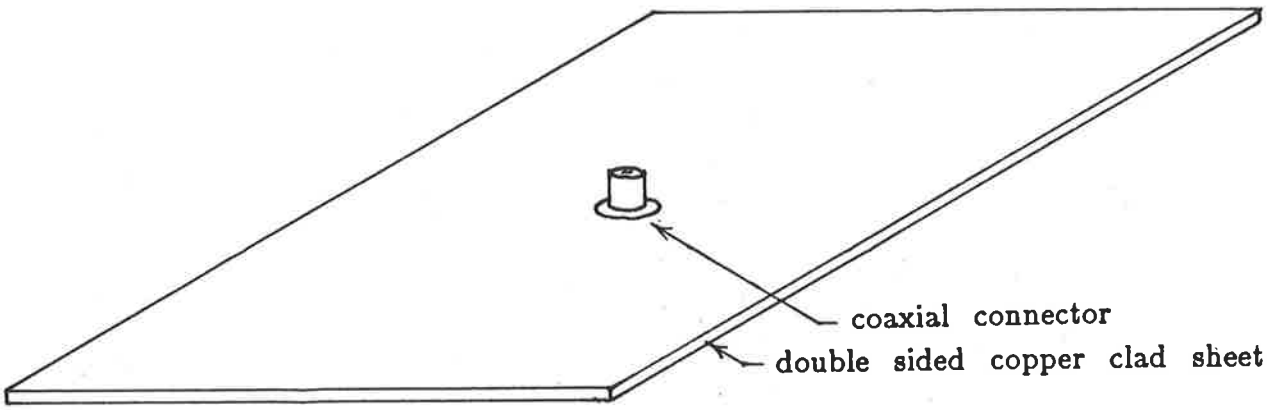

(a)

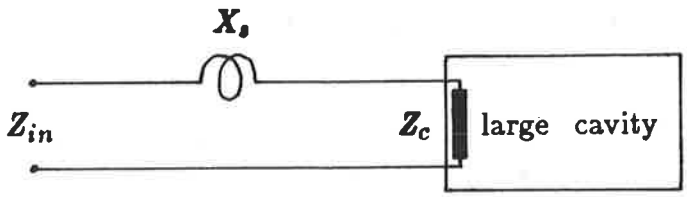

(b)

Figure 2.8: (a)The apparatus for the large cavity experiment and (b), its network model.

bination of the series reactance, X_s, and the cavity's input impedance, Z_c, where the contribution of the latter will be shown to be less significant.

A better understanding of the complex nature of this measured result is obtained if the magnitude and phase of the reflection coefficient versus frequency are presented separately. See figures 2.10 and 2.11. Both graphs show an almost random variation about a mean value, and in both cases the mean value is decreasing with frequency. The mean values of the amplitude and phase of the reflection coefficient at 5GHz are -5.2dB and 142^o, which is equivalent to an impedance of $16+j16.5\ \Omega$. Before a value for the series reactance at 5GHz can be derived from this measured result further explanation regarding the effect of the cavity impedance is required. Firstly the cavity impedance,

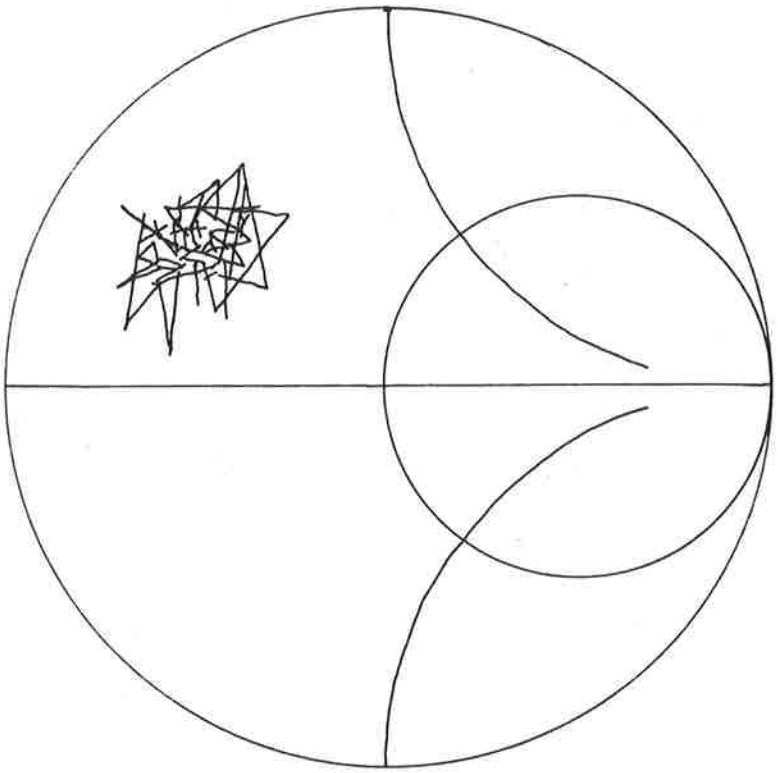

Figure 2.9: Smith chart plot of the measured reflection coefficient for a 1.57mm thick large cavity fed by an APC-7 probe.

Z_c, is calculated using a dual transmission line model and secondly a multi-mode cavity model is used to further explain the experimental observations.

The input impedance of the cavity excluding the series reactance is calculated using a model comprising two orthogonal parallel-plate transmission lines, refer to figure 2.12. The propagation constant, γ, and the characteristic impedance, Z_{om}, for each of the lines are calculated [47] using,

$$\gamma = \sqrt{(R + j\omega L)(G + j\omega C)} \tag{2.16}$$

$$Z_o = \sqrt{\frac{R + j\omega L}{G + j\omega C}} \tag{2.17}$$

where the distributed line constants are

$$R = \frac{2\ \mathrm{Real}(Z_s)}{W} \tag{2.18}$$

$$L = \frac{\mu h}{W} + \frac{2\ \mathrm{Imag}(Z_s)}{W} \tag{2.19}$$

$$G = \frac{W\sigma_d}{h} \tag{2.20}$$

$$C = \frac{\epsilon W}{h} \tag{2.21}$$

and Z_s is the surface impedance of the copper cladding given by

$$Z_s = \sqrt{\frac{j\omega\mu}{\sigma_c}} \tag{2.22}$$

Using the dielectric and copper conductivities

$$\sigma_d = 1.0\text{E} - 12 \quad \text{U/m}$$

$$\sigma_c = 5.8\text{E} + 7 \quad \text{U/m}$$

The per unit length line constants for the wide and narrow transmission lines are listed in Table 2.1. Also listed in the table are the input impedances, calculated using Harrington's equations (1.5) and (1.6), for the two radiating apertures at each end of the two transmission lines. The cavity impedance is calculated as a function of the frequency over a 3.5GHz to 6.5GHz bandwidth. Figures 2.13 and 2.14 show the magnitude and phase of the equivalent reflection coefficient normalised to 50Ω.

The magnitude of the calculated reflection coefficient, figure 2.13, displays a number of resonances across the band, where the typical quality factor is approximately equal to 600. Figure 2.14 shows that the phase of the calculated reflection coefficient is reflected through 180^o at each resonant frequency. The phase is bounded within plus or minus 3^o, and the average phase over the bandwidth is 180^o. So it can be concluded that the reflection coefficient of the cavity is

$$| k_c | \leq 0.8dB$$

and

$$\text{phase}(k_c) = 180^o \pm 3^o$$

or in terms of the cavity impedance

$$\text{Real}(Z_c) \begin{cases} \leq 2.3\Omega & \text{at any of the resonances} \\ \approx 0 & \text{otherwise} \end{cases}$$

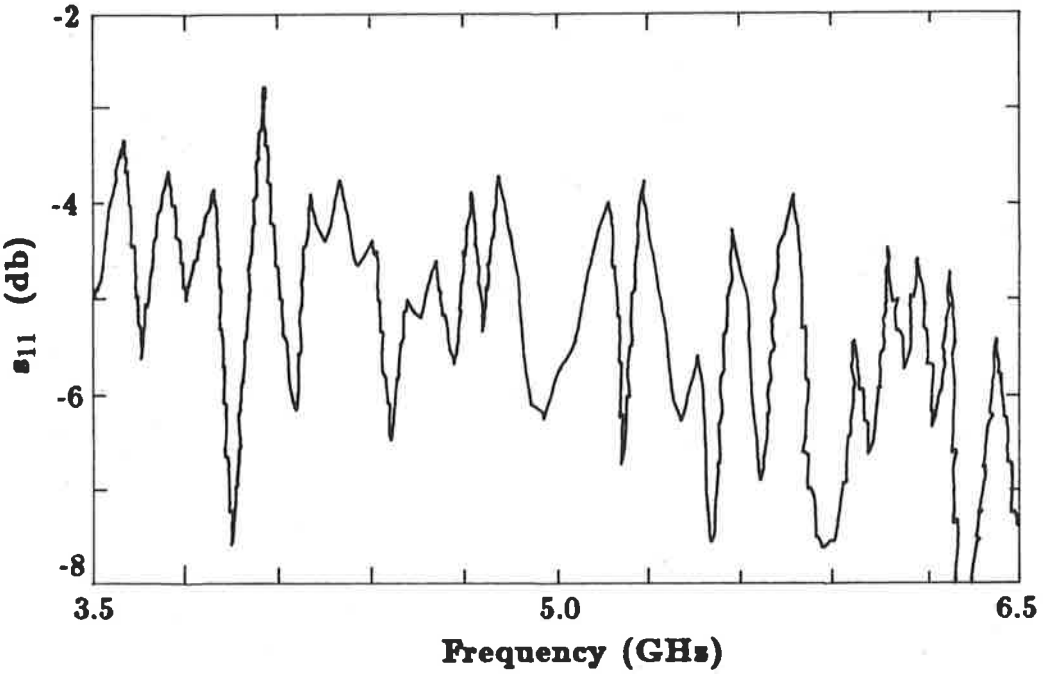

Figure 2.10: Magnitude of the measured reflection coefficient versus frequency for a 1.57mm thick large cavity fed by an APC-7 probe.

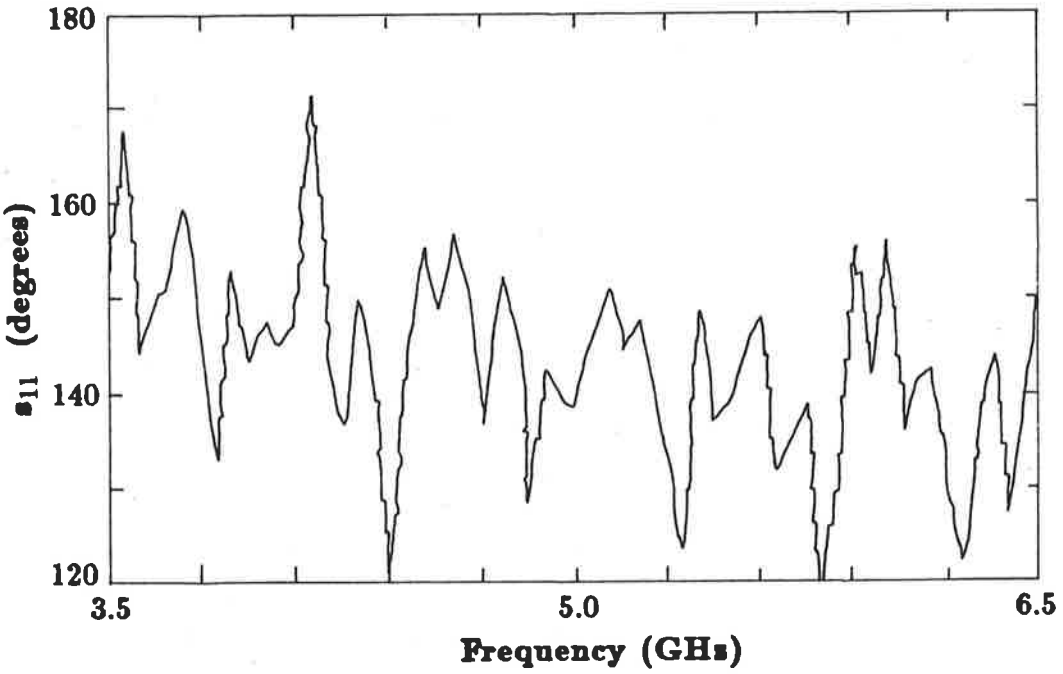

Figure 2.11: Phase of the measured reflection coefficient versus frequency for a 1.57mm thick large cavity fed by an APC-7 probe.

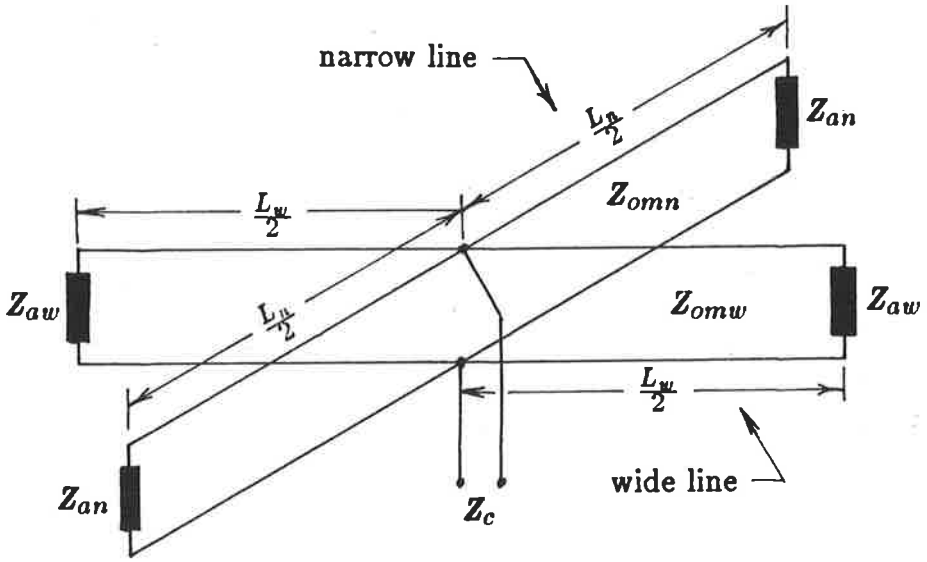

Figure 2.12: Transmission line model for the large cavity apparatus.

Large cavity model parameters at 5GHz		
Parameter	Wide line	Narrow line
h(mm)	1.57	1.57
L(mm)	913	406
W(mm)	406	913
α n/m	0.05	0.05
β rad/m	167.3	167.3
Re(Z_o) Ω	0.91	0.41
Im(Z_o) Ω	.0003	.0001
R Ω/m	0.09	0.04
ωL Ω/m	152.8	67.9
G $\mho$/m	0.26E-9	0.58E-9
ωC $\mho$/m	181.8	416.7
R_a Ω	5.5	2.4
X_a Ω	-8.2	-3.6

Table 2.1: Parameters for the large cavity transmission line model.

and

$$-1.3\Omega \leq \text{Imag}(Z_c) \leq +1.3\Omega$$

The average cavity impedance over the frequency bandwidth closely approximates a short circuit. Therefore, the input impedance of the overall structure can be equated to the series reactance of the probe. However, the measured input impedance has a significant real component, equal to 16Ω at 5GHz, which is hitherto unaccounted for in the dual transmission line model.

The complex nature of the measured input impedance can also be explained when it is appreciated that the probe is coupling into many closely spaced modes, all of high index, which are specified according to the cavity's length and width dimensions. At any single frequency, the degree of coupling into each mode is dependent on the position of the feed point relative to the field distribution of each and every mode, as well as the frequency and quality factor of that mode. Therefore due to the multiplicity of modes, it follows that their degrees of coupling and hence their reflection coefficients are almost random. Furthermore there are a large number of weakly coupled off-resonant modes both above and below the bandwidth of interest. The real part of the cavity impedance that is observed in the measurements, but not included in the results of the dual cavity model, is therefore attributed to the sum of the copper and dielectric losses associated with the multiplicity of off-resonant modes.

Greater insight into the measured input impedance of the overall structure is obtained if the complicated effects of the cavity resonances are removed from the magnitude and phase of the measured reflection coefficient. So the results of figures 2.10 and 2.11 are averaged over the frequency band by rejecting the excessive excursions, ±2dB or ±20 degrees respectively, and then deriving the lines of best fit. The figures show that the magnitude and phase of the average measured reflection coefficient decrease with frequency. These observations can be explained by considering the associated increase in the electrical length of the probe. This increased length will result in more energy

being coupled into the cavity as well as an increase in the effective inductance of the probe, as seen from the terminals of the cavity.

Figure 2.15 shows the resulting Smith chart plot of the reflection coefficient versus frequency that is constructed from the lines of best fit for the respective reflection coefficient magnitude and phase. This arc represents the measured input impedance of the large cavity apparatus without the complex resonance effects of the cavity. Using the same process of averaging, similar arcs were determined for the other connector and substrate thickness combinations. In each case the input reactance was equated to the equivalent series reactance of the feed probe. Table 2.2 lists the results obtained at 5GHz for the four connector and substrate thickness combinations.

This large cavity experiment has been useful in showing the frequency dependence of the series reactance. Figure 2.16 shows this dependence for the connector and substrate thickness combination of APC-7/1.57mm. The figure also shows the results of the shorted transmission line experiment, to be discussed next.

2.3.2 The short circuited transmission line method

A second technique to measure the series reactance directly provides a single frequency check of the experimental results already presented. Figure 2.17(a) shows the transmission line model of a general rectangular patch antenna with X_s included. For the purpose of measuring only X_s, the radiating walls at each end of the transmission line are replaced by short circuit loads, the feed point is moved to the transmission line's centre, and the line length, L, is chosen such that the distance between the plane of the feed point and each short circuit load is equal to half the wavelength in the dielectric. Refer to figure 2.17(b). Therefore, when the two short-circuit loads are transformed down the transmission lines to the feed, they form another short across the series combination of X_s and the feed terminals, refer to figure 2.17(c). Thus the measured reactance equals the series reactance.

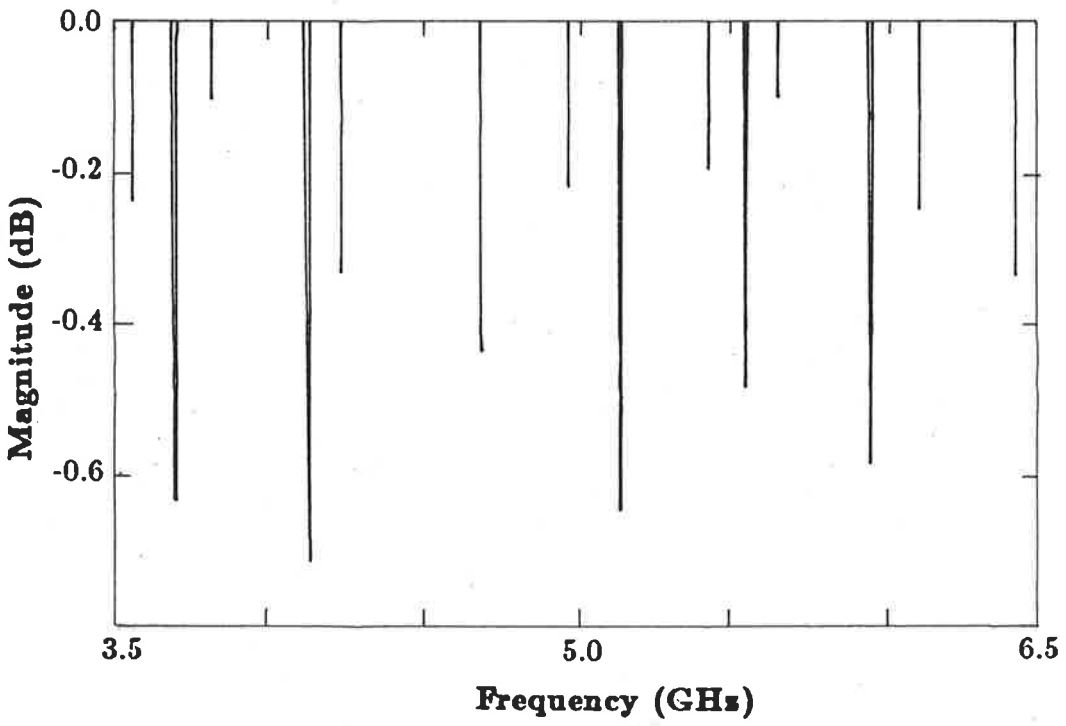

Figure 2.13: Using the dual transmission line model, the magnitude of the calculated reflection coefficient versus frequency for a 1.57mm thick large cavity fed by an APC-7 probe.

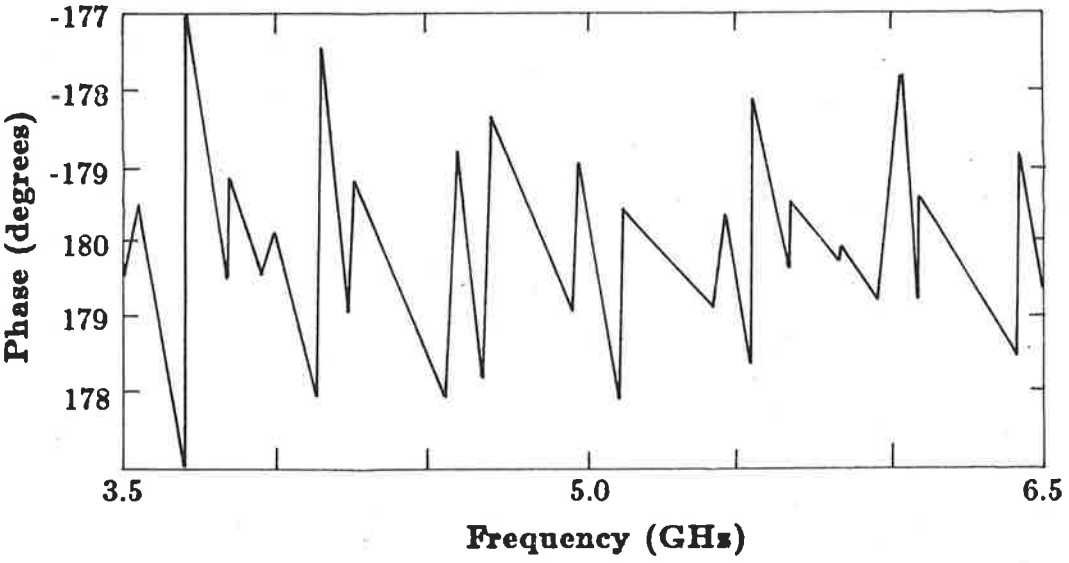

Figure 2.14: Using the dual transmission line model, the phase of the calculated reflection coefficient versus frequency for a 1.57mm thick large cavity fed by an APC-7 probe.

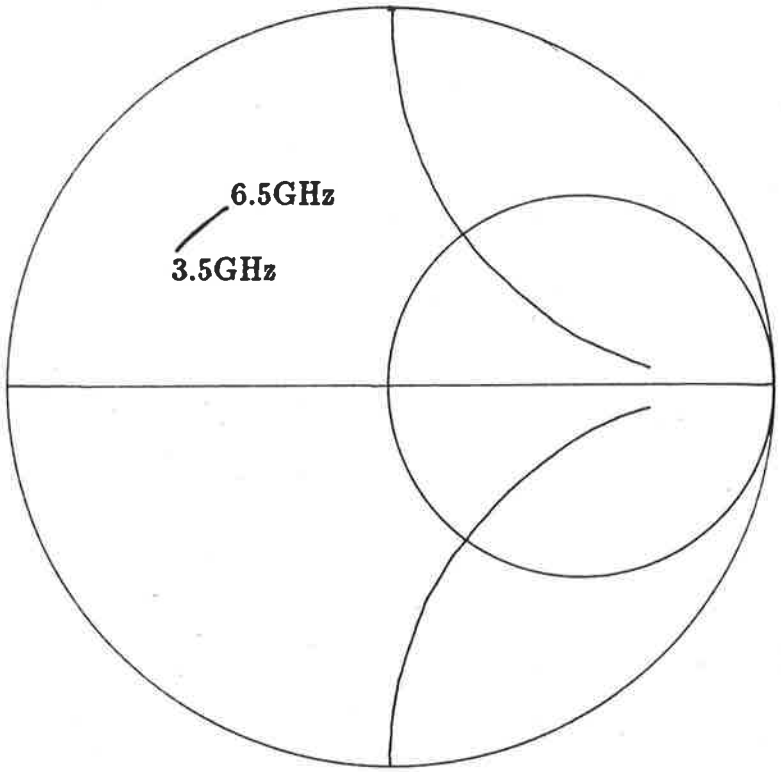

Figure 2.15: Averaged reflection coefficient for a 1.57mm thick large cavity fed by an APC-7 probe.

Series reactance using the large cavity method		
Probe type	Substrate thickness 0.80mm	Substrate thickness 1.57mm
APC-7	6.8 Ω	16.5Ω
SMA	11.7Ω	19.2Ω

Table 2.2: Measured series reactance at 5GHz for a large cavity: 424mm by 955mm by (1.57mm and 0.8mm), where ϵ_r=2.55.

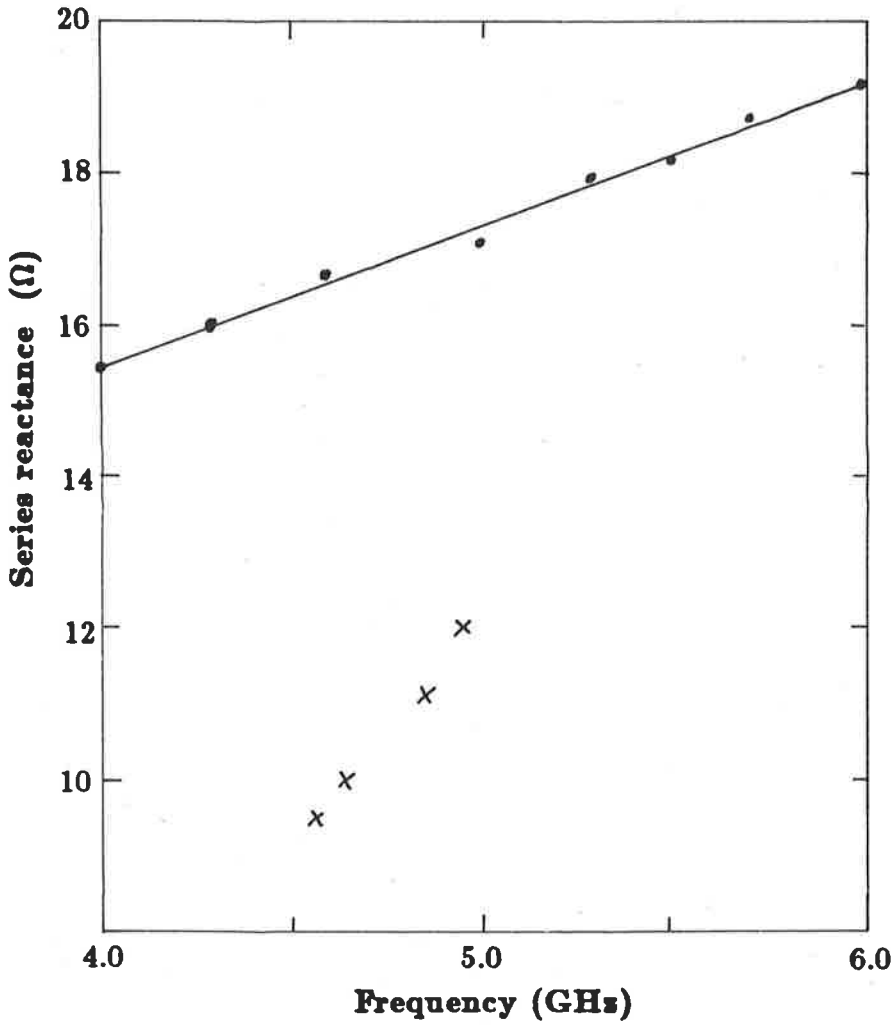

Figure 2.16: Series reactance versus frequency results for the large cavity(———) and shorted transmission line(× × ×) experiments, where an APC-7 connector is feeding a 1.57mm thick substrate.

Four experiments were carried out using an APC-7 probe with W=16mm, h= 1.57mm, and L=39.6mm, 39.0mm, 38.1mm and 37.0mm. Figure 2.17(d) illustrates the final apparatus.

Figure 2.18 shows the measured input impedance versus frequency on a Smith chart for the case where L = 39.6mm. The measured result can be interpreted using the network model of the parallel RLC single mode resonant circuit shown in figure 1.8(b), where the resistance represents the sum of the copper and dielectric losses and the small amount of radiation from the structure. The structure is observed to be resonant, that is $L = \lambda_g$, at the frequency for which the reflection coefficient is a minimum, which corresponds to a TEM_{020} mode resonance within the cavity. So it turns out that the

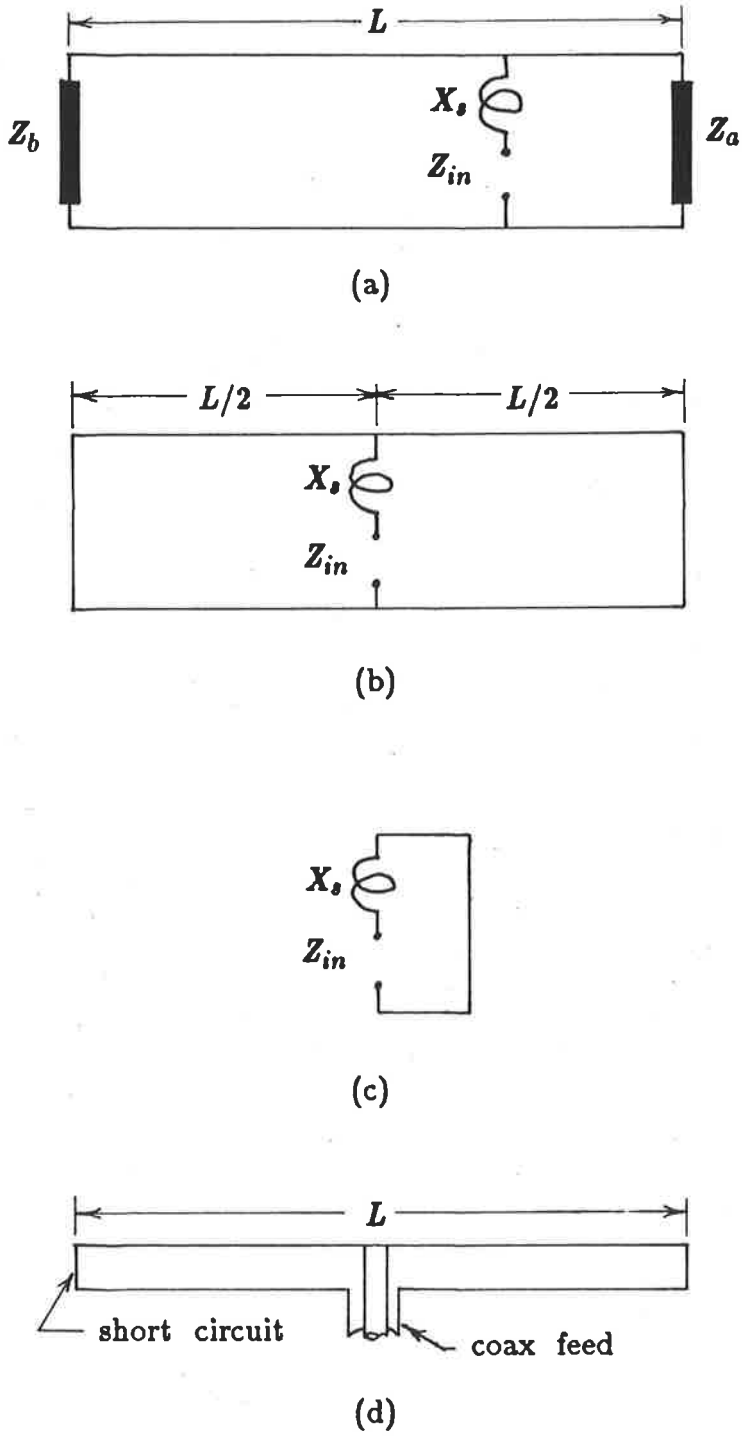

Figure 2.17: Measurement of the series reactance; (a)transmission line model, (b)model of the structure, (c)model after transformations and, (d) a side elevation sketch of the apparatus.

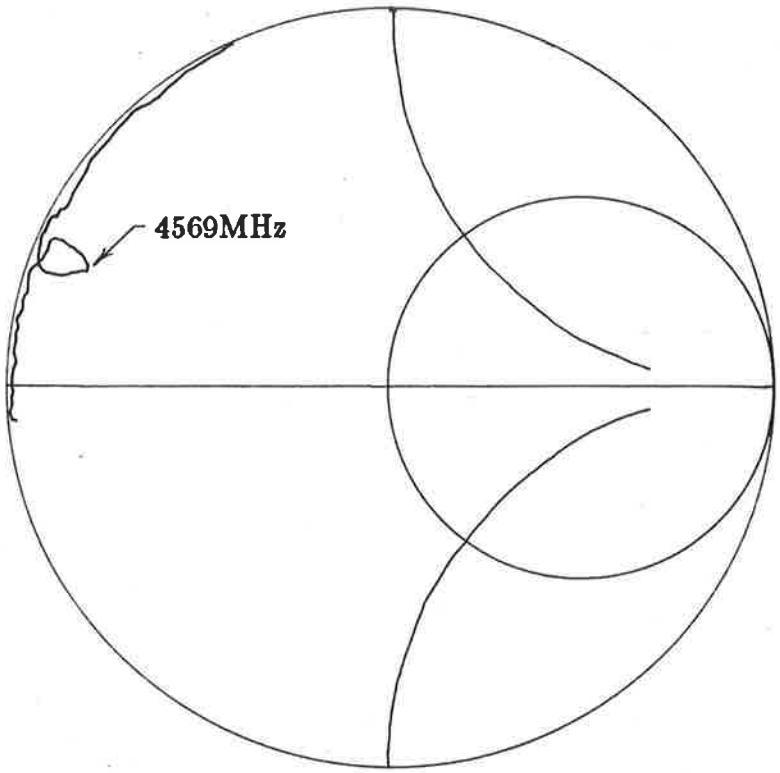

Figure 2.18: Measured reflection coefficient for the shorted transmission line fed by an APC-7 probe, where h=1.57mm, W=16mm, L=39.6mm, $\epsilon_r = 2.55$.

Series reactance using the shorted transmission line		
L(mm)	f_o(MHz)	$X_s(\Omega)$
39.6	4570	9.5
39.0	4640	10.0
38.1	4850	11.3
37.0	4950	12.0

Table 2.3: Series reactance measured using the shorted transmission line method.

resonant frequency is clearly indicated on the Smith chart plot, implying that the length of the apparatus need not be accurately predicted. The result displayed in figure 2.18 shows that resonance is achieved at 4569MHz. Here the input reactance is 9.5Ω which is attributed to the effective series reactance of the probe. Table 2.3 lists the results of the four experiments and figure 2.16 shows these four results as a plot of the series reactance versus frequency. The apparent inconsistency between these two sets of data can partly be explained if the widths of the two apparatuses are taken into account. This point is taken up in detail in Section 2.3.4.

2.3.3 The locus transformation method .

If the network model of the series reactance and leaky cavity resonator shown in figure 1.8(b) is accepted[1], then it follows that the series reactance can be obtained from a Smith chart plot of the measured input impedance versus frequency data by observing the extent of the reactive transformation of the locus of the cavity alone. This is easily done by approximating the measured impedance locus by a circle, which can then be related to the series reactance.

The process of deriving the series reactance from the centre of a circle of best fit to measured data is considered by introducing a hypothetical cavity having the following arbitrarily chosen specifications

$$f_{oc} = 5\text{GHz} \quad Q_o = 25 \quad R_o = 80\Omega \quad X_s = 20\Omega$$

Then using

$$f_o = \frac{1}{2\pi\sqrt{LC}} \tag{2.23}$$

$$Q_o = \frac{R_o}{\omega L} \tag{2.24}$$

[1] For the sake of correctness, it is necessary to point out that the network suggested by Carver[30], and shown in figure 1.8(b), needs to be amended to model the gap between the circle of best fit and the perimeter of the Smith chart. The gap resistance is not elaborated on here because it plays no part in the determination of the series reactance. It will be discussed in detail in Chapter IV.

the lumped circuit parameters for the parallel RLC plus series reactance equivalent circuit of figure 1.8(b) are

$$L = 1.018\text{E}-10\ H \quad C = 9.95\text{E}-12\ F \quad L_s = 6.37\text{E}-10\ H$$

The calculated input impedance data are plotted on figure 2.19. The centre of the circle of best fit is then located as equidistant from each data point, and then the circle is drawn. Notice that the calculated data does not form a perfect circular locus because the series reactance is a function of the frequency. More importantly however, notice that the centre of the circle of best fit is not on the X_s contour but on the line O-A. Therefore to determine the X_s parameter for the resonant cavity model of figure 1.8(b) from a measured input impedance locus, simply locate the centre of the circle of best fit to the measured data, and construct the line O-A. The reactance at point A is then equivalent to the series reactance. The process has also been verified for well over-coupled and under-coupled cavities. This technique has been applied to many sets of measured input impedance versus frequency data; both measured by the author and published in the open literature by other authors. The results are detailed in Table 2.4, section 2.4. For the case of an APC-7 probe feeding a 1.57mm thick substrate, figure 2.20 compares this method with those previously discussed and graphed in figure 2.6.

The technique has also been used to investigate the dependence of the series reactance on the position of the feed point along the E-plane of the patch; that is as a function of the distance D, defined in figure 1.5. Figure 2.21 shows that the effect of shifting the feed point is greater for the probe of larger electrical dimensions. The curve for $d/\lambda_s = 0.015$ is derived from the measured input impedance data published by Carver [30], and disagrees with his earlier direct measurements [34] of the series reactance as a function of the feed point position, shown in figure 2.3. A set of impedance loci for the case of $d/\lambda_s = 0.008$ have also been published [23], and the series reactances derived using the locus transformation method exhibit no dependence on the feed point position. Therefore it is concluded that the series reactance is a weak function of feed

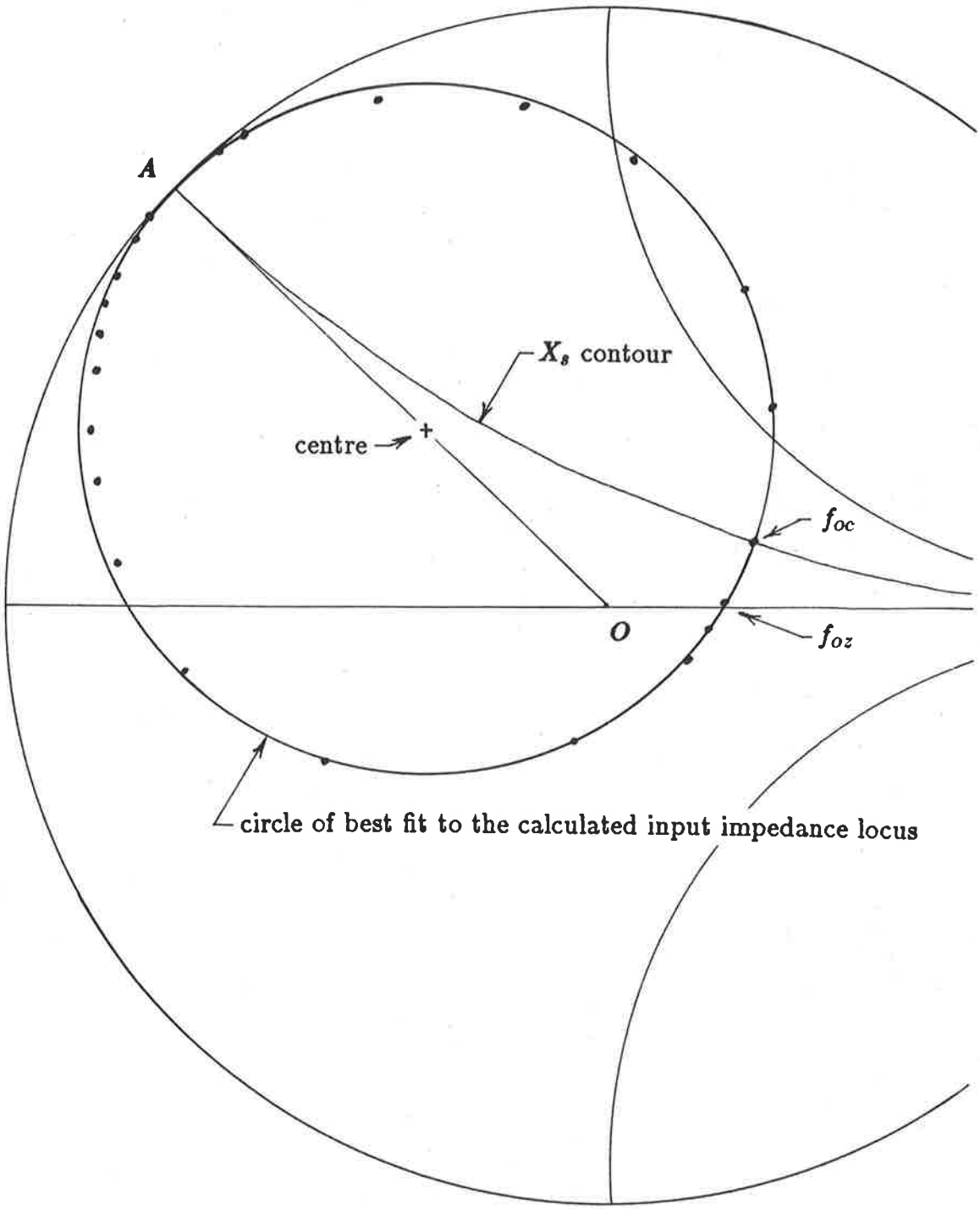

Figure 2.19: Determination of the equivalent series reactance from a set of calculated input impedance data for a hypothetical cavity.

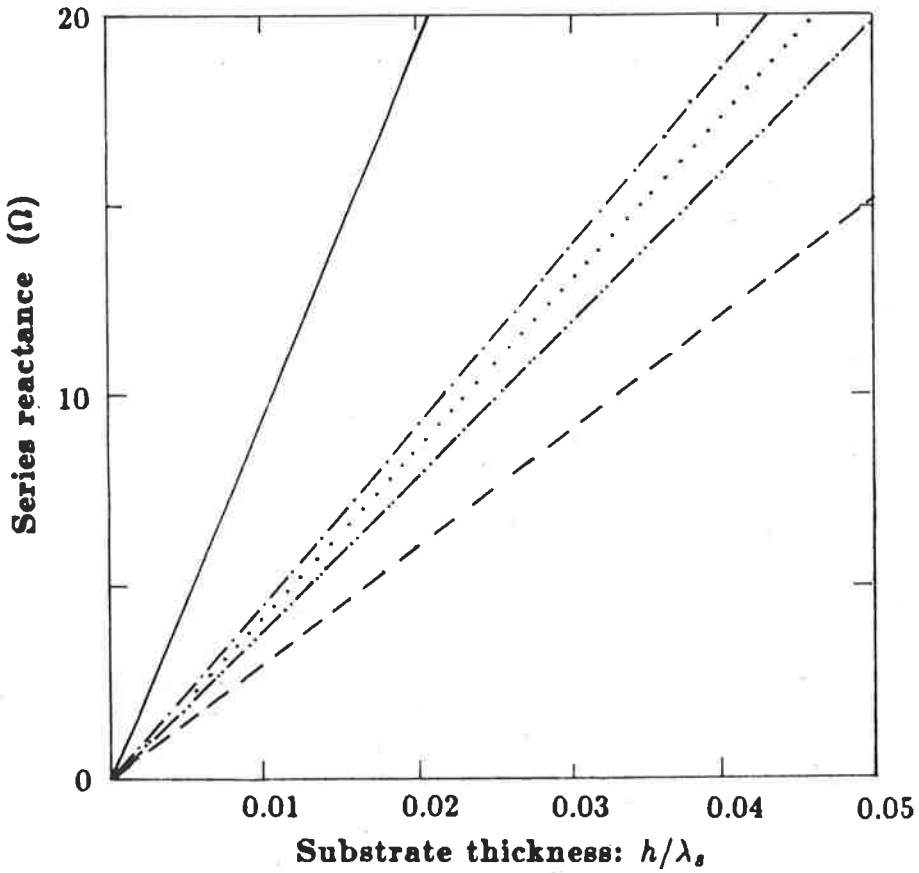

Figure 2.20: Calculated series reactance for the case of an APC-7 probe, where $d/\lambda_s = 0.08, h/\lambda_s = 0.04, \epsilon_r = 2.55$: calculated by Carver's transmission line model using λ_o (———), Griffin (—·—·—), Lier (·····), Sengupta (—··—··—) and the locus transformation method (– – – –).

point position and only becomes significant when the probe diameter increases beyond $0.008\lambda_s$.

A study of the effect that the aspect ratio has on the series reactance has also been carried out. Here the input impedance of a rectangular patch was measured as the width was varied. Figure 2.22 shows the series reactance versus aspect ratio for an antenna operating at about 5GHz and the results of the direct measurement of series reactance by Lier[46] for an antenna operating at 3.1GHz. Lier's experimental technique involved measuring the input reactance of a centre fed rectangular patch, where the electrical length of the patch was carefully calculated to ensure that it was half wave resonant at 3.1GHz. The absolute values of the series reactances from the

two experiments cannot be directly compared because the electrical dimensions of the probes and substrate heights differ, but the two sets of results are graphed side by side to show that both results exhibit a similar trend and generally support one another.

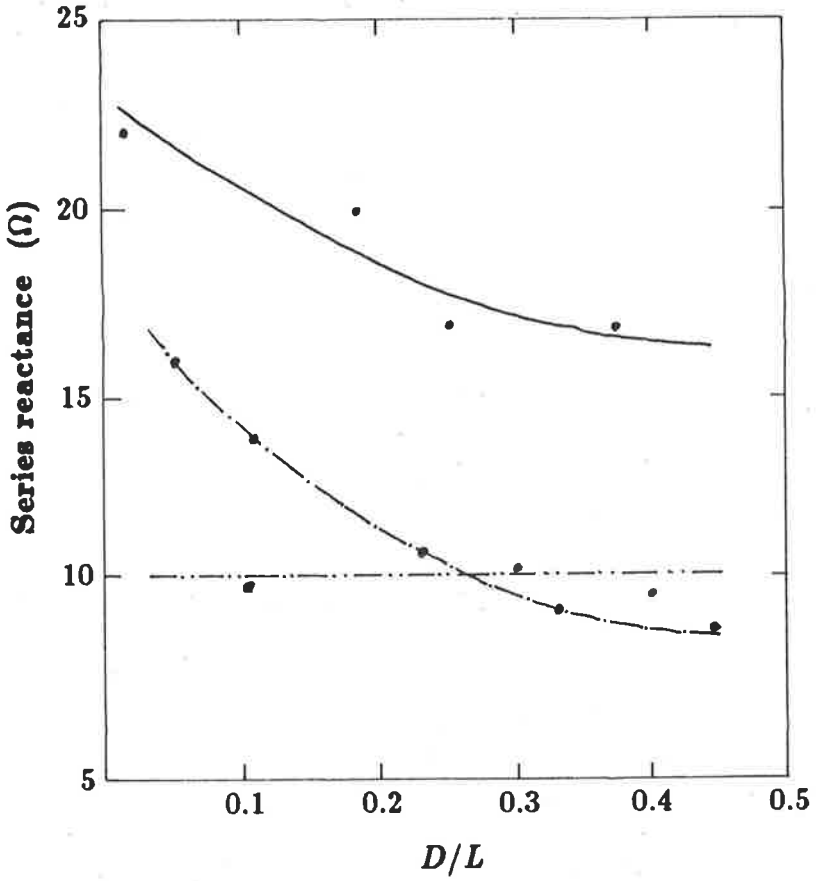

Figure 2.21: Series reactance, using the locus transformation method, as a function of the feed point position for: f_o=1189MHz, h=1.59mm, d/λ_s=0.008, ϵ_r=2.62 (—··—)[23]; f_o=2.2GHz, h=1.59mm, d/λ_s=0.015, ϵ_r=2.62 (———)[30]; f_o=4.9GHz, h=1.59mm, d/λ_s=0.076, ϵ_r=2.55 (—·—).

2.3.4 Comparisons between the results of the large cavity, short circuited transmission line, and locus transformation experiments

The series reactance results of the large cavity experiment are typically larger than those measured using the short circuited transmission line and the locus transfor-

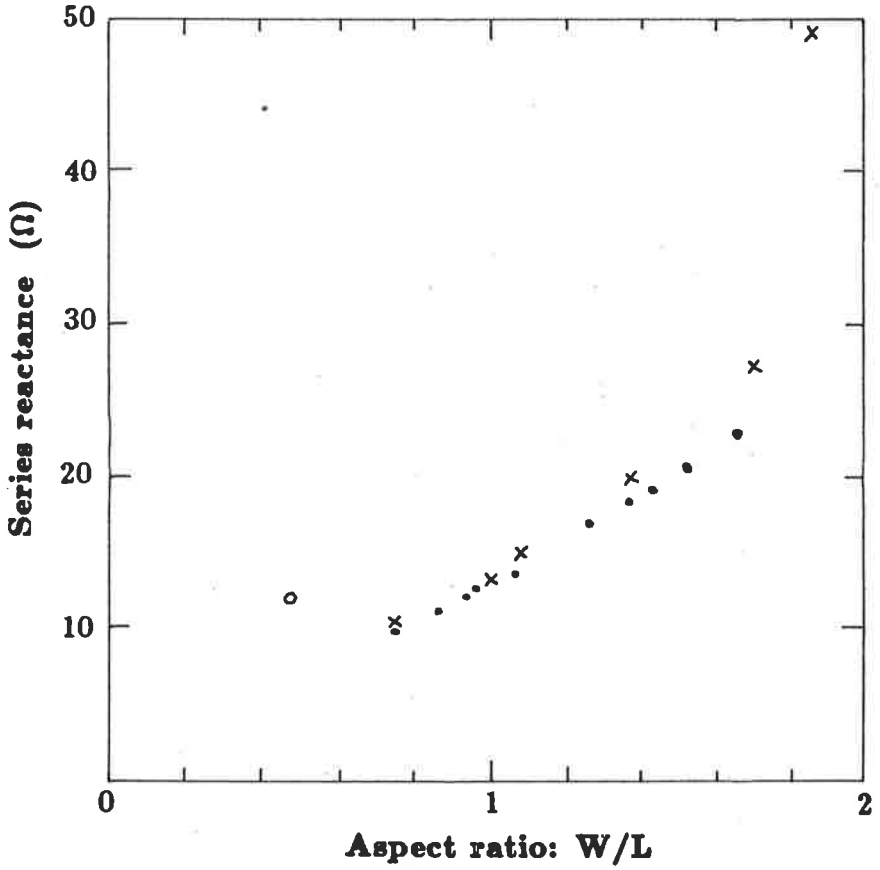

Figure 2.22: Measured series reactance as a function of the aspect ratio for: $f_o \approx 4.9GHz$, $h/\lambda_g=0.042$, $d/\lambda_g=0.076$, $\epsilon_r=2.55$ ($\bullet\ \bullet\ \bullet\ \bullet$); $f_o=3.1GHz$, $h/\lambda_g=0.025$, $d/\lambda_g=0.020$, $\epsilon_r=2.62$ ($\times\ \times\ \times\ \times$)[46]. Also included is a result obtained using the shorted transmission line method: $f_o=4.950GHz$, $h/\lambda_g=0.04$, $d/\lambda_g=0.08$, $\epsilon_r=2.55$ ($\circ$).

mation techniques. For example, for an APC-7 probe feeding a 1.57mm thick substrate at 5GHz, the results of the large cavity experiment are 5Ω and 4Ω greater than those of the short circuited transmission line and locus transformation methods respectively. This may be due to the absence of any patch edges in the large cavity case, thereby giving any energy stored in modes associated with the probe an effectively unlimited volume in which to establish themselves. The extra series reactance might be attributed to the energies stored in these modes that extend out from the probe in the volume over and above that available in the case of the other experiments where the dimensions of the structures are typically of the order of a half wavelength. It is tempting to attribute this extra series reactance to extra evanescent modes that might exist in the increased volume of the large cavity. However these modes are very localised within the proximity

of the probe. Although the physics of the modes associated with the probe is not understood, it is clear that the presence of the edges of the patch have an effect on the fields around the probe. This conclusion is based on two observations. Firstly the aspect ratio of the patch has already been demonstrated to influence the effective series reactance. The second observation will be discussed in detail in Chapter VI, where a liquid crystal film is used to visually display the field distributions around the edges of the patch. For frequencies and probe dimensions similar to those used in the large cavity experiments, the probe was seen to cause an increase in the level of radiation emanating from the end of the patch nearest to it. Thus if the probe has an effect on the fields at the edges, then it is possible that the presence or absence of the edges will effect the energy stored in the proximity of the probe, and hence the effective series reactance.

Even though the absolute values of the series reactances obtained using the large cavity experiments may be doubtful, the method still provides valuable information on the relative increase in the series reactance associated with an increase in the frequency. Refer to figure 2.16. A study of the frequency dependence of the series reactance is usually made difficult because of the frequency sensitivity of the rest of the antenna, or test structure. For example in the short circuited transmission line method, the isolation of the series reactance of the probe from the input impedance of the remaining apparatus could only be achieved at a single frequency because the success of the experiment depended on the effective length of the wide transmission line being resonant. For a similar reason the method used by Lier [46] is also a single frequency experiment. Alternatively the large cavity method can be used in a wide band investigation because of the extremely large length and width of the cavity, which means that the experiment is virtually independent of these parameters over the bandwidth of interest.Therefore, to a good approximation, figure 2.16 is displaying the change in the series reactance as the electrical length and diameter of the probe are effectively altered by a change in frequency. Similar results were obtained for the other probe and substrate thickness combinations.

At 5GHz the the short circuited transmission line experiment provides reactances that are roughly 1Ω below the results of the locus transformation method. This is consistent when account is taken of the aspect ratios of the apparatus used in each case. The shorted transmission line experiment has also been used to show the variation of the series reactance with frequency, see figure 2.16. The frequency dependence is observed to be stronger than that measured in the large cavity experiment. Recall that for the shorted transmission line experiment an increase in the test frequency corresponds to a decrease in the length of a constant width microstrip transmission line. Therefore the extra increase in the series reactance is due to the increasing width to length aspect ratio of the wide transmission line, and as just mentioned, the series reactance is a positive function of aspect ratio, refer to figure 2.22.

2.3.5 Comparisons between the results of the locus transformation method and measurements performed by other authors

Comparisons between the series reactances obtained from the locus transformation method and those measured by other authors are difficult unless the exact antenna dimensions and frequencies are duplicated. However, rough comparisons can be made if the differences in the effective electrical length and diameter of the probes are accounted for. This is achieved by extrapolating the results of other authors using the information on the characteristics of the probe obtained from locus transformation studies. Figure 2.23 is a plot of the series reactance, obtained from the locus transformation method, versus the substrate thickness as a function of the probe diameter. Because of the sensitivity of the series reactance to small changes in the substrate thickness, the results of figure 2.23 have been extrapolated to include data on probes thinner than those actually investigated using the locus transformation method. The line for $d/\lambda_s = 0.034$ is based on two points that were obtained from a locus transformation study at 5GHz on two rectangular elements fed through SMA probes, while the $d/\lambda_s = 0.08$ points are based on a similar investigation using APC-7 probes. The lines for the cases of $d/\lambda_s = 0.02$ and 0.016 are derived using figure 2.24, which is a graph of the series reactance ver-

sus the probe diameter using the same four results as were used in figure 2.23. Using figures 2.22 and 2.23 the measured reactances of other authors can be extrapolated to obtain equivalent reactances, for which locus transformation results exist with the same dimensions and frequencies.

Carver's average measured reactance of figure 2.3 is 17Ω for $W/L = 1.65$ and $h/\lambda_s = 0.018$, and can be extrapolated for comparison with results from the locus transformation method, where $W/L = 0.9$ and $h/\lambda_s = 0.02$. Firstly figure 2.23 implies that an addition of 1Ω to the 17Ω would account for an equivalent series reactance for the case of $h/\lambda_s = 0.02$ instead of the original $h/\lambda_s = 0.018$. In a similar manner, the graph of figure 2.22 implies that a lowering of the aspect ratio from 1.65 to 0.9 would involve the subtraction of 10Ω. The resultant equivalent reactance is $17 + 1 - 10 = 8\Omega$, which is plotted on figure 2.25. Two results from the locus transformation method, APC-7 and SMA probes feeding a 0.8mm thick substrate, are also graphed on figure 2.25, and a dashed curve is used to approximate the characteristic for the series reactance versus the probe diameter for patches of a common aspect ratio of 0.9. This figure includes curves repeated from figure 2.2 so that the reactances calculated by the modal-expansion method can be used to indicate the relative dependence of the series reactance on probe diameter. Because the dashed curve displays a similar characteristic to the curves obtained by the modal-expansion method, it is concluded that the results of the locus transformation method are consistent with Carver's measured result.

Figure 2.22 shows good agreement between the series reactances measured by Lier [46] and those obtained using the locus transformation method. For comparison of one data point, consider the case of Lier at $W/L = 1$, $h/\lambda_s = 0.025$, $d/\lambda_s = 0.02$, where the series reactance is 14Ω. Figure 2.23 is again used to imply that an increase in h/λ_s from 0.025 to 0.042 would correspond to an increase in the series reactance of 8Ω. Increasing in d/λ_s from 0.02 to 0.08, as shown for the h/λ_s=0.04 line in figure 2.24, results in a corresponding decrease in the series reactance of 4Ω. The resultant extrapolated series reactance of Lier for the $W/L = 1$ case is $14 + 8 - 4 = 18\Omega$, which is

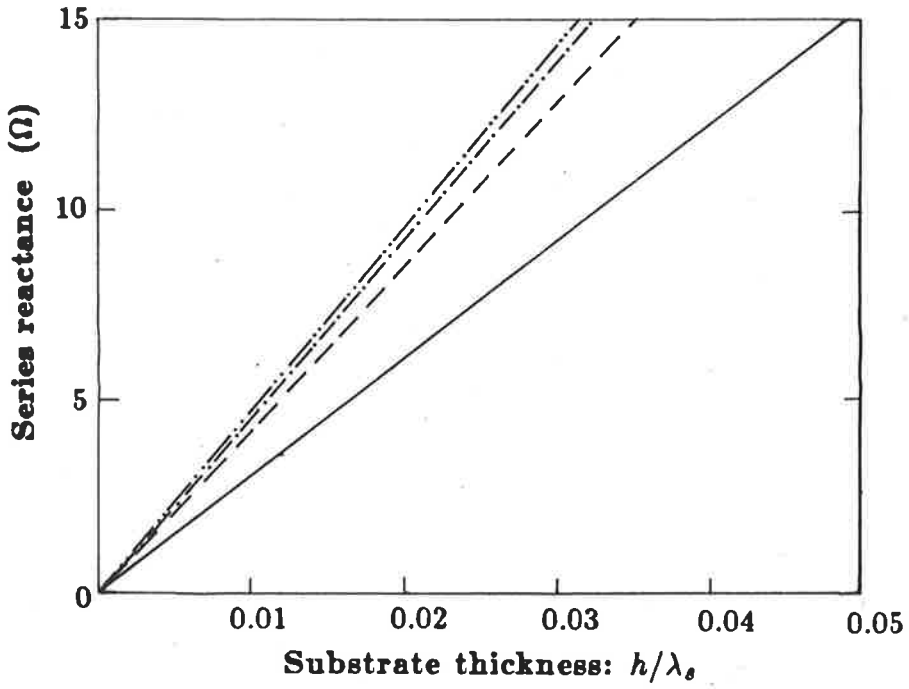

Figure 2.23: Series reactance using the locus transformation method as a function of substrate thickness for: $f_o \approx 5GHz$, $d/\lambda_s = 0.016$ (— ··—), 0.02 (— ·—) 0.034 (– – –) and 0.08 (———), where the 0.016 and 0.02 lines are based on extrapolated data, $\epsilon_r = 2.55$.

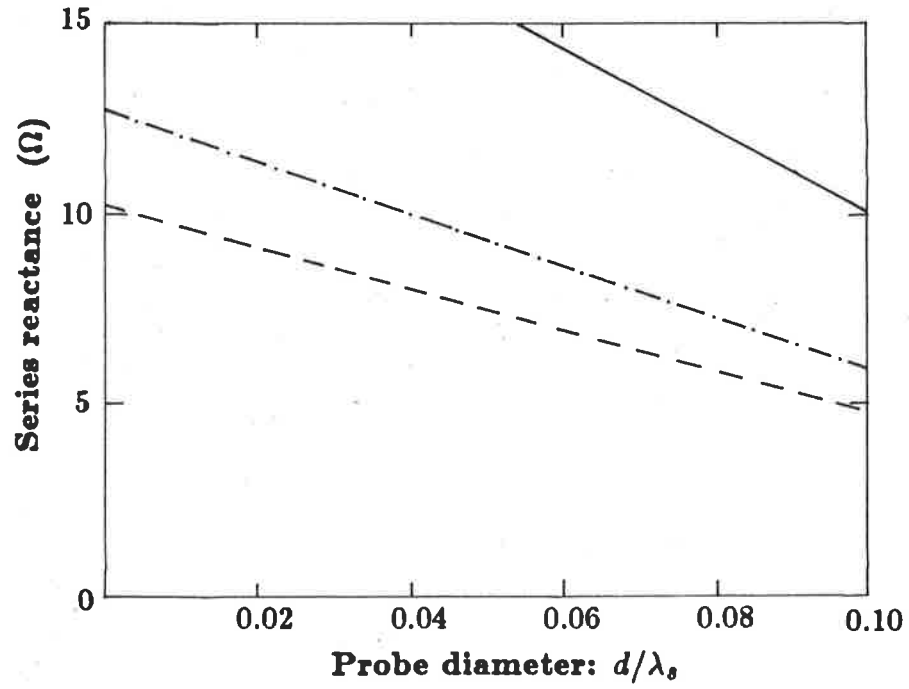

Figure 2.24: Series reactance using the locus transformation method as a function of probe diameter for: $f_o \approx 5GHz$, $h/\lambda_s = 0.04$ (———) and 0.025 (—·—) and 0.02 (– – –), where the 0.025 line is based in extrapolated data, $\epsilon_r = 2.55$.

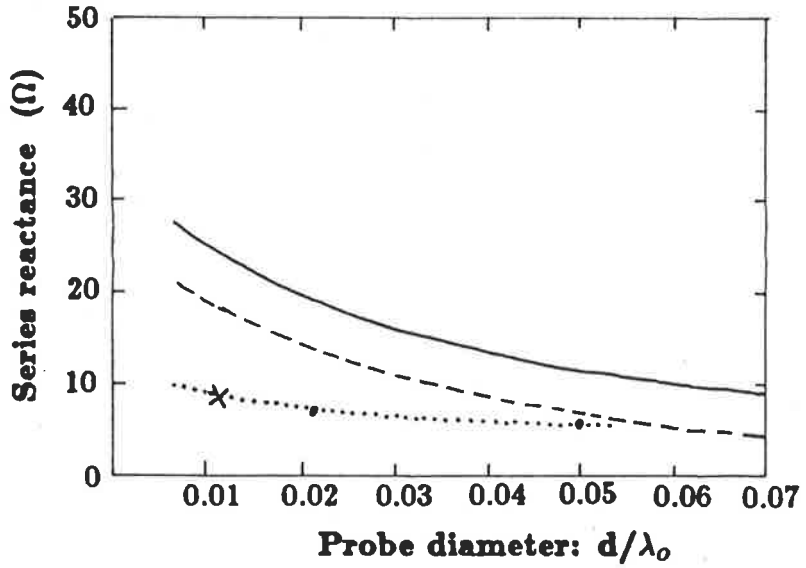

Figure 2.25: Series reactance calculated using the modal-expansion method for r=1.62 (———) and 0.98 (– – – –), where h=0.0116λ_o, ϵ_r = 2.5. Also a hybrid curve for r=0.9 (·····) comprising results from the locus transformation method (• •) and extrapolating Carver's measured result (×).

5Ω above the 13Ω result from the locus transformation method for the case of $W/L \approx 1$, h/λ_s=0.042 and d/λ_s=0.08.

2.3.6 Conclusions

The equivalent series reactance of the probe has been measured using the large cavity, the shorted transmission line, and the locus transformation methods. The results of these investigations have been shown to support each other and those performed by other authors.

Because the results of the locus transformation method agree with those of other experimental techniques proposed in this investigation, as well as those of other authors, its results will be used in the development of a new empirical model for the series reactance.

Table 2.2 shows that the short wire analogy of the probe is valid. An increase in the effective electrical length of the probe causes an increase in the self-inductance of an equivalent wire, and an increase in the diameter has an associated decrease in

inductance. Also the positive slope of the series reactance versus frequency lines in figure 2.16 indicates that the series reactance is a more sensitive function of the probe length than the diameter.

The results in figures 2.23, 2.22, 2.24, and 2.21 can be used to determine the relative dependence of the series reactance on substrate height, aspect ratio, probe diameter and feed point position respectively. As the stated aim of this investigation is to develop models for the computer aided design of rectangular microstrip antennas operating at about 5GHz, the most suitable indication of the sensitivity of the series reactance to the above parameters is obtained by considering a rectangular patch: $f_o \approx$5GHz, L=16.93mm, W=16mm, h=1.57mm fed by an APC-7 probe. The percentage change in the series reactance as the substrate height, aspect ratio, probe diameter and feed point position are in turn increased by 10% is: +11.5%, +10.0%, -8.2% and -2.1%. Therefore the new model to be developed in the next section will concentrate on the dependence of the series reactance on the substrate height, aspect ratio and probe diameter, feed point position being rejected because it only has a minor effect on the series reactance.

2.4 The tapered transmission line model

Although Carver's transmission line model is widely accepted, better agreement with experimental results can be obtained by a more detailed consideration of the field distribution in the region of the probe. A sketch of a cross-sectional view of the electric field in the probe region is shown in figure 2.26. Efforts have been made by Richards et.al. [35] to perform field analysis in the region of the probe using moment method techniques. However, in explaining this new model a sketch will suffice.

Using an electrostatic field analogy, the crosses in figure 2.27 approximate an equi-potential contour of mid-value between the two metal surfaces A and B. This contour can then be roughly approximated by the quarter-wave sinusoid shown in figure 2.28. Now if the outer conductor of a tapered transmission line is placed along this contour, then the fields along this short circuited transmission line will approximate

those in the proximity of the feed probe. This tapered line deviates from the equi-potential contour to make connection with the short circuiting patch in the $y = 0$ plane, but because the tapered line is feeding a short circuit load, the stored energy density decreases as x and y approach f and 0 respectively; that is, as the end of the line is approached. Therefore there is little error introduced by the approximation.

The reactance of the probe is now numerically evaluated using the transmission line equation (2.1) to transform the short circuit at $y = 0$ through a stair-case approximation to the tapered transmission line to the antenna terminals at the plane $y = -h$, where the reactance is renormalised to the characteristic impedance of the coaxial line used to feed the antenna, typically 50Ω. Therefore,

$$X_s = 50\frac{X_{st}}{Z_{ot}} \tag{2.25}$$

where Z_{ot} is the characteristic impedance of the coaxial tapered line at $y = -h$, and X_{st}, is the calculated series reactance normalised to Z_{ot}.

Using the mid-value equi-potential contour, the model has produced series reactances that are typically between 3Ω and 5Ω greater than those obtained by the locus transformation method. However, there is of course a multitude of equi-potentials that could be chosen for the model. An investigation into the agreement between the results of the locus transformation method and the reactances calculated using various contours has concluded that an empirically determined contour is the best choice; where e in figure 2.28 is chosen as $a + (b - a)/20$ and $(f - e)$ is made a function of the feed point's dimensions and aspect ratio of the patch. Hence the amplitude of the sinusoid, A_s, is a variable and will be used to determine the outer radius of the tapered coaxial line that is representing the probe. Figure 2.29 is a graph of the radius of the outer conductor at $y = 0$, r_{to}, versus the probe diagonal, p, normalised to the length of the patch, where

$$p^2 = h^2 + (b - a)^2 \tag{2.26}$$

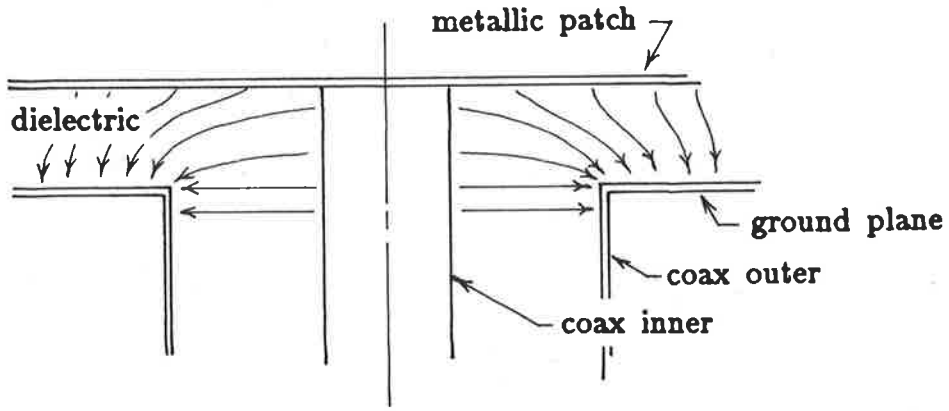

Figure 2.26: Fringing electric field around the probe.

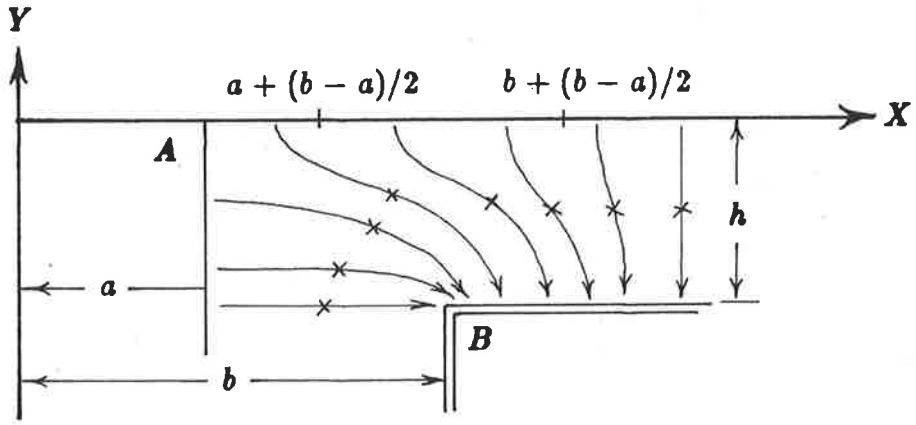

Figure 2.27: Electrostatic fringing field around the probe with an approximate equi-potential of mid-value.

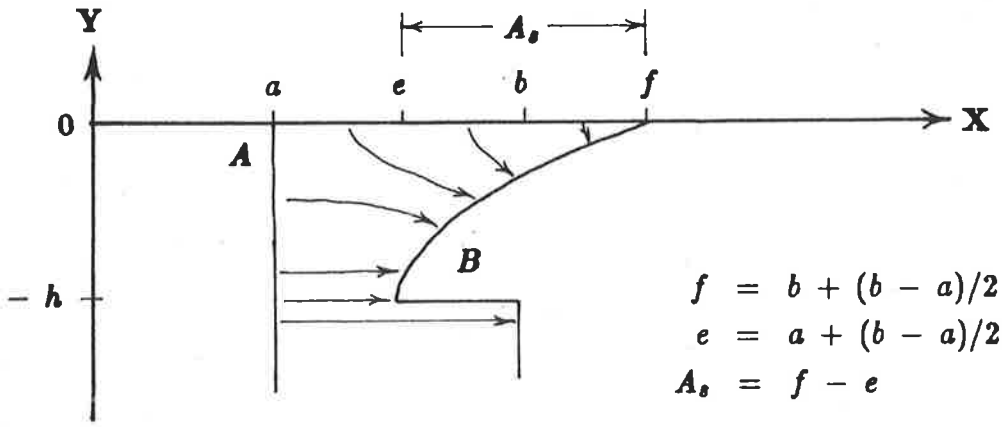

Figure 2.28: The field distribution of a sinusoidally tapered transmission line.

and is a measure of the probe's dimensions. These points describe the sinusoidal contour that was used with the tapered transmission line model to provide exact agreement with the measured impedance locus transformations. The data are actually derived for the case of an equivalent aspect ratio, $r \approx 0.9$. They have then been approximated by an exponential contour, using a curve fitting program, as follows

$$\frac{r_{to}}{a} = 1.929e^{-4.369\frac{p}{L}} \tag{2.27}$$

In a similar fashion figure 2.30 has been used to show the taper radius as a function of the aspect ratio of the patch and implies that for $p/L = 0.14$ the taper radius is almost independent of the aspect ratio. Again using a curve fitting program the approximate expression is

$$\frac{r_{to}}{a} = 0.935e^{0.153r} \tag{2.28}$$

The combined expression is then

$$\frac{r_{to}}{a} = 1.681e^{0.153r-4.369\frac{p}{L}} \tag{2.29}$$

Table 2.4 shows, that by using the empirically determined taper of equation (2.29), the tapered transmission line model calculates series reactances that are within plus or minus 3Ω of the measured input impedance locus transformations. Notice that the model has been tested over a large range of antenna dimensions and frequencies, all with relative dielectric constants between 2.5 and 2.55.

Figure 2.31 and 2.32 show excellent agreement between the results of the tapered transmission line model and those measured by the locus transformation method for reactance versus substrate height and aspect ratio respectively. Figure 2.33 displays series reactances versus frequency where the calculated results are compared with those of the large cavity experiment. Notice the similar slopes of the two lines. Recall that the results of the large cavity experiment are 3.5Ω higher than the accepted results of the locus transformation method .

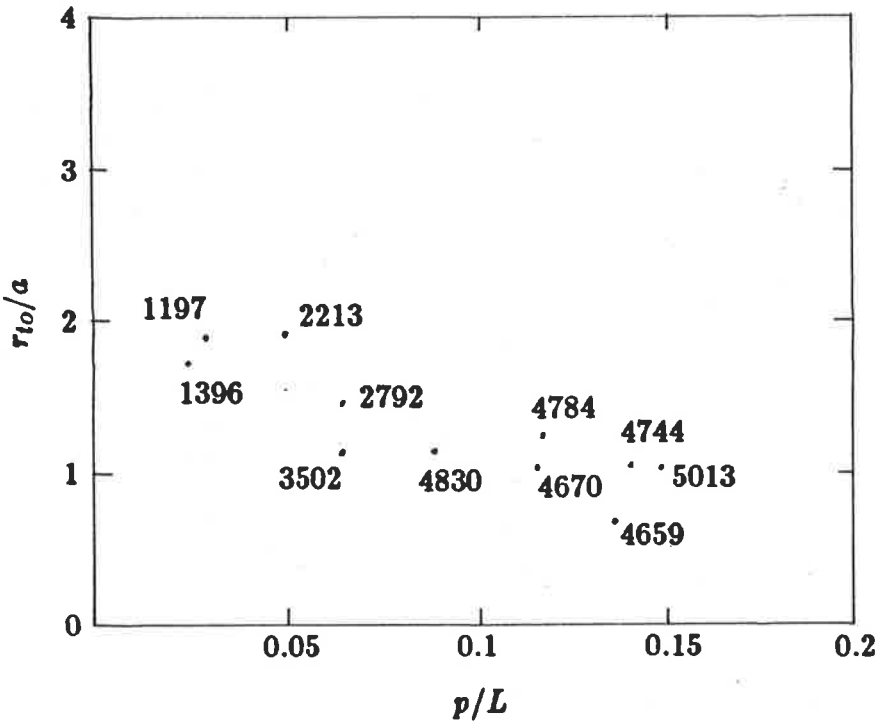

Figure 2.29: Empirical determination of the radius of the outer conductor at $y = -h$ as a function of the probe dimensions, where the numbers refer to the measured f_{oc} of the antennas concerned: full specifications can be found through Appendix A.

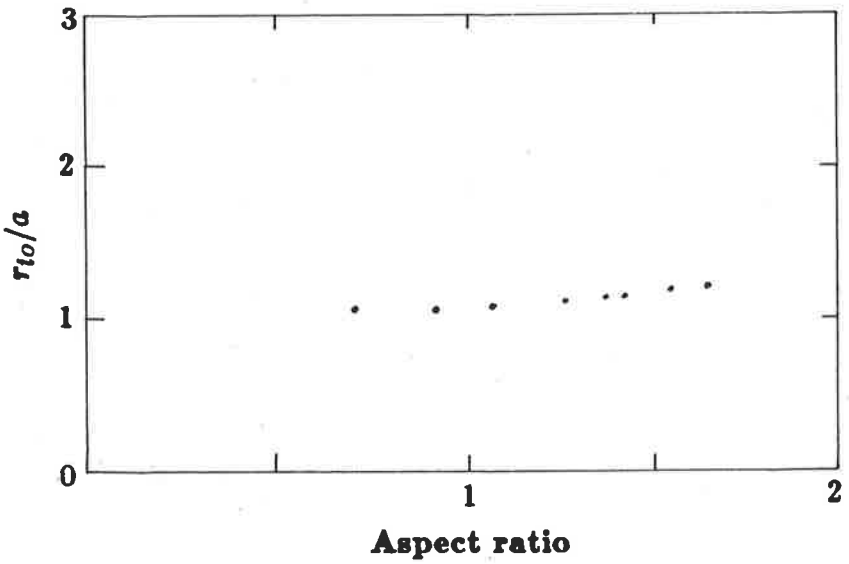

Figure 2.30: Empirical determination of the radius of the outer conductor at $y = -h$ as a function of the aspect ratio of the patch for the case p/L=0.14.

Series reactance					
Freq. MHz	h mm	r	Probe type	Calc'd Ω	Meas'd Ω
1189	1.59	1.5	SMA	10	10
1396	1.57	1.6	SMA	11	11
2213	1.59	1.7	SMA	16	19
2792	1.52	1.0	SMA	15	15
3387	0.80	0.9	SMA	9	7
3502	0.08	1.9	SMA	9	6
4659	1.57	1.6	APC-7	20	23
4670	0.08	0.9	APC-7	9	6
4744	1.57	0.9	APC-7	13	12
4784	1.57	0.9	SMA	15	18
4830	0.08	0.9	SMA	10	8
5013	1.57	1.0	APC-7	13	13

Table 2.4: Comparison between the series reactance calculated by the tapered transmission line model and measured by the locus transformation method.

2.5 Conclusions

The models proposed by other authors for the calculation of the series reactance have been reviewed and shown to be inadequate due to computational complexity or poor accuracy, especially as the substrate thickness increases.

The equivalent series reactance of the probe has been measured using the large cavity, the shorted transmission line, and the locus transformation method. The results of these methods have been shown to agree with each other and with those performed by other authors.

A novel tapered transmission line model, using an empirically determined contour, has been shown to provide series reactance results that are within ±3Ω of the

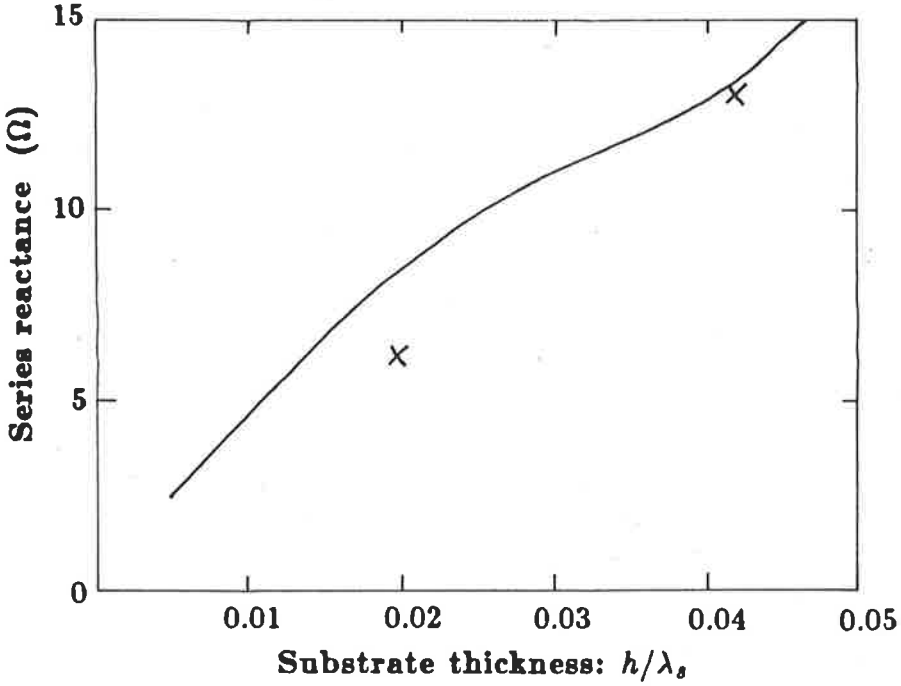

Figure 2.31: Series reactance versus substrate height for a rectangular element fed through an APC-7 probe: calculated using the tapered transmission line model (———), and measured using the locus transformation method (x x), where f_{oc} ≈5GHz, and $\epsilon_r = 2.55$.

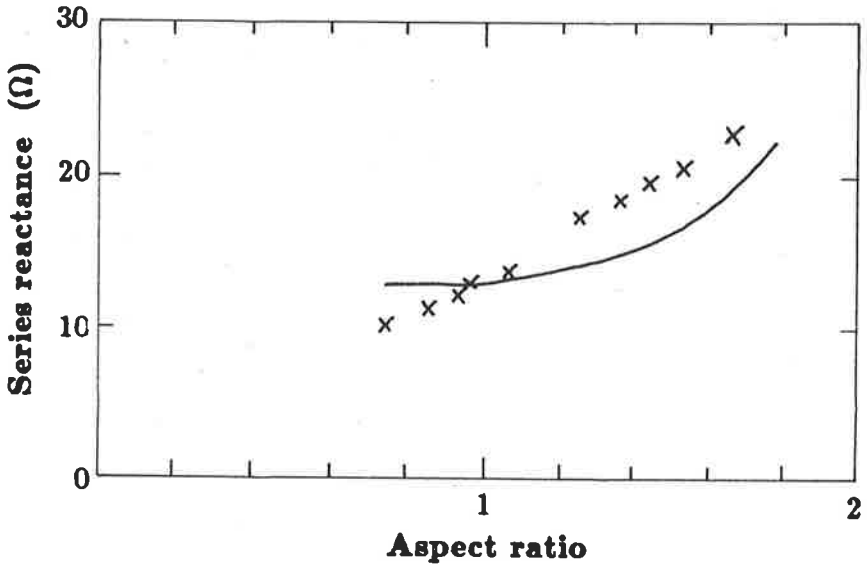

Figure 2.32: Series reactance versus aspect ratio for a set of a rectangular elements fed through APC-7 probes: calculated using the tapered transmission line model (———), and measured using the locus transformation method (x x x), where f_{oc} ≈5GHz, h=1.57mm, and $\epsilon_r = 2.55$.

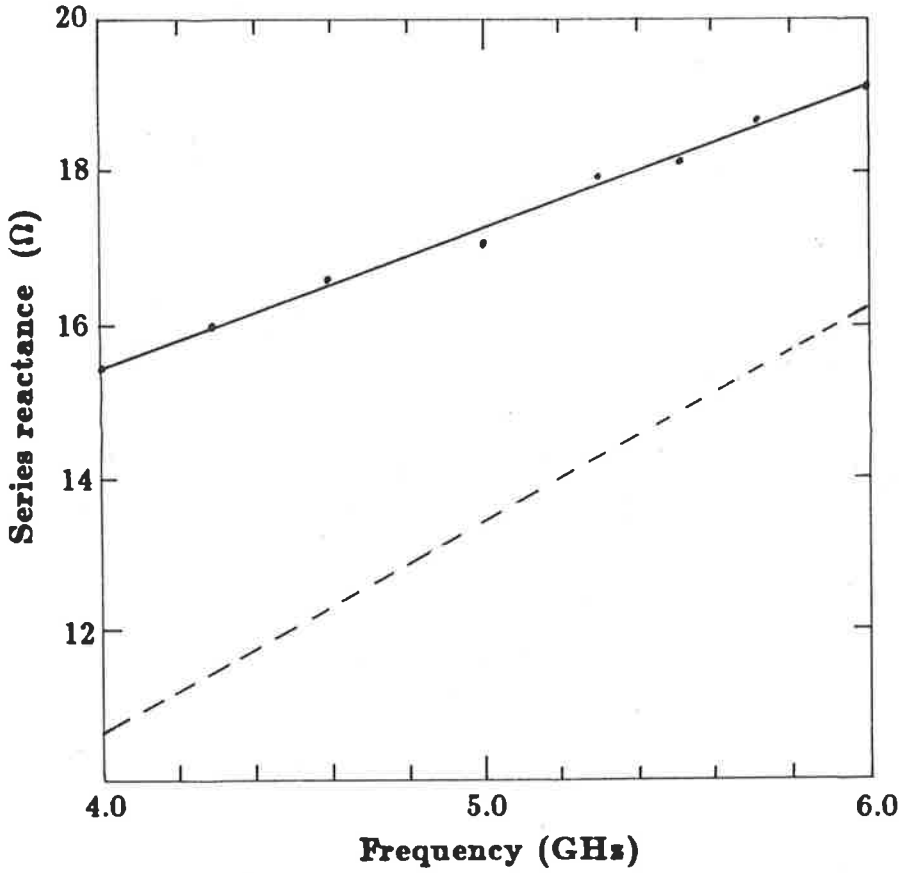

Figure 2.33: Series reactance versus frequency for a 1.57mm thick substrate fed through an APC-7 probe: calculated using the tapered transmission line model for a rectangular element $f_{oc} \approx 5GHz$ (– – –), and directly measured using the large cavity (———), where $\epsilon_r = 2.55$.

measured impedance locus transformations. Furthermore, this agreement is maintained over a very wide range of antenna and feed dimensions and frequencies.

This new empirical model for calculating the equivalent series reactance of the probe is incorporated into a computer-aided design program listed in Appendix C. The series reactance is numerically evaluated using the transmission line equation (2.1) to transform a short circuit load through a stair-case approximation to a tapered transmission line, where the taper is given by equation (2.29) and the length of the transformation is equal to the substrate thickness. At the terminals of the antenna the reactance is then re-normalised to the characteristic impedance of the coaxial line used to feed the antenna.

CHAPTER III

THE CALCULATION OF RESONANT FREQUENCY USING AN EMPIRICALLY DETERMINED EDGE EXTENSION PARAMETER

3.1 Introduction

The narrow bandwidth of the microstrip antenna means that it is crucial that the resonant frequency be accurately determined. The resonant frequency is very sensitive to the effective dielectric constant of the substrate and the effective electrical dimensions of the patch. Therefore the determination of the distance to which the fields fringe at each end of the rectangular microstrip antenna is a major step in determining the antenna's resonant frequency.

The methods to determine the resonant frequency suggested by other authors will be reviewed, where it will be noticed that the definition of resonant frequency being used is often unclear. It will also be shown that these methods give results that are in good agreement with measurements for antennas operating at frequencies up to the lower microwave band, but give misleading results as the frequency is increased, and especially at around 5GHz. The resonant frequency is clearly specified for probe fed microstrip antennas using the antenna's input impedance versus frequency locus plotted on a Smith chart. The poor performance of the published models in predicting the resonant frequency prompted the development of a new empirical model for the

edge extension that will be shown to lead to resonant frequencies that are in excellent agreement with measurements carried out at frequencies up to 5GHz.

3.2 A literature survey of the analytical and empirical models used to calculate the resonant frequency

The procedures of other authors to calculate the resonant frequency of rectangular patch antennas are now reviewed. Most use a resonant length transmission line or cavity model together with equations for the effective dielectric constant and edge extension which may or may not be their own.

To analyse the resonant frequency of rectangular microstrip antenna's Howell [2,3] used a rectangular cavity model and assumed the cavity to be driven at its fundamental TEM_{010} mode. Then at resonance

$$f_o = \frac{c}{2\sqrt{\epsilon_r}L} \tag{3.1}$$

where L is the antenna's physical length. This model was tested at 3.5GHz on a rectangular patch mounted on a 0.8mm thick substrate. The calculated resonant frequency was 2.8% above the measured frequency. The method is however only useful at low frequencies, because as the frequency is increased effects of the fringing fields at each end of the patch extend its effective electrical dimensions. Howell also ignored the fact that the medium around the antenna is partially filled with air and a substrate material having a non-unity dielectric constant, and that the effective dielectric constant of the overall medium must therefore be between that of the air and the substrate material.

Derneryd [12] added to this simple model the effects of the non-uniform medium and the fringing fields at each end of the patch by letting

$$f_o = \frac{c}{2\sqrt{\epsilon_e}(L + 2\delta L)} \tag{3.2}$$

where ϵ_e is the effective dielectric constant and δL is the effective length to which the fields fringe at each end of the patch, and is called the edge extension. Hence

the accuracy of Derneryd's model for the resonant frequency depends on the accurate determination of the effective dielectric constant of the substrate and the total electrical length of the antenna or cavity, $L + 2\delta L$. Derneryd applied to microstrip antennas the approximate electrostatic expressions for the effective dielectric constant and the edge extension that were proposed for use with microstrip transmission lines by Schneider [13] and Hammerstad [14],

$$\epsilon_e = \frac{\epsilon_r + 1}{2} \frac{\epsilon_r - 1}{2} (1 + \frac{10h}{W})^{-0.5} \tag{3.3}$$

$$\delta L = 0.412h \frac{\epsilon_e + 0.300}{\epsilon_e - 0.258} \frac{W/h + 0.262}{W/h + 0.813} \tag{3.4}$$

where the equation for the effective dielectric constant was obtained by empirically modifying the theoretical data of Schneider [13] and Wheeler [17]. The edge extension equation is an empirical expression based on the theoretical results of Silvester et.al. [49].

Six years later Hammerstad [50] proposed another empirical equation based on the calculations for the edge extension associated with the open circuited end of a microstrip transmission line, and furthermore recommended its use in the design of rectangular microstrip antennas

$$\delta L = \frac{h}{2\pi} \frac{W/h + 0.366}{W/h + 0.556} [0.28 + \frac{\epsilon_r + 1}{\epsilon_r} [0.274 + \ln(W/h + 2.518)]] \tag{3.5}$$

Using a computer-aided matching technique Kirschning et.al. [51] derived the following expressions from a rigorous numerical hybrid mode solution of the end effect of a microstrip line,

$$\delta L = \frac{h \xi_1 \xi_3 \xi_5}{\xi_4} \tag{3.6}$$

where

$$\xi_1 = 0.434907 \frac{\epsilon_e^{0.81} + 0.26}{\epsilon_e^{0.81} - 0.189} \frac{(W/h)^{0.8544} + 0.236}{(W/h)^{0.8544} + 0.87} \tag{3.7}$$

$$\xi_2 = 1 + \frac{(W/h)^{0.371}}{2.358\epsilon_r + 1} \tag{3.8}$$

$$\xi_3 = 1 + \frac{0.5274 \arctan(0.084(W/h)^{1.9413/\xi_2})}{\epsilon_e^{0.9236}} \tag{3.9}$$

$$\xi_4 = 1 + 0.0377 \arctan(0.067(W/h)^{1.456})[6 - 5e^{0.036(1-\epsilon_r)}] \tag{3.10}$$

$$\xi_5 = 1 - 0.218e^{-7.5W/h} \tag{3.11}$$

The authors recommend using a third equation published by Hammerstad [52] for the calculation of the effective dielectric constant,

$$\epsilon_e = \epsilon_r - \frac{\epsilon_r - \epsilon_{eo}}{1 + G(f/f_p)^2} \tag{3.12}$$

where

$$f_p = \frac{Z_{om}}{2\mu_o h} \tag{3.13}$$

$$G = \frac{\pi}{12}^2 \frac{\epsilon_r - 1}{\epsilon_{eo}} \sqrt{\frac{2\pi Z_{om}}{\eta_o}} \tag{3.14}$$

and

$$\epsilon_{eo} = \frac{\epsilon_r + 1}{2} + \frac{\epsilon_r - 1}{2}(1 + \frac{10h}{W})^{-a\,b} \tag{3.15}$$

where

$$a = 1 + \frac{1}{49} \ln \frac{(W/h)^4 + (W/52h)^2}{(W/h)^4 + 0.432} + \frac{1}{18.7} \ln 1 + (W/18.1h)^3 \tag{3.16}$$

$$b = 0.564 \left(\frac{\epsilon_r - 0.9}{\epsilon_r + 3.0}\right)^{0.053} \tag{3.17}$$

These equations are all empirical modifications of theoretical models. Equations (3.12) (3.13) and (3.14) are based on the work of Getsinger [48] which will be presented in section 3.5.

Using the transmission line model for rectangular microstrip antennas Sengupta [16] developed formulas for the resonant frequency that include the frequency shift due to the effect of feeding the antenna through a coaxial feed probe. For the admittance at each end of the transmission line Sengupta used the expressions of Marcuvitz [42] for the admittance of a parallel-plate waveguide radiating into free space. Ignoring the

probe, an expression for the resonant frequency is derived by determining the frequency at which the input impedance is real

$$f_r = f_o \frac{1 - \frac{2h}{\epsilon_e L \pi \alpha}}{1 + \frac{2h}{\epsilon_e L \pi \alpha} \ln \frac{\sqrt{\epsilon_e} 2L}{\gamma h}} \tag{3.18}$$

where

$$f_o = \frac{c}{2L\sqrt{\epsilon_e}} \tag{3.19}$$

and the relative shift in the resonant frequency caused by the probe is

$$\frac{\delta f_r}{f_r} = \frac{\pi h^2 W}{2\alpha \epsilon_e^2 L^3} \ln \frac{4L}{\gamma \pi d} \tag{3.20}$$

where α is evaluated using equation (1.14). Sengupta also recommends using equation (3.3) for the effective dielectric constant.

These formulas are used in the next section to calculate the resonant frequency of a number of antennas, and when the results are compared with measurements the agreement is shown to decrease with increasing frequency.

3.3 The limitations of the published formulas used in the calculation of the resonant frequency

Resonant frequencies have been calculated using the equations of other authors for a number of rectangular patch antennas. The resonant frequency at which the comparison is made is the cavity resonant frequency, f_{oc}, which will be defined in the next section. Suffice to say that for a probe fed antenna, this is the frequency at which the input impedance is real when the effects of the probe are removed. The effect of the probe on the measured resonant frequency can be compensated for by first determining the series reactance of the probe using the locus transformation method described in Chapter II. Then the cavity resonant frequency is the frequency at which the input reactance is equal to the series reactance of the probe.

Table 3.1 shows the percentage difference between the calculated and measured resonant frequencies. The first column lists the measured cavity resonant frequencies of a number of antennas, where this frequency can be used as a guide to identify the complete specifications of the antennas which can be found through Appendix A. Column two lists the resonant frequencies calculated using the method of Derneryd [12] based on equation (3.2) and Hammerstad's expressions for the effective dielectric constant and edge extension; equations (3.3) and (3.4). Hammerstad's equations (3.3) and (3.5) are used in column three and the results obtained using the equations of Kirschning et.al. are listed in column four. The fifth column shows the results using Sengupta's method.

Most of the above equations for the edge extension have been published for use with microstrip transmission lines and provide unsatisfactory results when applied to antennas, especially as the frequency is increased. The typical bandwidth of microstrip antennas operating at 5GHz is 4%, therefore methods that give a 6% error in the prediction of the resonant frequency are of little use. This error in the resonant frequency is possibly because the antenna's length is only half of a wavelength in the dielectric, therefore evanescent and hybrid modes caused by perturbations in the cavity's field by the feed may be present in the fringing fields. This point is taken up in more detail in Chapter VI. Sengupta's expression was published for the specific application to rectangular microstrip antennas. However, it too gives poor results for resonant frequency when applied to antennas operating above 4GHz. An empirical model to determine the edge extension is now developed, but first the input impedance versus frequency locus is used to specifically define the resonant frequencies of the antenna.

3.4 The definition of resonant frequency

In dealing with resonant structures and their feeds there are at least three definitions for determining the frequency at which resonance occurs:

i when the structure, excluding the feed network, is resonant. Typically this implies the frequency at which an electrical dimension of a cavity or antenna is a

Resonant frequency percentage error				
Freq.(MHz)	Derneryd	Hammerstad	Kirschning	Sengupta
633	−0.94	−2.21	+1.49	+1.43
658	+0.80	+0.69	+0.47	+0.28
1189	+1.15	−1.04	+0.57	+0.51
1197	+0.74	−1.45	+0.15	+0.01
1396	+1.31	−1.15	+0.62	+0.56
1410	+0.53	−1.91	−0.16	−0.26
2195	+1.98	−1.24	+0.89	+1.10
2224	+2.32	+0.39	+1.32	+1.82
3387	+3.26	+1.17	+2.42	+2.67
3502	+3.52	+1.34	+2.66	+2.90
4672	+5.59	+1.16	+3.40	+4.70
4744	+5.84	+3.19	+3.91	+6.15
4770	+5.85	+3.66	+4.04	+6.43
4784	+4.52	+1.92	+2.63	+4.69
4792	+4.26	+1.87	+3.12	+3.75
4830	+3.82	+1.44	+2.68	+3.32
5013	+6.11	+3.31	+4.07	+6.43

Table 3.1: For the formulas of various authors, a comparison between the percentage difference in the calculated and measured cavity resonant frequency.

multiple number of half-wavelengths.

ii when the input impedance, referred to the input terminals, is real.

iii when the VSWR, referred to the input terminals, is a minimum.

Furthermore when working with resonant type antennas and their feeds, the above definitions typically do not lead to the same frequency value. Notice also that the use of definition ii can lead to either two closely spaced resonant frequencies or no resonant

frequency at all, as shown in the measured input impedance versus frequency results of figures 5.12(a) and 5.11(b) respectively.

The Smith chart display of the input impedance versus frequency characteristic of a cavity excited about its fundamental mode resonant frequency is shown in figure 3.1, and suggests that a microstrip patch antenna can be modelled as a leaky cavity coupled through a series reactance. In the region near the centre of the operational bandwidth of the antenna either of two values for resonant frequency can be identified: f_{oc}, the frequency at which the cavity itself resonates, or f_{oz}, the frequency at which the input impedance of the antenna is real. The definition of resonant frequency using the VSWR is not considered any further because this investigation is primarily concerned with antennas that are matched to their feeding transmission lines, and when this is the case, the frequency at which the VSWR is a minimum is equal to the frequency at which the input impedance is real. A new empirical model for the calculation of the cavity and impedance resonant frequencies will now be developed.

3.5 The calculation of the cavity resonant frequency using an empirically determined edge extension parameter

Equations for the effective dielectric constant and edge extension are now proposed. These equations are necessary inorder that equation (3.2) may be used to calculate the cavity resonant frequency, and obtain an agreement with measurements that is better over a wider frequency bandwidth than that obtained using the equations of other authors. This section describes an equation for the effective dielectric constant derived by another author, and the development of an empirical model for the effective edge extension.

The effective dielectric constant, ϵ_e, is calculated using an expression developed by Getsinger [48] for use with microstrip transmission lines

$$\epsilon_e = \epsilon_r - \frac{\epsilon_r - \epsilon_{eo}}{1 + G(f^2/f_p^2)} \tag{3.21}$$

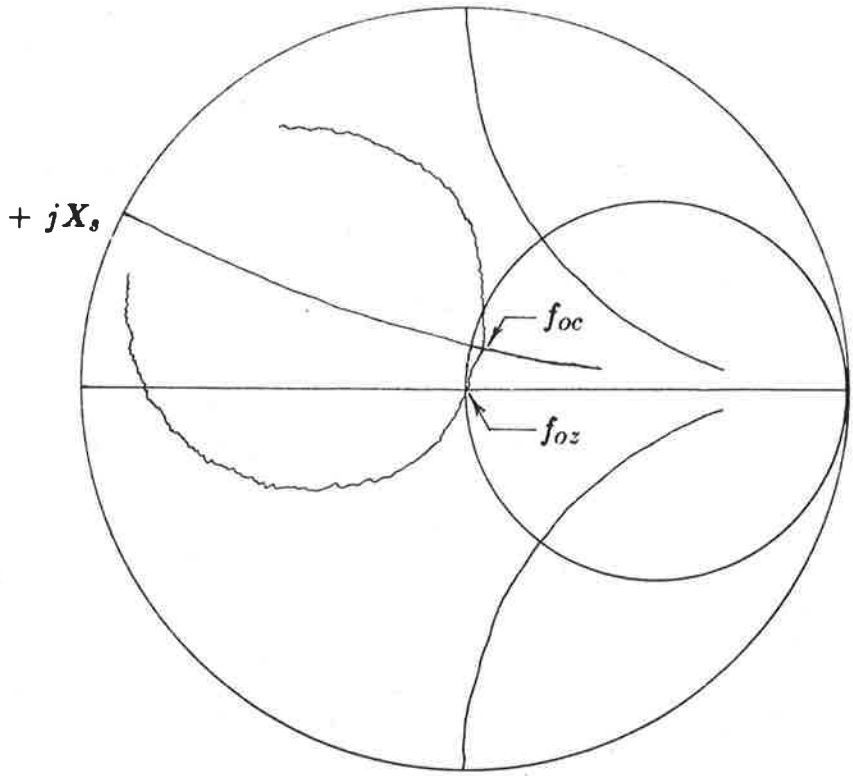

Figure 3.1: The definition of resonant frequency; f_{oc} the resonant frequency of the cavity and f_{oz}, the frequency at which the input impedance is real.

where

$$f_p = \frac{Z_{om}}{2\mu_o h} \tag{3.22}$$

$$G \approx 0.6 + 0.009 Z_{om} \tag{3.23}$$

This analytical expression was derived for an approximation to a microstrip line; that is, a transmission line supporting a single longitudinal section electric (LSE) mode. Equation (3.22) may be regarded as an approximation to the first TE-mode cut-off frequency while G is an empirically determined factor. The application of this expression to microstrip antennas was recommended by James et.al. [40] because it can be used to attribute the frequency dispersion effects that may be observed to the effective dielectric constant. The calculation includes the zero frequency effective dielectric constant, ϵ_{eo}, which is obtained from equation (3.3). A model for the edge extension is now developed on the assumption that the effective dielectric constant calculated by equation (3.21) is

a correct result that accurately describes the physical phenomenon.

An empirical equation for the edge extension, δL, is determined using equation (3.2), by substituting the measured results for the cavity resonant frequency, f_{oc}, and the effective dielectric constant, ϵ_e, calculated using equation (3.21). Figure 3.2 shows for a range of antennas the calculated results for the edge extension as a function of the dimensions of the W by h aperture located at each end of the antenna. The calculations were carried out for a range of antennas of different dimensions built on substrates of relative dielectric constants between 2.5 and 2.62. Because this small range in dielectric constant is so widely used in antenna applications, the dielectric constant will not be included in the model for the edge extension. It is therefore understood that the model will only be applicable to antennas on substrates of dielectric constant between these values. Based on the formulas of the previous authors, the empirical equation for the edge extension will primarily be a function of W/h; the aspect ratio of the cross-section through the dielectric filled region under the patch. Shown in figure 3.3 is the extrapolated edge extension at $W/h = 0$ versus the electrical substrate thickness. This graph has no physical interpretation, but it is used to determine a correction term that takes into account the substrate thickness. The overall expression of best fit for the effective edge extension as a function of the dimensions of the aperture and frequency is

$$\beta_s \delta L = \frac{322.5}{10^6}\frac{W}{h} + C \tag{3.24}$$

where

$$C = \begin{cases} 0.606 + 0.128 \ln \frac{h}{\lambda_s}; & h/\lambda_s \geq 0.009 \\ 0; & \text{otherwise.} \end{cases}$$

Here h and W are the aperture width and length respectively which correspond to the substrate height and patch width of the antenna. Equation (3.24) has been evaluated for h/λ_s=0.01, 0.02, 0.03, 0.04, and the lines of $\beta_s \delta L$ versus W/h have been superimposed on the points of figure 3.2. The specifications of the antennas used are referred to in Appendix A.

Using this empirical approach, any error in the calculated effective dielectric

constant due to the failure of equation (3.21) to accurately represent the physical phenomenon is accounted for in the edge extension term. In the next section the combination of equations (3.2), (3.21) and (3.24) are shown to lead to calculated results for f_{oc} that are within 2% of measured ones for a wide variety of antennas. However, in any design exercise the frequency at which the input impedance is real, f_{oz}, is of primary concern, so the impedance resonant frequency will now be calculated from the cavity resonant frequency.

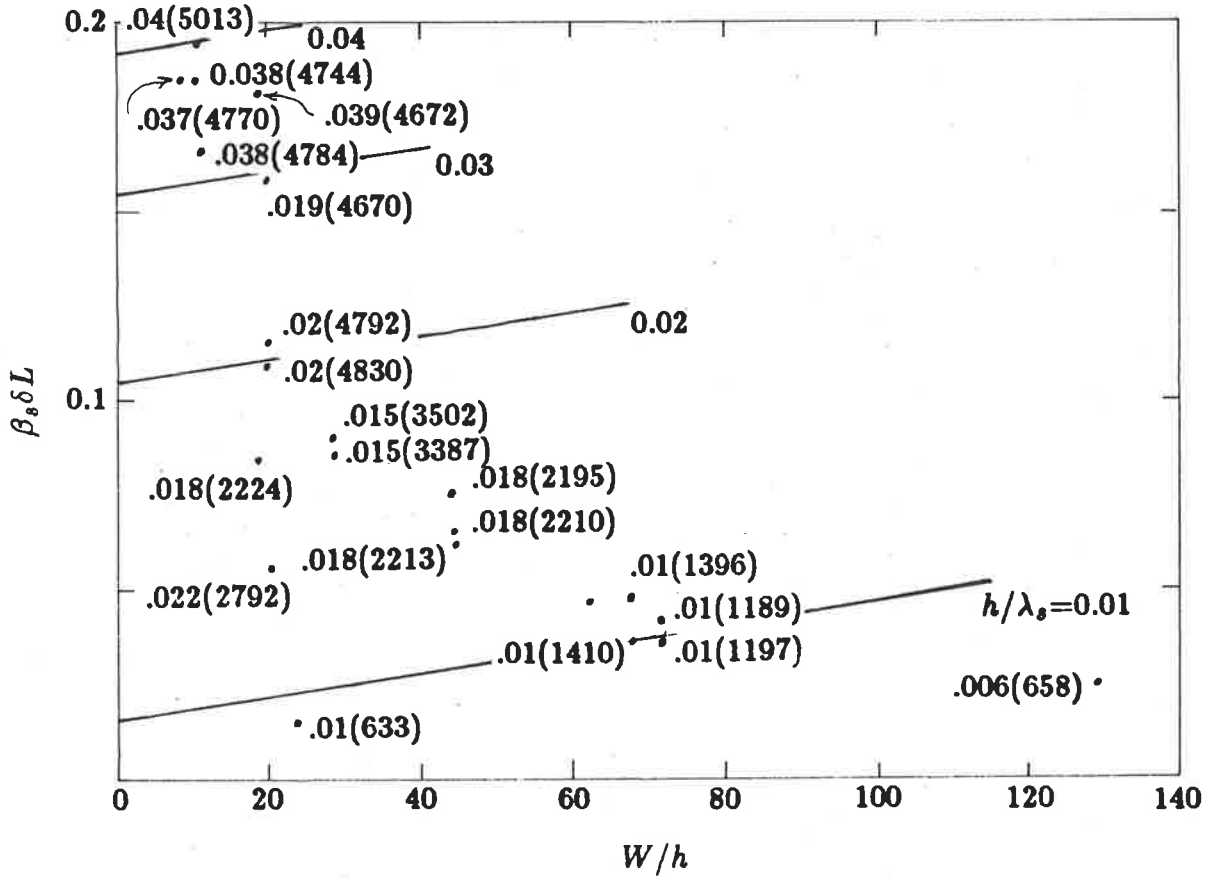

Figure 3.2: Empirical determination of the edge extension as a function of the aperture dimensions, where the numbers along side each point refer to the h/λ_s and f_{oc} MHz.

3.6 The impedance resonant frequency

To determine f_{oz} from f_{oc}, the equation for the circle of best fit to the input

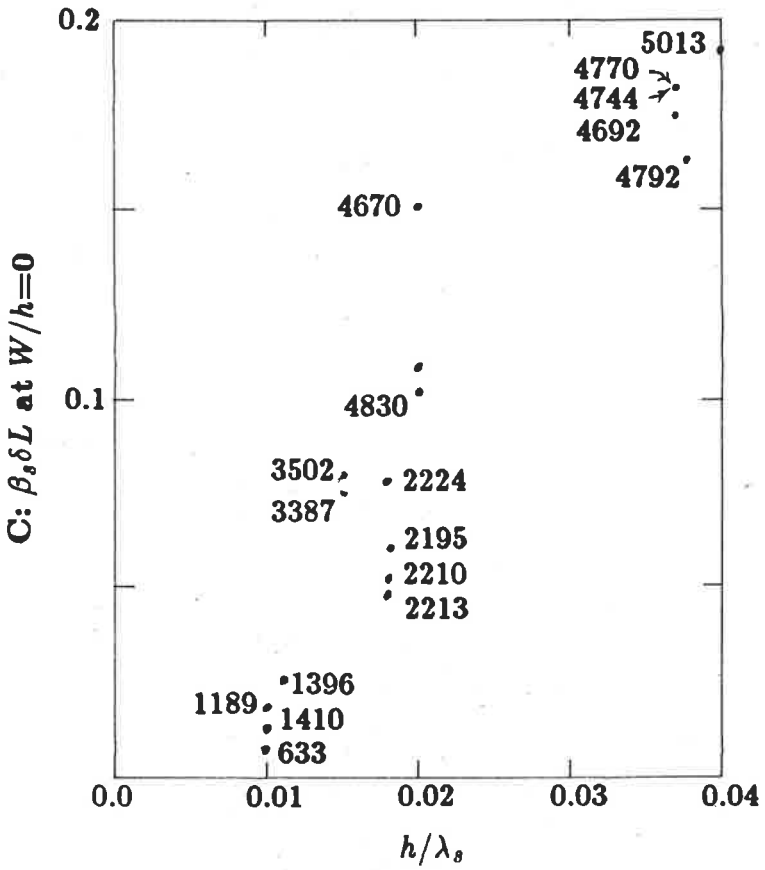

Figure 3.3: Empirical determination of the edge extension as a function of the substrate height, where the numbers along side each data point refer to f_{oc}MHz.

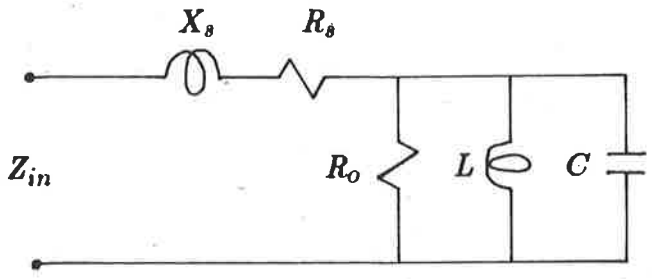

Figure 3.4: Network model of a leaky resonant cavity.

impedance versus frequency locus must be obtained. The network model of the antenna suggested by Carver [15,30] and shown in figure 1.8(b) is a good starting point because it has been useful in the calculation of the input impedance of microstrip antennas operating at lower microwave frequencies. However for the 3GHz and 5GHz antennas studied in this investigation, there is typically a gap between the impedance locus and the perimeter of the Smith chart. This gap can be observed in the measured input impedance results of figure 2.1. Carver's network of figure 1.8(b) can therefore be improved by adding a series resistance, R_s, to the circuit, as shown in figure 3.4. It turns out that the equation for the resonant frequency is independent of the series resistance. The series resistance will be treated in more detail in Chapter IV.

Using normalised parameters the equation for the input impedance of the network of figure 3.4 is

$$z_{in} = r_s + jx_s + \frac{r_o}{1 + jQ_o(f^2/f_{oc}^2 - 1)} \tag{3.25}$$

and was obtained using

$$f_{oc} = \frac{1}{2\pi\sqrt{LC}} \tag{3.26}$$

and for a parallel RLC circuit

$$Q_o = \frac{R_o}{\omega L} \tag{3.27}$$

where

$$z_{in} = \frac{Z_{in}}{Z_o} \tag{3.28}$$

$$r_o = \frac{R_o}{Z_o} \tag{3.29}$$

$$r_s = \frac{R_s}{Z_o} \tag{3.30}$$

$$x_s = \frac{X_s}{Z_o} \tag{3.31}$$

Note that r_o is the resonant resistance, that is the input resistance at resonance f_{oz}, and that Z_o is the characteristic impedance of the transmission line feeding the cavity.

Because only the relationship between the closely spaced frequencies f_{oz} and f_{oc} is of interest, let $f \approx f_{oc}$ so that the classical definition of the frequency tuning

parameter [41] can be used

$$\delta = \frac{f - f_{oc}}{f} \tag{3.32}$$

Substituting the frequency tuning parameter into equation (3.25) results in an expression for the input impedance versus frequency locus

$$z_{in} = r_s + jx_s + \frac{r_o}{1 + j2Q_o\delta} \tag{3.33}$$

To calculate f_{oz}, substitute f_{oz} for f and then equate the imaginary part of equation (3.33) to zero to obtain a quadratic equation in δ:

$$\delta^2 - \frac{r_o}{2Q_o x_s}\delta + \frac{1}{4Q_o^2} = 0 \tag{3.34}$$

Equation (3.32) can be used to determine f_{oz} from f_{oc}, where the series reactance term, x_s, is calculated using the tapered transmission line model, and the unloaded quality factor, Q_o, for a lossy dielectrically filled rectangular cavity is given by [53]

$$\frac{1}{Q_o} = \frac{1}{Q_{rad}} + \frac{1}{Q_{die}} + \frac{1}{Q_{cu}} \tag{3.35}$$

and is evaluated using [24]

$$Q_{rad} = \frac{\pi W}{4G_{rad}\mu_o h f_{oc} L} \tag{3.36}$$

$$Q_{die} = \frac{1}{\tan\delta} \tag{3.37}$$

$$Q_{cu} = \frac{h}{\delta_s} \tag{3.38}$$

$$G_{rad} = \frac{1}{60\pi^2}\int_0^{\pi} \frac{(1 + J_o(\beta_o L \sin\theta))\sin^2(\frac{\beta_o W}{2}\cos\theta)\sin^3\theta}{\cos^2\theta}\, d\theta \tag{3.39}$$

$$\delta_s = \sqrt{\frac{2}{\omega\mu_o\sigma}} \tag{3.40}$$

The transmission line model for the input impedance of a rectangular patch antenna, to be discussed in Chapter V, can be used to derive an expression for the resonant resistance, r_o, in terms of the radiation conductance

$$r_o = \frac{Z_o}{2G_{rad}} \tag{3.41}$$

where the radiation conductance can be calculated using equation (3.39), or one of the many other expressions to be reviewed in Chapter V.

3.7 Discussion of results

Table 3.1 clearly shows that the agreement between the measured cavity resonant frequencies and those calculated using the formulas of other authors falls off as the frequency is increased. Typically the difference exceeds 2% for frequencies greater than 2.5GHz, and up to an average difference of 5% at 5GHz.

The first and second columns of Table 3.2 compare the measured cavity resonant frequencies with those calculated using equation (3.2), where equations (3.21) and (3.24) were used for the effective dielectric constant and the empirically determined edge extension respectively. The third column of Table 3.2 lists the percentage difference between the measured and calculated frequencies. For frequencies less than 3.5GHz, the agreement between the calculated and measured results is similar to that obtained using the formulas of other authors, as listed in Table 3.1. However the frequencies calculated using the accurately determined parameters are within 2% of measurements for frequencies up to 5GHz. Furthermore there is no indication of the agreement falling off as the frequency increases.

The sixth column of Table 3.2 shows that the maximum percentage difference between the measured and calculated impedance resonant frequencies is less than 2%. The antennas tested represent a wide range of aspect ratios (W/L), substrate heights, feed point positions, and frequencies. The dielectric constant of the substrate materials was between 2.5 and 2.62.

The computational effort required to determine the impedance resonant frequency can be decreased if the resonant resistance, r_o, is assumed to have a value equal to one; that is, the antenna is assumed to be critically coupled to the transmission line feeding it. This assumption was made during the calculation of the results

Cavity and impedance resonant frequencies					
f_{oc} meas'd	f_{oc} calc'd	% error	f_{oz} meas'd	f_{oz} calc'd	% error
633	627	−1.03	634	628	−0.95
658	652	−0.96	658	652	−0.91
1189	1190	+0.09	1190	1193	+0.25
1197	1193	−0.36	1197	1195	−0.17
1396	1389	−0.51	1393	1393	0.00
1410	1392	−1.25	N/A	1396	N/A
2195	2153	−1.93	N/A	2175	N/A
N/A	2203	N/A	2224	2209	−0.70
3387	3422	+1.02	N/A	3428	N/A
3502	3539	+1.06	3507	3547	+1.10
4659	4630	−0.62	N/A	4702	N/A
4744	4725	−0.39	N/A	4751	N/A
4770	4756	−0.29	4778	4779	+0.02
4784	4707	−1.59	4798	4740	−1.20
4792	4805	+0.28	4794	4818	+0.50
4830	4822	−0.17	4833	4835	+0.04
5013	5000	−0.26	5028	5031	+0.06

Table 3.2: Calculated and measured resonant frequencies, where N/A refers to cases where the data was not available.

listed in the fifth column of Table 3.2. The resonant resistance is used in the evaluation of the frequency tuning parameter; equation (3.34). The assumption that the antenna is critically coupled can be justified for two reasons. Firstly, the resonant resistance is difficult to calculate because it depends on the radiation conductance, and it will be shown in Chapter V that the expressions for the radiation conductance proposed by other authors disagree with conductances derived from experiments by up to 70% when used with microstrip elements at frequencies of 5GHz. The second justification

for assuming $r_o = 1$ is that the effect on the calculated impedance resonant frequency is demonstrated in figure 3.5 to be small. Shown are the results of the calculation of the impedance resonant frequency as a function of the resonant resistance. Here f_{oc} has been calculated for a 16.93mm by 16mm by 1.57mm rectangular element to be 5GHz, and when the normalised resonant resistance is equal to one, the corresponding calculated f_{oz} is 5.033GHz. The value of r_o was then varied between 0.6 and 2.5, and the resulting change in f_{oz} expressed as a percentage of 5.033GHz. The figure shows that the impedance resonant frequency is a weak function of the resonant resistance, especially as the coupling moves from critical to over-coupled; that is, r_o greater than one.

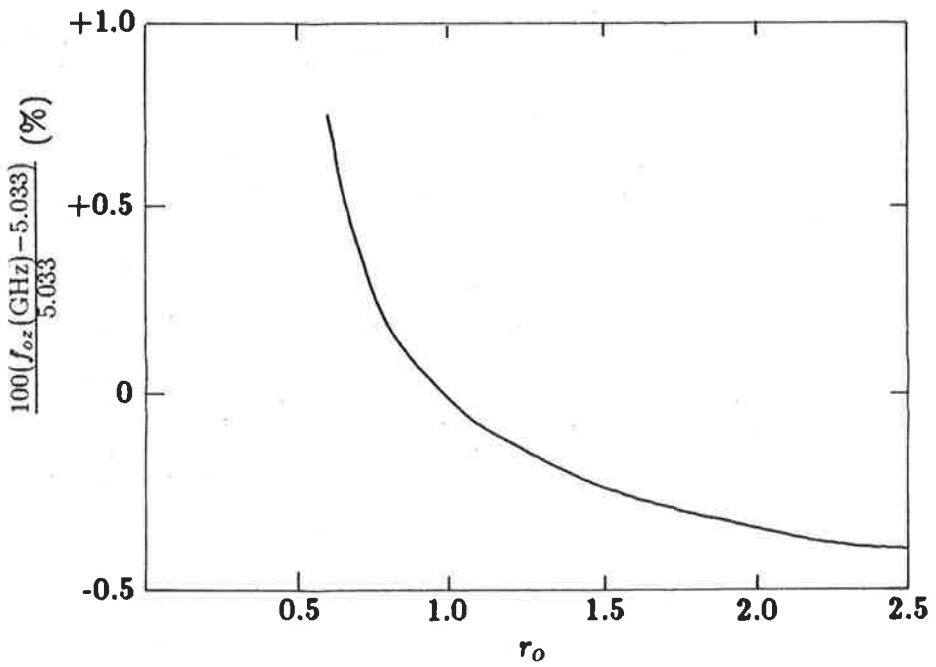

Figure 3.5: Sensitivity of the impedance resonant frequency to the resonant resistance.

Figure 3.6 shows a comparison between the calculated and measured cavity resonant frequencies as a function of the patch width, for a set of antennas of different widths. Notice that the agreement between the two results is independent of width.

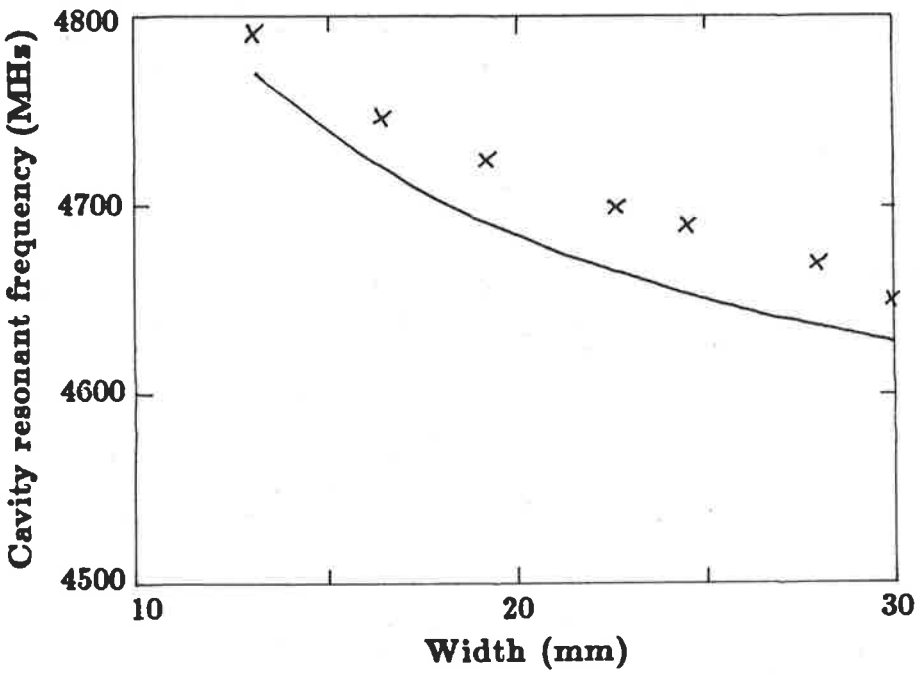

Figure 3.6: Calculated (——) and measured (× × ×) cavity resonant frequency versus the width for a 18.01mm by W by 1.57mm rectangular antenna, where ϵ_r=2.55.

3.6 Conclusions

Specific definitions of the resonant frequencies of a microstrip antenna have been proposed. A new empirical model for the effective edge extension of rectangular microstrip antennas has been shown to provide cavity resonant frequencies that are within 2% of measurements. A method for determining the impedance resonant frequency from the cavity resonant frequency is also proposed; it again provides results that are within 2% of measurements. The models have been tested on a wide variety of antenna geometries, including a study on the variation of the accuracy as a function of the width of the patch. The new formulas represent a significant improvement on those of other authors because of their simplicity and the fact that they produce accurate results up to a frequency of 5GHz.

In the computer-aided design program listed in Appendix C the cavity resonant frequency is calculated from the dimensions of the rectangular patch antenna using equations (3.2), (3.21), and (3.24). The impedance resonant frequency is then calculated from the cavity resonant frequency using equations (3.32) to (3.40), where the series

reactance is calculated using the tapered transmission line model outlined in Chapter II. The value of the resonant resistance is assumed equal to one.

CHAPTER IV

THE APPLICATION OF THE DEFINITION OF BANDWIDTH FOR SINGLE PORT RESONATORS TO MICROSTRIP ANTENNAS

4.1 Introduction

The bandwidth of an antenna can be defined in many ways: in terms of a change in the far field radiation pattern's shape, direction, polarisation, loss in the gain, or an increase in side-lobe levels or, as is usually the case with microstrip antennas, a change in the VSWR. The VSWR definition of bandwidth is however not suitable for comparative studies of bandwidth because it requires the antennas to be matched or driven by the same degree of mismatch. In other words, the VSWR definition is suitable for determining the bandwidth of an antenna by direct measurements where a specific antenna is being tested. However, when studying the effect of antenna geometry on the bandwidth of a family of antennas an experimentally evaluated comparison may be difficult, because the coupling between the feed and each antenna in the investigation may have to be adjusted to give a match at a specific frequency. The bandwidth definition used for single port resonators is applicable to microstrip patch antennas because they are, in essence, cavity resonators with leaky side walls. In this chapter the classical definition of bandwidth is proposed as the most suitable definition for carrying out comparative studies between microstrip antennas.

4.2 The resonant cavity definition of bandwidth

It has already been mentioned in Chapters II and III that the input impedance of a microstrip antenna can be closely approximated by the circular locus that characterises a single mode resonant cavity. The Smith chart of Figure 4.1 shows how the measured input impedance versus frequency locus can be approximated by a circle of best fit, where the measurements were carried out on a 18.1mm by 16mm rectangular patch over a 3.5GHz to 6.5GHz bandwidth; the resonant frequency being about 5GHz. The lumped network model for the approximating circle response is given in Figure 3.4, where R_o represents the sum of the copper and dielectric losses in the cavity as well as the radiation from the cavity. Thus

$$R_o = R_{cu} + R_{die} + R_{rad} \tag{4.1}$$

where $R_{rad} \gg R_{cu} + R_{die}$. The LC terms account for the energy stored in the antenna structure. The X_s term is the equivalent series reactance of the probe, which is only included in the network when probe fed antennas are considered. The series resistance term, R_s, models the gap between the locus and the perimeter of the Smith chart. The gap was originally attributed by Ginzton [41] to resistive losses in the coupling structure. More recently however, Griffin [54] pointed out that the gap is a consequence of the fundamental difference between a distributed parameter resonator, which the antenna is, and a lumped fixed element equivalent circuit: moreover, the gap is mostly due to the residual effects of higher order modes rather than losses in the coupling structure. Therefore let

$$R_s = R_l + R_h \tag{4.2}$$

where R_l represents the losses in the coupling structure, and the energy radiated and dissipated in the higher order modes is represented by the R_h term. For the representation of the antenna operating about a single resonant mode the R_h term can be approximated to zero, and because R_l is negligible in value then to a good approximation R_s can be removed from the circuit model.

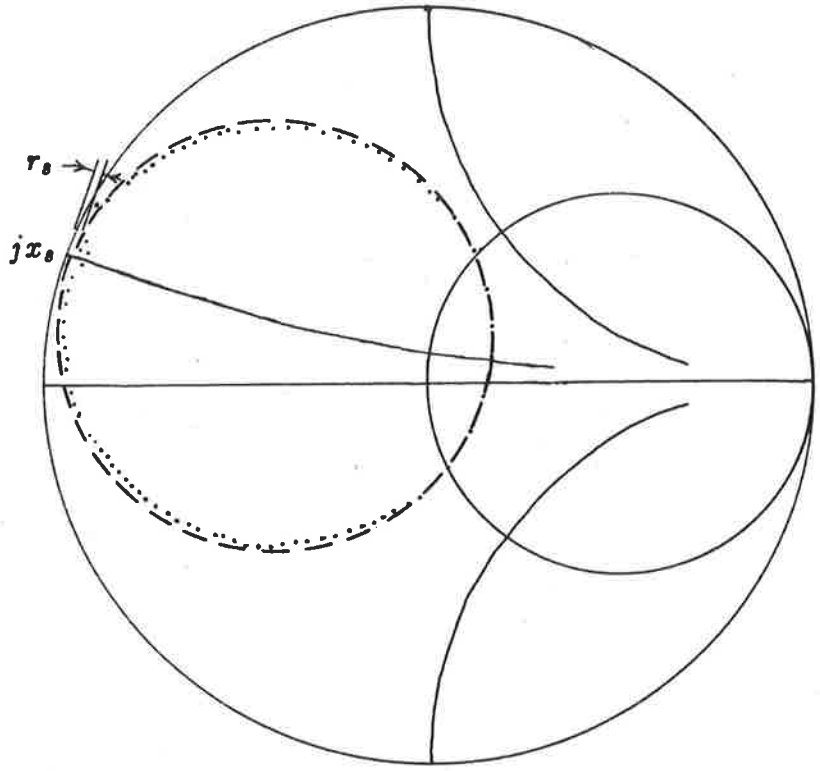

Figure 4.1: The input impedance response of a rectangular microstrip antenna, 18.1mm by 16mm by 1.57mm, D =6mm, $\epsilon_r = 2.55$, measured over a ±30% bandwidth about the resonant frequency: f_{oc} ≈5GHz. Measured data (·····) and the circle approximation (– – –).

The classical method [41] for determining the terminal characteristics of a single port single mode resonator requires that the locus be symmetrical about the real axis of the Smith chart. This is usually achieved by choosing a special reference plane along the transmission line feeding the cavity at which the series reactance term representing the coupling structure disappears. This happens at a series of singular positions, a half wavelength apart, called the detuned-short positions. This shift in the reference plane is usually achieved by rotating the locus around the chart until symmetry about the real axis is achieved, where the off-resonance region of the locus is located near the short circuit end of the chart. It is however more accurate to directly subtract the value of the series reactance, jX_s. The equivalent series reactance of the feed probe is inductive. Therefore, the input impedance locus is made symmetrical about the real axis of the Smith chart by subtracting the value of $j\omega L_s$ from each point on the locus. The resulting

transformed circle of best fit is shown in figure 4.2. For the parallel RLC circuit of figure 3.4, the unloaded quality factor, Q_o, describes the ratio of the energy dissipated to the energy stored within the cavity. The unloaded quality factor can be expressed in terms of the half power point frequencies, f_1 and f_2. These points represent the intersections of the $r = x$ contour with the locus of the transformed impedance. Thus

$$Q_o = \frac{f_{oc}}{f_2 - f_1} \tag{4.3}$$

where f_{oc} is the cavity resonant frequency defined in Chapter III.

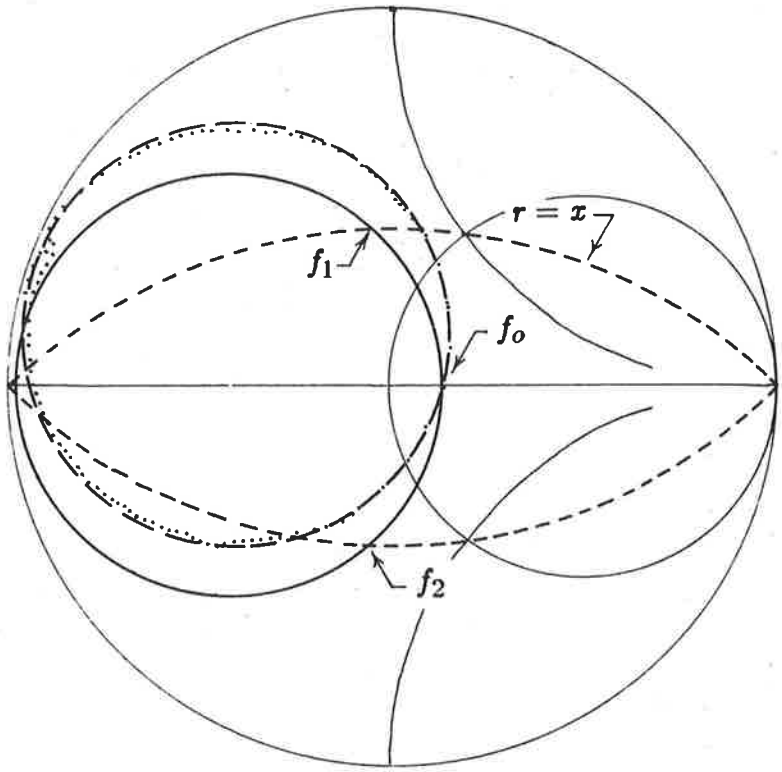

Figure 4.2: The transformed circle approximation for the input impedance response of a rectangular microstrip antenna, 18.1mm by 16mm by 1.57mm, D =6mm, ϵ_r = 2.55, measured over a ±30% bandwidth about the resonant frequency: f_{oc} ≈5GHz.

The loaded quality factor is defined as the ratio of the total reactance to the total series loss, and is a function of the unloaded quality factor, Q_o, and the coupling coefficient, β. Thus

$$Q_L = \frac{Q_o}{1 + \beta} \tag{4.4}$$

and

$$\beta = \beta_1 \frac{1}{1 + x_s^2} \tag{4.5}$$

where β_1 is the ratio of the coupled resistance to the cavity resistance, R_O. When $\beta_1 = 1$ the cavity is critically coupled. When $\beta_1 < 1$ the cavity is under coupled, and over coupled when $\beta_1 > 1$. Also β is related to the resonant resistance by

$$\beta = \begin{cases} r_o & \text{for the over coupled cavity} \\ \frac{1}{r_o} & \text{for the under coupled cavity} \end{cases}$$

When comparing the bandwidths of a number of microstrip antennas, it is helpful to use a definition of bandwidth that is independent of the degree of coupling between the antennas and their respective feeds, which in practice typically means the positions of the feed points along the E-planes of the patches. The bandwidth between the half power point frequencies is expressed in terms of the unloaded coupling factor

$$BW = \frac{1}{Q_o} \tag{4.6}$$

Therefore the bandwidth can be determined for differently shaped patches for comparative bandwidth studies, without the need to match each antenna to the transmission line feeding it.

The application of the single port cavity definition of bandwidth to microstrip antennas is based on the assumption that these antennas can be modelled as cavities with the network model shown in figure 3.4. This assumption can be easily tested because one of the results of the classical theory is that, for the definition of bandwidth based on the unloaded cavity factor, the bandwidth is independent of changes in the coupling coefficient, which in this case is achieved by altering the feed point position. The results of an experimental investigation carried out to test this assumption are show in figure 4.3. Here the bandwidth is calculated from the measured input impedance versus frequency data of a set of rectangular patches and is plotted against the feed point position, D. Here $D \approx 6.4$mm corresponds to a critically coupled antenna, and

$D < 6.4$mm and $D > 6.4$mm corresponds to the over coupled and under coupled cases respectively. The bandwidth can be seen to be almost independent of the changes in the coupling mechanism.

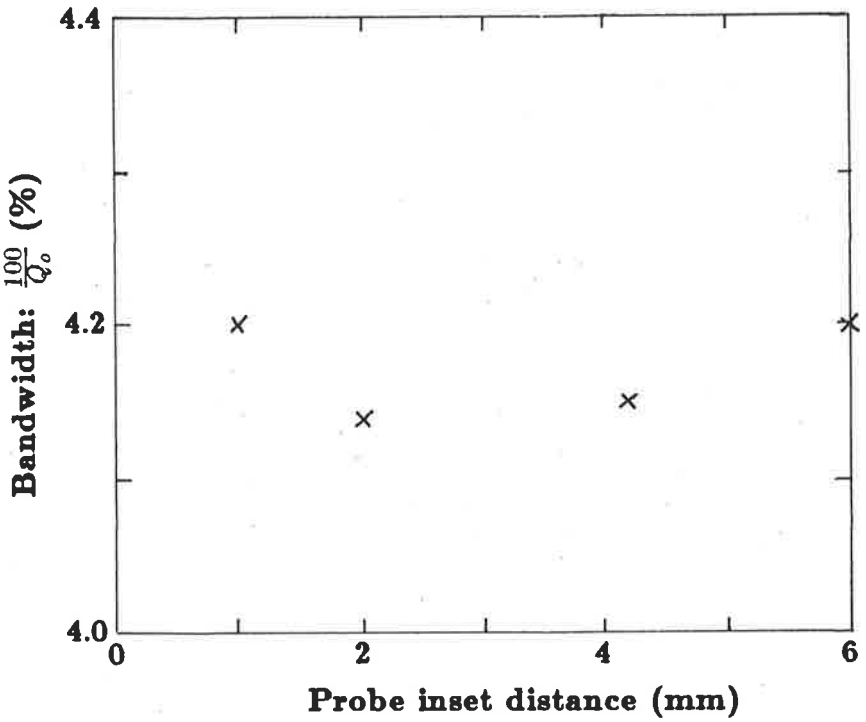

Figure 4.3: Bandwidth versus feed point inset distance for a 18.1mm by 16mm by 1.57mm rectangular element, $f_{oc} \approx 5GHz$, $\epsilon_r = 2.55$.

Specifying an antenna's bandwidth in terms of Q_o has two advantages over specifying it in terms of the VSWR. Firstly, the antenna bandwidth can be investigated without regard for the feeding structure. This means, for example, that the bandwidth of two antennas can be compared even though neither may be matched to its feeding structure nor mismatched by equal amounts. The other advantage of this definition is that once the locus has been transformed so that it is symmetrical about the real axis of the Smith chart, there is no ambiguity in specifying the resonant frequency because

there is now only one frequency at which the input impedance is real, the cavity field structure resonant and the VSWR a minimum.

4.3 Conclusion

The classical definition of bandwidth, as used for single port resonant cavities, is regarded as a more appropriate quantity for comparative studies between microstrip antennas whether they are matched or not. The use for this bandwidth definition will be described in Chapter VIII, where an experimental investigation into the bandwidth performance of a novel hexagonal patch is presented.

CHAPTER V

THE CALCULATION OF THE INPUT IMPEDANCE USING THE TRANSMISSION LINE MODEL WITH EMPIRICALLY DETERMINED APERTURE ADMITTANCES

5.1 Introduction

The accuracy of the original models devised for designing rectangular microstrip antennas can be improved if new empirical formulas are used to determine key parameters in these simple models. The particular quantity for which new formulas are proposed is the equivalent impedance of the radiating apertures that are assumed to be located at each end of the antenna element. These quantities are incorporated in a simple model that consists of two aperture antennas separated by a low characteristic impedance microstrip transmission line that is connected part way along its length to a coaxial feed line. In the past the model has predicted resonant frequencies and input impedances that were only in agreement with measurements at low frequencies, which led to the discarding of the simple transmission line model in favour of more comprehensive modal-expansion cavity models [29,32]. It will be shown that the empirical formulas for parameters presented here give design results that are in accurate agreement with measurements for the input impedances of rectangular elements operating at frequencies up to 5GHz.

5.2 Survey of the methods used to calculate the effective aperture admittance at each end of the patch

A major part of modelling the input impedance and far field radiation pattern is the determination of the effective admittance which the walls present to the fields within the cavity. When the resonant frequency was initially considered, the antenna was modelled as a lossless cavity bounded by two short circuit and four open circuit walls. This rudimentary model predicts frequencies that are higher than those measured because it ignores the extent to which the fields fringe beyond the physical dimensions of the patch. The radiated and stored power associated with the fringing fields are represented by an effective aperture admittance. For the case of a rectangular element, the side walls are assumed to be open circuited and the effective aperture admittances of the two end walls are determined by modelling them as radiating apertures, both with input admittances, Y_a, referred to as the aperture admittance. This parameter is also referred to in the literature as the wall admittance. There are no rigorous solutions for the aperture admittance, but several authors have published approximate solutions and the results of these formulas will now be reviewed, tested, and compared.

One appropriate model for the aperture admittance has been developed by Marcuvitz [42] for the case of a semi-infinite parallel-plate feeding an aperture in a ground plane which is then radiating into free space. If the height of the guide is h', then the expressions in units of mho per unit length of aperture are

$$G_a \approx \frac{Y_o \pi h'}{2\lambda_o} \tag{5.1}$$

$$B_a \approx \frac{2Y_o h'}{\lambda_o} \ln\left(\frac{e\lambda_o}{\gamma h'}\right) \tag{5.2}$$

where Y_o is the characteristic admittance of the air-filled guide, and is given by

$$Y_o = \frac{1}{\eta_o h'} \tag{5.3}$$

and

$$e = 2.71828$$

$$\gamma = 1.78107$$

These formulas have been applied to microstrip antennas by Sengupta [16]. If a rectangular antenna of width W is mounted on an substrate of thickness h, then

$$Y_{om} = \frac{\alpha W \sqrt{\epsilon_e}}{h\eta_o} \quad \text{mho} \tag{5.4}$$

where

$$\alpha = 1 + 1.393(h/W) + 0.667(h/W)\ln(W/h + 1.44) \tag{5.5}$$

Then

$$G_a = \frac{Y_{om}\beta_s h}{2\alpha\epsilon_e} \quad \text{mho} \tag{5.6}$$

$$B_a = \frac{Y_{om}\beta_s h}{\pi\alpha\epsilon_e} \ln\left(\frac{\sqrt{\epsilon_e}2\pi e}{\gamma\beta_s h}\right) \quad \text{mho} \tag{5.7}$$

where

$$\beta_s = \beta_o\sqrt{\epsilon_e} \tag{5.8}$$

Sengupta's equations for the admittance of the radiating apertures can be derived from the expressions of Marcuvitz by firstly taking into account the image beneath the ground plane of the aperture at each end of the antenna. Thus

$$h' = 2h \tag{5.9}$$

is substituted into equations (5.1) and (5.2). Secondly because the characteristic impedance of the transmission line between the ends of the antenna is independent of any radiation considerations, Sengupta has substituted

$$h' = h \tag{5.10}$$

into equation (5.3). When both these substitutions are made equations (5.6) and (5.7) are the result.

Another expression that has been widely used with the transmission line model was proposed by Harrington [9] for the input admittance of a parallel-plate guide feeding an aperture in a metallic plane, and radiating into a half-space. The expressions for a slot of width h in units of mho per unit length are

$$G_a = \frac{\pi(1 - \frac{(\beta_o h)^2}{24})}{\eta_o \lambda_o} \tag{5.11}$$

$$B_a = \frac{3.135 - 2\log\beta_o h}{\eta_o \lambda_o} \tag{5.12}$$

where the aperture is assumed narrow; that is $h/\lambda_o \leq 0.1$. Expression (5.12) is based on the quasi-static capacitance associated with the fields fringing from the end of the antenna element.

Derneryd [12] suggested modelling the aperture admittance as the input impedance of an equivalent slot radiator above the ground plane. Referring to figure 1.5, the length and width of the slots at each end of the transmission line are respectively W and h, and the electric field distribution across the slot is constant in the y-direction. The radiation field was determined by replacing the slot's electric field by a longitudinal magnetic current distribution. The effect of the image slot beneath the ground plane was taken into account by multiplying the magnitude of the magnetic current by a factor of two. The slot's radiation conductance was determined by integrating the real part of the Poynting vector over a hemisphere of large radius. The approximate solutions in the units of mho are

$$G_a = \begin{cases} \frac{W^2}{90\lambda_o^2} & W \leq \lambda_o \\ \frac{\pi W}{\eta_o \lambda_o} & W > \lambda_o \end{cases} \tag{5.13}$$

The aperture's input susceptance was obtained using a static capacitance representation of the fringing field in the region beyond the end of a microstrip transmission line. The equivalent capacitance of the slot is

$$C_a = \frac{\delta L}{v_{ph} Z_{om}} \tag{5.14}$$

where v_{ph} is the substrate phase velocity and Z_{om} is the characteristic impedance of

the microstrip line. The approximate expression [14] for the edge extension is

$$\delta L = 0.412h\frac{\epsilon_e + 0.300\,W/h + 0.262}{\epsilon_e - 0.258\,W/h + 0.813} \tag{5.15}$$

where ϵ_e is the effective dielectric constant.

Carver [32] assumes the aperture conductance is that of a parallel-plate TEM waveguide slot radiating into a half-space, and suggests using an approximation to Harrington's [9] expression for a narrow slot,

$$G_a = \frac{\pi W}{\eta_o \lambda_o} \quad \text{mho} \tag{5.16}$$

This expression is used on the assumption that only a dominant TM_{10} mode is excited in the cavity. Therefore the waves within the cavity are normally incident on the two radiating ends of the antenna producing uniform field intensities across each aperture. Carver also suggests that the susceptance may be approximated using Hammerstad's [14] formula for the capacitance of an open circuited microstrip line

$$B_a = \frac{0.01668\delta LW\epsilon_e}{h\lambda_o} \quad \text{mho} \tag{5.17}$$

Carver [32] goes on to suggest an empirical modification to the aperture admittance given by equations (5.16) and (5.17). This modification is based on an analysis of the zig-zag nature of the quasi-TEM plane waves in the cavity reported by Chang and Kuester [55]. The analysis of this condition was carried out as a function of the patch aspect ratio, W/L, and showed that the aperture admittance is a function of both the frequency and the angle of incidence of waves on the cavity walls, suggesting that the normal incidence assumed above is inadequate. By probing the fields near the cavity's walls, Carver has shown empirically that expressions (5.16) and (5.17) may be multiplied by an aspect ratio factor given by

$$F(W/L) = 0.7747 + 0.5977(W/L - 1) - 0.1638(W/L - 1)^2 \tag{5.18}$$

which is recommended to provide improved agreement with the measured input impedance loci of microstrip antennas operating at frequencies lower than about 3.5GHz.

Newman [19] also recommended using Carver's equations (5.16) and (5.17). However Newman has incorrectly quoted Carver for the conductance equation. Newman published the expression

$$G_a = \frac{\pi W}{\eta_o \lambda_s} \quad \text{mho} \tag{5.19}$$

where

$$\lambda_s = \frac{\lambda_o}{\sqrt{\epsilon_e}} \tag{5.20}$$

which is only true if the free space wavelength in Carver's equation (5.16) is replaced by the substrate wavelength.

5.2.1 A comparison between the aperture admittance formulas

For typical microstrip antenna geometries, where $(\beta_o h)^2/24 \ll 1$, equation (5.11) reduces to (5.16) and (5.13) for the aperture conductance when $W > \lambda_o$. Equations (5.11) and (5.6) can be derived when (5.3) is substituted into (5.1). Also (5.19) is equivalent to (5.11) using the substrate wavelength. Furthermore each of the formulas imply that the conductance is proportional to the effective electrical width of the aperture. The main difference between them is the constant factor.

For the aperture susceptance, (5.12) was obtained using a quasi-static capacitance approach, while (5.14) and (5.17) were determined using the static capacitance. Also equation (5.17) can be derived from (5.14) using:

$$| B_a | \approx | \omega C_a | \tag{5.21}$$

$$Z_{om} \approx \frac{h\eta_o}{W\sqrt{\epsilon_e}} \tag{5.22}$$

$$v_{ph} = \frac{\omega}{\beta_o \sqrt{\epsilon_e}} \tag{5.23}$$

$$\beta_o = \frac{2\pi}{\lambda_o} \tag{5.24}$$

Also expression (5.7) can be derived from (5.2). The similarities in the susceptance expressions are not as obvious as those found with the conductance. However in the next paragraph they are evaluated and shown to produce similar susceptance versus frequency characteristics. The main difference again being the factor of proportionality.

Figures 5.1(a) and (b) compare these published aperture admittances for a typical antenna geometry operating at about 1.4GHz. Because of the large variation between the results of the different formulas, it is concluded that the input impedance results obtained using the transmission line model are greatly dependent on the choice of the correct aperture admittance. Each of the formulas was used in turn with the transmission line model to calculate the input impedance and the results compared with measurements for the case of $f_{oc} \approx 1.4$GHz. The best agreement was obtained with Carver's expressions (5.16), (5.17) and (5.18). The calculated and measured input impedances are shown in figure 5.2. The same equations also provide useful results at 2.2GHz, shown in figure 5.3, but are shown in figure 5.4 to be worthless when applied to an antenna operating at about 5GHz.

It is therefore necessary to develop accurate empirical equations for the aperture admittance that are applicable to rectangular elements on electrically thick substrates; that is, during operation at mid-microwave frequencies, say 5GHz for example.

5.3 The determination of an empirical equation for the aperture admittance

Modelling the microstrip antenna as a multi-mode lossy cavity has tended to replace the transmission line model in recent work. However, if the width of the patch is restricted, then the fundamental resonant mode field distributions are the same for both the transmission line and the cavity models. Therefore good results might be expected for the transmission line model if its parameters are empirically determined to account for the residual effects of other modes.

The transmission line model is used to derive an empirical equation for the aperture admittance parameter. The input admittance of the similar effective aperture

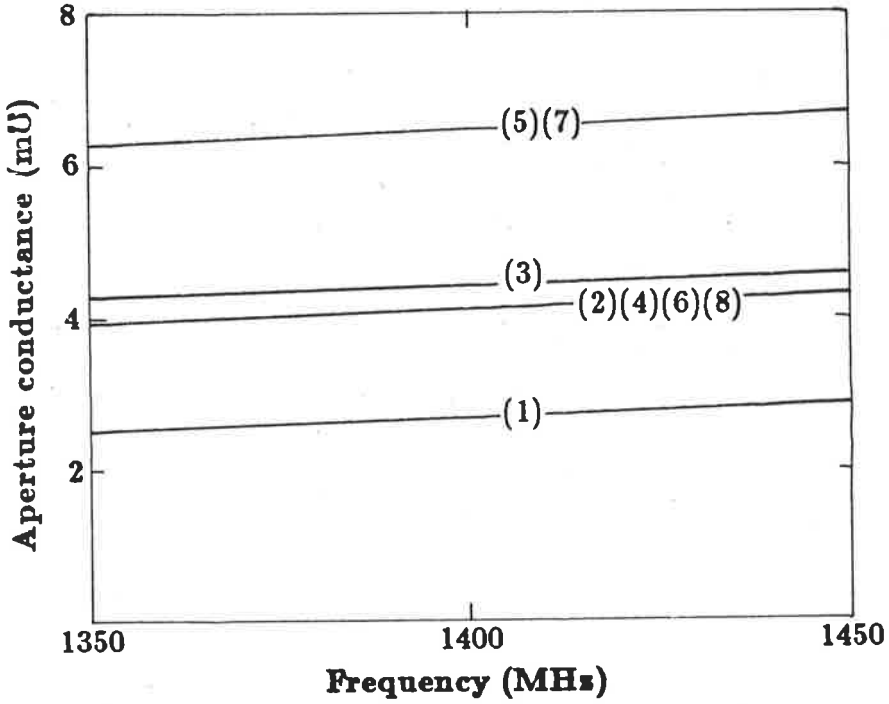

(a)

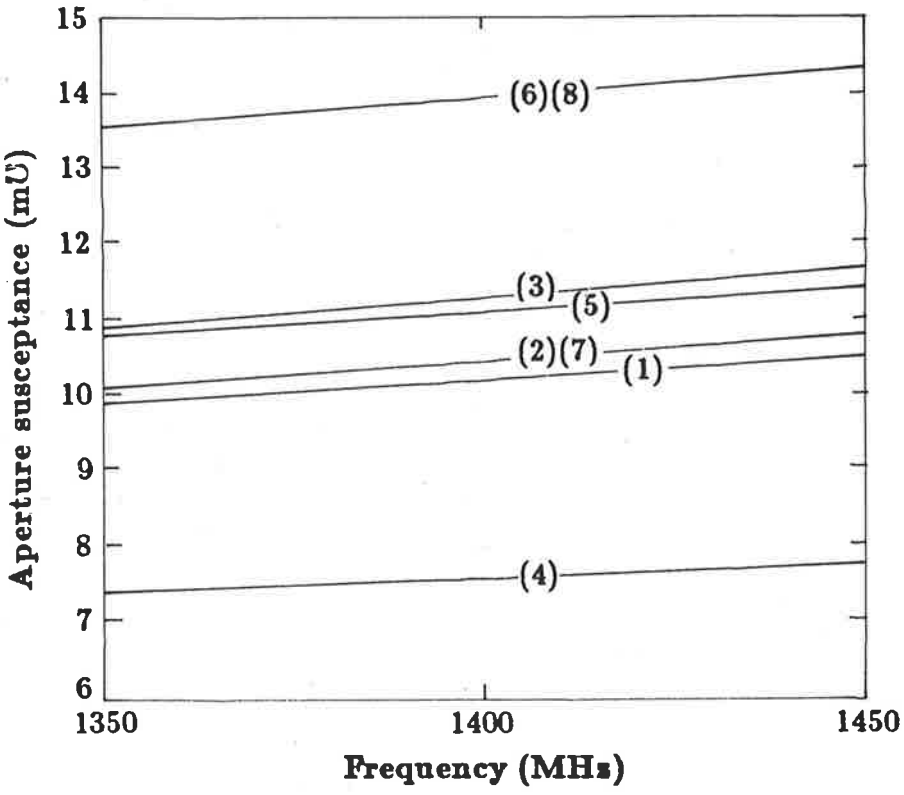

(b)

Figure 5.1: Calculated aperture conductances (a) and susceptances (b) using the published equations for a rectangular element: 65.5mm by 105.6mm by 1.57mm, SMA, D=17mm, ϵ_r = 2.55: (1) Derneryd, (2) Carver, (3) Carver with aspect ratio factor, (4) Harrington using λ_o, (5) Harrington using λ_s, (6) Marcuvitz, (7) Newman, and (8) Sengupta.

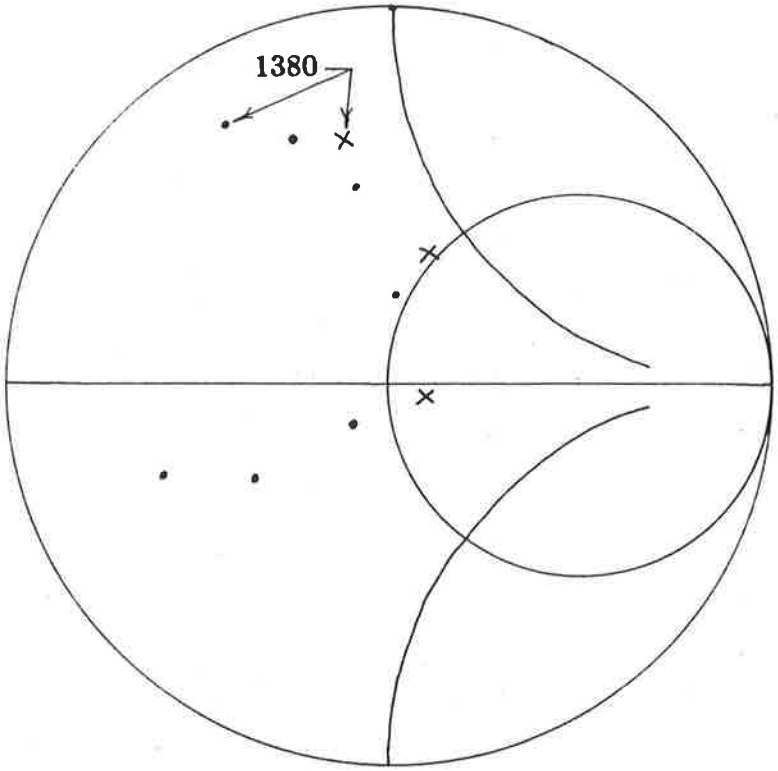

Figure 5.2: Measured (× × ×) and calculated (• • •) input impedances using Carver's aperture admittance for a rectangular element: 65.5mm by 105.6mm by 1.57mm, SMA, D=17mm, $\epsilon_r = 2.55$, where f=1380MHz plus 10MHz increments.

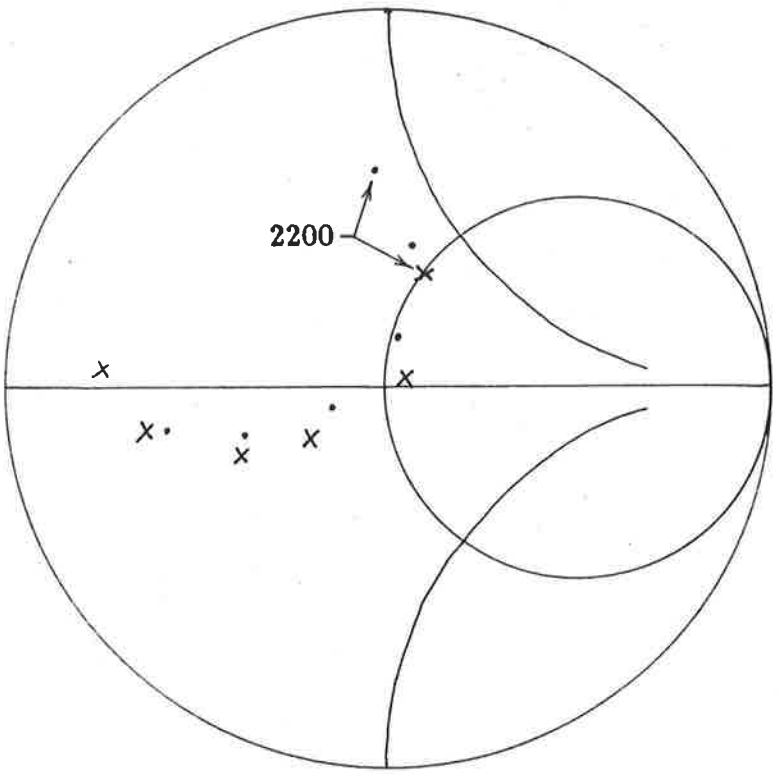

Figure 5.3: Measured (× × ×) and calculated (• • •) input impedances using Carver's aperture admittance for a rectangular element: 41.4mm by 68.58mm by 1.59mm, SMA, D=10.16mm, $\epsilon_r = 2.5$, where f=2200MHz plus 20MHz increments.

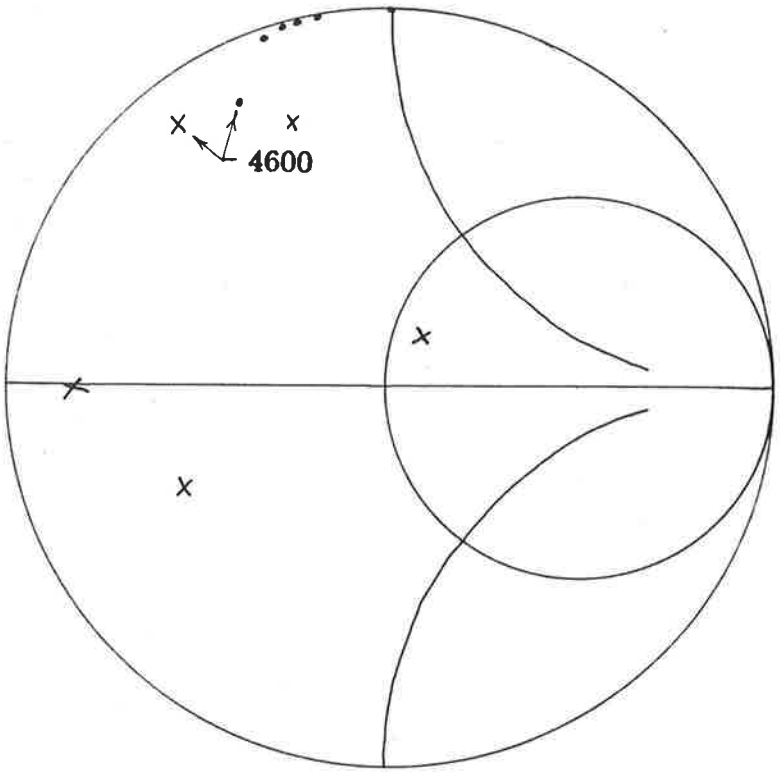

Figure 5.4: Measured (× × ×) and calculated (• • •) input impedances using Carver's aperture admittance for a rectangular element: 16.93mm by 16mm by 1.57mm, APC-7, D=5.5mm, $\epsilon_r = 2.55$, where f=4600MHz plus 200MHz increments.

antennas, one at each end of the line, is determined using measured input impedance data. The calculated aperture admittances resulting from this technique will be referred to as empirical admittances. Where necessary the effect of the feed probe is modelled by a series reactance, the value of which is determined using the locus transformation method already outlined in Chapter II. This derivation of the empirical admittances has been completed for two rectangular elements: 18.03mm by 16mm and 16.93mm by 16mm, both mounted on 1.57mm thick substrates each having a dielectric constant of 2.55. Figures 5.5(a) and (b) show the empirical aperture admittances together with values obtained using the formulas of other authors. The figures also show the close agreement between the two sets of empirical conductance and susceptance data. It is interesting to note that Derneryd's expressions (5.13) and (5.14) can be modified to achieve better agreement with the empirical values. This is done by using the conductance expression for a long aperture, even though for the apertures under consideration

$W/\lambda_0 = 0.27$. Also the susceptance is calculated using equation (5.14) with the empirically determined expression for δL, equation (3.24), and Getsinger's equation (3.21) for the effective dielectric constant. In contrast, Derneryd recommended using equations (1.10) and (1.9) for the edge extension and the effective dielectric constant, respectively. With these modifications Derneryd's formulas for the aperture admittance give results that are close to the empirically derived aperture admittance. Figure 5.6 shows the calculated input impedance locus using these modified equations for the aperture admittance. There is a 1% error in the impedance resonant frequency and a 12% error in resonant resistance when the results are compared with measurements. However this excellent agreement is not maintained over a very large frequency range. Therefore due to the sensitivity of the calculated input impedance to the aperture admittance, it is necessary to determine an accurate empirical equation for the aperture admittance.

A simple approach to the determination of an empirical model for the aperture admittance of antennas operating at around 5GHz might be the approximation of the empirical aperture data shown in figure 5.5 by lines of best fit. This approach would provide very accurate input impedances for antennas operating at about 5GHz, but would be of limited use at other frequencies and geometries. Instead it was decided to aim at developing a set of equations that will enable the transmission line model to be used to calculate the input impedance to sufficient accuracy for the design of antennas operating over a wide range of frequencies; say 0.5GHz to 5GHz.

The modified set of Derneryd's equations are in fair agreement with measurements so they are used as a starting point in the development of new empirical equations for the aperture admittance. Derneryd's equations (5.13) and (5.14) can be used to show that the conductance is a function of the effective electrical length of the aperture, while the susceptance is a function of the effective electrical length of the aperture and the edge extension normalised to the substrate thickness. That is,

$$G_a = \text{function}\left(\frac{W}{\lambda_0}\right) \tag{5.25}$$

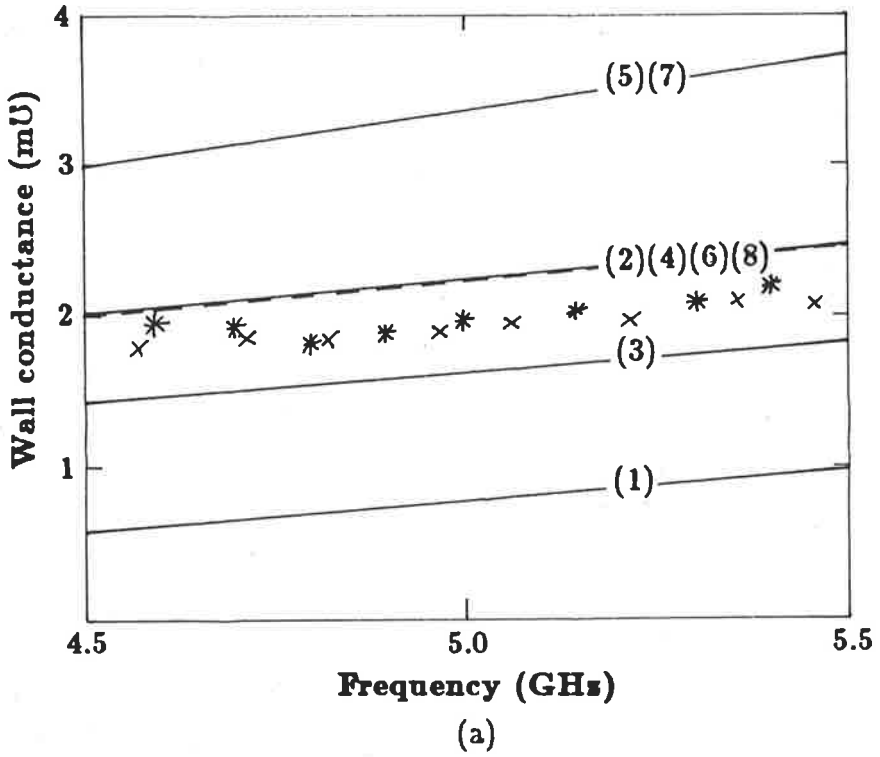

(a)

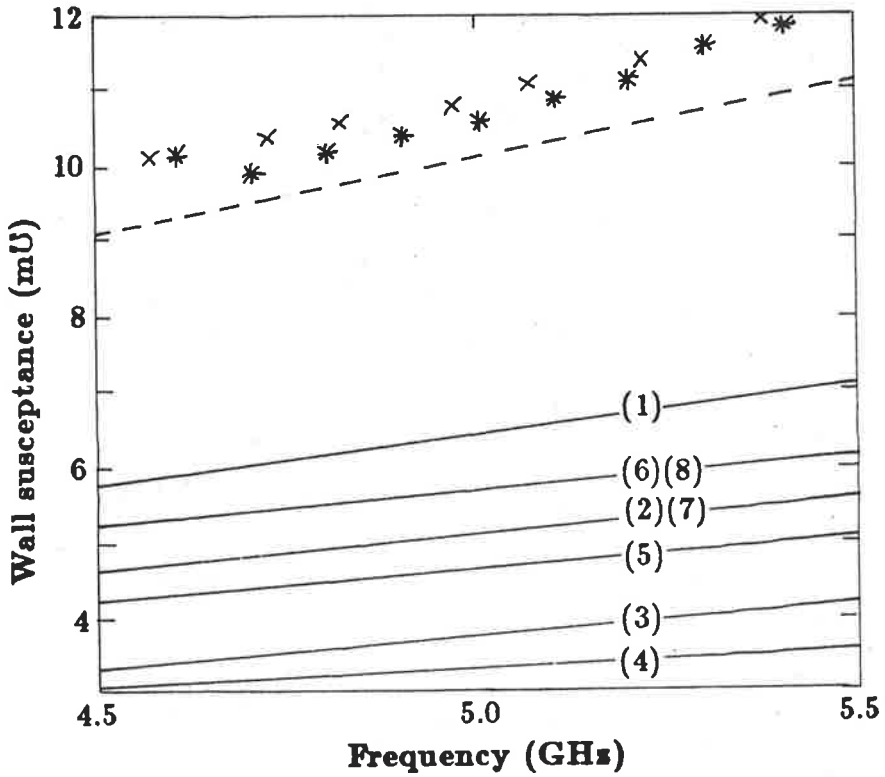

(b)

Figure 5.5: Aperture conductances (a) and susceptances (b) versus frequency for a rectangular element: 16.93mm by 16mm by 1.57mm, APC-7, D=5.5mm, $\epsilon_r = 2.55$: (1) Derneryd, (2) Carver, (3) Carver with aspect ratio factor, (4) Harrington using λ_o, (5) Harrington using λ_s, (6) Marcuvitz, (7) Newman, (8) Sengupta, Empirical: 16.93mm by 16mm by 1.57mm (×) and 18.03mm by 16mm by 1.57mm (✱), and Modified Derneryd (− − −).

and

$$\omega C_a = \text{function}\left(\frac{\delta L}{h}\frac{W}{\lambda_o}\right) \tag{5.26}$$

The aperture susceptance can also be considered in terms of a classical parallel-plate capacitor, where the equivalent capacitor has a plate area of δL by W and a plate separation of h. It is worth noting that the ratio $\delta L/h$ only varies between 0.7 and 0.9 for typical antenna geometries. Therefore it is concluded that the aperture susceptance, like the conductance, is predominantly a function of the effective electrical length of the aperture.

An experiment was carried out to determine the empirical aperture admittance as a function of the aperture dimensions using a 16.93mm long antenna on a 1.57mm thick substrate of dielectric constant 2.55. The width of the patch was varied between 13mm and 30mm. The empirical conductance data is given in figure 5.7, and approximated by the exponential equation of best fit

$$G_a = \frac{546}{10^6} e^{\frac{4.47W}{\lambda_o}} \quad \text{mho} \tag{5.27}$$

The aperture susceptance is graphed in figure 5.8, and the straight line of best fit is

$$\omega C_a = 0.0455\frac{\delta L}{h}\frac{W}{\lambda_o} + \frac{5}{10^4} \tag{5.28}$$

Strictly speaking ωC_a is an approximation to the aperture susceptance because a susceptance is only the reciprocal of the reactance when the resistance is equal to zero. Therefore an iterative routine is used to determine the aperture admittance from the aperture conductance, G_a, and reactance, $1/\omega C_a$.

Notice that both the aperture conductance and susceptance are increasing functions of the frequency. This is because these aperture admittance parameters now include many other characteristics of the antenna that were hitherto ignored in the transmission line model. For example, copper and dielectric losses are combined with the aperture conductance, and the aperture susceptance includes the energy stored in

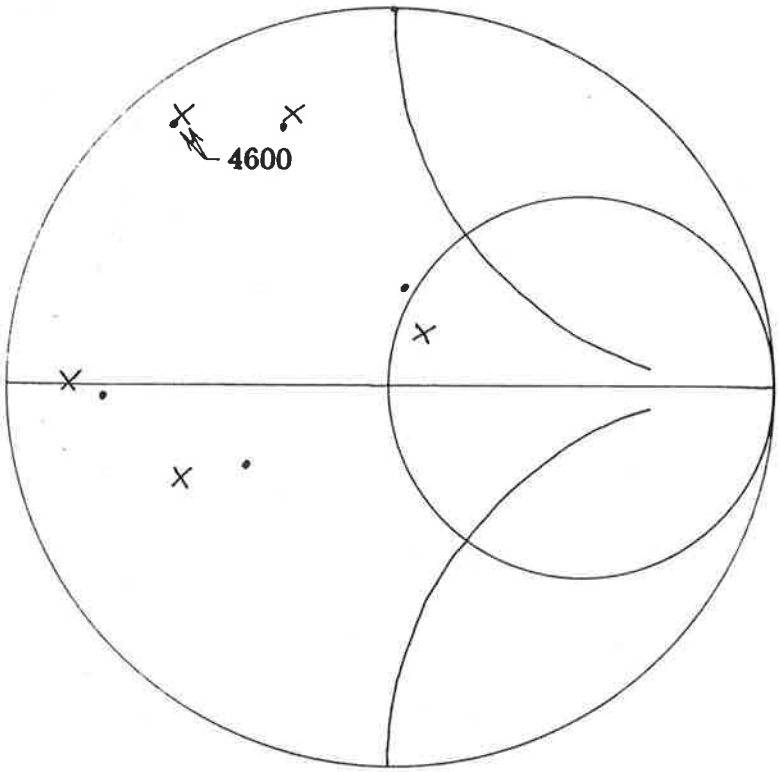

Figure 5.6: Measured (× × ×) and calculated (• • •) input impedances using a modified set of Derneryd's equations for the aperture admittance of a rectangular element: 16.93mm by 16mm by 1.57mm, APC-7, D=5.5mm, $\epsilon_r = 2.55$, where f=4600MHz plus 200MHz increments.

evanescent modes. These parameters also account for the residual effects of higher order modes.

5.4 Calculating the input impedance using the empirically determined aperture admittance parameters

The transmission line model as described by equation (1.15) in Chapter I is now used with the empirically determined aperture admittances to calculate the input impedance loci of a number of rectangular elements of differing feed types, and operating from 600MHz to 5GHz. The tapered transmission line model described in Chapter II is used to model the effects of the feed when probe fed structures are considered.

Figures 5.9 and 5.10 show the combination of results for four 5GHz antenna elements on 1.57mm and 0.8mm thick substrates fed through APC-7 and SMA probes.

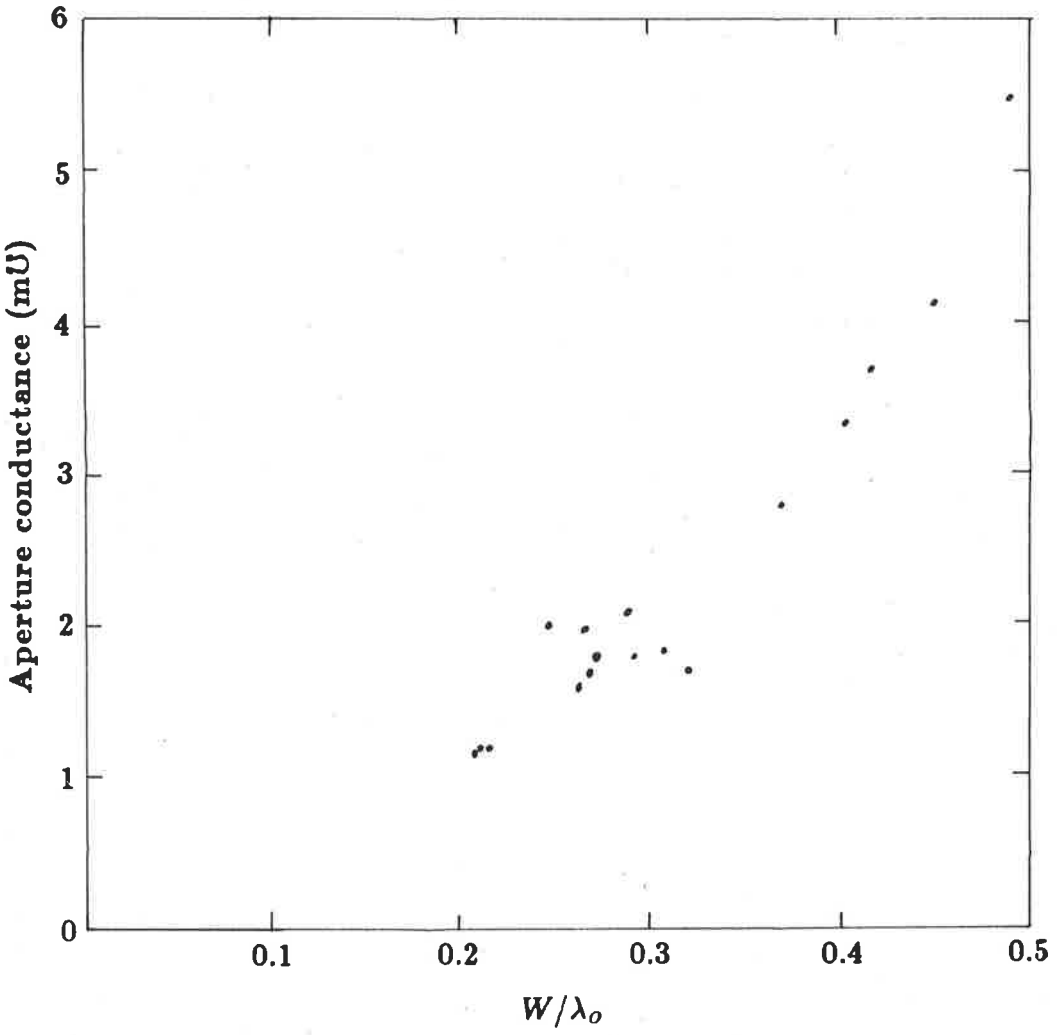

Figure 5.7: Empirical aperture conductance versus aperture width.

It can be seen that the proposed models provide good results for different feeds and substrate thicknesses. It is also concluded that the previous assumptions are acceptable. That is, the aperture conductance is independent of the substrate thickness and the aperture susceptance is only weakly dependent on the ratio of the effective edge extension to the substrate thickness. Figure 5.11 also shows good agreement between calculated and measured results for extremes in patch aspect ratio, 0.8 and 1.65 respectively. Figures 5.12 and 5.13 demonstrate that the accuracy of the models is maintained as the frequency is decreased. Shown are the calculated and measured input impedance loci for elements operating at 3.5, 2.2, 1.2 and 0.63GHz respectively. Notice also that the 1.2GHz element in figure 5.13(a) is fed through a microstrip transmission line.

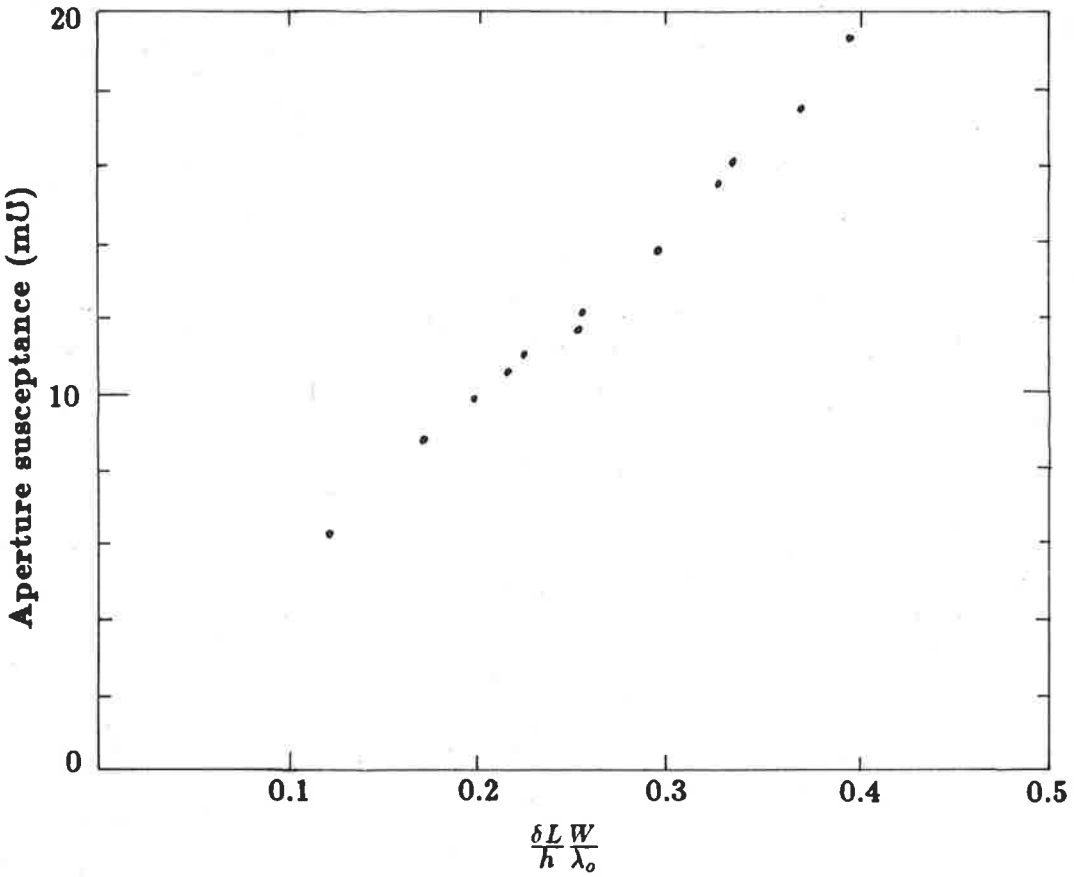

Figure 5.8: Empirical aperture susceptance versus aperture dimensions.

Where they exist, table 5.1 lists the resonant resistances and impedance resonant frequencies for the antennas under consideration, together with the percentage errors between the calculated and measured results.

5.5 Conclusions

The accuracy of the transmission line model in determining input impedances of rectangular microstrip antennas has been greatly improved by the use of accurately determined empirical equations for the input admittances of the effective apertures located at each end of the transmission line where, if necessary, the effects of the feed probe are evaluated using the tapered transmission line model. The accuracy of this impedance modelling combination has been extensively tested on typical antenna ge-

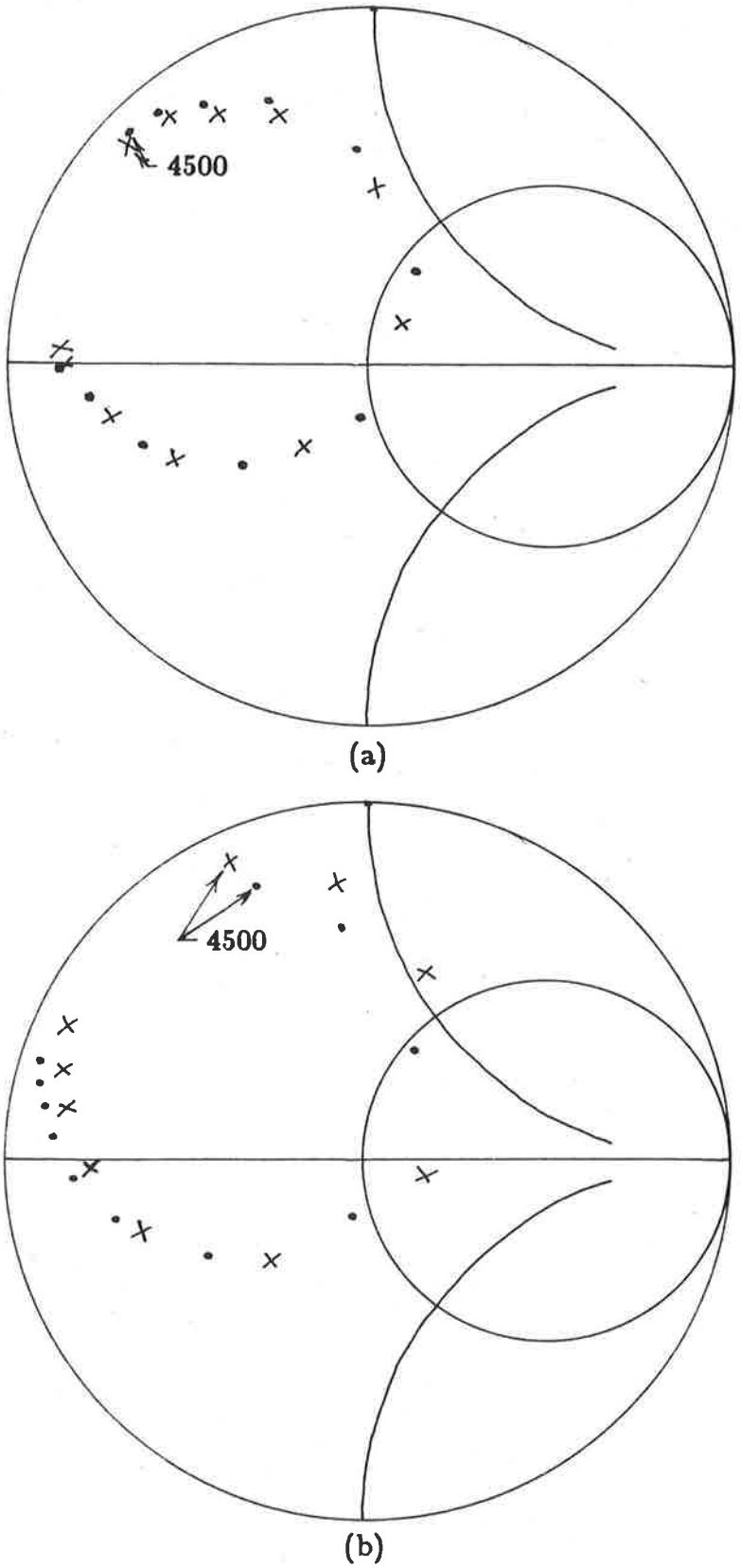

Figure 5.9: Calculated (• • •) and measured (× × ×) input impedances for rectangular elements with W=16mm, ϵ_r = 2.55, h=1.57mm: (a) L=16.93mm, D=5.5mm, APC-7 and (b), L=18.11mm, D=6mm, SMA, where f=4500MHz plus 100MHz increments.

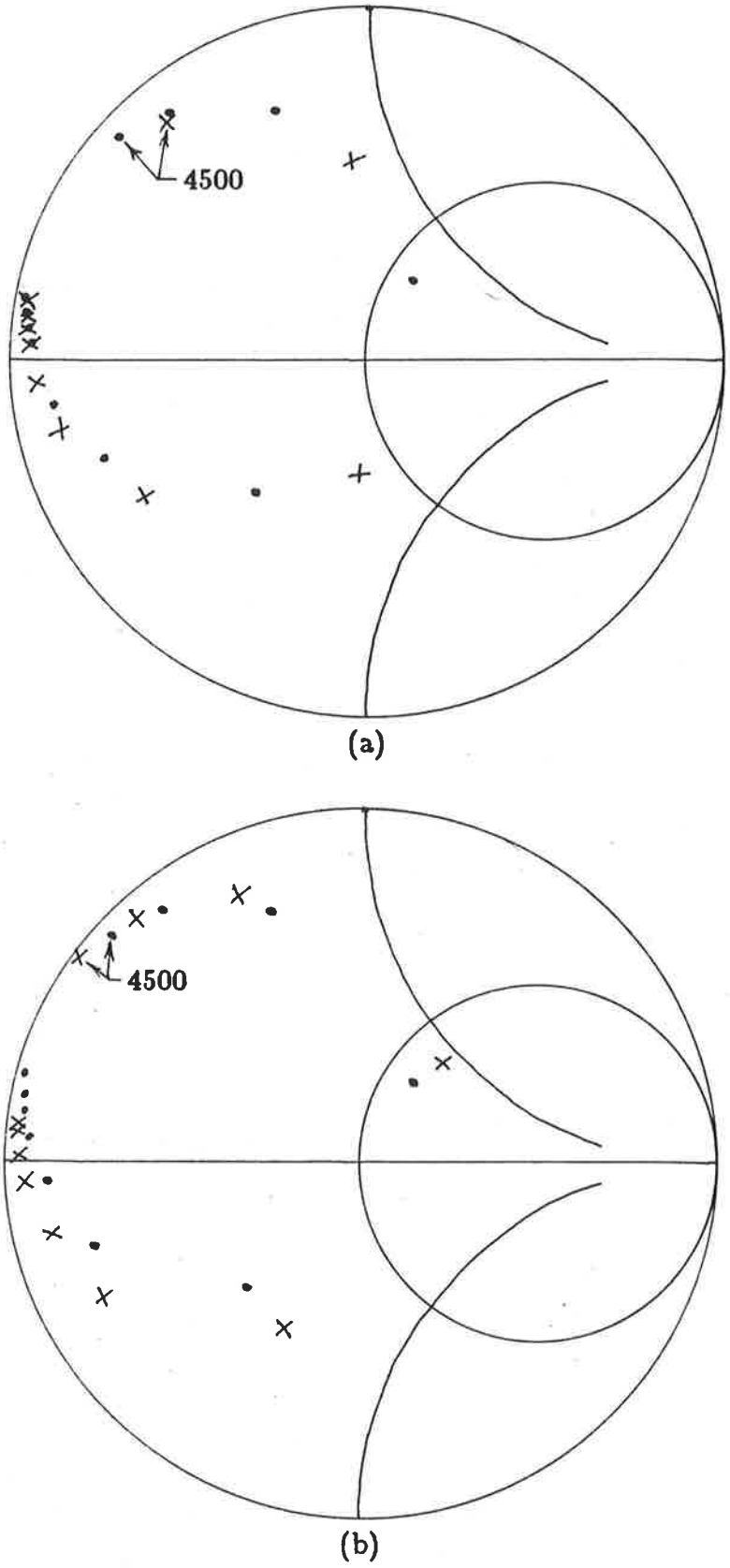

Figure 5.10: Calculated (• • •) and measured (× × ×) input impedances for rectangular elements with ϵ_r = 2.55, h=0.8mm: (a) L=18.47mm, APC-7, D=6.14mm and (b), L=18.47mm, SMA, D=6.14mm, where f=4500MHz plus 100MHz increments.

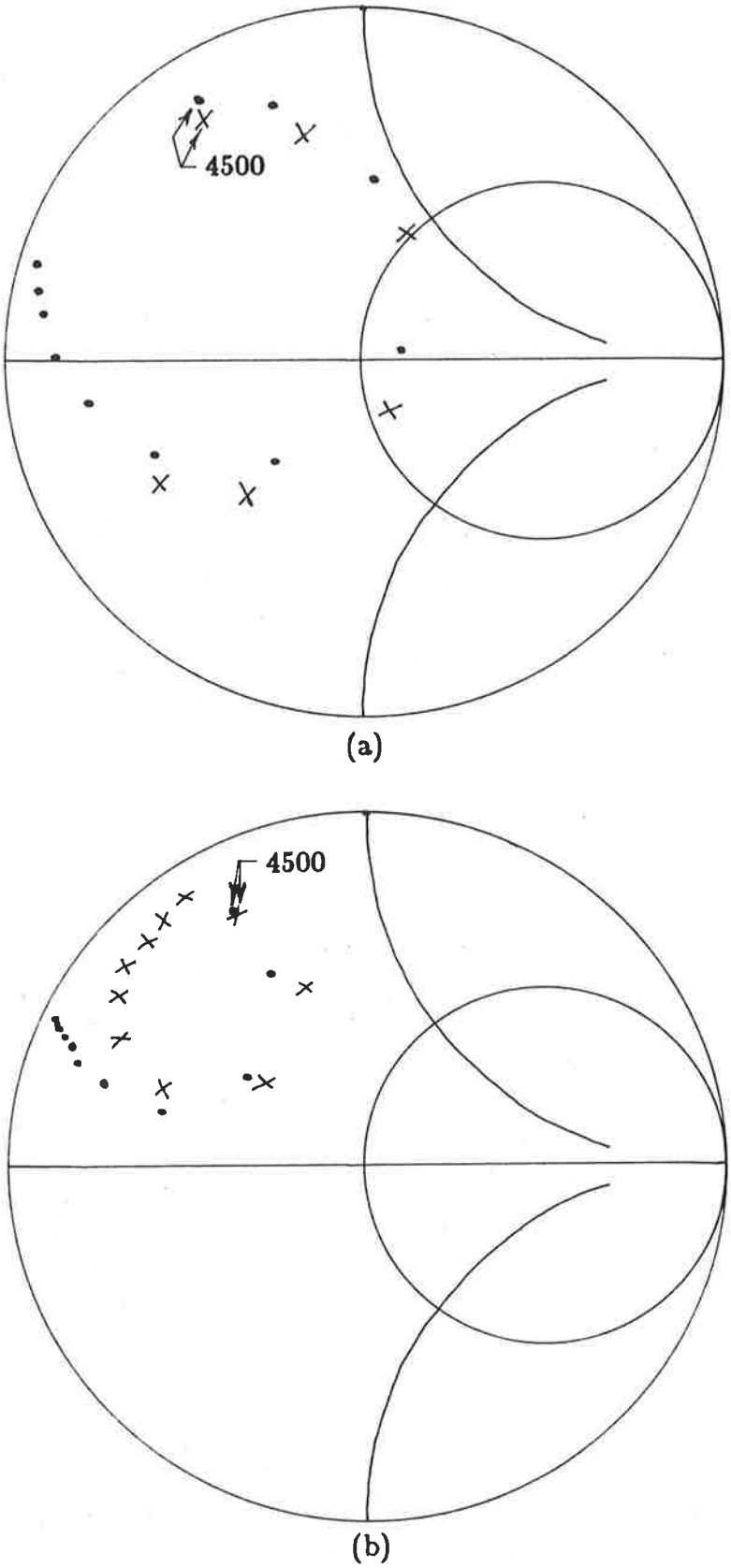

Figure 5.11: Calculated (• • •) and measured (× × ×) input impedances for rectangular elements with L=18.03mm, h=1.57mm, ϵ_r = 2.55, APC-7, D=6.21mm, where (a) W=13.5mm, and (b) W=28mm, where f=4500MHz plus 100MHz increments.

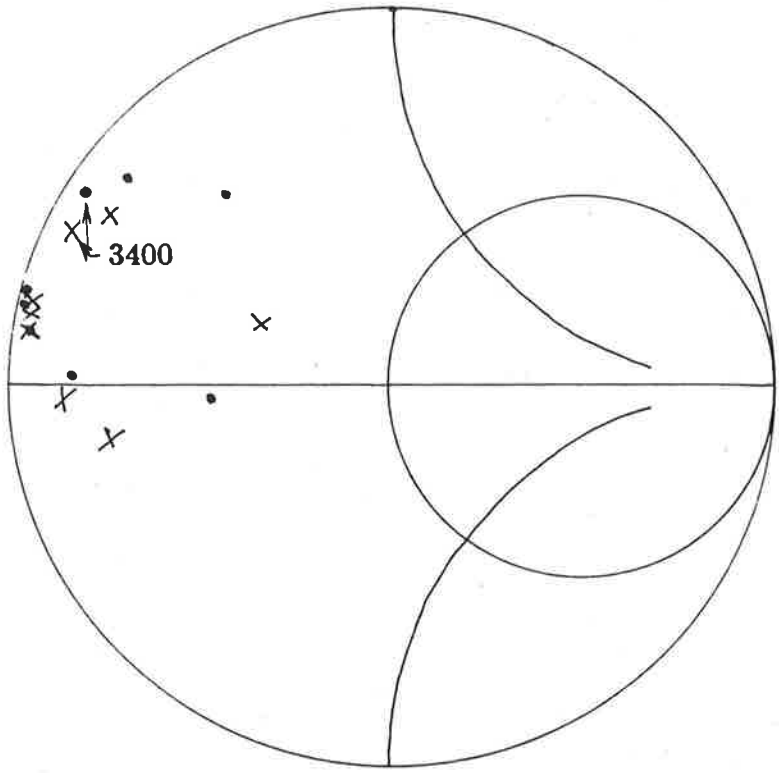

(a)

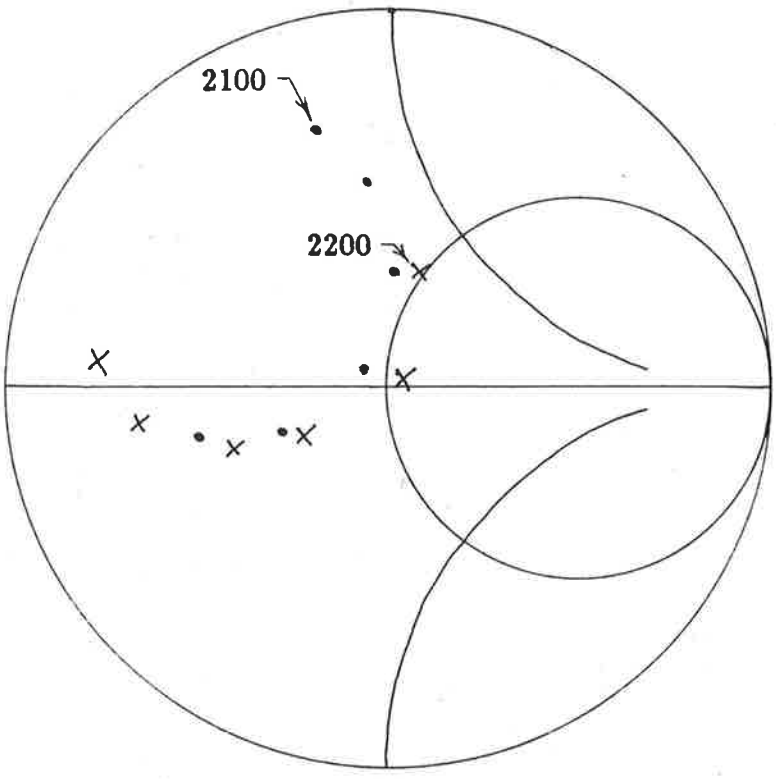

(b)

Figure 5.12: Calculated (• • •) and measured (× × ×) input impedances for rectangular elements: (a) 25.66mm by 23.1mm by 0.8mm, D=10.15mm, ϵ_r=2.55, where f=3400MHz plus 50MHz increments and (b), 41.4mm by 68.58mm by 1.59mm, D=10.16mm, SMA, ϵ_r=2.5, where f=2200MHz plus 20MHz increments for the measurements, and for the calculated data f=2100MHz plus 20MHz increments.

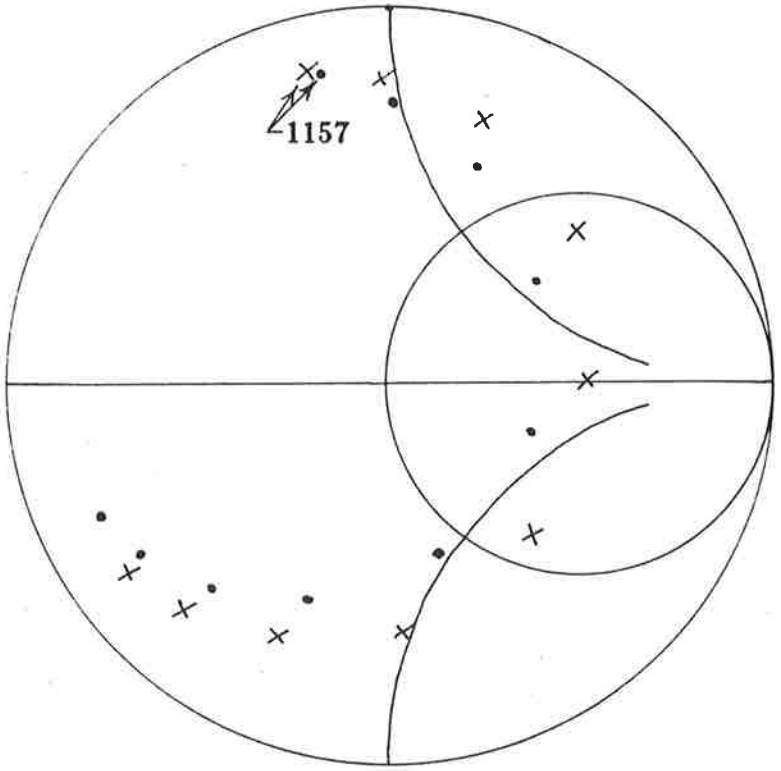

(a)

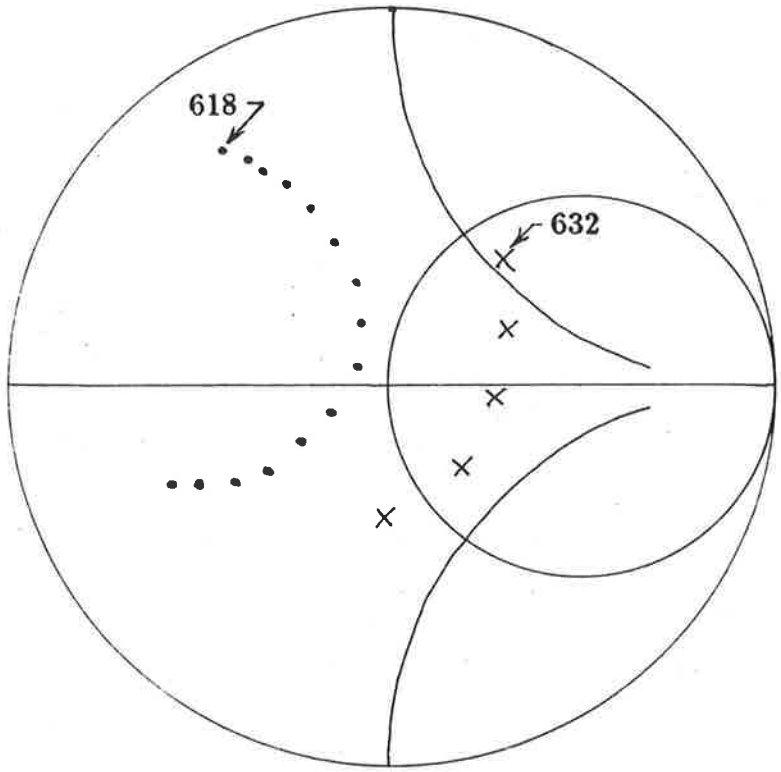

(b)

Figure 5.13: Calculated (• • •) and measured (× × ×) input impedances for rectangular elements: (a) 76mm by 114mm by 1.59mm, transmission line fed, ϵ_r=2.62, where f=1157MHz plus 10MHz increments and (b), 150mm by 75mm by 3.18mm, D=60mm, SMA, ϵ_r=2.56, where f=632MHz plus 1MHz increments for the measurements, and for the calculated data f=618MHz plus 1MHz increments.

Resonant frequency and resonant resistance						
L/W mm/mm	f_{oz} meas'd	f_{oz} calu'd	% error	R_o meas'd	R_o calu'd	% error
16.93/16.00	5028	5060	+0.6	52	59	+13
18.11/16.00	4795	4760	−0.7	68	59	−13
18.47/16.00	4674	4825	+3.2	69	63	− 9
18.47/16.00	4825	4824	−.02	85	64	−25
18.03/13.50	4770	4805	+0.7	65	62	− 5
25.66/23.10	3510	3542	+0.9	23	23	0
41.40/68.58	2221	2164	−2.6	50	41	−18
76.00/144.0	1197	1194	−0.3	150	118	−21
150.0/75.00	633	626	−1.1	90	41	−54

Table 5.1: Calculated and measured resonant resistances and impedance resonant frequencies.

ometries operating up to a frequency of 5GHz. Errors in the resonant resistance and the impedance resonant frequency are typically of the order of 17% and 2% respectively.

In the computer-aided design program listed in Appendix C the input impedance of a rectangular microstrip antenna is calculated using equation (1.15); a form of the transmission line equation adopted to model the microstrip antenna fed at a general point along its E-plane axis. An iterative routine is used to determine the aperture admittance from the aperture conductance and susceptance equations (5.27) and (5.28) respectively. When required, the equations of the tapered transmission line model developed in Chapter II are used to calculate the equivalent series reactance of the feed probe.

CHAPTER VI

THE CALCULATION OF THE FAR FIELD RADIATION PATTERN USING A TWO APERTURE ARRAY

6.1 Introduction

Each of the analytical models introduced in Chapter I involves an approximation for the field distribution around the boundary of the antenna so that it is expressed in terms of the components of the electric field normal to the ground plane, $E_z(x, y)$. The far field radiation pattern can be obtained by the application of Huygen's principle to the equivalent magnetic current sources [29,56], or obtained directly from equivalent electric current sources on the top side of the patch and the ground plane [15]. Because the near fields along the sides of the element are polarised in such a direction that they have no effect on the far field radiation in the main E- and H-planes, their contribution is usually omitted, leaving only the two sources at each end of the antenna. With these approximations the radiation problem is reduced to the analysis of a two aperture array, where the apertures are modelled as slot antennas or equivalent magnetic dipoles [12]. The far field radiation from a two aperture array was also obtained using the vector Kirchhoff relationship [57]. Agrawal et.al. [36] calculated the radiation pattern of the antenna directly from a numerical solution for the electric current distributions on the segments of two fine wire grids which model the patch and its image beneath the ground plane. In all of these models the accuracy of the far field radiation pattern

is directly dependent on a knowledge of either the electric currents on the patch and ground plane or the field distributions around the boundary of the antenna element. In the analyst's favour, however, is the fact that the radiation pattern is not sensitive to small changes in the near field distribution. Therefore radiation patterns that are accurate enough for design purposes are not difficult to obtain. However detailed near field information is required when the far field radiation pattern needs to be accurately investigated away from the E- and H-planes, or when cross-polarisation, or side-lobe information is required.

This chapter describes an investigation into the fundamental radiation mechanism of rectangular elements mounted on typical substrates and operating at frequencies up to 5GHz. In order to base the two aperture array model on a good foundation, the radiation characteristics of the individual apertures are studied in detail using a liquid crystal film to observe the near field distributions. The far fields of the individual apertures are measured. Finally a two aperture side by side array model is proposed for the calculation of the far field radiation patterns, where the aperture width and separation parameters take into account the effective distance to which the fields at each end of the patch fringe.

6.2 Examination of the near fields using a liquid crystal film

A liquid crystal film [58,59] was previously used by Derneryd [60] to verify the standing-wave nature of the fields under the patch by viewing the distributions of the fringing fields. When the film is placed on the patch, the component of the electric field intensity in the plane of the film induces a voltage in the resistive coating on the film surface, causing localised heating, the extent of which is seen using a heat sensitive liquid crystal. Thus the coloured patterns on the surface of the film give a relative indication of the power associated with the electric field intensity. The high to low field intensity scale is indicated by the colours blue through to yellow. The black areas correspond to intensity levels outside of the dynamic range of the detector; that is, saturation and

under excitation. Plate 6.1 shows a liquid crystal display of the fringing fields of a 18.47mm by 16mm by 0.8mm rectangular antenna fed by a SMA probe located 6.14mm from the right hand edge. Figure 6.1 can be used in conjunction with the plates to indicate the position of the liquid crystal film on the antenna. The antenna was driven at its cavity resonant frequency, 4830MHz, with a power level of 0.001mW. An asymmetry in the size of the blue areas at each end of the antenna can be observed. This indicates that in the $z = h$ plane, refer to figure 1.1, the electric field intensity is stronger at the aperture closest to the feed point. This effect is consistent for rectangular, circular or hexagonal antennas mounted on 0.8mm or 1.57mm thick substrates and fed through SMA or APC-7 probes, when the operating frequency is of the order of 5GHz. No asymmetry in the power level was observed for transmission line fed antennas, or antennas operating at 3.1GHz or 3.3GHz. Therefore it is concluded that the effect can be associated with any probe fed antenna built on substrates of typical thickness and operating at mid-microwave frequencies, say 5GHz. The asymmetry is attributed to two frequency dependent phenomena. Firstly, as the frequency is increased the effective electrical dimensions of the probe are also increased, which will in turn increase the distortion of the field distribution under the patch caused by the presence of the probe. Also the amount of energy stored in the evanescent modes associated with the probe will be increased. Secondly an increase in the effective electrical substrate thickness occurs when the frequency is increased, thereby accommodating an increase in the residual effects of higher order modes. The difference in the power levels radiated from the two apertures was tested for the previously mentioned combinations of substrate thickness and probe dimensions, and estimated to be 1.0±0.4dB. This was done by observing the size of the illuminated area associated with the aperture emanating the greater power, then noting the increase in input power level required to obtain a similar sized blue area for the low power aperture. This increase in the input power is then a rough estimate of the difference between the power levels of the two apertures.

Plate 6.2 shows the distribution of the field intensity of the fringing field off the

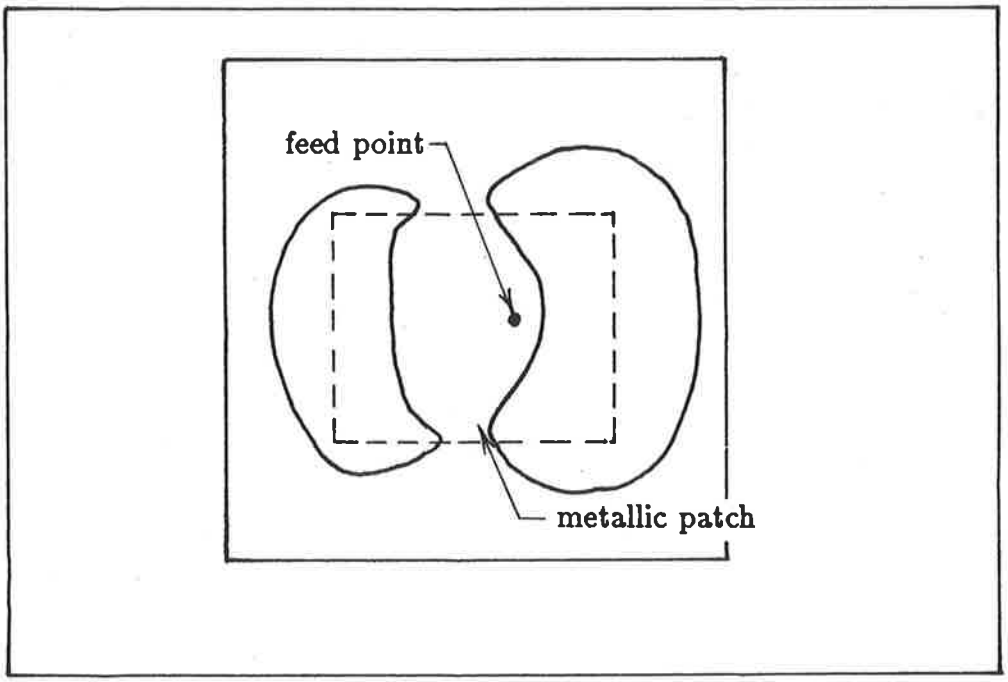

(a)

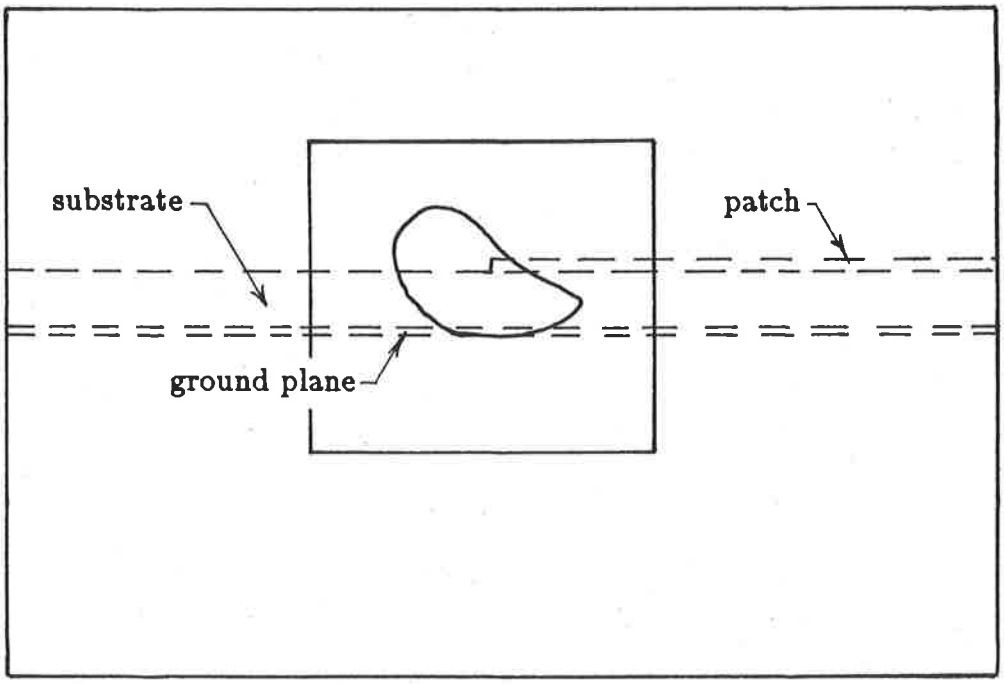

(b)

Figure 6.1: Sketches indicating the location of the antenna behind the liquid crystal film for (a) plate 6.1 and (b) plate 6.2.

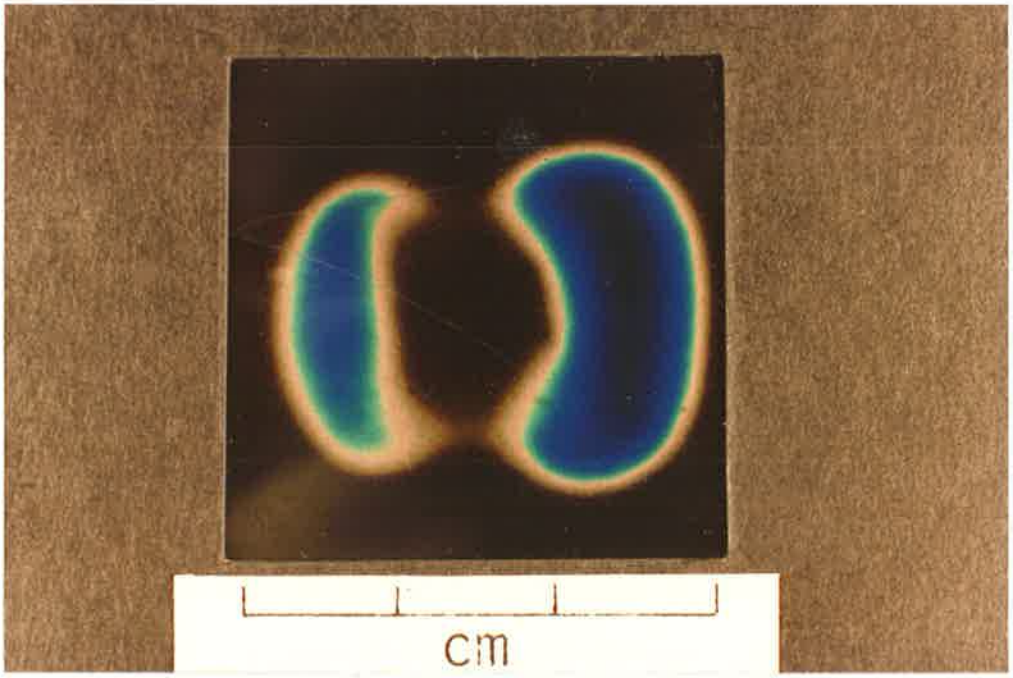

Plate 6.1: Liquid crystal display of the fields around the periphery of a rectangular patch.

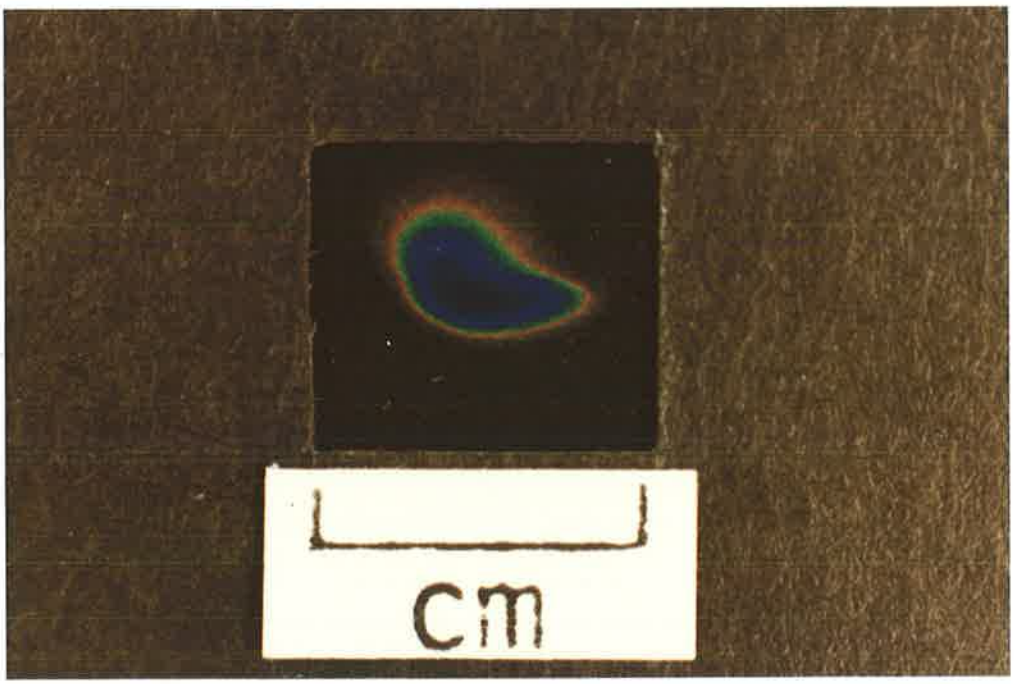

Plate 6.2: Liquid crystal display of the fields off the end of a rectangular patch.

edge of the patch, where the crystal film is aligned in the E-plane of a 16.93mm by 16mm by 1.57mm antenna, operating at f_{oc}=5013MHz. Again the blue area indicates the region of highest electric field intensity in the plane of the film. Therefore it is concluded that the direction of maximum radiation is roughly normal to the patch. This observation is consistent with Derneryd's [12] approach to modelling the radiation pattern of the antenna, where the radiation is considered to be emanating from two slot antennas in the $z = h$ plane, refer to figure 1.1. However closer examination of the plate leads to the conclusion that the direction of maximum radiation is slightly tilted off the normal in a direction away from the patch, where this angle shall be called the tilt angle, ϕ_t. This tilting of the angle of maximum radiation in the indicated direction was also observed for the short circuited patch on a 1.57mm thick substrate to be described in the next section, but not detectable for the case of antennas mounted on substrates of electrical thickness less than those considered here; that is $0.042\lambda_s$, which is equal to 1.57mm at 5GHz.

Increasing the substrate thickness has been widely used to decrease the quality factor and therefore increase the bandwidth of the antenna. However plates 6.1 and 6.2 show that the radiation sources and hence the radiation from antennas on thick substrates appears to be subject to undesirable properties. The effects on the far fields of the tilt and power level asymmetry of the apertures at each end of a $0.042\lambda_s$ thick antenna will now be examined in an experimental investigation.

6.3 Measured far field radiation pattern of a single aperture

The following far field measurements were carried out to further verify the power level asymmetry and beam tilting effects that were observed when using a liquid crystal film to examine the near fields of antennas mounted on electrically thick substrates.

Because of the difficulties of separating the far field radiation from the individual apertures located at each end of a rectangular element, the rectangular antenna was modified so that the radiation from one of the apertures was shielded. The resulting

structure is the short circuit patch shown in figure 6.2(a). Here the radiation from the aperture furthermost from the feed point, aperture B, is shielded by connecting a wide microstrip transmission line to the end of the antenna. This line presents an open circuit at the reference plane of aperture B and so the field distribution under the short circuit patch is the same as that for the original rectangular patch antenna. At plane B the transmission line presents an open circuit to the original half wavelength long antenna because it is transforming, along a length $\lambda_g/4$, the short circuit at its other end. Because the measured input impedance shown in figure 6.2(b) is close to that of the original rectangular antenna, it is therefore concluded that the field distributions under the patch and fringing around its boundary are a very good approximation to those of the original antenna. Moreover a liquid crystal examination of the structure's fringing fields in the X-Y plane shows that the only significant fringing is along aperture A. Fringing from aperture B is thus successfully shielded.

For the purpose of defining measurement planes and aiding analysis, a general A_l by A_w rectangular aperture is now defined and placed in the spherical coordinate system of figure 6.3. Notice that the aperture's field distribution is left unspecified so that it can be used to represent either the end or the side magnetic walls of the rectangular patch antenna. For the isolated aperture, the E- and H-plane radiation patterns are represented by the far field distributions in the X-Y and Z-Y planes of the coordinate system respectively.

Figure 6.4 shows the measured E-plane far field pattern for the single aperture of the short circuit patch. Notice the small gain in the broadside ($\phi = \pi/2$) direction, again justifying the use of apertures in the $z = h$ plane for a radiation pattern model. Refer to figure 1.1. The low gain also leads to the conclusion that the equivalent radiating aperture is quite thin. However, this figure gives no indication of the beam tilt referred to in the preceding section.

In order to increase the sensitivity of the experiment to the direction of the main lobe, microwave energy absorbent pads were placed equi-distant from the axis of

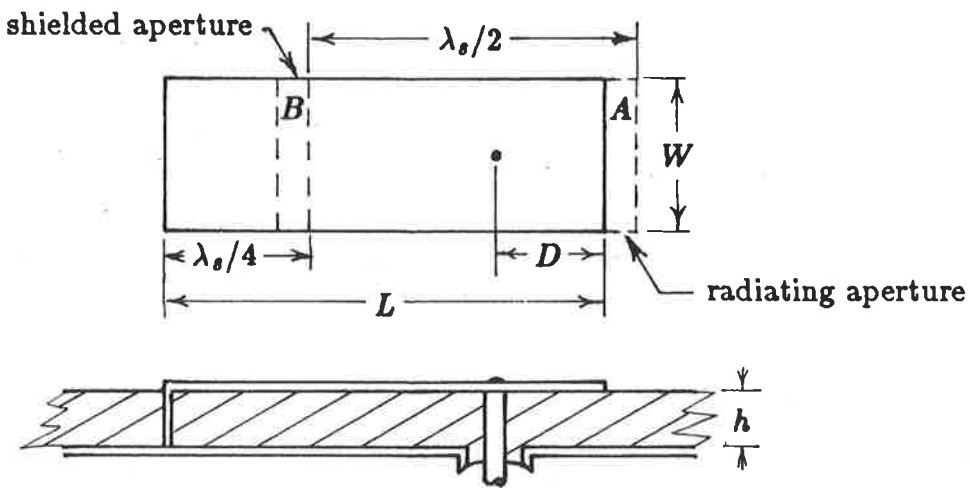

(a)

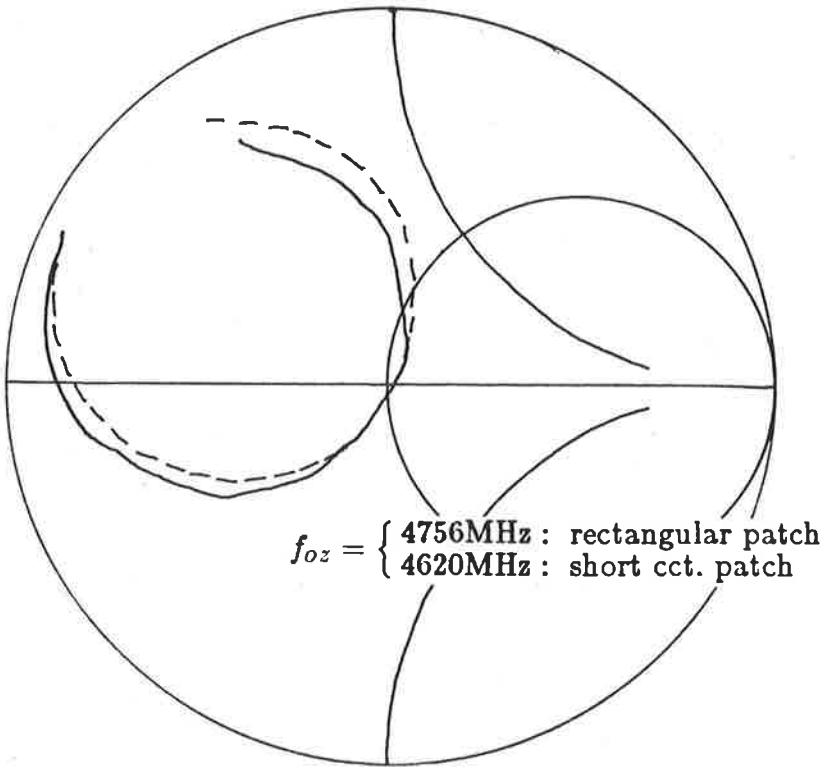

(b)

Figure 6.2: The short circuit patch; (a) sketch of the structure where L=29.16mm, W=16mm, D=6.3mm, and (b), the measured input impedance locus (——) compared with the locus of a rectangular element: 18.03mm by 16mm by 1.57mm, D=6.21mm, APC-7, ϵ_r=2.55 (– – –).

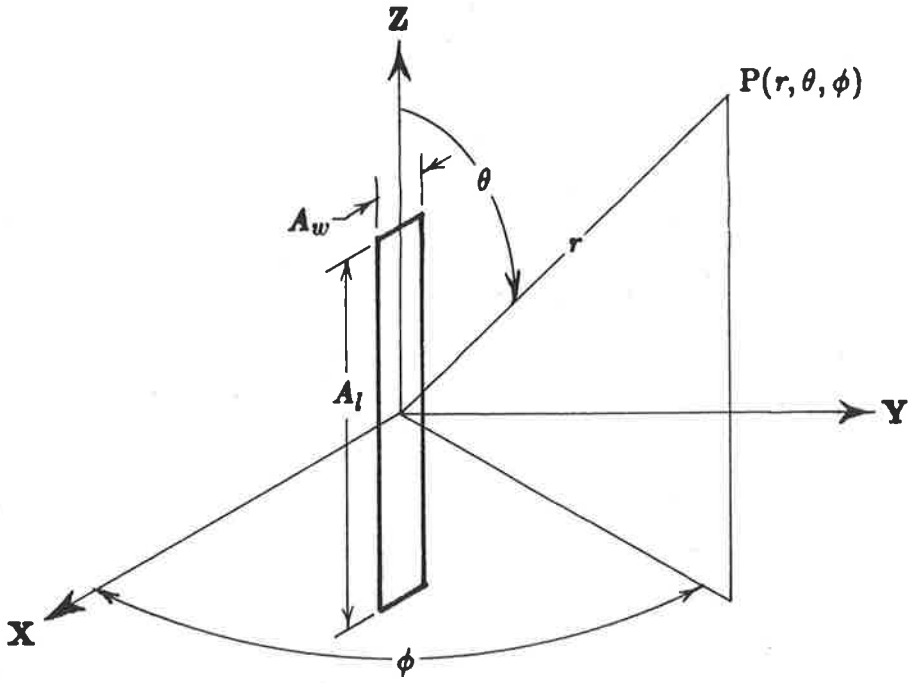

Figure 6.3: Rectangular aperture in a spherical coordinate geometry.

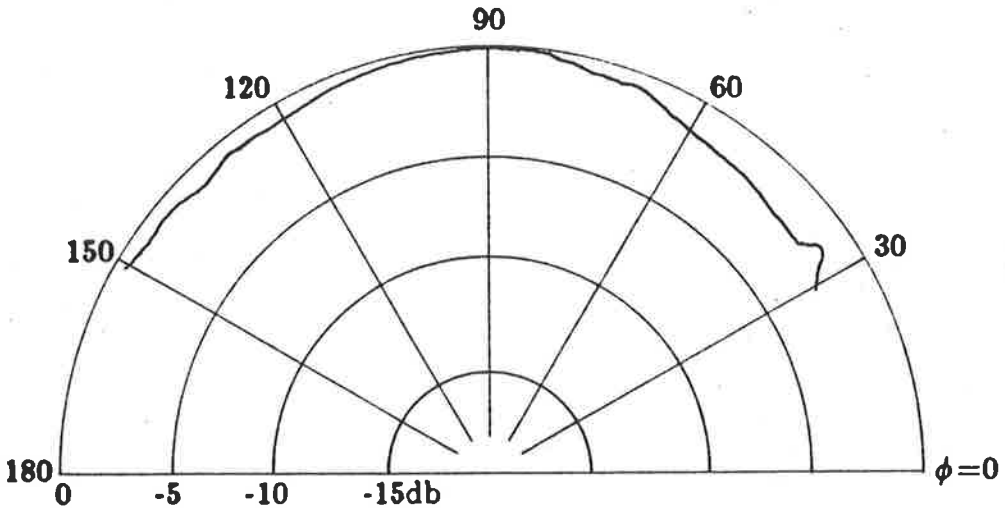

Figure 6.4: Measured E-plane pattern for the short circuited patch.

the radiating aperture to ensure significant absorption of the radiation emanating from the edges of the dielectric sheet. Thus the single aperture of the short circuit patch was effectively radiating through a window as shown in figure 6.5, where the window width refers to the distance between the pads. The pads were 15mm thick and made by slicing up a commercially available absorber of the type typically used to line the walls of anechoic chambers. The measured patterns shown in figure 6.6 indicate that the pads do not interfere with the general operation of the antenna. Here radiation patterns are compared for a 16.93mm by 16mm by 1.57mm rectangular element, with and without 30mm of absorber tightly pressed totally over the face of the patch. Only minor changes in the shape of the pattern are observed whilst, in fact, the measured pattern with the absorber in position is 6.7dB down on the unobstructed pattern. It is therefore concluded that the absorber material does not interfere with the shape of the radiation pattern.

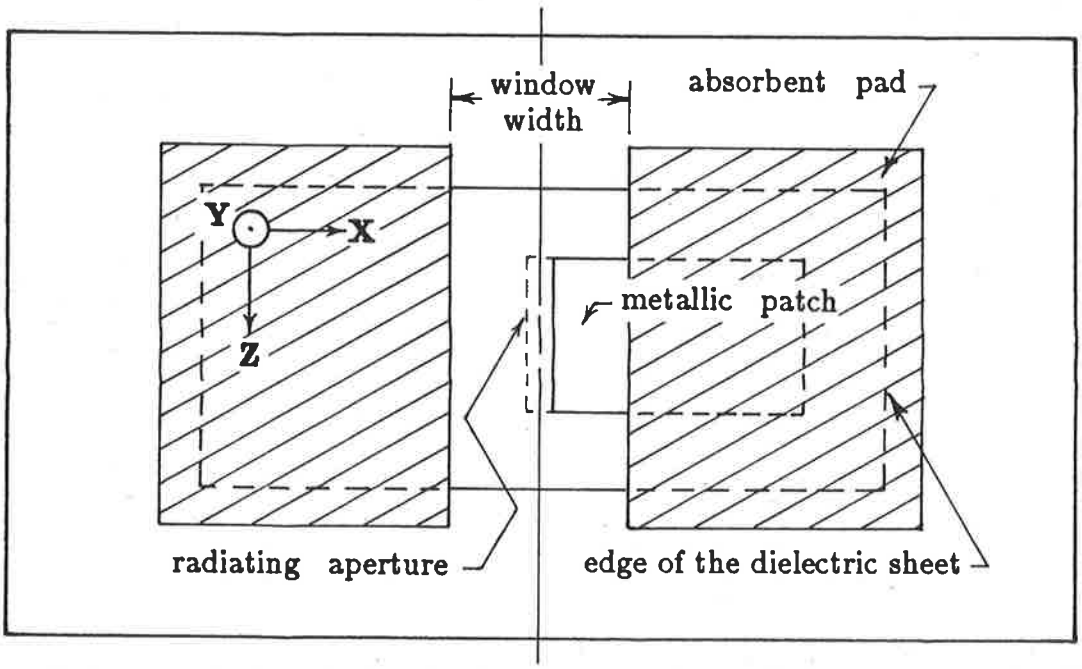

Figure 6.5: The placing of absorbent pads around a radiating aperture for E-plane measurement.

Figure 6.7 shows the radiation pattern of the short circuit patch measured through a 40mm wide window. Notice that the maximum in the radiation pattern is tilted roughly 5^o off the normal in a direction away from the antenna, thereby ver-

ifying the near field observations referred to earlier. Figure 6.8 illustrates a section through the short circuit patch and the coordinate system used. The measured direction of maximum radiation is also indicated. The lobes in the pattern of figure 6.7 at 30^o and 150^o are due to secondary radiation from the edges of the dielectric substrate on which the short circuited patch is mounted. These lobes can be observed on all of the far field radiation patterns presented.

Absorbent pads were also placed on each side of one of the two apertures of a 16.93mm by 16mm by 1.57mm rectangular patch antenna with the aim of measuring in turn the radiation from the apertures at each end of the antenna. The window width was chosen at 30mm in order to significantly absorb the radiation from the aperture that was not of interest. This process was, in turn, applied to the apertures near to and distant from the feed point. For these respective apertures the measured far field E-plane patterns are given in figures 6.9 and 6.10. Again notice a small but distinguishable tilt in the direction of maximum radiation. In both cases the tilt represents a 5^o squint off the normal direction away from the patch itself. The conclusion again verifies the near field observations using the liquid crystal film.

Comparing the absolute maximum signal levels of the radiation patterns from the individual apertures reveals a 0.9dB difference, thereby supporting the near field liquid crystal observations which indicated a 1.0±0.4dB difference.

These far field measurements have served to independently verify the observations that the aperture nearest the feed point is radiating at a higher signal level than the other, as well as confirming the existence of a 5^o tilting of the beams off the normal and in directions away from the antenna element. Although these characteristics of the apertures are now established, it still remains to be determined whether or not their effect on the far field radiation pattern is significant enough to include them in an analytical model of the two aperture array; that will be used to calculate the radiation pattern of the rectangular antenna element.

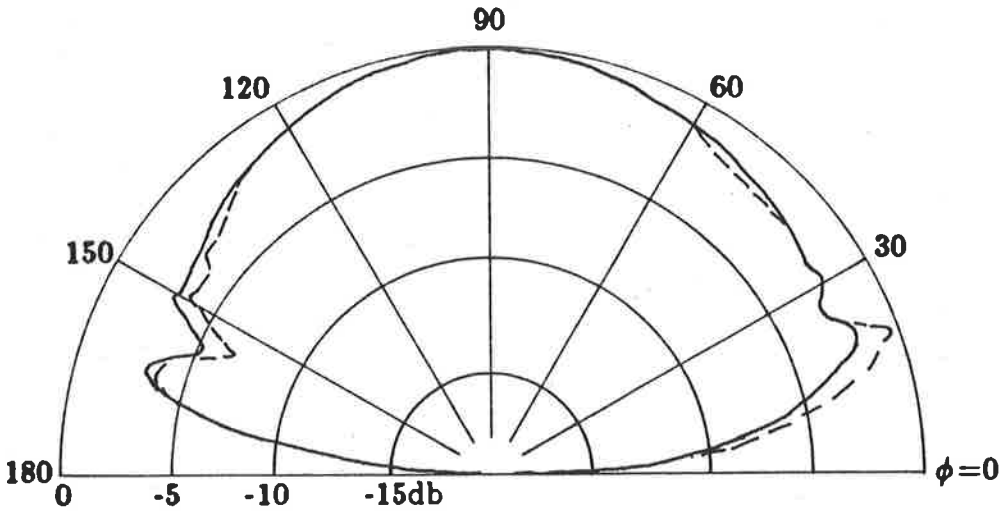

Figure 6.6: Measured E-plane patterns for a 16.93mm by 16mm by 1.57mm rectangular element with (— — —) 30mm of absorbent pad and without (———).

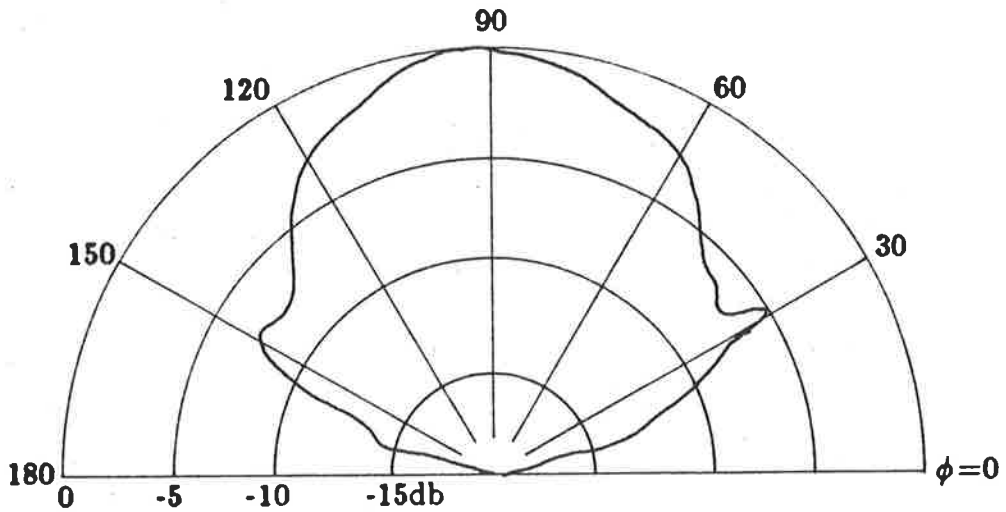

Figure 6.7: Measured E-plane patterns for the short circuited patch through a 40mm window.

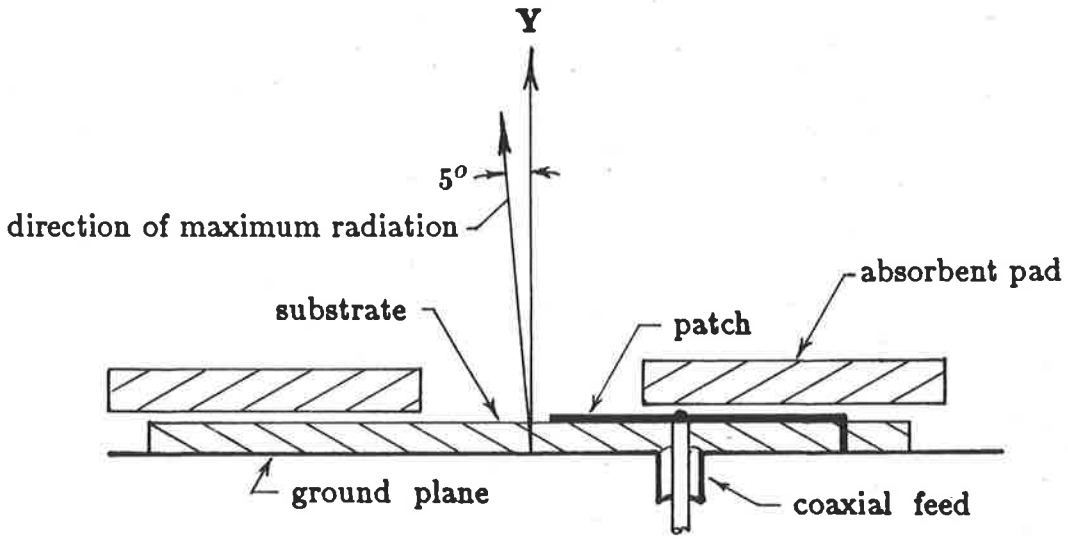

Figure 6.8: Sketch of a section through the short circuit patch.

6.4 Calculation of the far field radiation pattern of a rectangular microstrip antenna using a two aperture array

In developing a model for the far field radiation pattern it is advantageous to continue with the transmission line analogy introduced in Chapter V so that the same model is being used for the radiation pattern and the input impedance. Here a quasi-TEM_{010} mode is again assumed to exist under the patch. If the leakage from the sides of the element is ignored and the fringing fields across the ends of the patch are assumed to be the only sources of far field radiation in the E- and H-planes then, as was previously proposed by Derneryd [12], the rectangular antenna element is represented by a two element side by side array of uniformly illuminated apertures. However unlike Derneryd's model, the equivalent apertures are not necessarily excited at the same signal level, nor are they radiating in a direction normal to the patch.

The expressions for the far field of a single uniformly illuminated aperture have been obtained by considering the case of an equivalent magnetic dipole with a time

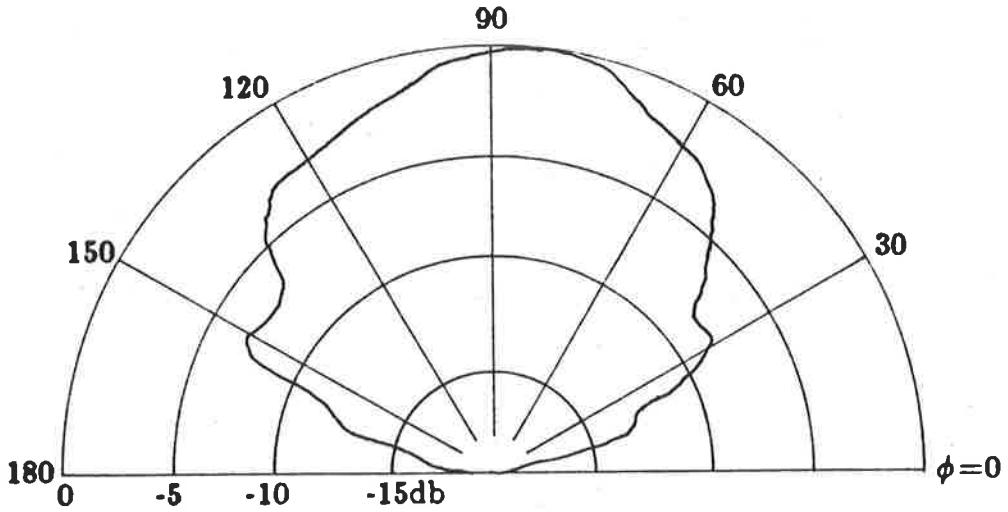

Figure 6.9: Measured E-plane pattern for the aperture near to the feed point of a 16.93mm by 16mm by 1.57mm rectangular element.

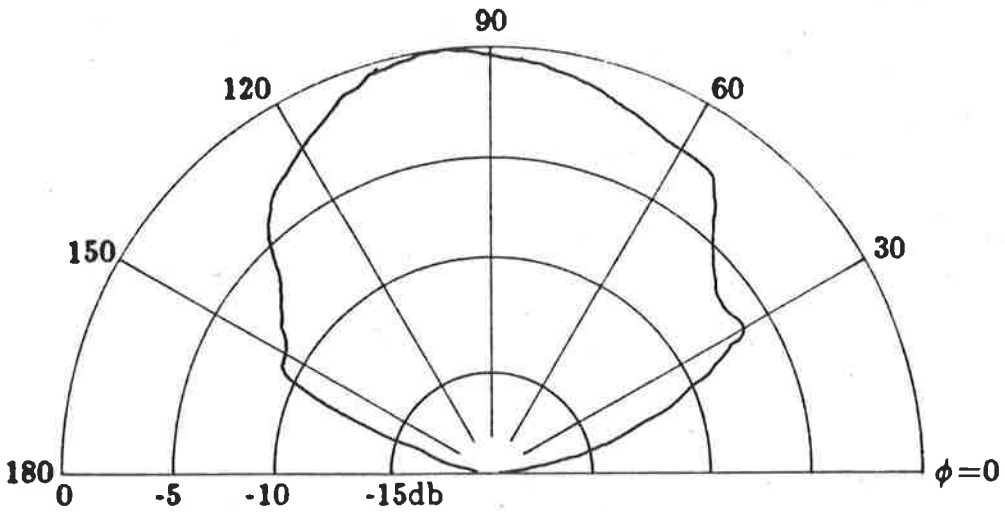

Figure 6.10: Measured E-plane pattern for the aperture far from the feed point of a 16.93mm by 16mm by 1.57mm rectangular element.

harmonic magnetic current

$$\underline{M} = \underline{u}_z 2E_x = \underline{u}_z \frac{2V_o}{A_w} \tag{6.1}$$

where the factor 2 accounts for the image of the magnetic current beneath the ground plane, and V_o is the voltage across the aperture. According to Bahl et.al. [61] the far field at a distance r from the origin is given by

$$\underline{E}_\phi = \frac{-j\underline{u}_\phi 2V_o A_l \beta_o e^{-j\beta_o r}}{4\pi r} F(\theta,\phi) \tag{6.2}$$

$$\underline{E}_\theta = 0 \tag{6.3}$$

where

$$F(\theta,\phi) = \frac{\sin(\frac{\beta_o A_w}{2}\sin\theta\cos\phi)}{\frac{\beta_o A_w}{2}\sin\theta\cos\phi} \frac{\sin(\frac{\beta_o A_l}{2}\cos\theta)}{\frac{\beta_o A_l}{2}\cos\theta}\sin\theta \tag{6.4}$$

For the E-plane pattern let $\theta = \pi/2$, then:

$$F(\phi) = \frac{\sin(\frac{\beta_o A_w}{2}\cos\phi)}{\frac{\beta_o A_w}{2}\cos\phi} \tag{6.5}$$

and for the pattern in the H-plane let $\phi = \pi/2$, so that

$$F(\theta) = \frac{\sin(\frac{\beta_o A_l}{2}\cos\theta)}{\frac{\beta_o A_l}{2}\cos\theta}\sin\theta \tag{6.6}$$

Now the E-plane pattern of the two aperture array is obtained by the vector addition of the contributions to the far fields from the two apertures shown in figure 6.11. Thus

$$\underline{E}_\phi = \underline{E}_{\phi a} + \underline{E}_{\phi b} \tag{6.7}$$

$$= \frac{-j\underline{u}_\phi 2A_l\beta_o}{4\pi}\left[V_{oa}\frac{e^{-j\beta_o r_a}}{r_a}\frac{\sin(\frac{\beta_o A_w}{2}\cos\phi_d)}{\frac{\beta_o A_w}{2}\cos\phi_d} + V_{ob}\frac{e^{-j\beta_o r_b}}{r_b}\frac{\sin(\frac{\beta_o A_w}{2}\cos\phi_s)}{\frac{\beta_o A_w}{2}\cos\phi_s}\right] \tag{6.8}$$

where

$$\phi_s = \phi + \phi_l \tag{6.9}$$

$$\phi_d = \phi - \phi_l \tag{6.10}$$

$$r_a \approx r - \frac{A_s}{2}\cos\phi \tag{6.11}$$

$$r_b \approx r + \frac{A_s}{2}\cos\phi \tag{6.12}$$

Then letting $r_a \approx r_b \approx r$ in the denominator and substituting (6.11) and (6.12) into the numerator gives an equation for the E-plane pattern of a patch antenna that includes the excitation level and beam tilting of the radiation from the individual apertures.

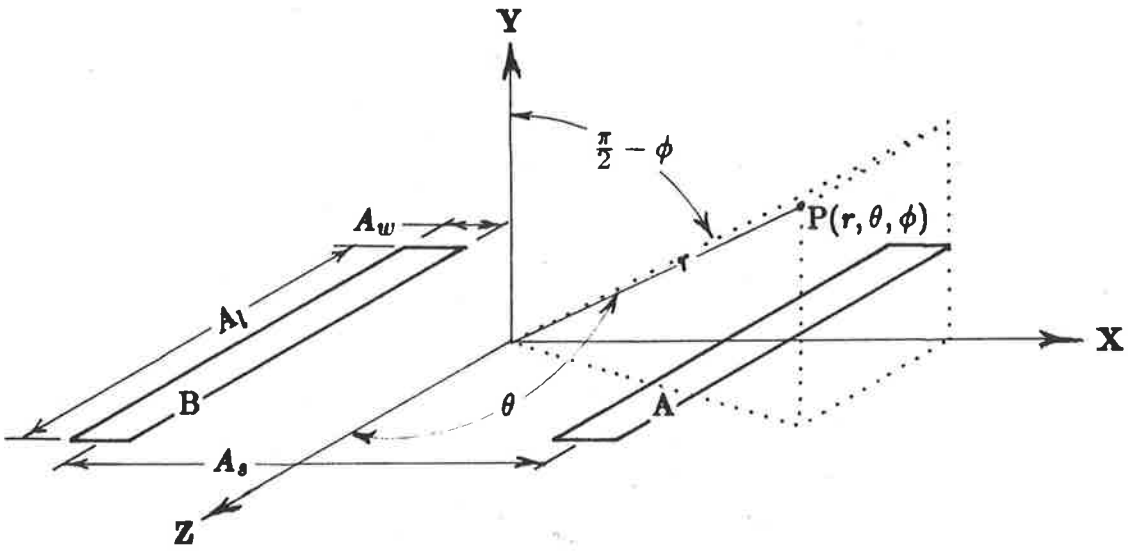

Figure 6.11: Coordinate geometry for the two aperture side by side array.

The H-plane radiation pattern is independent of the nature of the array and therefore can be obtained using the equation for the H-plane pattern of a single aperture, equation (6.6). The magnitudes of equations (6.6) and (6.8) are normalised and compared with measured H- and E-plane far field radiation patterns in the next section.

6.5 Discussion of results

The asymmetry in the power level of the two apertures has been established in antennas of electrically thick substrates of the order of $0.02\lambda_s$ and $0.042\lambda_s$, while the beam tilting was only observed for the $0.042\lambda_s$ substrates. Equation (6.8) for the

E-plane far field radiation pattern of the rectangular antenna can be used to show that the effect of the asymmetry in the excitation level is to cause a slight ripple in the calculated pattern, the magnitude of which is smaller than the tolerances of the experimental technique. Therefore ripple due specifically to asymmetrical excitation of the apertures could not observed in the measured patterns.

The effects on the antenna's far field pattern of the beam tilting also turns out to be minor because the single thin aperture is characterised by an E-plane radiation pattern that is almost omni-directional. So the orientation of the aperture has little affect upon the analytical results. Figure 6.4 showed that the measured pattern of a single aperture has a slight gain roughly in the $\phi = \pi/2$ direction. Also, the calculated gain is almost 0dB_i.

Further investigations with the equations for the far field radiation patterns showed that their accuracy is mainly dependent on the aperture separation term, A_s. Furthermore, other authors [4,12,61] have suggested using the length of the patch for the aperture separation; however, this approach was found to constantly predict patterns of lower gain than those measured for the antennas on electrically thick substrates operating around 5GHz.

A more accurate representation of the two aperture array is obtained when the aperture separation is made to include the aperture width. Referring to figure 6.11 indicates that

$$A_s = L + A_w \tag{6.13}$$

Inclusion of the aperture width into the separation term is necessary for antennas operating at mid-microwave frequencies because the width of the aperture is significant when compared to the patch length. For example, following the recommendations of other authors, let the equivalent aperture width equal the substrate thickness. Then for typical antennas operating at 1.2GHz and 5GHz, the ratios of the substrate thicknesses to the patch lengths are 2.1% and 9.3% respectively. So it is concluded that the width of the aperture can no longer be ignored.

It was also found that the equivalent aperture width is best represented by the equivalent length to which the fields fringe beyond the end of the patch; that is, the effective edge extension as calculated in Chapter III. Moreover the dielectric substrate is taken into account by using an equivalent free space edge extension. Therefore

$$A_w = \sqrt{\epsilon_r}\delta L \tag{6.14}$$

and hence

$$A_s = L + \sqrt{\epsilon_r}\delta L \tag{6.15}$$

and as previously recommended by other authors, let the length of the apertures be

$$A_l = W \tag{6.16}$$

For most antennas in general use the equivalent free space edge extension will be greater than the substrate height. This increased aperture width will have an associated increase in the gain of the patterns radiated by the individual apertures, however in practice this will be negligible because the apertures are still very thin compared with the wavelength. However, increasing the width of the apertures will significantly add to the array separation and cause a marked increase in the gain of the radiation pattern of the antenna. This increase represents improved agreement with measurements over the patterns obtained using $A_s = L$ and $A_w = h$, as recommended by other authors. Figure 6.12 compares with measurements the E-plane patterns calculated by the substitution of equations (6.14) (6.15) and (6.16) into (6.8). The figure also includes the calculated result obtained when the patch length is substituted for the array separation. The improved agreement between the results of this new model and the measured pattern is easily seen.

The model is also used to calculate the H-plane pattern to good agreement with measurements, as shown in figure 6.13. Figures 6.14 and 6.15 show comparisons with measurements for 5GHz and 3.5GHz antennas on thin substrates.

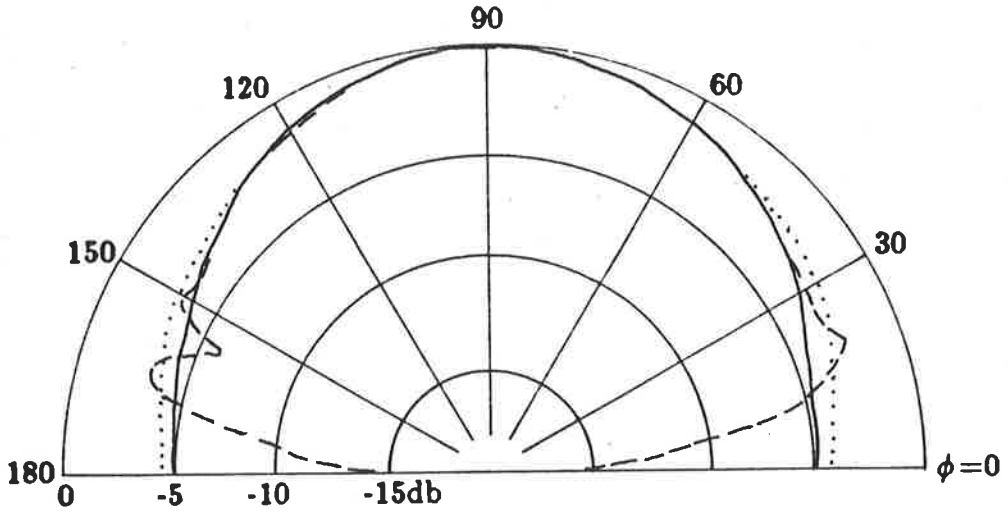

Figure 6.12: Measured (— — —) E-plane pattern for a 16.93mm by 16mm by 1.57mm rectangular element at f_{oc}=5013MHz, with the calculated results of the new model (———) and old model (·····).

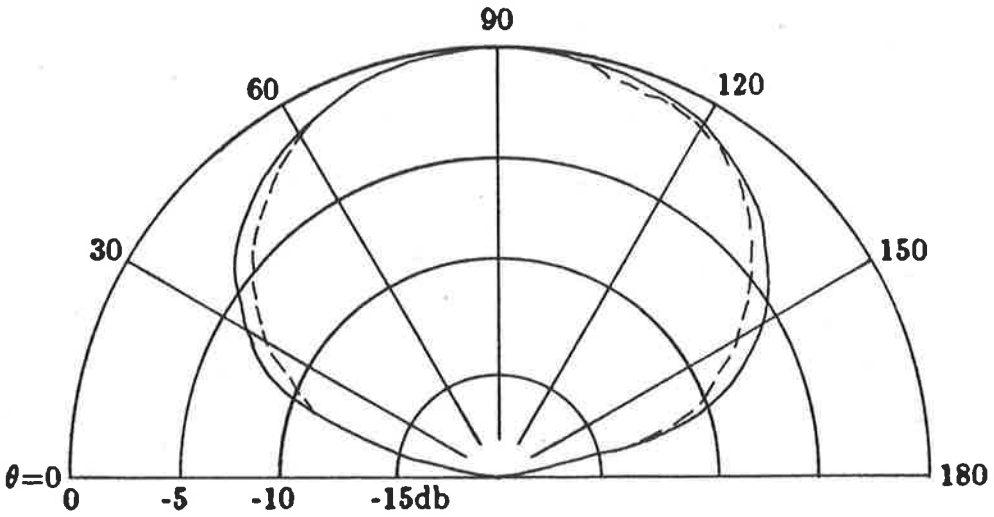

Figure 6.13: Measured (— — —) and calculated (———) H-plane pattern for a 16.93mm by 16mm by 1.57mm rectangular element at f_{oc}=5013MHz.

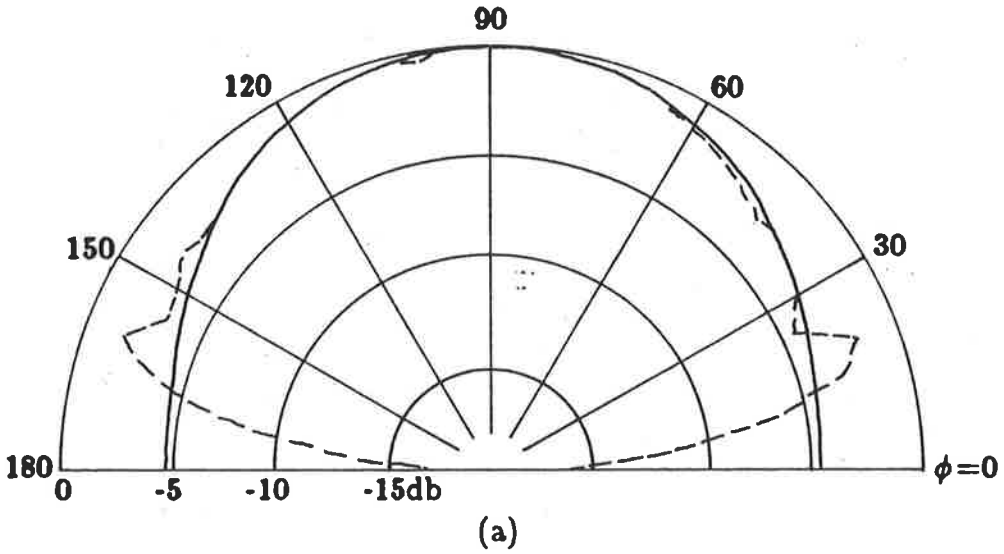

(a)

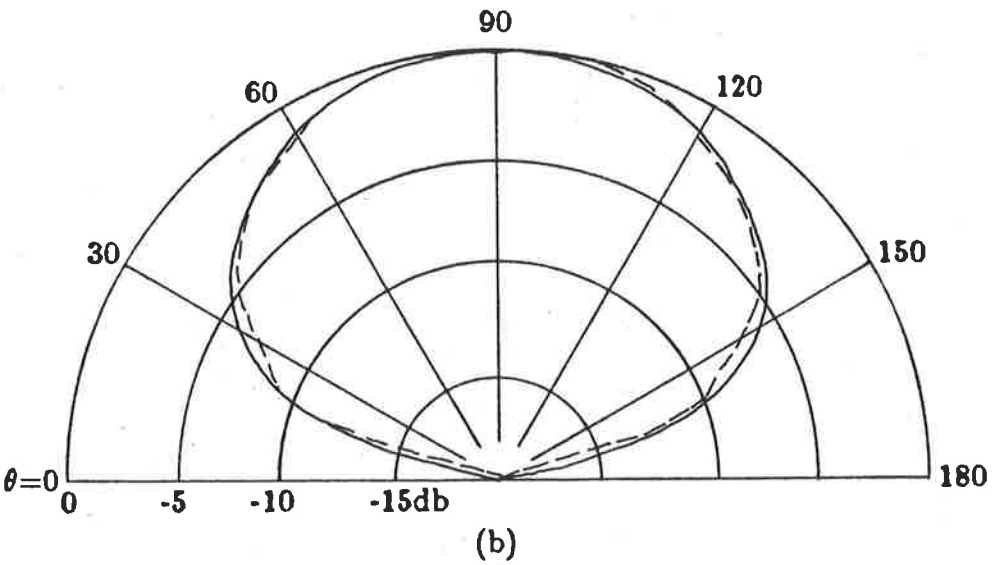

(b)

Figure 6.14: Measured (– – –) and calculated (———) patterns for a 18.47mm by 16mm by 0.8mm rectangular element at f_{oc}=4670MHz, (a) E-plane and (b) H-plane.

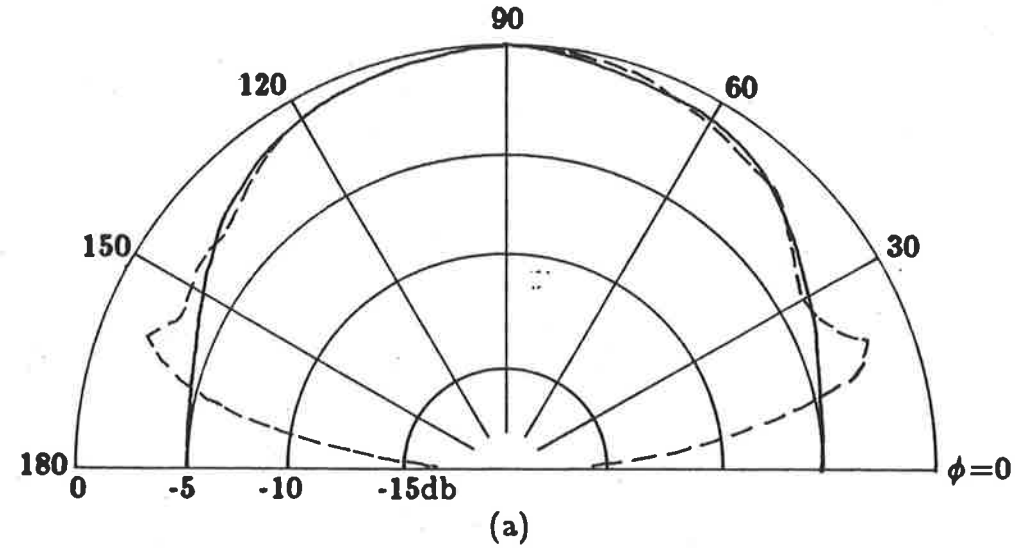

(a)

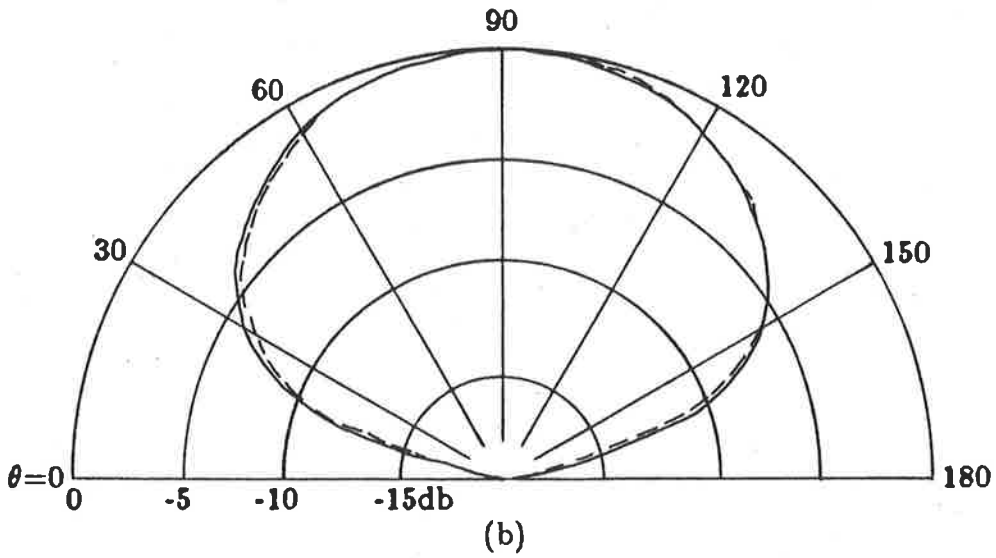

(b)

Figure 6.15: Measured (– – –) and calculated (———) patterns for a 25.66mm by 23.1mm by 0.8mm rectangular element at f_{oc}=3502MHz, (a) E-plane and (b) H-plane.

6.6 Conclusions

A study of the fundamental radiation characteristics of the apertures at each end of electrically thick rectangular antennas has been carried out. The aperture nearest the feed point was shown to be excited at a higher relative signal level than the other, and a tilt off the normal direction of the radiation beams of both apertures was also observed. However, both phenomena were shown to have little effect on the E- and H-plane radiation patterns of the overall antenna, mainly because the apertures are so thin that their E-plane radiation patterns are almost omni-directional. However these characteristics of the apertures may be, and probably are, significant if a detailed knowledge of the far field radiation pattern is required, particularly that off the main planes, or when side-lobe and cross-polarisation information needs to be determined. The two aperture side by side array model was improved through an accurate representation of the array separation which takes into account of the equivalent free space edge extension associated with the fringing fields at the end of the patch.

The computer-aided design program listed in Appendix C enables the calculation of far field radiation patterns of rectangular microstrip antennas using equations (6.8) and (6.6) for the E-plane and H-plane patterns respectively. The two apertures in the model are assumed to have approximately the same characteristics, that is, $V_{oa} \approx V_{ob}$ and $\phi_t \approx 0$. The dimensions of the effective radiating apertures are calculated using equations (6.15) and (6.16).

CHAPTER VII

AN ANALYTICAL MODEL FOR THE MUTUAL COUPLING BETWEEN TWO RECTANGULAR PATCH ANTENNAS

7.1 Introduction

Mutual coupling between two microstrip antenna elements can result in the degradation of the radiation pattern and VSWR performance of each of the elements. These effects are difficult to predict, especially in scanned arrays where they are sensitive to the scan angle.

In 1979 Jedlicka and Carver [62] published a comprehensive set of measurements of mutual coupling as a function of the spacing between two rectangular microstrip antennas. The results have been widely used as a basis for comparison with many analytical models. A new analytical model for the mutual coupling is compared with these measurements and others performed as part of this investigation. The model is very simple and is used to study the mechanism of the coupling phenomenon.

7.2 Survey of models for the calculation of mutual coupling

Various analyses of mutual coupling between rectangular microstrip antennas have been published. Krowne et.al. [63] modelled the H-plane coupling between two rectangular elements using a coupled transmission line approach and the method of

moments technique to calculate even and odd mode transmission line parameters. In a second paper Krowne [64] modelled the E-plane coupling using an equivalent π-network of capacitances, where the capacitance values were obtained by an approximation to a quasi-static formulation of the gap in a microstrip line. The rectangular antennas themselves were represented by transmission lines.

Penard and Daniel [65] have used the equivalence theorem to reduce the problem to one of coupling between two loops of magnetic current and then used the reaction theorem to calculate the coupling. The calculated magnitude of the transfer coefficient is shown to agree with their own measurements to within 1dB for separations greater than 0.1λ.

Pozar [39] has presented a moment method solution which uses an exact Green's function for the dielectric slab. This is regarded as rigorously accounting for surface waves and other coupling mechanisms between patches. Pozar's results show good agreement with the measurements of Jedlicka et.al., however the value of the effective dielectric constant was chosen to ensure this agreement.

The analytical models published by the above authors rely on extensive numerical calculation which tends to impede development of a physical understanding of the phenomena involved and engineering insight for their exploitation. This investigation into a simpler analytical technique that models the coupling as the power transfer between two aperture antennas was undertaken to promote understanding and insight.

7.3 A radiation based model for the mutual coupling between well separated rectangular patch antennas

A simple radiation based model for determining the mutual coupling between rectangular microstrip patch antennas is developed for the case where the separation is greater than the classical $2D^2/\lambda_o$ far field distance. The antennas are modelled by resonant cavities radiating through the four rectangular apertures that form the sides

of each cavity. The coupling mechanism is then modelled as the power transfer that occurs when the far field radiation pattern of the transmitting aperture illuminates the receiving aperture as shown in figure 7.1(a). Only the two apertures facing each other are considered to have an effect on mutual coupling.

This model is developed with the aim of accounting for the mutual coupling, between two antennas, that is measured at reference planes located at the coaxial connections to each of the coupled antennas. Therefore it is necessary to consider the cascade of two-port equivalent networks shown in figure 7.1(b) to relate the parts of the model to the different mechanisms of signal flow from the transmitting to the receiving coaxial connections. Ports 1 and 2 are the terminals of the transmitting and receiving elements and the apertures responsible for the coupling are at ports A and B. With the elements isolated from each other it is assumed that s_{11} and s_{22} are set to zero at some specified frequency which is the resonant frequency of each element and also the frequency at which experimental data has been gathered. Also s_{aa} and s_{bb} are the reflection coefficients of the transmitting and receiving apertures respectively. The s_{43} term represents the forward and reverse transfer coefficients between the two aperture antennas. The transfer coefficients s_{a1} and s_{2b} account for transmission between the antenna terminals at ports 1 and 2 and the apertures at ports A and B.

In terms of the scattering parameters, the total forward transfer coefficient between the terminals of the two elements is s_{21} and is expressed in terms of a set of scattering transfer parameters for the cascaded two-port networks in figure 7.1(b)

$$s_{21}^{-1} = T_{2b}(T_{a1}T_{33} - T_{aa}T_{43}) - T_{22}(T_{a1}T_{43} - T_{aa}T_{44}) \tag{7.1}$$

The patch elements are matched to their external coaxial connections so that

$$s_{11} = s_{22} = 0 \tag{7.2}$$

and expression (7.1) becomes

$$s_{21} = s_{a1}s_{43}s_{2b} \tag{7.3}$$

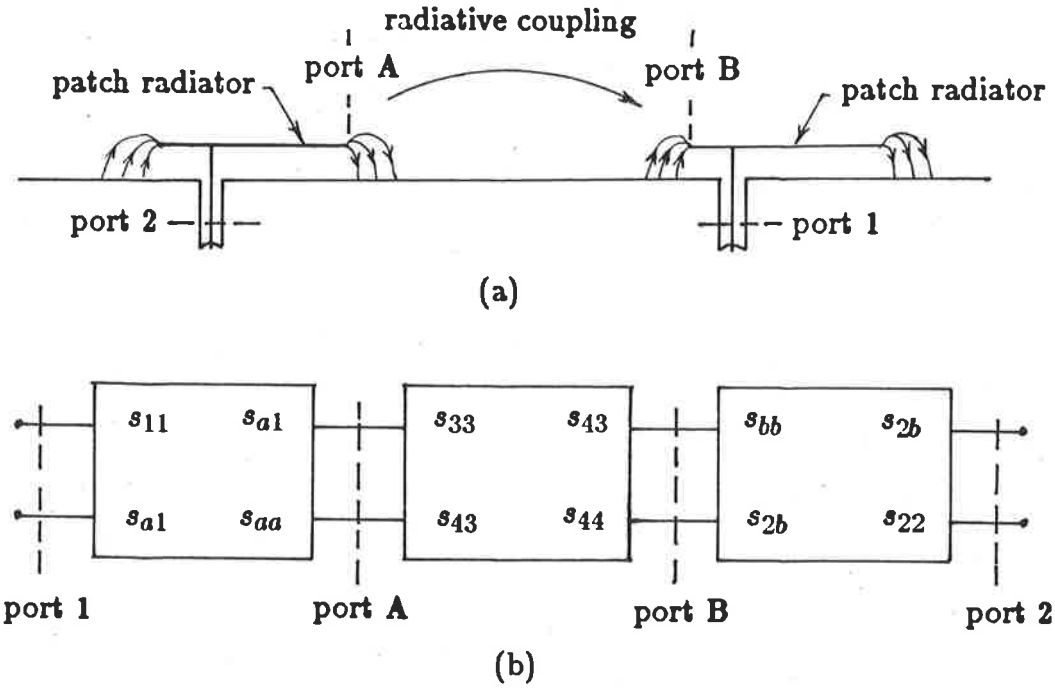

Figure 7.1: Mutual coupling between two patch antennas located in each others far field: (a) side-elevation sketch of two antennas coupled in the E-plane, and (b) the equivalent network in terms of the scattering coefficients.

The transfer coefficient, s_{43}, models the power transfer between two aperture antennas and the s_{a1} and s_{2b} coefficients represent the ratios of the wave amplitudes at the coaxial connections to those in the associated radiating apertures taking part in the coupling. Each of these three transfer coefficients will now be considered in detail.

7.3.1 The transfer coefficient modelling the radiative coupling: s_{43}

Regard the two rectangular elements as resonant cavities with electric fields distributed over the aperture-like four magnetic walls. The equivalence theorem is used to replace the electric fields of the walls by equivalent magnetic currents. Also the ground plane of figure 7.1(a) is replaced by the image of these magnetic currents for the purpose of determining the radiation in the half space above the ground plane. The coupling is

evaluated on the basis of the power transfer that occurs when the transmitting aperture illuminates the receiving aperture.

The two antennas are assumed to be in each others far field to the extent that the separation is at least $2D^2/\lambda_o$ where D is the largest dimension of the radiating (or receiving) aperture. Referring to figure 1.1, the aperture field distributions are taken to be the z-directed electric field around the patch's perimeter. This choice of orientation of the effective aperture at each end of the antenna does not conflict with the use of the y-component of the fringing field in the models for the antenna's input impedance and radiation pattern. Appreciate that it is the electric field distributions in the magnetic walls of the cavity that are being used in the coupling model rather than a component of the curved field lines of the fringing field that exists out from the edges of the patch, as shown in figure 7.1(a). Both elements are assumed to be operating at a common resonant frequency and in their fundamental TM_{01} modes. Referring to the aperture and coordinate geometry shown in figure 6.3, the time harmonic electric field distributions of the apertures located along the edges of the patch can be expressed as follows. At each end of the patch

$$\underline{E_x} = \underline{u_x} E_m \qquad -A_l/2 \leq z \leq A_l/2 \tag{7.4}$$

and for each side of the patch,

$$\underline{E_x} = \underline{u_x} E_m \sin \frac{2\pi z}{\lambda_o} \qquad -A_l/2 \leq z \leq A_l/2 \tag{7.5}$$

where the length of the effective free space aperture is resonant, that is, $A_l = \lambda_o/2$.

In both cases the far field radiation pattern is calculated by taking the equivalent magnetic current density of the source distributions and integrating over the source points to obtain the electric vector potential F_z. The far field approximation is used to obtain the E_ϕ-component of the electric field in terms of F_z through the approximate relation;

$$\underline{E_\phi} = -\underline{u_\phi} j\beta_o F_z \sin\theta \tag{7.6}$$

The resulting expressions for the H-plane far fields of the end [12] and side [66] apertures are

$$\underline{E}_\phi = -\underline{u}_\phi j E_m A_w e^{-j\beta_o r} \frac{\sin((\pi A_l/\lambda_o)\cos\theta)\tan\theta}{\pi r} \tag{7.7}$$

$$\underline{E}_\phi = \frac{-\underline{u}_\phi j E_m A_w e^{-j\beta_o r} \cos((\pi A_l/\lambda_o)\cos\theta)}{\pi r \tan\theta} \tag{7.8}$$

where A_w and A_l are the width and length of the equivalent aperture being considered.

Equations (7.7) and (7.8) are now used to calculate the transmitted and received power. The transmitted power is given by the Poynting vector $\underline{P}$ where

$$P = \frac{E^2}{\eta_o} \tag{7.9}$$

and η_o is the characteristic impedance of free space. The radiation intensity is the power per unit solid angle, and is given in the units of watt per sterradian by

$$\Phi(\theta,\phi) = r^2 P \tag{7.10}$$

The total power radiated by the aperture is found by the integration of equation (7.10) over a spherical surface that encloses the aperture so that

$$P_t = \frac{\pi r^2}{\eta_o} \int_0^\pi E^2(\theta) \sin\theta \; d\theta \quad \text{Watt} \tag{7.11}$$

The power received by the equivalent aperture in the coupled antenna is derived in a similar way

$$P_r = \frac{2A_w}{\eta_o} \int_0^{A_l} E^2(z) \; dz \quad \text{Watt} \tag{7.12}$$

and $| s_{43} |^2$ follows as the ratio of (7.12) and (7.11)

$$| s_{43} |^2 = \frac{P_r}{P_t} \tag{7.13}$$

7.3.2 Transfer coefficients within the antenna elements: s_{a1} and s_{2b}

The coefficients s_{a1} and s_{2b} represent the ratios of the wave amplitudes at the coaxial connections to those in the associated radiating apertures selected in the previous

section for the determination of s_{43}. Simple reasoning in terms of the distribution of the power at the coaxial connection port and the equivalent radiating apertures around the four edges of the rectangular patches yields values for these transfer coefficients.

Because each antenna element is assumed to be matched to its coaxial connection, and if the antenna's copper and dielectric losses are assumed negligible, then all of the input power must be radiated. Only a fraction of that power is considered in the determination of s_{43}. Thus, in the case of two elements with their ends facing each other, only the power passing through the apertures equivalent to those ends is considered. For the case of element sides facing each other, the power passing through the equivalent apertures is considered with accurate account being taken of the level relative to the power through the end apertures. This is done by assuming unit amplitude for the aperture distributions at the positions that are common to the end and side apertures; namely the corners of the rectangular patch. This means that the coefficients s_{a1} and s_{2b} are the same for both the "ends facing" and the "sides facing" or, more succinctly, the E-plane and H-plane coupling cases.

For rectangular geometries that are nearly square only a small fraction of the total input power is radiated through the side apertures and therefore nearly half of the input power is radiated through each end aperture. This means that

$$| s_{a1} |^2 \approx 0.5 \tag{7.14}$$

and

$$10 \log | s_{a1} |^2 = -3dB \tag{7.15}$$

If the only contribution to the power in the receiving antenna is through an end or a side aperture, then reciprocity applies so that

$$| s_{2b} |^2 = | s_{a1} |^2 \approx 0.5 \tag{7.16}$$

7.4 Discussion of results

The mutual coupling is calculated using a free space equivalent to the experimental study, where the dimensions of the patch elements are multiplied by $\sqrt{\epsilon_r}$ in order that the free space wavelength be used throughout the model.

Jedlicka and Carver [62] published the set of mutual coupling measurements for two substrate thicknesses shown in figure 7.2. Although these experimental results have been widely referred to by other researchers, Jedlicka et.al. omits details of the tuning and matching conditions maintained as the spacing between the elements is varied. However, it is reasonable to assume that each element was resonant and matched to its coaxial connection at the specified test frequency when isolated from other elements. There is no information given on the mismatches that may occur due to the interaction between elements as the spacing decreases. Experiments carried out as part of this investigation show that this is only important at spacings smaller than the minimum tested by Jedlicka and Carver. The measured results correspond to the $|\ s_{21}\ |^2$ scattering transfer coefficient in figure 7.1.

Figure 7.2 shows the agreement between the calculated and measured coupling for two substrate thicknesses. For separations greater than $0.75\lambda_o$, the calculated mutual coupling is within 3dB of the measurements for both the E- and H-plane cases. Excellent agreement with measurements is also shown in figure 7.3 for the coupling between two elements excited at 5GHz. These results also show that the model holds for separations less than the far field distance, which is equal to $1.2\lambda_o$ and $0.5\lambda_o$ for the E- and H-plane coupling cases respectively. The good agreement between the results of this simple radiation coupling model and measurements indicates that the amount of coupling by a surface wave mechanism is negligible, even at 5GHz.

7.4 Conclusions

This work has shown that for E- and H-plane coupling between rectangular

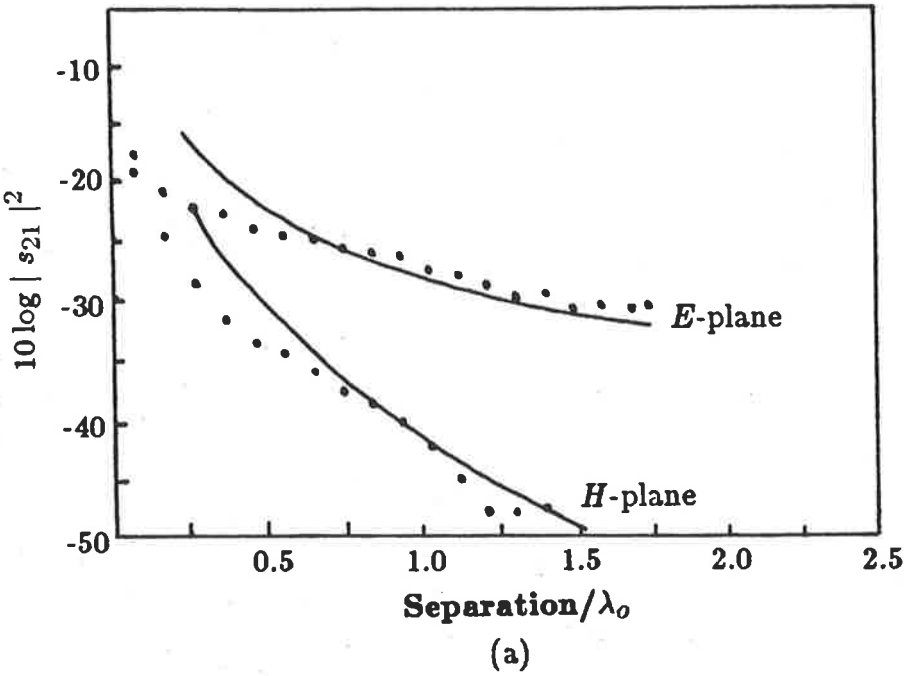

(a)

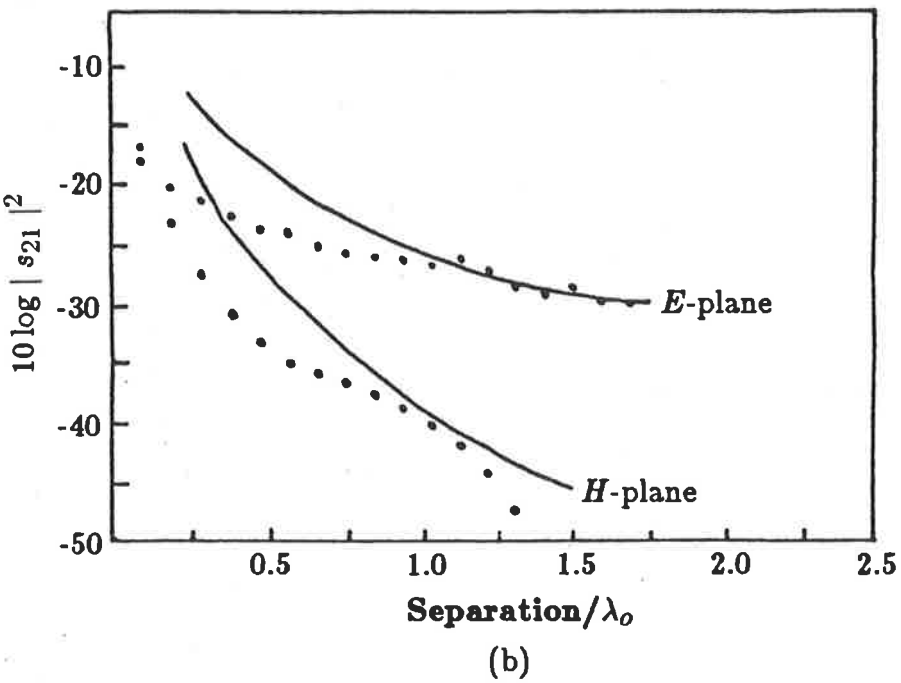

(b)

Figure 7.2: Measured (• • •) and calculated (——) mutual coupling as a function of separation for two 66mm by 105.6mm rectangular elements of thickness (a) 1.57mm and (b) 3.2mm, where f_o=1.4GHz.

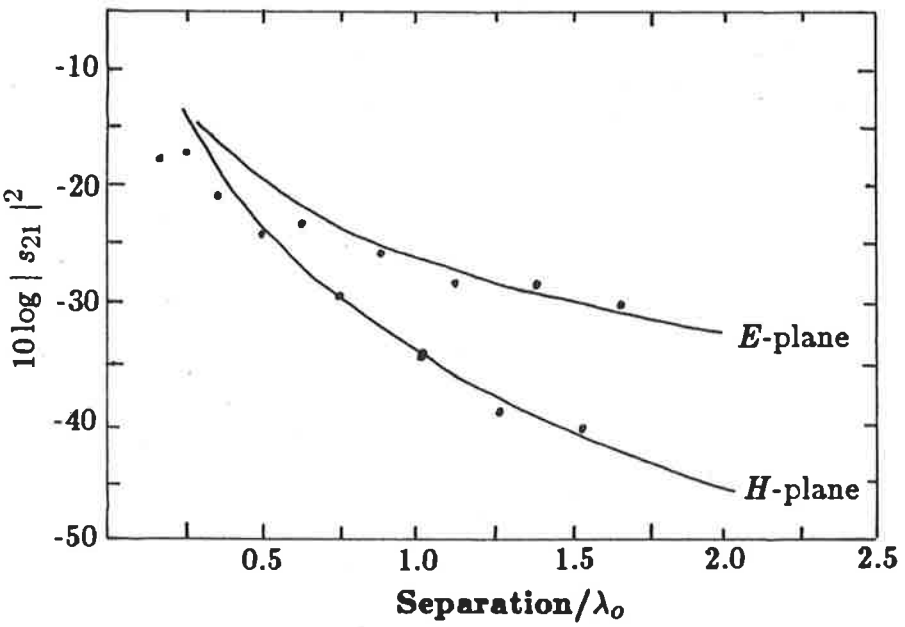

Figure 7.3: Measured (• • •) and calculated (———) mutual coupling as a function of separation for two 16.93mm by 16mm by 1.57mm rectangular elements, where f_o=5GHz.

patches separated by at least $0.75\lambda_o$, a very simple space radiation based transmission model of the coupling phenomena can provide results of comparable accuracy with those obtained by more sophisticated analytical techniques. Furthermore the model has been shown to give excellent results for antennas operating up to a frequency of 5GHz.

This model for calculating the mutual coupling between neighbouring rectangular microstrip antennas is used in the program listed in Appendix C. The coupling is expressed in terms of the magnitude of the scattering transfer coefficient. Given the dimensions of the two antennas, the frequency and the separation, the program evaluates the coupling using equations (7.3), and (7.11) through to to (7.14).

CHAPTER VIII

THE BANDWIDTH CHARACTERISTICS OF THE RECTANGULAR PATCH ANTENNA AND ITS EXTENSION USING A HEXAGONALLY SHAPED PATCH

8.1 Introduction

This chapter does not contribute to the computer-aided design of rectangular microstrip antennas but rather is in part an application of the work described in the previous chapters. The transmission line model described in Chapter V is used to investigate the dependence of the bandwidth on other antenna parameters. The efforts of other authors to increase the bandwidth of rectangular patch antennas are reviewed. Finally the definition of bandwidth introduced in Chapter IV is used to identify the hexagonally shaped patch as exhibiting a greater bandwidth than an equivalent rectangular patch, and a comparable bandwidth to a circular patch.

8.2 Using the transmission line model to study the effect of antenna parameters on the bandwidth of the antenna

The transmission line model has been used to account for the variation in the bandwidth of the rectangular patch antenna as other antenna parameters are varied. For example figure 8.1 shows that at 5GHz the bandwidth, expressed as a function of

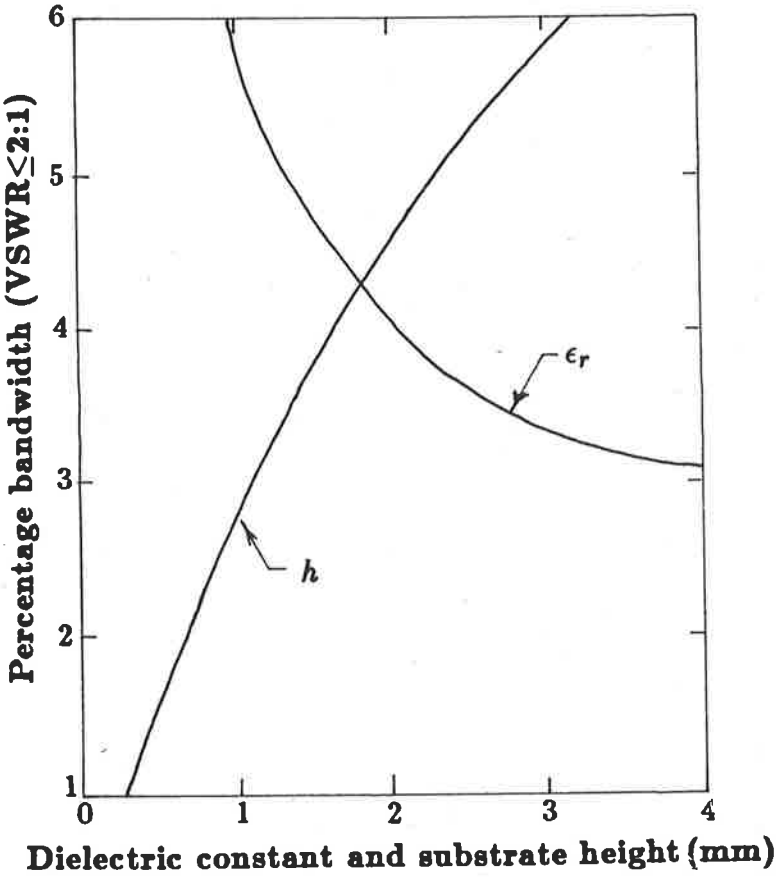

Figure 8.1: Bandwidth versus substrate height and relative dielectric constant.

the operating frequency, is an increasing function of the substrate thickness, h, and a decreasing function of the relative dielectric constant, ϵ_r.

The narrow bandwidth of the antenna was explained in Chapter III in terms of the cavity model as being due to the high quality factor of the equivalent cavity. The same conclusion can be reached using the transmission line model by calculating the antenna's input impedance as a function of frequency. Thus the frequency sensitivity of the input impedance can be attributed to the large ratio of aperture impedance, Z_a, to the characteristic impedance of the transmission line, Z_{om}. Refer to figure 1.4. This result is shown in figure 8.2, where the VSWR is plotted as a function of normalised frequency for three values of the characteristic impedance of the microstrip line. An extension to figure 8.2 is figure 8.3 where the percentage bandwidth is plotted against the characteristic impedance of the microstrip line. The transmission line model was

also used to calculate the bandwidth versus frequency relationship for different substrate thicknesses and substrate dielectric constants. Refer to figure 8.4.

8.3 A review of the techniques used by other authors to increase the bandwidth of microstrip antennas

There are many ways of increasing the bandwidth of microstrip antennas. However, all methods represent a compromise of bandwidth against substrate thinness, efficiency, or complexity in the antenna's structure. The techniques to increase the bandwidth can be combined into two groups.

The first group involves alterations to the fundamental element. The reason for the increase in the bandwidth can be explained by considering either a decrease in the antenna's quality factor or, appealing to the transmission line model, by an increase in the characteristic impedance of the microstrip line. An increase in the substrate thickness, h, will increase the bandwidth but at the cost of the antenna's low profile advantage. Karlsson [67] achieved a 17% bandwidth (VSWR$\leq$2:1) for a 6GHz square patch by increasing the substrate height to 8mm, where $\epsilon_r = 4$. Hall [68] showed that an increase in the loss tangent of the substrate material will lower the quality factor of the cavity, however, a decrease in the radiation efficiency will also result. Wiesbeck [69] loaded the cavity by cutting holes and slots into the metallic patch. This improvement may be explained in terms of lowering the quality factor of the cavity, or increasing the inductance per unit length of the transmission line, thus increasing the characteristic impedance of the line. A decrease in the dielectric constant has also been used to increase the bandwidth [2,70].

The other group of bandwidth broadening techniques involves a major alteration to the antenna's structure. The shape of the patch element has a small effect on bandwidth. The circular patch usually has a one to two percent wider bandwidth than its rectangular equivalent. When the patch is fed from a microstrip line, it is usually necessary to use a transmission line transformer to match the input impedance

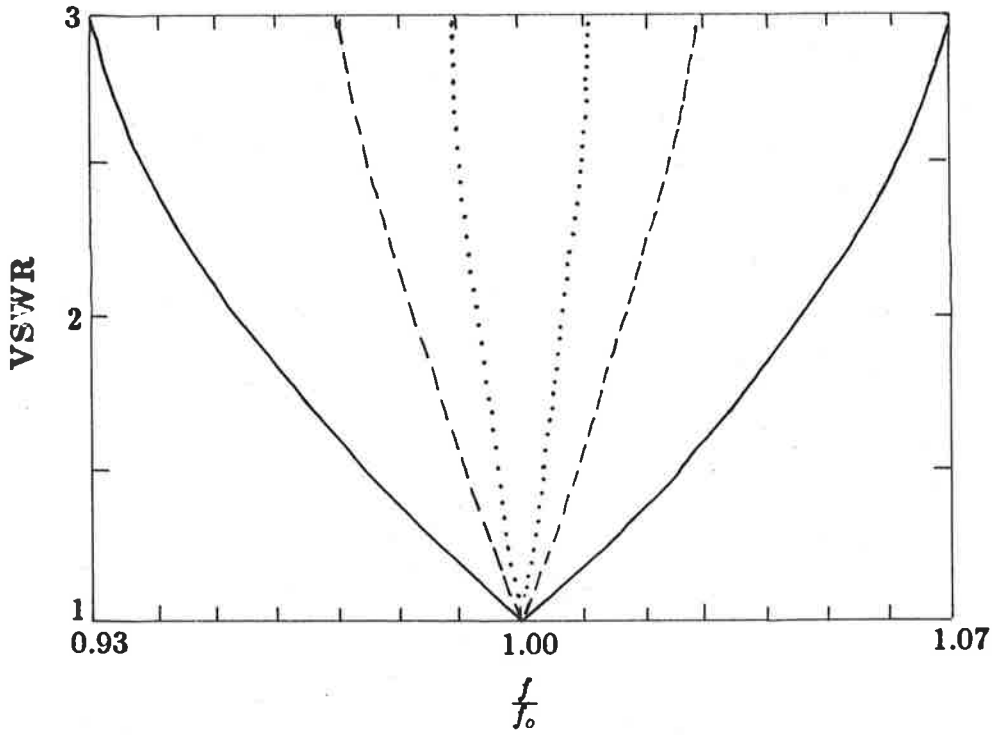

Figure 8.2: VSWR versus frequency for a rectangular element with the aperture resistance, R_a, arbitrarily chosen to be 100Ω, where the characteristic impedance of the transmission line, Z_{om}=10Ω(——), 4Ω(– – –), and 1.3Ω(· · · · ·).

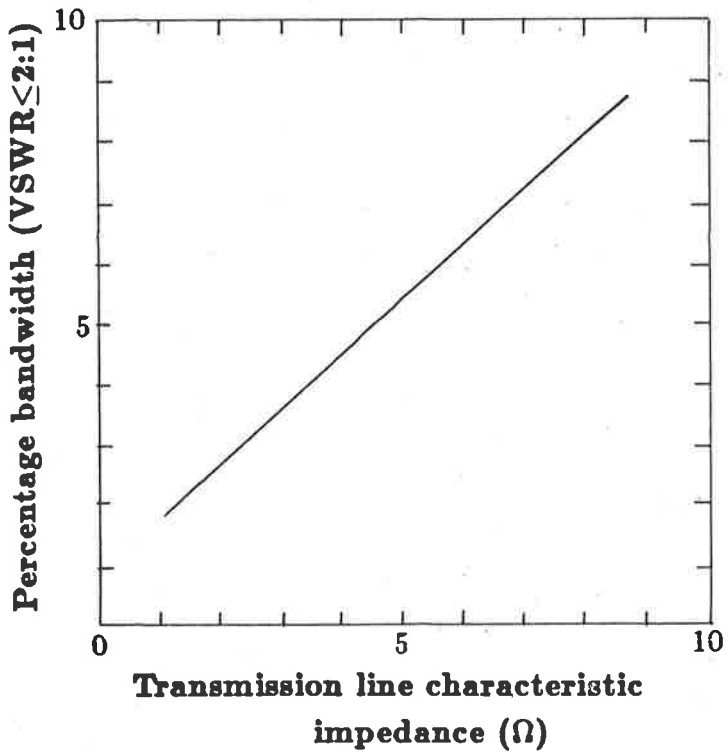

Figure 8.3: Bandwidth versus transmission line characteristic impedance Z_{om}, where the aperture resistance has been arbitrarily chosen to be 100Ω.

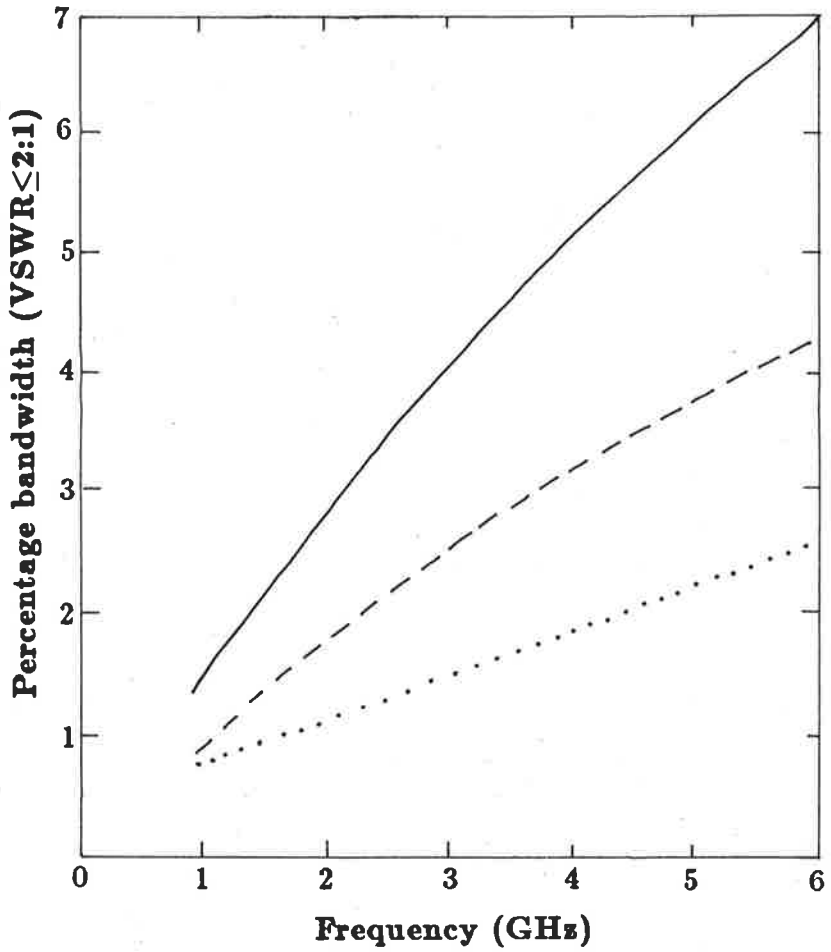

Figure 8.4: Bandwidth versus frequency for different substrate heights and relative dielectric constants, where h=1.57mm and $\epsilon_r = 2.55$ (– – –), h=0.8mm and $\epsilon_r = 2.55$ (· · · · · ·), h=1.57mm and $\epsilon_r = 1.0$ (——).

of the patch to the characteristic impedance of the microstrip feed line. The resulting bandwidth of the antenna system is then limited by the transformer rather than by the patch. However Howell [2] and Derneryd [71] have used a computer optimised two section transmission line transformer to match the element without decreasing the system bandwidth. Derneryd also used this technique to enhance the system's bandwidth by matching the element at two frequencies, ±12% each side of the element's resonant frequency. The usefulness of an antenna may be extended by a dual band configuration [71,72,73]. Here the element or the feed is constructed so that the antenna appears to be resonant at more than one frequency. However, the bandwidth is still a problem because at each of the resonant frequencies it is still only of the same order as the

bandwidth of a simple element. Ito et.al. [74] obtained a bandwidth improvement of two and a half times that of a single linear strip element by placing a window in the ground plane, directly behind the element. Here the antenna will radiate from both sides, and the antenna's electrical characteristics will depend on the size and location of the window. Multilayer elements were used by Hall [70] to achieve a bandwidth of 18% (VSWR$\leq$1.2:1). Two rectangular patches were placed above a smaller feeder patch which excited the top two patches by electromagnetic coupling. Broad-band microstrip antennas have also been constructed by combining together into arrays a number of stagger-tuned elements. The simplest case being a microstrip power divider feeding two rectangular patches located side by side, each resonant at a slightly different frequency. A more complex log-periodic type array has been built by Hall [68] and achieved a 30% bandwidth (VSWR$\leq$2.2:1) without any loss of radiation efficiency, or increased substrate thickness compared to the single element. The antenna was constructed of nine rectangular patches placed in a line and fed, via electromagnetic coupling, by a microstrip line buried in the centre of the substrate. The sizes of the patches were increased as the feed progressed through the array. Travelling wave antennas have also been constructed using microstrip techniques. However, there is a problem with mode control because these antennas are usually many wavelengths long. It has been shown that a microstrip line will radiate from discontinuities such as bends, and Wood [75] used this principle to design a spiralling line antenna that produced circularly polarised radiation over a 40% bandwidth (VSWR$\leq$1.3:1). Table 8.1 summarises the bandwidth related properties of the antennas that have been discussed.

8.4 Bandwidth of the hexagonal patch

A new hexagonally shaped patch exhibits a bandwidth greater than an equivalent rectangular element and comparable to that of a circular element. Figure 8.5 shows that the hexagon is formed by adding triangles along the sides of the rectangular patch, where the extension from the original rectangle is described in terms of the apex distance, a, measured from the original side of the rectangle. Also positive and negative apex

Microstrip antenna structures						
Antenna type	h mm	ϵ_r	f_{oz} MHz	η	Bandwidth %	VSWR
Rec. patch	1.59	2.32	10	90	5	≤2.0:1
Cir. patch	1.59	2.32	10	90	7	≤2.0:1
Lossy sub't	1.59	2.32	10	16	40	≤2.2:1
Spiral	1.59	2.32	10	50	40	≤1.3:1
Stacked	4.77	2.32	10	80	18	≤1.2:1
Log periodic	1.59	2.32	10	70	30	≤2.2:1
Window	0.80	2.60	3	N/A	6	N/A

Table 8.1: A summary of the bandwidth characteristics of microstrip antenna structures, where N/A refers to cases where no data is available.

distances are considered.

Input impedances were measured for a series of hexagonal elements with different apex distances as a function of frequency over a 1.6:1 range of variation. The impedance behaviour was then expressed in terms of the bandwidth using the definition presented in Chapter IV. Figure 8.6 shows that the bandwidth is proportional to the apex distance. It also shows that for the 0 to +3mm range of apex distances the resonant frequency is increased by 3.5 percent and the resonant resistance decreased by 11Ω.

The increase in the bandwidth with increasing apex distance is believed to be due to enhanced radiation from the sides of the patch. Hence the quality factor is decreased because the energy lost by the cavity through radiation is increased. This explanation is based on the changes in the far field radiation pattern that will be discussed in the next section.

8.5 Far field radiation pattern of the hexagonal patch

As the apex distance increases from 0 to +4mm, the gain is increased by 2dB,

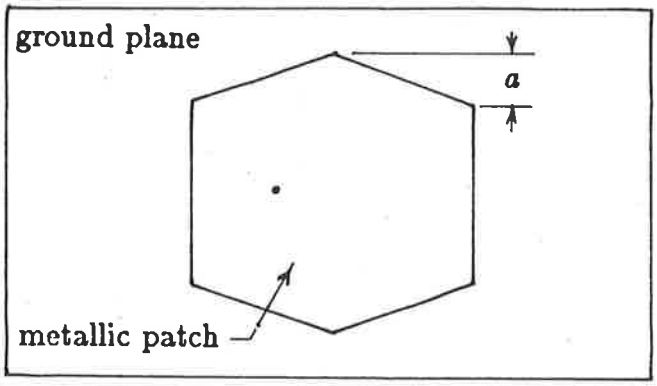

Figure 8.5: The basic geometry of the hexagonal patch.

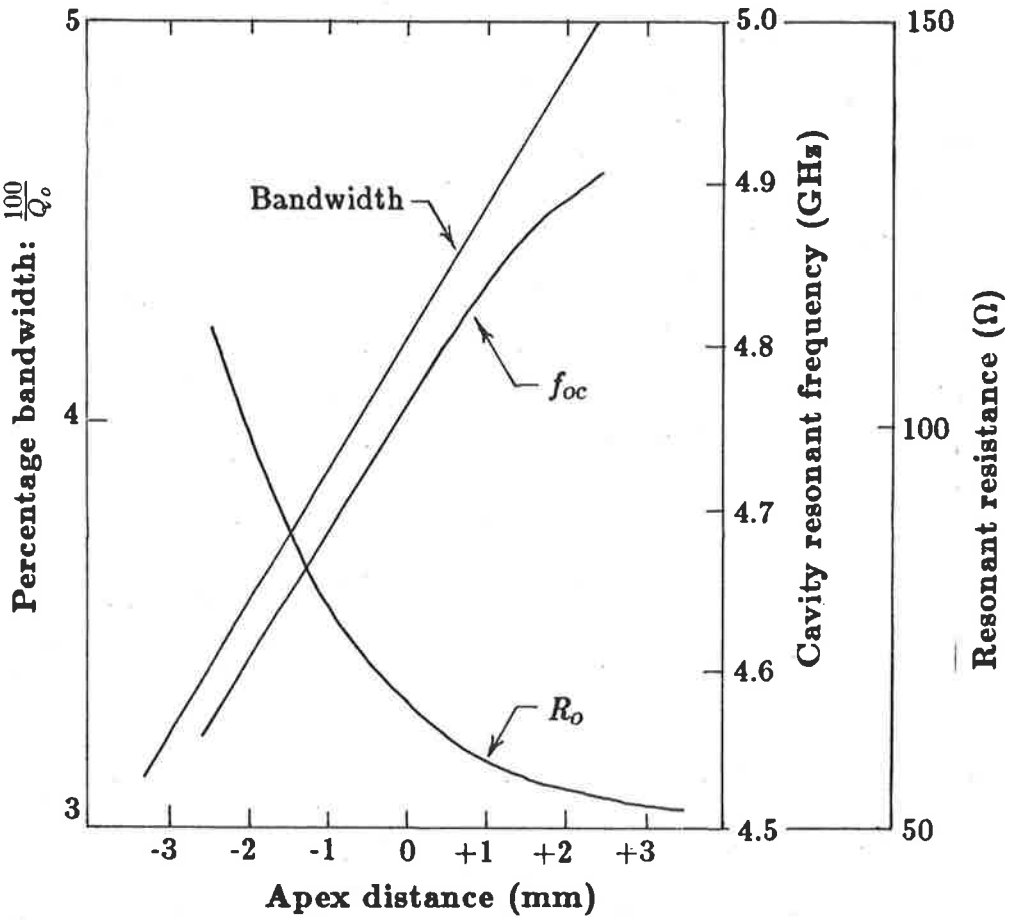

Figure 8.6: Bandwidth, impedance resonant frequency, and resonant resistance versus the apex distance.

the E-plane beam-width increases from 62 to 72 degrees and the H-plane beam-width decreases from 65 to 59 degrees. Figure 8.7 shows typical E-plane radiation patterns for both the rectangular and hexagonal, a=+4mm, patch antennas.

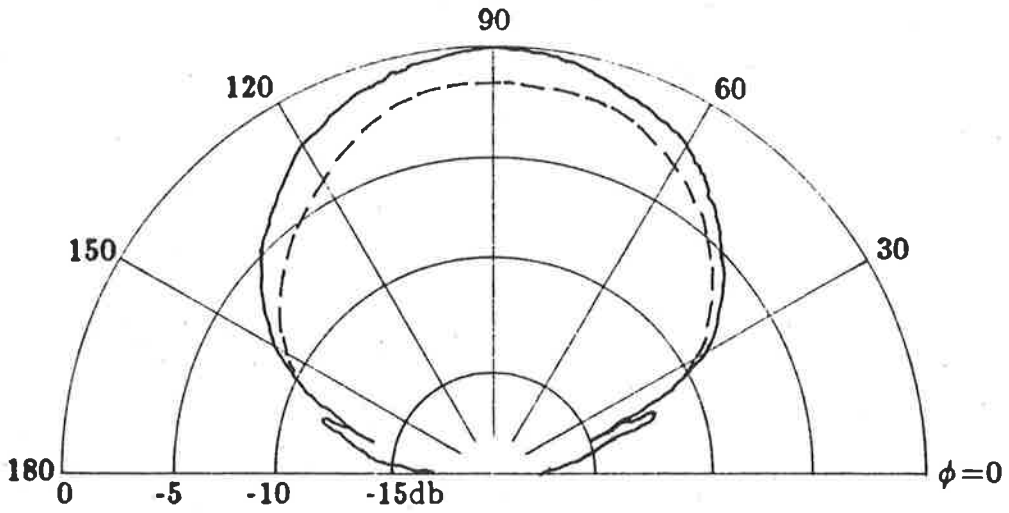

Figure 8.7: E-plane far field radiation patterns for a rectangular (– – –), 18.1mm by 16mm by 1.57mm, and hexagonal (———) a=+4mm, element.

8.6 Conclusions

The transmission line model has been used to account for some of the bandwidth properties of rectangular patch antennas. The results of an experimental investigation into the bandwidth performance of a novel hexagonal element have been presented. This element exhibits a wider-band and greater gain performance than an equivalent rectangular patch antenna.

CHAPTER IX

CONCLUSIONS

9.1 Conclusions

Models for inclusion in a computer-aided design program have been developed for rectangular microstrip antennas, fed by either a coaxial probe or a microstrip transmission line. Both the leaky resonant cavity and transmission line models were used to calculate the main electrical characteristics of the antenna to an accuracy sufficient for most design purposes. The accuracy of the new models for the probe reactance, resonant frequency, and input impedance all relied on empirically determined key parameters, while the radiation pattern and mutual coupling models represent the application of existing classical techniques of electromagnetic analysis.

The major achievement of this research was the presentation of formulas for critical antenna characteristics that produced results in very good agreement with measurements for antennas on typical substrates operating from 600MHz to 5GHz. The model for the feed probe predicted equivalent series reactances that were within $\pm 3\Omega$ or 15% of measurements. This was very satisfying alongside errors of up to 350% for models suggested by other authors. For the resonant frequency models the agreement with measurements was within $\pm 2\%$. This was achieved through specific definitions of the cavity and impedance resonant frequencies and the accurate empirical determination of

the effective edge extension. Again these models provided consistently accurate results for a very wide variety of antenna geometries. The accuracy of the transmission line model in calculating the input impedance was greatly improved by the use of empirically determined aperture admittances. The calculated loci gave resonant frequencies and resonant resistances that were on average within 2% and 17% of measurements. This agreement represents a significant improvement over the results that are obtained if an aperture admittance calculated using one of the published expressions is substituted into the transmission line model. The near field investigations carried out using the liquid crystal film produced some very interesting results regarding the radiation characteristics of the apertures located at each end of the antennas mounted on electrically thick substrates. However, the asymmetry in the excitation level and the beam tilting were later shown to be of little significance to the antenna's radiated field in the main E- and H-planes. Furthermore, the widely used two aperture array model has already been frequently shown in the literature to produce results in good agreement with measurements. Even for the case of an electrically thick substrate the model, as stated in the literature, provides results within 3dB of measurements. However, the agreement was improved to 2dB by correctly accounting for the array separation in terms of the effective width of the apertures at each end of the patch. This is regarded as a minor achievement of the research because the current state of the radiation pattern models provides main plane patterns that are sufficiently accurate for most design purposes. Another achievement of the research was the modelling of the mutual coupling in terms of the power transfer between two apertures located in each others far field. This work demonstrated that useful results can be obtained from a simple model. Although limited to cases where the separation was at least $0.75\lambda_o$, it gave both E- and H-plane mutual coupling results that were within 3dB of measurements for antennas operating up to and including 5GHz.

Areas within the microstrip antenna field that need immediate attention include a rigorous solution for the aperture admittance. Like the effective dielectric constant,

the aperture admittance parameter affects the accuracy of the analysis of all of the important electrical characteristics of the antenna. The great variation between the approximations that are currently being used has already been highlighted. The empirical equations for the aperture admittance presented here will certainly be useful until a rigorous approach is found. However, a more accurate empirical approach would be to determine a set of aperture admittance equations that cover a set of frequency bands of interest rather than the approach taken here where the aim was to present equations that were widely applicable. This aperture admittance problem is also evident from the liquid crystal near field investigations, which indicated a need for further work on the detailed nature of the mode structure of the fields under and fringing from the patch. Only when the types of observations described here are accounted for in an analytical model will all of the properties of the radiation field be predictable. Such a complete analysis would also permit the accurate calculation of input impedance and mutual coupling between antennas on thick substrates, even when they are so closely spaced that they are loading each others field distributions.

Because the brightest future of microstrip antenna technology lies in array applications, there is still a need for further work in developing new antenna geometries. This may include new patch shapes, or making major changes to the antenna's structure by cutting notches in the substrate, or even its total removal from around the patch. A new hexagonal element with enhanced bandwidth and gain performance over the rectangular antenna has been introduced but further work is needed to determine its suitability as an array element.

This thesis describes the development of simple models requiring moderate computing power for the major electrical characteristics of rectangular microstrip antennas. The models have been incorporated in a computer-aided design program which has been extensively tested on antennas representing a wide variety of those commonly encountered, and proven to provide results that are accurate enough for most design purposes.

REFERENCES

[1] G.A.Deschamps, "Microstrip microwave antennas," Third USAF Antenna Symposium, '53.

[2] J.Q.Howell, "Microstrip antennas," IEEE Antennas and Propagation Society International Symposium, Digest, pp177-180,'72.

[3] J.Q.Howell, "Microstrip antennas," IEEE trans. Antennas Propagat., pp90-93 Jan'75.

[4] R.E.Munson, "Conformal microstrip arrays and microstrip phased arrays," IEEE trans. Antennas Proagat., pp74-78, Jan'74.

[5] H.D.Weinschel, "A cylindrical array of circularly polarised microstrip antennas," IEEE Antennas and Propagation Society International Symposium, Digest, pp177-180, '75.

[6] P.S.Hall, J.R.James, "Survey of design techniques for flat profile microwave antennas and arrays," IERE proc., vol 48, no 11, pp549-565, Nov'78.

[7] I.J.Bahl, "Build microstrip antennas with paper-thin dimensions," Microwaves, pp50-63, Oct'79.

[8] W.C.Johnson, "Transmission lines and networks," McGraw-Hill, pp105, '50.

[9] R.F.Harrington, "Time harmonic electromagnetic fields," New York, McGraw-Hill, pp183, '61.

[10] T.A.Milligan, "Bandwidth and efficiency of a microstrip patch antenna," IEEE Antennas and Propagation Society International Symposium, Digest, pp585-588,'80.

[11] S.Silver, "Microwave antenna theory and design," McGraw-Hill,'49.

[12] A.G.Derneryd, "Linearly polarised microstrip antennas," IEEE trans. Antennas Propagat., pp846-851, Nov'76.

[13] M.V.Schneider, "Microstrip lines for microwave integrated circuits," Bell System T.J. vol 48 no 5, pp1421-1444, May-Jun, '69.

[14] E.O.Hammerstad, "Equations for microstrip circuit design," 5th European Microwave Conference. pp268-272, Sep'75.

[15] K.R.Carver, J.W.Mink, "Microstrip antenna technology," IEEE trans. Antennas Propagat., pp2-24, Jan'81.

[16] D.L.Sengupta, "Approximate expression for the resonant frequency of a rectangular patch antenna," Electron. Lett. vol 19, no 20, pp834-835, '83.

[17] H.A.Wheeler, "Transmission line properties of parallel strips separated by a dielectric sheet," IEEE trans. Microwave Theory and Technique, pp172-185, Mar'65.

[18] W.L.Weeks, "Antenna engineering," New York, McGraw-Hill, pp8-26,'68.

[19] E.H.Newman, P.Tulyathan, "Microstrip analysis technique," Proc. workshop on printed circuit antenna technology, New Mexico State Univ., Las Cruces, pp9.1-9.8, Oct 17-19, '79.

[20] T.Okoshi, T.Miyoshi, "The planar circuit - an approach to microwave integrated circuitry," IEEE trans. Microwave Theory and Technique, vol MTT-20, no 4, pp245-253, Apr'72.

[21] T.Itoh, R.Mittra, "A new method for calculating the capacitance of a circular disc for microwave integrated circuits," IEEE trans. Microwave Theory and Technique, pp431-432, Jan'73.

[22] T.Itoh, "Analysis of microstrip resonators," IEEE trans. Microwave Theory and Technique, vol MTT-22, no 11, pp946-952, Nov'74.

[23] Y.T.Lo, D.Solomon, W.F.Richards, "Theory and experiment of microstrip antennas," IEEE trans. Antennas Propagat., vol AP-27, no 2, pp-137-145, Mar'79.

[24] A.G.Derneryd, "Circular and rectangular microstrip antenna elements," Ericsson Technics no 3, pp160-171, '78.

[25] J.Watkins, "Circular resonant structures in microstrip," Electron. Lett., vol 5, pp524-525, 16th Oct'69.

[26] K.R.Carver, "The radiation pattern of a microstrip disc antenna," Physical Science Laboratory, New Mexico State Univ., Las Cruces PSL Tech Memorandum, 29th Nov'76.

[27] A.G.Derneryd, "Analysis of the microstrip disc antenna element," RADC-TR-77-383, Nov'77.

[28] S.A.Long, L.C.Shen, "The circular disc, printed circuit antenna," IEEE Antennas and Propagation Society International Symposium Digest, pp100-103, Jun'77.

[29] W.F.Richards, Y.T.Lo, D.D.Harrison, "An improved theory for microstrip antennas and applications," IEEE trans. Antennas Propagat., vol AP-29, no 1, pp38-46 Jan'81.

[30] K.R.Carver, E.L.Coffey, "Theoretical investigation of the microstrip antenna," ARO semi-annual research report, PT-00929, Jan'79.

[31] R.M.Foster, "A reactance theorem," Bell System Tech.J, vol 3, pp259-267, Apr '24.

[32] K.R.Carver, "Practical analytical techniques for the microstrip antenna," Proc. workshop on printed circuit antenna technology, New Mexico State Univ., Las Cruces, pp7.1-7.20, Oct'79.

[33] A.H.Mohammadian, N.M.Martin, D.W.Griffin, "A theoretical and experimental study of mutual coupling in microstrip antenna arrays," in preparation.

[34] K.R.Carver, "Input impedance to probe-fed microstrip antennas," IEEE Antennas and Propagation Society International Symposium, Digest, Quebec, pp617-620, Jun'80.

[35] W.F.Richards, Y.T.Lo, P.Simon, D.D.Harrison, "Theory and applications for microstrip antennas," Proc. workshop on printed circuit antenna technology, New Mexico State Univ., Las Cruces, pp8.1-8.23, Oct'79.

[36] P.K.Agrawal, M.C.Bailey, "An analysis technique for microstrip antennas," IEEE trans. Antennas Propagat., vol AP-25, no 6, pp756-759, Nov'77.

[37] E.H.Newman, "Strip antennas in a dielectric slab," IEEE trans. Antennas Propagat., vol AP-26, no 6, pp647-653, Sep'78.

[38] E.H.Newman, P.Tulyathan, "Analysis of microstrip antennas using moment method," IEEE trans. Antennas Propagat., vol AP-29, no 1, pp47-53, Jan'81.

[39] D.M.Pozar, "Input impedance and mutual coupling of rectangular microstrip antennas," IEEE trans. Antennas Propagat., vol AP-30, no 5, pp1191-1196, Nov'82.

[40] J.R.James, P.S.Hall, C.Wood, "Microstrip antenna theory and design," Peter Peregrinus, '81

[41] E.L.Ginzton, "Microwave measurements," McGraw-Hill,New York, '57, pp391-428.

[42] N.Marcuvitz, "Waveguide handbook," McGraw-Hill, New York, '51, pp183-184.

[43] J.M.Griffin, J.R.Forest, "Broadband circular disc microstrip antenna," Electron. Lett. vol 18, no 6, pp266-269, Mar'82.

[44] D.L.Sengupta, L.F.Martins-Camelo, "Theory of dielectric filled edge slot antennas," IEEE trans. Antennas Propagat., vol AP-28, no 4, pp481-490, Jul'80.

[45] D.L.Sengupta, "The transmission line model for rectangular patch antennas," IEEE Antennas and Propagation Society International Symposium, Digest, pp158-160, May'83.

[46] E.Lier, "Improved formulas for input impedance of coax-fed microstrip patch antennas," IEE proc, vol 129, pt H, no 4, pp161-164, Aug '82.

[47] E.C.Jordan, K.G.Balmain, "Electromagnetic waves and radiating systems," Prentice-Hall, '68, pp154,212.

[48] W.J.Getsinger, "Microstrip dispersion model," IEEE trans. Microwave Theory and Technique, vol MTT-21, no 1, pp34-39, Jan'73.

[49] P.Silvester, P.Benedek, "Equivalent capacitances of microstrip open circuits," IEEE trans. Microwave Theory and Technique, vol MTT-20, Aug'72.

[50] E.O.Hammerstad, "Computer-aided design of microstrip couplers with accurate discontinuity models," IEEE Microwave Theory and Technique Society International Symposium, Digest, pp54-56,'81.

[51] M.Kirschning, R.H.Jansen, N.H.L.Koster, "Accurate model for open end effect of microstrip lines," Electron. Lett, vol 17, no 3, pp123-125, Feb'81.

[52] E.O.Hammerstad, O.Jensen, "Accurate models for microstrip computer-aided design," IEEE Microwave Theory and Technique Society International Symposium, Digest, pp407-409, May'80.

[53] I.Wolff, N.Knoppik, "Rectangular and circular microstrip disc capacitors and

resonators," IEEE trans. Microwave Theory and Technique, vol MTT-22, pp857-864, Oct'74.

[54] D.W.Griffin, "Computer-aided determination of resonator characteristics based on expansion in normal modes and using automatic network analyser data," IEEE Microwave Theory and Technique Society International Symposium, Digest, '82.

[55] D.C.Chang, E.F.Kuester, "Resonance characteristics of a rectangular microstrip antenna," Proc. workshop on printed circuit antenna technology, New Mexico State Univ., Las Cruces, pp28.1-28.18, Oct'79.

[56] P.Hammer, D.Van Bouchaute, D.Verschraeven, A.Van De Capelle, "A model for calculating the radiation field of microstrip antennas," IEEE trans. Antennas Propagat., vol AP-27, no 2, pp267-270, Mar'79.

[57] J.R.James, C.J.Wilson, "Microstrip antennas and arrays," Pt. I, Fundamental action and limitations, IEE proc. pt H, Microwaves, Optics and Acoustics, vol 1, pp165-174, '77.

[58] N.P.Kernweis, J.F.McIlvenna, "Liquid crystal diagnostic techniques, an antenna design aid," Microwave journal, vol 20, pp47-51, 58, Oct'77.

[59] J.McIlvenna, N.Kernweis, "Diagnostic use of liquid crystal detectors in microstrip antenna design," RADC-TR-77-250, Jul'77.

[60] A.J.Derneryd, "A theoretical investigation of the microstrip antenna element," IEEE trans. Antennas Propagat., vol AP-26, no 4, pp532-536, Jul'78.

[61] I.J.Bahl, P.Bhartia, "Microstrip antennas," Artech House, '80, pp48-50.

[62] R.P.Jedlicka, K.R.Carver, "Mutual coupling between microstrip antennas," Proc workshop on printed circuit antenna technology, New Mexico State Univ., Las Cruces, pp4.1-4.19, Oct'79.

[63] C.M.Krowne, A.R.Sindoris, "H-plane coupling between rectangular microstrip antennas," Electron. Lett. vol 16, pp211-213, '80.

[64] C.M.Krowne, "E-plane coupling between two rectangular microstrip antennas," Electron. Lett. vol 16, no 16, pp635-636, '80.

[65] E.Penard, J.P.Daniel, "Mutual coupling between microstrip antennas," Electron. Lett. vol 18, no 14, pp605-607, Jul'82.

[66] D.W.Griffin, "Cross-polarised radiation from metal patch type microstrip antenna elements," IEEE Antennas and propagation Society International Symposium, Los Angeles, pp31-34, Jun'81.

[67] I.Karlsson, "Broadband microstrip antenna array," IEEE Antennas and Propagation Society International Symposium, Digest, pp593-596, '80.

[68] P.S.Hall, "New wideband microstrip antenna using log-periodic technique," Electron Lett. vol 16, no 4, pp127-128, Feb'80.

[69] W.Wiesbeck, "Miniaturisierte antenne in mikrowellenstreifen lectungstechnik," Nackrichtentechn Zeitschrift vol NTZ-28, pp156-159, May'75.

[70] P.S.Hall, C.Wood, C.Garrett, "Wide bandwidth microstrip antennas for circuit integration," Electron Lett. vol 15, pp458-460, '79.

[71] A.G.Derneryd, "Microstrip disc antenna covers multiple frequencies," Microwave journal, vol 21, pp77-79, May '78,

[72] G.G.Stanford, R.E.Munson, "Conformal VHF antenna for the Apollo-Soyuz test project," IEE conference proceedings, no 128, pp130-135, '75.

[73] J.L.Kerr, "Other microstrip antenna applications," Proc. of the 1977 Antenna Applications Symposium, Univ. of Illinois.

[74] K.Ito, N.Aizaira, N.Goto, "Increasing the bandwidth of circularly polarised

printed array antennas composed of strips and slots," IEEE Antennas and Propagation Society International Symposium, Digest, pp597-600, '80.

[75] C.Wood, "Curved microstrip lines as compact wideband circularly polarised antennas," IEE proc. pt. H, Microwaves, Optics and Acoustics, vol 3, no 1, pp5-13, Jan'79.

APPENDIX A

ANTENNA MANUFACTURE AND SPECIFICATIONS

All of the antennas and microstrip transmission lines were manufactured using DI-CLAD CUT-N-PEEL woven PTFE laminate made by Keene Corporation, where: ϵ_r=2.55, h=1.57mm or 0.735mm, and t=0.05mm.

The antennas were manufactured using standard precision workshop equipment, including: a flat table, a right angle block, and a scalpel blade fixed to a height vernier. The copper clad substrate was mounted in the vertical position while the blade in the height vernier was used to successively scribe and eventually cut through the copper. After all of the horizontal cuts were made, the substrate was rotated by 90^o to facilitate cutting in the direction perpendicular to those taken first. Any lifting along the edges was then lightly smoothed down. The technique produced a consistent undersized product, however this was taken into account by adding 0.03mm to all dimensions before cutting. The final manufacturing accuracy was $\pm$0.04mm.

APC-7 and SMA connectors were used throughout this project, the relevant dimensions of which are given in table A.1. For the case of probe fed antennas, the inner conductors of either APC-7 or SMA type connectors were extended through the dielectric substrate to make connection with the metallic patch. Hence these probes are referred to as either APC-7 or SMA in dimension.

Coaxial connector dimensions		
Type	inner radius a(mm)	outer radius b(mm)
APC-7	1.520	3.50
SMA	0.635	2.05

Table A.1: Dimensions of the coaxial connectors feeding the antenna, where the inner conductor is extended to become the probe.

The complete manufacturing data for the antennas referred to in the thesis are listed in the "DATA" statements near the start of the computer program in Appendix C. The order of information is:

Measured f_{oc}, L, W, h, D, ϵ_r, Feed type

Note that due reference is given to the data obtained from measurements published by other authors. Experiments that were incomplete in their description were quite common. However, the parameters could often be pieced together through reference to successive papers published by the author or members of the same research group. In the cases of [19],[29],and [30] however, it was necessary to directly write to the authors concerned seeking full details of their experiments. Without exception these researchers did not reply to the request, necessitating the guessing of some of the parameters of their experiments in order to make up the data sets.

APPENDIX B

RADIATION PATTERN, INPUT IMPEDANCE, AND MUTUAL COUPLING MEASUREMENT

All of the experimental techniques were built around an automatic network analyser system (ANA) based on the HP8410 controlled by a HP9845 mini-computer.

The far field radiation patterns were measured in a 3m by 3m by 9.1m anechoic chamber lined on all faces with 46cm high pyramidal absorbers. The test path of the ANA was used to measure the radiation pattern of the antenna by determining the s_{21} scattering transfer coefficient for the free space path loss between the rotating test antenna and the receiving horn. Figure B.1 shows a schematic of the measurement system where the HP9845 was used to plot out the radiation patterns in polar coordinates.

Input impedances were also measured using the ANA where the reference plane was defined at the back of the ground plane through the use of in-house constructed calibration terminations. The gold plated APC-7 short and open circuited terminations were used to move the reference plane 33.6mm away from the face of the connector in the test port of the ANA, permitting the easy manufacture of numerous extended flange mount receptacles that were used to feed the antennas. The SMA calibration terminations were constructed using a commercial flange mount receptacle for the short circuit and a modified in-line female-female adapter for the open circuit. Again, the reference plane was the back of the ground plane. The HP9845 was used to present the

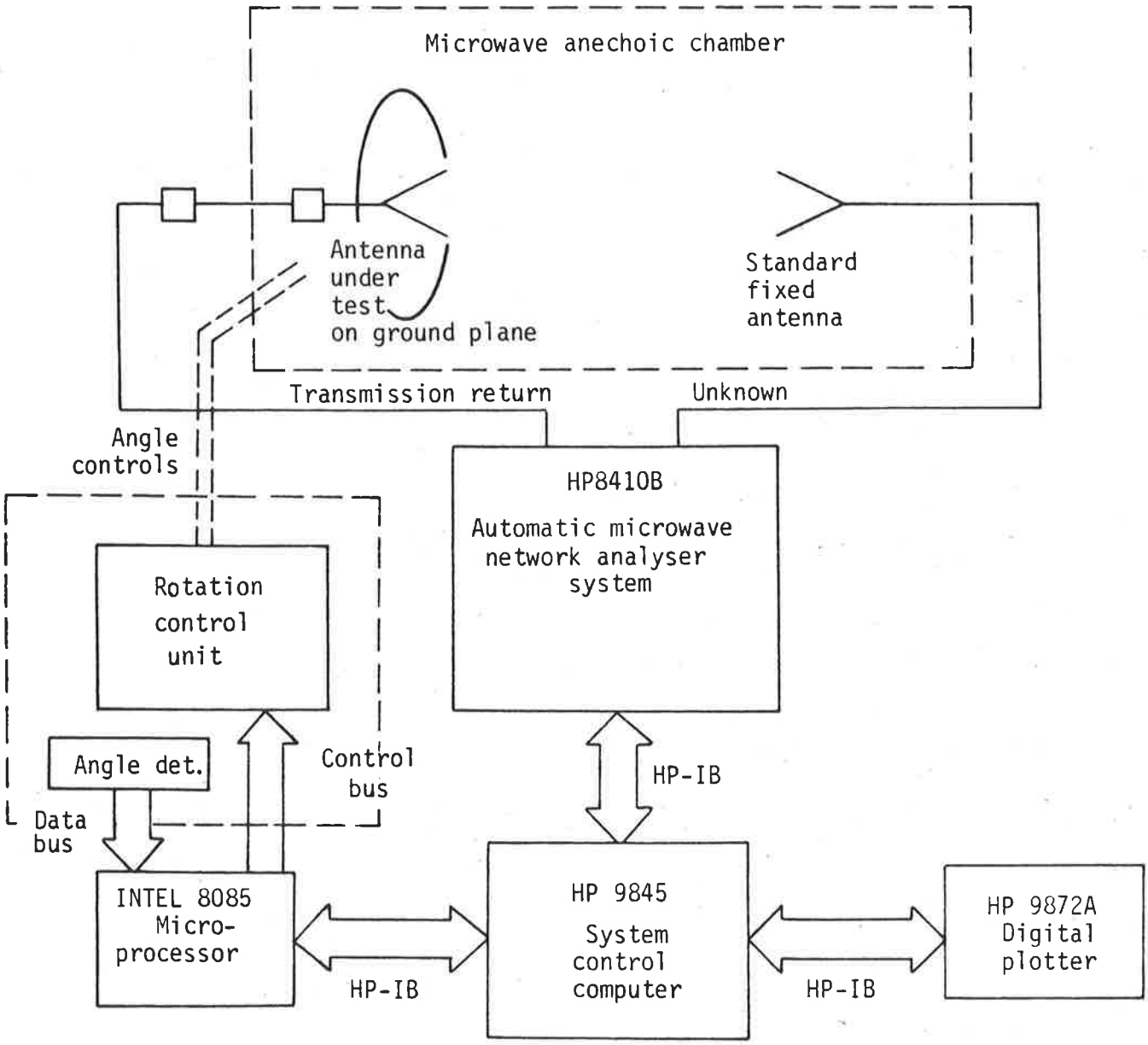

Figure B.1: Schematic of the equipment used to measure far field radiation patterns.

s_{11} results for the input impedance in Smith chart form. Also a HP5245L frequency counter and HP5257A transfer oscillator were used to calibrate the frequency of the ANA.

The mutual coupling between the antennas shown in figure 7.1 was measured with an ANA in terms of s_{21} using the same technique as proposed by Jedlicka et.al. [62], where in order to establish two antennas of varying separation, a set of substrate inserts were placed between the antennas to form a continuous substrate of variable length.

APPENDIX C

COMPUTER-AIDED DESIGN PROGRAM FOR RECTANGULAR MICROSTRIP ANTENNAS

The following is a listing of the computer-aided design program for rectangular microstrip antennas. It includes all of the new models introduced in the body of this thesis and, through the use of multiple option flags, can be used to execute many of the models suggested by other authors. The program is written in BASIC computer language and is suitable for execution on a HP9845 mini-computer.

```
10    !  ************************************************************************
20    !  ************************************************************************
30    !  **                                                                    **
40    !  **                      COMPUTER AIDED DESIGN                         **
50    !  **                             OF                                     **
60    !  **                 RECTANGULAR MICROSTRIP ANTENNAS                    **
70    !  **                                                                    **
80    !  **              Part of the research effort towards the               **
90    !  **                degree of Doctor of philosophy by:                  **
100   !  **                                                                    **
110   !  **                       NOEL MAXWELL MARTIN                          **
120   !  **                                                                    **
130   !  **                      University of Adelaide                        **
140   !  **               Department of Electrical and Electronic              **
150   !  **                          Engineering                               **
160   !  **                                                                    **
170   !  **                          December 1984                             **
180   !  **                                                                    **
190   !  **                                                                    **
200   !  **                   Supervisor:Dr.D.W.Griffin                        **
210   !  **                                                                    **
220   !  ************************************************************************
230   !  ************************************************************************
240   !
250   !
260   !
270   !
280   !
290   !
300   ! This is a computer-aided design program for rectangular microstrip
310   ! antennas. The design and analysis are carried out using the formulas
320   ! presented in the thesis of the same title. The equation numbers
330   ! in the thesis can be used to identify the  same equations in
340   ! the program.
350   !
360   ! The general layout of the program is shown below. If the designer is
370   ! starting with a desired resonant frequency and a specified patch width,
380   ! substrate height, dielectric constant and feed type, then the length
390   ! of the patch must be designed before analysis can take place. Refer
400   ! to line 'Ddesign'. The analysis of a fully specified patch starts at
410   ! line 'Analysis'. From this point the designer can choose to analyse
420   ! for the series reactance of the probe and the resonant frequency,
430   ! the input impedance, the far field radiation pattern or the mutual
440   ! coupling between two antennas of the same dimensions. If the measured
450   ! resonant frequency is put into the program then the radiation pattern
460   ! and mutual coupling are evaluated at this frequency. However if the
470   ! resonant frequency is calculated, then this calculated value replaces
480   ! the measured frequency in any further analysis.
490   !
500   ! Two sets of flags, located at lines 'F1' and 'F2', permit the
510   ! evaluation of the equations proposed by other authors for various
520   ! antenna and transmission line parameters. This program also includes
530   ! the code that was used to determine the empirical equations for the
540   ! effective edge extension and the aperture admittance. The aperture
550   ! admittance being the reciprocal of the impedance referred to as the
560   ! slot impedance in the program.
570   !
580   !
590   ! The analysis of a rectangular resonant cavity is also included in the
600   ! program. These subroutines enable the calculation of the resonant
610   ! frequencies from a set of dimensions and the dielectric constant,
620   ! or the calculation of the dielectric constant from two sets of measured
630   ! resonant frequencies obtained from two cavities of slightly different
640   ! dimensions.
650   !
660   !
670   !
```

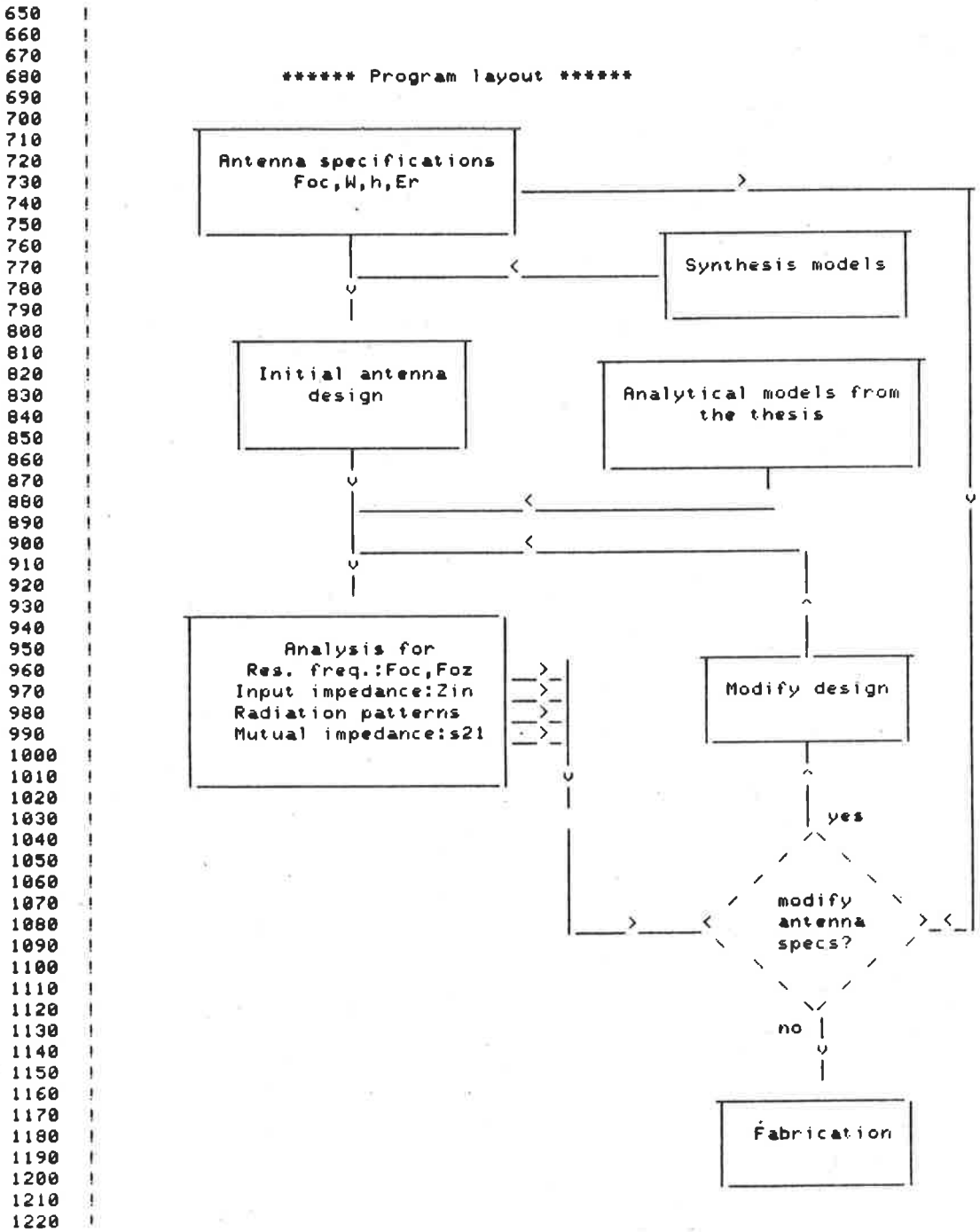
****** Program layout ******
Antenna specifications
Foc,W,h,Er
Synthesis models
Initial antenna
design
Analytical models from
the thesis
Analysis for
Res. freq.:Foc,Foz
Input impedance:Zin
Radiation patterns
Mutual impedance:s21
Modify design
yes
modify
antenna
specs?
no
Fabrication

```
1220  !
1230  !
1240  !            ****** subroutine listing ******
1250  !
1260  !                  Description                    Name          Line(no.)
1270  ! Input impedance of a rectangular patch         Zin           Zin(5900)
1280  ! Input impedance of an aperture antenna         Zslot         Zsl(6180)
1290  ! Empirical development of an expression
1300  ! for the aperture input impedance               Zslotsyn      Zsy(7630)
1310  ! Effective dielectric constant                 Effer         Eff(8080)
1320  ! Characteristic imp. of a parallal plate
1330  ! transmission line                             Zom           Zom(8250)
1340  ! Edge extension                                Deltal        Del(8400)
1350  ! Microstrip feed point                         Msfp          Msf(9580)
1360  ! Mutual coupling                               Couplingfar   Mut(10890)
1370  ! Mutual coupling with E-plane orientation      Eplane        Epl(12520)
1380  ! Mutual coupling with H-plane orientation      Hplane        Hpl(12750)
1390  ! Transmission line equation                    Tll           Tle(13190)
1400  ! Simpsons rule                                 Simp          Sim(12930)
1410  ! Polar to rectangular                          Ptor          Ptr(13540)
1420  ! Rectangular to polar                          Rtop          Rtp(13640)
1430  ! Complex multiply                              Cmult         Cmu(13750)
1440  ! Complex divide                                Cdiv          Cdi(13840)
1450  ! Characteristic impedance of a coax line       Zo            Zoc(14140)
1460  ! Capacitance of a parallal plate               Cpp           Cpp(14240)
1470  ! Quality factor and radiation conductance      Qandgrad      Qan(14388)
1480  ! Resonant cavity analysis                      Cavity        Cav(14690)
1490  ! Solution of a quadratic equation              Quadratic     Qua(15760)
1500  ! Parallel combination of two impedances        Parallel      Par(15890)
1510  ! Factorial                                     Factorial     Fac(16010)
1520  ! Bessel's function of order zero               Bessel        Bes(16130)
1530  ! Sine and cosine integrals                     Sici          Sci(16360)
1540  ! Radiation pattern                             Rad           Rad(16640)
1550  ! Resonant frequency                            Fo            Res(17460)
1560  !
1570  !
1580  !
1581  !                  ****** main program ******
1582  !
1583  !
1590  !
1600  TRACE ALL VARIABLES
1610  PRINT ALL IS 16
1620  PRINTER IS 0
1630  FIXED 2
1640 Start:!
1650  PRINTER IS 16
1660  PRINT "Computer-aided design of a rectangular patch Antenna or"
1670  PRINT "analysis of a rectangular resonant Cavity A/C ?"
1680  INPUT Ans$
1690  IF Ans$="A" THEN GOTO 1720
1700  CALL Cavity
1710  GOTO Start
1720  PRINTER IS 0
1730  PRINT "*************************************************************************"
1740  PRINT "*************************************************************************"
1750  PRINT "**                    COMPUTER-AIDED DESIGN                            **"
1760  PRINT "**                          OF                                         **"
1770  PRINT "**              RECTANGULAR MICROSTRIP ANTENNAS                        **"
1780  PRINT "*************************************************************************"
1790  PRINT "*************************************************************************"
1800  !
1810 F1: ! **********Flags for the analysis**************************************
1820  Tlflag$="Sinusoidal"          !Caver/Newman/Sengupta/Sinusoidal/Straight
1830  !                              type of TL model for the feed.
1840  Foflag$="Martin"              !Martin/Sengupta/out
1850  Fringeflag$="Empirical"       !Factor/Hamm1/Hamm2/KIR/Experimental/Empirical
1860  Erflag$="Getsinger"           ! Getsinger/Hammerstad
1870  ! *************************************************************************
1880  PRINTER IS 16
```

```
1890  PRINT "Do you need to Design an antenna length for a specified"
1900  PRINT "resonant frequency, or do you want to Analyse a full set of"
1910  PRINT "dimensions    D/A?"
1920  PRINTER IS 0
1930  INPUT Ans$
1940  IF Ans$="D" THEN GOTO Ddesign
1950  GOTO Adata
1960  !
1970  !
1980  !
1990 Ddesign:! Data for the design of the antenna length
2000  !
2010  PRINT
2020  PRINT
2030  PRINT "-------INITIAL DESIGN FOR THE LENGTH  OF A RECTANGULAR PATCH -----"
2040  PRINT
2050  INPUT "Foc:cavity res freq(Mhz),Width(mm),Height(mm),Dielectric const,Feed
type?",Focmhz,Wmm,Hmm,Er,Feed$
2060  CALL Zom(Wmm,Hmm,Zom) !Hammerstad
2070  CALL Effer(Erflag$,Focmhz,Zom,Er,Wmm,Hmm,Effer)
2080  Fochz=Focmhz*1E6
2090  Vlengthmma=3E8/(2*Fochz*SQR(Effer))  !Approximate antenna length to be
2100  !    used in the expression for Deltal                                    (3.1)
2110  CALL Deltal(Fringeflag$,Wmm,Hmm,Vlengthmma,Er,Effer,Focmhz,Deltalmm)
2120  Deltalm=Deltalmm/1000
2130  Vlength=(3E8-4*Fochz*Deltalm*SQR(Effer))/(2*Fochz*SQR(Effer))
2140    ! Res half wave(m)                                                      (3.2
)
2150  Vlengthmm=Vlength*1000 !mm
2160  CALL Qandgrad(Focmhz,Hmm,Vlengthmm,Wmm,Grad,Qrad,Qdi,Qcu,Qo)
2170  Rrad=1/Grad !ohm
2180  Re=Rrad/2 !Rrad=Rslot,Re:resistance at the end=Rslot//Rslot
2190  D=Vlengthmm*ACS(SQR(50/Re))/PI !Caver APS Jan 81 pp12
2200  PRINT "Design cavity resonant frequency(Foc)=";Focmhz;"Mhz"
2210  PRINT "Calculated patch length=";Vlengthmm;"mm"
2220  PRINT "Initial guess of the feedpoint for Zin = 50ohm is ";D;"mm"
2230  GOTO Cont
2240  !
2250  !
2260 Adata: !
2270  !
2280  INPUT "Enter antenna specs. from the Key board or Array K/A",Ans$
2290  IF Ans$="A" THEN GOTO Data
2300  INPUT "Do you have a measured resonant frequency Y/N ?",Ans$
2310  IF Ans$="N" THEN GOTO Dims
2320  PRINTER IS 16
2330  PRINT "Foc:cavity res freq(Mhz),Length(mm),Width(mm),Height(mm),Feed inset
 distance(mm),Dielectric const,Feedtype?"
2340  PRINTER IS 0
2350  INPUT Focmhz,Vlengthmm,Wmm,Hmm,D,Er,Feed$
2360  PRINT "Measured cavity resonant frequency(Foc)=";Focmhz;"Mhz"
2370  PRINT "Specified patch length=";Vlengthmm;"mm"
2380  PRINT "Specified feedpoint=";D;"mm"
2390  GOTO Cont
2400 Dims: PRINTER IS 16
2410  PRINT "Lengthmm,Width(mm),Height(mm),Feed inset distance(mm),Dielectric co
nst,Feedtype?"
2420  PRINTER IS 0
2430  INPUT Vlengthmm,Wmm,Hmm,D,Er,Feed$
2440  Focmhz=.9*300/(2*(Vlengthmm/1000)*SQR(Er))!approximate resonant frequency
2450  ! needed for the determination of Deltal and Effer, where the .9 accounts
2460  ! for the effect of fringing.
2470  PRINT "Approximate resonant frequency=";Focmhz;"MHz"
2480  PRINT "Specified patch length=";Vlengthmm;"mm"
2490  PRINT "Specified feedpoint=";D;"mm"
2500  GOTO Cont
2510 Data: !
2520  PRINT "Data set:  633.5/658/915/1189/1197/1396/1396/1410/1518/2195/2210"
2530  PRINT "             2213/2224/2792/3387/"
2540  PRINT "           3502/4670/4672/4744*/4770/4784/4792/4830/5013 ?"
```

```
2550  INPUT "Foc of data array set ?",Data
2560  ! Data=5013
2570  RESTORE
2580  FOR N=1 TO 40
2590  READ Focmhz,Vlengthmm,Wmm,Hmm,D,Er,Feed$
2600  IF Focmhz=Data THEN GOTO Enddata
2610  NEXT N
2620  PRINT
2630  PRINT " Data not available"
2640  GOTO Start
2650  ! Frequency corrected foc.
2660  DATA 4659,18.03,30.0,1.57,6.21,2.55,"APC7"
2670  DATA 4669,18.03,28.0,1.57,6.21,2.55,"APC7"
2680  DATA 4674,18.03,25.65,1.57,6.21,2.55,"APC7"
2690  DATA 4687,18.03,24.75,1.57,6.21,2.55,"APC7"
2700  DATA 4700,18.03,22.66,1.57,6.21,2.55,"APC7"
2710  DATA 4724,18.03,19.40,1.57,6.21,2.55,"APC7"
2720  DATA 4751,18.03,16.49,1.57,6.21,2.55,"APC7"
2730  DATA 5007,18.03,13.04,1.57,6.21,2.55,"APC7"
2740  !
2750  DATA 633.5,150,75,3.175,60,2.56,"SMA" !Pozar APS Nov82 [39]
2760  !                                      & Newman 'Workshop'[19]
2770  DATA 658,139.7,204.5,1.588,63.50,2.59,"SMA" !Pozar APS Nov82 [39]
2780  DATA 915,57.7,50,1.57,0,2.1,"SMA"
2790  DATA 1189,76.2,114.3,1.59,22.9,2.62,"SMA" !Richards APS Jan'81 [29]
2800  DATA 1197,76.0,114.0,1.59,00,2.62,"SMA"
2810  DATA 1396,65.5,105.6,1.57,17,2.55,"SMA"
2820  DATA 1410,66,105.6,1.57,17,2.5,"SMA"
2830  DATA 1518,59.5,100,1.59,0,2.62,"TL"
2840  DATA 2195,41.4,68.58,1.588,00.00,2.50,"TL"!Carver/Coffey ARO pp52 [30]
2850  !                                  and Er=2.5 from APS Jan'81 [29] pp13
2860  DATA 2210,41.4,68.58,1.588,00.00,2.50,"SMA"!      [30] pp53
2870  DATA 2213,41.4,68.58,1.588,10.16,2.50,"SMA"!      [30] pp54
2880  DATA 2224,41.4,48,1.59,7.62,2.50,"SMA"
2890  !                                refer Carver/Mink APS Jan'81 [15] for Er=2.5
2900  DATA 2792,33.0,33.0,1.524,11.50,2.55,"SMA" !Derneryd Ericson [24]
2910  DATA 3387,26.63,23,.8,10.15,2.55,"SMA"
2920  DATA 3502,25.66,23.10,0.80,10.15,2.55,"SMA"
2930  DATA 4670,18.47,16,0.80,6.14,2.55,"APC7"!4663
2940  DATA 4672,18.03,30,1.57,6.21,2.55,"APC7"
2950  DATA 4744,18.03,16,1.57,6.21,2.55,"APC7"
2960  DATA 4770,18.03,13.5,1.57,6.21,2.55,"APC7"
2970  DATA 4784,18.11,16,1.57,6,2.55,"SMA"
2980  DATA 4792,18.54,16.04,.8,6.14,2.55,"SMA"
2990  DATA 4830,18.47,16,.8,6.14,2.55,"SMA"
3000  DATA 5013,16.93,16,1.57,5.5,2.55,"APC7"
3010  ! DATA 5013,27.04,25.55,2.51,5.5,1.,"APC7"
3020 Enddata: !
3030  PRINT
3040  PRINT "Measured cavity resonant frequency(Foc)=";Focmhz;"Mhz"
3050  !
3060  !
3070  !
3080  !
3090  PRINT "Specified patch length=";Vlengthmm;"mm"
3100  PRINT "Specified feedpoint position=";D;"mm"
3110 Cont:!
3120  PRINT
3130  IF Feed$="SMA" THEN GOTO 3210
3140  IF Feed$="APC7" THEN GOTO 3180
3150  IF Feed$="TL" THEN GOTO 3230
3160  PRINT "feed not specified correctly"
3170  GOTO Start
3180  Radiusi=1.52 !mm
3190  Radiuso=3.5 !mm
3200  GOTO 3230
3210  Radiusi=.64 !mm
3220  Radiuso=2.05 !mm
3230  !
3240  Rr=Wmm/Vlengthmm
```

```
3250  !
3260  PRINT "Patch width=";Wmm;"mm"
3270  PRINT "Substrate height=";Hmm;"mm "!100*h/lamdas @ Foc=";Hdlams
3280  PRINT "Dielectric constant=";Er
3290  PRINT "Feed type=";Feed$
3300  !
3310  !
3320  !
3330 Analysis: !
3340  PRINT "-------------------------------------------------------------------"
3350  PRINT "-------------ANALYSIS OF A RECTANGULAR PATCH----------------------"
3360  PRINT "-------------------------------------------------------------------"
3370  !
3380  CALL Zom(Wmm,Hmm,Zom) !Hammerstad
3390  CALL Effer(Erflag$,Focmhz,Zom,Er,Wmm,Hmm,Effer)
3400  CALL Deltal(Fringeflag$,Wmm,Hmm,Vlengthmm,Er,Effer,Focmhz,Deltalmm)
3410  !
3420  ! ##Zom by other authors##
3430  ! Carver APS trans Jan '81 pp5 [15]
3440  Zomcaver=Hmm*377/(Wmm*SQR(Er))
3450  ! Sengupter APSIS '83 pp159 [45]
3460  Alpha=1+1.393*(Hmm/Wmm)+.667*(Hmm/Wmm)*LOG(Wmm/Hmm+1.444)
3470  Zomsen=377*Hmm/(Wmm*Alpha*SQR(Effer))
3480  !
3490  Deltalm=Deltalmm/1000
3500  Fochz=Focmhz*1E6
3510  Vlamom=3E8/Fochz!m
3520  Vlamsm=Vlamom/SQR(Effer)!m
3530  Vlamsmm=Vlamsm*1000
3540  Vlamomm=Vlamom*1000
3550  Zoms=Zom/SQR(Effer)
3560  !
3570  PRINTER IS 16
3580  PRINT " The order of analysis is:-"
3590  PRINT "              Series reactance of the probe,"
3600  PRINT "              Resonant frequency,"
3610  PRINT "              Input impedance,"
3620  PRINT "              Radiation pattern, and"
3630  PRINT "              Mutual coupling."
3640  PRINT "              Empirical determination of Zslot"
3650  PRINT "However these analyses do not need to be done in order."
3660  PRINTER IS 0
3670  INPUT "Do you want to follow the above order Y/N ?",Ans$
3680  IF Ans$="Y" THEN GOTO Feedpt
3690  INPUT "Go immediately to the input impedance analysis Y/N ?",Ans$
3700  IF Ans$="Y" THEN GOTO Ti
3710  INPUT "Go immediately to the radiation pattern analysis Y/N ?",Ans$
3720  IF Ans$="Y" THEN GOTO Pattern
3730  INPUT "Go immediately to the mutual impedance analysis Y/N ?",Ans$
3740  IF Ans$="Y" THEN GOTO Mutual
3750  INPUT "Determine values for Zslot Y/N ?",Ans$
3760  IF Ans$="Y" THEN GOTO Sy
3770  GOTO 3580
3780  PRINT
3790  PRINT
3800  PRINT
3810  !
3820  !
3830  !
3840 Feedpt: PRINT
3850  PRINT "-------------------Analysis of the probe--------------------------"
3860  !
3870  IF Feed$="TL" THEN GOTO 3910
3880  CALL Msfp(Tlflag$,Focmhz,Er,Effer,Wmm,Deltalmm,Hmm,Radiusi,Radiuso,Xseries
)
3890  PRINT "Series reactance of the probe @  Foc = +j";Xseries;"ohm  (";Tlflag$
;")"
3900  GOTO Fo
3910  Xseries=0! the case for a transmission line feed
3920  PRINT "For the transmission line fed case the series reactance = +j";Xseri
```

```
es;"ohm  (";Tlflag$;")"
3930  !
3940  !
3950  !
3960 Fo: PRINT
3970  PRINT "----------Analysis for the resonant frequency--------------------"
3980  !
3990  Hdlams=100*Hmm/Vlamsmm
4000  CALL Fo(Foflag$,Feed$,Er,Effer,Vlengthmm,Radiusi,Radiuso,Wmm,Deltalmm,Hmm,
Xseries,Focmhz)
4010  PRINT
4020  PRINT "Wavelength in the free space @ Foc=";Vlamomm;"mm"
4030  PRINT "Wavelength in the substrate @ Foc(using effective Er)=";Vlamsmm;"mm
"
4040  PRINT "Aspect ratio=";Wmm/Vlengthmm
4050  FIXED 4
4060  PRINT "Substrate height(h/lamdas @ Foc)=";Hdlams
4070  FIXED 2
4080  PRINT "Effective dielectric constant=";Effer;"  (";Erflag$;")"
4090  PRINT "Characteristic impedance of MS line,freespace=";Zom
4100  PRINT "Characteristic impedance of MS line,substrate=";Zoms;"(Hammerstad)"
4110  PRINT "Characteristic impedance of MS line,substrate=";Zomcaver;"(Caver)"
4120  PRINT "Characteristic impedance of MS line,substrate=";Zomsen;"(Sengupta)"
4130  PRINT "Edge extension=";Deltalmm;"mm  (";Fringeflag$;")"
4140  !
4150  !
4160  !
4170  GOTO T1   !Program development
4180  !
4190 ! ----- Calculate Zin using the cavity model for a frequency Freqmhz------"
4200  INPUT "Freqmhz ?",Freqmhz
4210  Ftp=(Freqmhz-Focmhz)/Freqmhz   !frequency tuning parameter
4220  P1=Rr !r
4230  P2=0
4240  P3=1
4250  P4=Ftp*Qo
4260  CALL Cdiv(P1,P2,P3,P4,P5,P6)
4270  Rezin=P5*50
4280  Vimzin=(P6+Xseries/50)*50
4290  PRINT "Freq=";Freqmhz;"Zin=";Rezin,Vimzin;Focmhzc;Xseries
4300  PRINT
4310  !
4320  !
4330  !
4340 T1: INPUT "Modify antenna specs. Y/N ?",Ans$
4350  IF Ans$="N" THEN GOTO 4390
4360  PRINT
4370  PRINT " Change in the dimensions"
4380  GOTO Dims
4390  INPUT "Go to the input impedance or  start of the analysis I/A ?",Ans$
4400  IF Ans$="A" THEN GOTO Analysis
4410  PRINT
4420  !
4430  !
4440  !
4450 T12: PRINT "----------Analysis for the input impedance--------------------"
4460  !
4470  PRINT
4480  !
4490 F2: ! ************************FLAGS*************************************
4500  Slotflag$="M"       ! C/N/Cf/D/Md/Ma/Sen/Ho/Hs/M/.....refer to SUB Zslot
4510  Lengthflag$="P"     !P/physical,E/eleltrical..Transmission line model only
4520  Fpflag$="IN"        !Feedpoint model   IN/OUT
4530  ! ********************************************************************
*
4540  PRINT "Lengthflag=";Lengthflag$
4550  PRINT "Slotflag=";Slotflag$
4560  PRINT "Fpflag=";Fpflag$
4570  PRINT "Fringeflag=";Fringeflag$
4580  PRINT
```

```
4590  PRINT
4600  !
4610  !
4620  !
4630  INPUT "START,STOP,STEP   FREQUENCY Mhz?",Fstart,Fstop,Fstep
4640  ! Fstart=4500
4650  ! Fstop=5500
4660  ! Fstep=500
4670  FOR Freqmhz=Fstart TO Fstop STEP Fstep
4680  PRINT
4690  PRINT "Freq=";Freqmhz;"Mhz"
4700  FIXED 3
4710  Hdlams=Hmm/Vlamsmm
4720  ! PRINT "h/lams=";Hdlams                                                    P
4730  FIXED 2
4740  Vlamomm=3E5/Freqmhz
4750  CALL Effer(Erflag$,Freqmhz,Zom,Er,Wmm,Hmm,Effer)
4760  Vlamsmm=Vlamomm/SQR(Effer)
4770  IF Feed$="TL" THEN GOTO 4800
4780  CALL Msfp(Tlflag$,Freqmhz,Er,Effer,Wmm,Deltalmm,Hmm,Radiusi,Radiuso,Xserie
s)
4790  GOTO 4810
4800  Xseries=0
4810  CALL Zin(Vlengthmm,Vlamomm,Vlamsmm,Zoms,Er,Effer,Wmm,Hmm,Deltalmm,Slotflag
$,Lengthflag$,D,Zpr,Zpi,Zsr,Zsi)
4820  Zinr=Zpr
4830  ! Now include the effect of the probe
4840  IF Fpflag$="IN" THEN GOTO 4860
4850  IF Fpflag$="OUT" THEN Xseries=0
4860  Zini=Zpi+Xseries
4870  R1=Zinr-50
4880  R2=Zinr+50
4890  CALL Cdiv(R1,Zini,R2,Zini,Rcr,Rci)
4900  PRINT "Series reactance=";Xseries;"ohm"
4910  PRINT "Reflection coeff.=";Rcr;"+j";Rci
4920  PRINT "Zin=";Zinr;"+j";Zini;"ohm"
4930  NEXT Freqmhz
4940  !
4950  !
4960  !
4970  INPUT "Stay in impedance routine and new feedpoint  YY/YN/NN ?",Ans$!SP
4980  IF Ans$="YY" THEN GOTO 5060
4990  IF Ans$="YN" THEN GOTO T1
5000  INPUT "Go back to the start of the analysis Y/N ?",Ans$!SP
5010  IF Ans$="Y" THEN GOTO Analysis
5020  INPUT "Calculate the Pattern or the Mutual coupling P/M ?",Ans$!SP
5030  IF Ans$="M" THEN GOTO Mutual
5040  IF Ans$="P" THEN GOTO Pattern
5050  GOTO 4970
5060  INPUT "New feedpoint(mm) ?",D
5070  PRINT "Feedpoint position=";D;"mm"
5080  GOTO T12
5090  !
5100  !
5110 Pattern: !
5120  PRINT
5130  PRINT "----------Analysis for the radiation pattern----------------------"
5140  PRINT
5150   CALL Rad(Focmhz,Er,Vlengthmm,Wmm,Hmm,Deltalmm)
5160  INPUT "Calculate the Mutual coupling or go to the start M/S ?",Ans$!SP
5170  IF Ans$="S" THEN GOTO Start
5180   !
5190   !
5200   !
5210  PRINT
5220 Mutual: ! PRINT"-------Anslysis for the mutual coupling-------------------"
5230  ! Coupling$="E"!.........E/H-PLANE COUPLING
5240  ! Dlamo=.5
5250  INPUT "Separation in free space wavelengths ?",Dlamo
5260  INPUT "Direction of coupling E/H ?",Coupling$
```

```
5270  CALL Couplingfar(Dlamo,Focmhz,Er,Coupling$,Vlengthmm,Wmm,Hmm,Deltalmm)
5280  INPUT "Stay in mutual coupling or go to the start of analysis M/A ?",Ans$
5290  IF Ans$="A" THEN GOTO Analysis
5300  GOTO 5250
5310  !
5320  INPUT "Synthesis of patch or array P/A ?",Ans$
5330  IF Ans$="A" THEN GOTO 5820
5340  !
5350  !
5360  !
5370 Sy: PRINT "--------------Zslot synthesis-----------------------------------"
5380  !
5390  INPUT "Xseries @ Foc rom measurements(ohm) ?",Xseries
5400  Vls=Xseries/(2*PI*Focmhz*1E6)
5410  Vlsp=Vls*1E12
5420  PRINT "Xs @ Foc=";Xseries,"Ls=";Vls*1E12;"pH"
5430  PRINT
5440  PRINT
5450  PRINT "frequ.Mhz                Zin     Xseries     Zslot     Yslot(mmho)"
5460  INPUT "Frequency Mhz,Input impedance R,X ?",Freqmhz,Zinr,Zini
5470  Xseries=2*PI*Freqmhz*Vls*1E6
5480  CALL Effer(Erflag$,Freqmhz,Zom,Er,Wmm,Hmm,Effer)
5490  Vlamsmm=3E5/(Freqmhz*SQR(Effer))
5500  ! Zin:  Input impedance at the terminals
5510  ! Zp:   Parelleled trasferred impedances
5520  ! Zs:   Input impedance of the slot antenna
5530  ! Vll mm
5540  Zpr=Zinr
5550  IF Fpflag$="OUT" THEN GOTO 5590
5560  ! CALL Msfp(Freqmhz,Er,Hmm,Radiusi,Radiuso,Xseries)                    T
5570  Zpi=Zini-Xseries!Inputted
5580  GOTO 5600
5590  Zpi=Zini
5600  CALL Zslotsyn(Zoms,D,Vlengthmm,Vlamsmm,Zpr,Zpi,Zsr,Zsi)
5610  IF Fpflag$="OUT" THEN GOTO 5460
5620  Zsrpl=Zsr*1000/Wmm  !Zslot/length (ohm/m)
5630  Zsipl=Zsi*1000/Wmm
5640  Ysr=1000*Zsr/(Zsr^2+Zsi^2)
5650  Ysi=-1000*Zsi/(Zsr^2+Zsi^2)
5660  PRINT Freqmhz,Zinr;Zini;Xseries;Zsr;Zsi;Ysr;Ysi
5670  GOTO 5690
5680  PRINT Freqmhz,Zinr;Zini;"-----";Zsr;Zsi;Zsrpl;Zsipl
5690  PRINT
5700  PRINT
5710  INPUT "Stay in Zslot determination or goto Analysis S/A ?",Ans$
5720  IF Ans$="A" THEN GOTO Analysis
5730  GOTO Sy
5740  !
5750  !
5760  !
5770  !
```

```
5750  !
5760  !
5770  !
5780  !
5790  !
5800  !
5810 Sub: !
5820  ! ************************************************************************
5830  ! ************************************************************************
5840  ! ************************SUBROUTINES*************************************
5850  ! ************************************************************************
5860  ! ************************************************************************
5870  !
5880  !
5890  !
5900 Zin: ! Input impedance of a rectangular patch antenna using a transmission
5910  ! line model*************************************************************
5920  !
5930  SUB Zin(Vlengthmm,Vlamomm,Vlamsmm,Zoms,Er,Effer,Wmm,Hmm,Deltalmm,Slotflag$
,Lengthflag$,Vl1,Zinr,Zini,Zsr,Zsi)
5940  Freqhz=3E11/Vlamomm
5950  D2=(Vlengthmm-Vl1)/1000 !m  PHYSICAL LENGTH
5960  D1=Vl1/1000 !m PHYSICAL LENGTH
5970  IF Lengthflag$="P" THEN GOTO 6010
5980  D1=D1+Deltalmm/1000 ! m ELECTRICAL LENGTH
5990  D2=D2+Deltalmm/1000 ! m ELECTRICAL LENGTH
6000  ! INPUT "Slotflag:C/N/Cf/Md/D/Ma/Sen/Ho/Hs/M ?",Slotflag$!                T
6010  CALL Zslot(Slotflag$,Vlamomm,Vlamsmm,Vlengthmm,Wmm,Hmm,Effer,Deltalmm,Zoms
,Zsr,Zsi)
6020  ! GOTO 4060!                                                              T
6030  ! INPUT "?",Zsr,Zsi
6040  CALL Tl(Freqhz,Effer,D1,Zoms,0,Zsr,Zsi,Zin1r,Zin1i)
6050  CALL Tl(Freqhz,Effer,D2,Zoms,0,Zsr,Zsi,Zin2r,Zin2i)
6060  FIXED 6
6070  ! PRINT "ZA'=";Zin1r;Zin1i;"(short distance)","ZB'=";Zin2r;Zin2i
6080  FIXED 2
6090  ! Paralleling Zin1 and Zin2
6100  CALL Cmult(Zin1r,Zin1i,Zin2r,Zin2i,D1,D2)
6110  Denr=Zin1r+Zin2r
6120  Deni=Zin1i+Zin2i
6130  CALL Cdiv(D1,D2,Denr,Deni,Zinr,Zini) !ohm
6140  SUBEND
6150  !
6160  !
6170  !
6180 Zsl: ! Input Impedance of a slot antenna*************************************
6190  !
6200  SUB Zslot(Slotflag$,Vlamomm,Vlamsmm,Vlengthmm,Wmm,Hmm,Effer,Deltalmm,Zoms,
Zsr,Zsi)
6210  ! Input impedance of a slot antenna using the formulae of....
6220  !   Slotflags:C.... Carver using free space wavelength
6230  !             N.... Newman:Carver with the substrate wavelength for G
6240  !             Cf... Carver with the empirical factor
6250  !             D.... Derneryd
6260  !             Md... Derneryd with a wide slot
6270  !             Ho... Harrington using free space wavelength
6280  !             Hs... Harrington using substrate wavelength
6290  !             Ma... Marcuvitz pp179
6300  !             Sen.. Sengupta  APSIS '83 pp159
6310  !             M.... Martin by empirical methods
6320  !
6330  !
6340  Freqmhz=3E5/Vlamomm
6350  IF Slotflag$="C" THEN GOTO 6480
6360  IF Slotflag$="N" THEN GOTO 6530
6370  IF Slotflag$="Cf" THEN GOTO 6580
6380  IF Slotflag$="Md" THEN GOTO 6660
6390  IF Slotflag$="D" THEN GOTO 6680
6400  IF Slotflag$="Ma" THEN GOTO 6960
6410  IF Slotflag$="Sen" THEN GOTO 7040
```

```
6420  IF Slotflag$="Ho" THEN GOTO 7170
6430  IF Slotflag$="Hs" THEN GOTO 7170
6440  IF Slotflag$="M" THEN GOTO 7300
6450  PRINT "Slotflag error"
6460  GOTO 7500 !EXIT
6470  !
6480  ! Carver PT00929pp42
6490  G=.00836*Wmm/Vlamomm!                                          (5.16)
6500  B=.01668*Deltalmm*Wmm*Effer/(Hmm*Vlamomm)!                     (5.17)
6510  GOTO 7270
6520  !
6530  ! Newman Mexico pp9.2
6540  G=.00836*Wmm*SQR(Effer)/Vlamomm
6550  B=.01668*Deltalmm*Wmm*Effer/(Hmm*Vlamomm)!                     (5.17)
6560  GOTO 7270
6570  !
6580  ! Carver Mexico pp7.6 & APS trans Jan 81
6590  Wdl=Wmm/Vlengthmm
6600  Fwl=.7747+.5977*(Wdl-1)-.1638*(Wdl-1)^2!                       (5.18)
6610  PRINT "F(w/l)=";Fwl
6620  G=Fwl*.00836*Wmm/Vlamomm
6630  B=Fwl*.01668*Deltalmm*Wmm*Effer/(Hmm*Vlamomm)
6640  GOTO 7270
6650  !
6660  ! Modified Derneryd
6670  GOTO 6740 !wide slot
6680  !
6690  ! Derneryd APS Nov 76
6700  Wdlam=Wmm/Vlamomm
6710  IF Wdlam>1 THEN GOTO 6740
6720  G=(Wmm/Vlamomm)^2/90 !narrow                                   (5.13)
6730  GOTO 6750
6740  G=Wmm/(120*Vlamomm) !wide                                      (5.13)
6750  Freq=3E11/Vlamomm !Hz
6760 D: C=Deltalmm/(Freq*Zoms*Vlamsmm)!                              (5.14)
6770  N=0 !nth guess
6780  S=-1
6790  Error=.002*C
6800  Bt=2*PI*Freq*C*(1+S*N/1000)  !Test or First approximation
6810  Rt=G/(G^2+Bt^2)
6820  Xt=-Bt/(G^2+Bt^2)
6830  Ct=ABS(1/(2*PI*Freq*Xt))
6840  IF ABS(C-Ct)<Error THEN GOTO 6890
6850  IF N>0 THEN GOTO 6870
6860  IF Ct<C THEN S=-S
6870  N=N+1
6880  GOTO 6800
6890  Zsr=Rt
6900  Zsi=Xt
6910  B=-Xt/(Rt^2+Xt^2)
6920  GOTO 7500
6930  !
6940  ! Marcuvitz pp179
6950  Ha=2*Hmm/1000 !Aperture height(m)
6960  Yom=1/(377*(Hmm/1000))   !mho  Sengupta APS July '80 pp481 [44]  (5.13)
6970  Ha=2*Hmm/1000 !Aperture height(m)
6980  G=Yom*PI*Ha*(Wmm/1000)/(2*Vlamomm/1000) !mho                     (5.1)
6990  B=LOG(2*2.71828*(Vlamomm/1000)/(1.78107*Ha))!                    (5.2)
7000  B=Yom*B*Ha*(Wmm/1000)/(Vlamomm/1000) !mho
7010  ! * W because G & B are per length expressions in Macuvitz.
7020  GOTO 7260
7030  !
7040  ! Sengupta APSIS '83 pp159
7050  Alpha=1+1.393*(Hmm/Wmm)+.667*(Hmm/Wmm)*LOG(Wmm/Hmm+1.444)!       (5.5)
7060  ! Alpha=1
7070  Beta=2*PI*SQR(Effer)/(Vlamomm/1000)
7080  ! PRINTER IS 0
7090  ! PRINT "Alpha=";Alpha
7100  Yom=Alpha*Wmm*SQR(Effer)/1000/(377*(Hmm/1000))!mho
7110  !  Carver APS Jan'81 [15]                                       (5.4)
```

```
7120  G=Yom*Beta*(Hmm/1000)/(2*Alpha*Effer)!                                    (5.6)
7130  B=LOG(SQR(Effer)*2*PI*2.71828/(1.78107*Beta*(Hmm/1000)))!                 (5.7)
7140  B=B*Yom*Beta*(Hmm/1000)/(PI*Alpha*Effer)
7150  GOTO 7260
7160  !
7170  ! Harrington "Time Harmonic EM Fields" pp183 [9]
7180  IF Slotflag$="Hs" THEN GOTO 7210
7190  Vlam=Vlamomm
7200  GOTO 7220
7210  Vlam=Vlamsmm
7220  Beta=2000*PI/Vlam
7230  Betah=Beta*Hmm/1000
7240  G=Wmm*(1-Betah^2/24)/(120*Vlam)!                                          (5.11)
7250  B=(3.135-2*LGT(Betah))*Wmm/(377*Vlam) !base 10                            (5.12)
7260  ! ##Yslot to Zslot##
7270  Zsr=G/(G^2+B^2)
7280  Zsi=-1*B/(G^2+B^2)
7290  GOTO 7500
7300  !
7310 W: ! Martin:Empirical Zslot  @ 5GHz
7320  G=546/1E6*EXP(4.47*Wmm/Vlamomm)      !mho,26/5                            (5.27)
7330  Wc=.0455*(Deltalmm*Wmm/Hmm/Vlamomm)+5E-4 !mho,26/5                        (5.28)
7340  C=Wc/2/PI/Freqmhz/1E6
7350  N=0 !nth guess
7360  S=-1
7370  Error=.002*C
7380  Bt=2*PI*Freqmhz*1E6*C*(1+S*N/1000)  !Test or First approximation
7390  Rt=G/(G^2+Bt^2)
7400  Xt=-Bt/(G^2+Bt^2)
7410  Ct=ABS(1/(2*PI*Freqmhz*1E6*Xt))
7420  IF ABS(C-Ct)<Error THEN GOTO 7470
7430  IF N>0 THEN GOTO 7450
7440  IF Ct<C THEN S=-S
7450  N=N+1
7460  GOTO 7380
7470  Zsr=Rt
7480  Zsi=Xt
7490  B=-Xt/(Rt^2+Xt^2)
7500  ! PRINT "Slotflag=";Slotflag$!                                            P
7510  FIXED 6
7520  PRINT "Zslot=";Zsr;Zsi;"ohm"!                                             P
7530  Gm=G*1000
7540  Bm=B*1000
7550  PRINT "Yslot=";Gm;Bm;"mmho"!                                              P
7560  PRINT "W/lamo=";Wmm/Vlamomm;"dLW/hlamo=";Deltalmm*Wmm/Hmm/Vlamomm
7570  PRINT "wC=";2*PI*Freqmhz*1E6*C*1000;"mho"
7580  FIXED 2
7590  SUBEND
7600  !
7610  !
7620  !
7630 Zsy: ! Synthesis of the slot input impedance*********************************
7640  !
7650  SUB Zslotsyn(Zoms,Vl1,Vlengthmm,Vlamsmm,Zinr,Zini,Zsr,Zsi)
7660  !
7670  ! Vl1  mm
7680  ! all impedances in Ohm
7690  D1=Vl1/1000 !m
7700  D2=(Vlengthmm-Vl1)/1000 !m
7710  Beta=2000*PI/Vlamsmm
7720  RAD
7730  C1=COS(Beta*D1)
7740  C2=COS(Beta*D2)
7750  S1=SIN(Beta*D1)
7760  S2=SIN(Beta*D2)
7770  CALL Crec(Zinr,Zini,Yinr,Yini)
7780  Yo=1/Zoms
7790  S6=S1*C2+C1*S2
7800  C=C1*C2
7810  S=S1*S2
```

```
7820  Ar=Yinr*C
7830  Ai=Yini*C-Yo*S6
7840  Br=-2*C+2*S-Yini*Zoms*S6
7850  Bi=Yinr*Zoms*S6
7860  Cr=-1*Yinr*S*Zoms^2
7870  Ci=-1*(Yini*S*Zoms^2+Zoms*S6)
7880  ! Evaluate ZA
7890  P3=2*Ar
7900  P4=2*Ai
7910  CALL Cdiv(Br,Bi,P3,P4,Z1,Z2)
7920  Z1=-Z1
7930  Z2=-Z2
7940  CALL Cmult(Br,Bi,Br,Bi,B1,B2)
7950  P5=4*Ar
7960  P6=4*Ai
7970  CALL Cmult(P5,P6,Cr,Ci,P7,P8)
7980  P9=B1-P7
7990  P10=B2-P8
8000  CALL Csqr(P9,P10,P11,P12)
8010  CALL Cdiv(P11,P12,P3,P4,Z3,Z4)
8020  Zsr=Z1-Z3 !Zslot
8030  Zsi=Z2-Z4
8040  SUBEND
8050  !
8060  !
8070  !
8080 Eff: ! Effective dielectric constant of a microstrip t.l.******************
8090  !
8100  SUB Effer(Erflag$,Freqmhz,Zom,Er,Wmm,Hmm,Effer)
8110  Effer=(Er+1)/2+(Er-1)/(2*SQR(1+10*Hmm/Wmm))!                          (1.9)
8120  IF Erflag$="Hammerstad" THEN GOTO 8210
8130  IF Erflag$="Getsinger" THEN GOTO 8160
8140  PRINT "error 0 Eff"
8150  PAUSE
8160  Zoms=Zom/SQR(Effer)
8170  Fp=Zoms/(.8*PI*Hmm)   !                                               (3.22)
8180  Effer1=Effer
8190  G=.6+.009*Zoms!                                                       (3.23)
8200  Effer=Er-(Er-Effer1)/(1+G*(Freqmhz/1000)^2/Fp^2)!                     (3.21)
8210  SUBEND
8220  !
8230  !
8240  !
8250 Zom: ! Characteristic imp. of a Microstrip transmission line***************
8260  !
8270  SUB Zom(Wmm,Hmm,Zom)
8280  ! M.V.Schneider,"Microstrip lines for MICs",BSTJ,May/June,1969,Vol 48
8290  ! pp1421-1444,pp1430
8300  Wh=Wmm/Hmm
8310  Hw=Hmm/Wh
8320  IF Hw>1 THEN GOTO 8350
8330  Zom=120*PI/(Wh+2.42-.44*Hw+(1-Hw)^6)
8340  GOTO 8360
8350  Zom=60*LOG(8*Hw+Wh/4)
8360  SUBEND
8370  !
8380  !
8390  !
8400 Del: ! Fringing length of a microstrip open circuit*************************
8410  !
8420  SUB Deltal(Fringeflag$,Wmm,Hmm,Vlengthmm,Er,Effer,Fmhz,Deltalmm)
8430  Vlamsmm=3E5/(Fmhz*SQR(Effer))
8440  IF Fringeflag$="Hamm1" THEN GOTO 8510
8450  IF Fringeflag$="Hamm2" THEN GOTO 8640
8460  IF Fringeflag$="KIR" THEN GOTO 8750
8470  IF Fringeflag$="Empirical" THEN GOTO 9320
8480  IF Fringeflag$="Experimental" THEN GOTO 8930
8490  PRINT "Fringeflag error"
8500  PAUSE
8510  ! E.O.Hammerstand"Equations for microstrip circuit design"
```

```
8520  ! EMC'75,pp268-272
8530  ! ....with factor .412
8540  Wh=Wmm/Hmm
8550  Efferh=(Er+1)/2+(Er-1)/(2*SQR(1+10*Hmm/Wmm))!                    (1.9)
8560  ! Effer using Hammerstad EMC'75
8570  Deltalmm=.412*Hmm*(Efferh+.3)*(Wh+.262)/((Efferh-.258)*(Wh+.813))!  (1.10)
8580  Deltalmmdh=Deltalmm/Hmm
8590  Focmhz=300/(2*(Vlengthmm/1000+2*Deltalmm/1000)*SQR(Efferh))!      (3.2)
8600  Error=(Focmhz-Fmhz)*100/Fmhz
8610  ! PRINT "HAM1/h=";Deltalmmdh,"Freq=";Focmhz,"%e=";Error
8620  GOTO 9540
8630  !
8640  ! Hammerstad :Int. MTT Conf.'81 pp54-56/Lier IEE-H Aug'82 pp161-163
8650  Wh=Wmm/Hmm
8660  Deltalmm=Hmm/2/PI*((Wh+.366)/(Wh+.556))
8670  Deltalmm=Deltalmm*(.28+(Er+1)/Er*(.274+LOG(Wh+2.518)))  !ln       (3.5)
8680  Deltalmmdh=Deltalmm/Hmm
8690  Focmhz=300/(2*(Vlengthmm/1000+2*Deltalmm/1000)*SQR(Efferh))
8700  ! Change above Effer using MTT'80 later
8710  Error=(Focmhz-Fmhz)*100/Fmhz
8720  ! PRINT "HAM2/h=";Deltalmmdh,"Freq=";Focmhz,"%e=";Error
8730  GOTO 9540
8740  !
8750 K: ! Kirschning Elect Lett Feb 81 pp123-125
8760  Efferh=(Er+1)/2+(Er-1)/(2*SQR(1+10*Hmm/Wmm)) !Effer using Hammerstad
8770  RAD
8780  Z1=.434907*(Efferh^.81+.26)*((Wmm/Hmm)^.8544+.236)!              (3.7)
8790  Z1=Z1/((Efferh^.81-.189)*((Wmm/Hmm)^.8544+.87))
8800  Z2=1+(Wmm/Hmm)^.371/(2.358*Er+1)!                                (3.8)
8810  Z3=1+.5274*ATN(.084*(Wmm/Hmm)^(1.9413/Z2))/Efferh^.9236!          (3.9)
8820  Z4=1+.0377*ATN(.067*(Wmm/Hmm)^1.456)*(6-5*EXP(.036*(1-Er)))!     (3.10)
8830  Z5=1-.218*EXP(-7.5*(Wmm/Hmm))!                                   (3.11)
8840  Deltalmm=Hmm*Z1*Z3*Z5/Z4!                                        (3.6)
8850  Focmhz=300/(2*(Vlengthmm/1000+2*Deltalmm/1000)*SQR(Efferh))
8860  Error=(Focmhz-Fmhz)*100/Fmhz
8870  Deltalmmdh=Deltalmm/Hmm
8880  ! PRINT "KIR/h=";Deltalmmdh,"Freq=";Focmhz,"%e=";Error
8890  ! PRINT "Er=";Er,"Effer=";Effer,"Efferh=";Efferh
8900  ! PRINT "Z12345=";Z1;Z2;Z3;Z4;Z5
8910  GOTO 9540
8920  !
8930  ! Experimental determination of deltalmm
8940  ! INPUT "Patch length(mm) ?",Vlengthmm
8950  ! PRINT "Freq.=";Fmhz
8960  Deltalmm=500*(150/(SQR(Effer)*Fmhz)-Vlengthmm/1000)
8970  ! Hh=1000*(Hmm/Wmm)^2!
8980  ! PRINT "(h/W)^2*1000=";Hh
8990  Vlamsmm=3E5/(Fmhz*SQR(Effer))
9000  Vlamsmm=3E5/(Fmhz*SQR(Effer))
9010  Vlamomm=3E5/Fmhz
9020  ! PRINT "lamo=";Vlamomm,"lams=";Vlamsmm
9030  Ww=Wmm/Vlamsmm
9040  ! PRINT "W/lamdas=";Ww
9050  ! Aa=1000*Hmm*Wmm/Vlamsmm^2
9060  ! Aao=1000*Hmm*Wmm/Vlamomm^2
9070  ! PRINT "1000*Wh/lams^2";Aa,Aao
9080  ! Aaaa=Hmm*Wmm
9090  ! PRINT "Wh=";Aaaa
9100  FIXED 6
9110  Hhs=Hmm/Vlamsmm
9120  Hho=Hmm/Vlamomm
9130  Wwo=Wmm/Vlamomm
9140  Wws=Wmm/Vlamsmm
9150  ! PRINT "W/lamdas=";Wws!,"W/lamdao=";Wwo
9160  ! PRINT "----hh h/lamdas=";Hhs;"hh"!,"h/lamdao=";Hho
9170  Wh=Wmm/Hmm
9180  ! PRINT "----WWW W/h=";Wh;"WWW"
9190  Deltalmmdh=Deltalmm/Hmm
9200  ! PRINT "Synthesis"
9210  ! PRINT "----Deltalmm=";Deltalmm,"Deltal/h=";Deltalmmdh
```

```
9220  Deltalmmds=Deltalmm/Vlamsmm
9230  Deltalmmdo=Deltalmm/Vlamomm
9240  ! PRINT "Deltalmm/Lamdas=";Deltalmmds,"Deltalmm/Lamdao=";Deltalmmdo
9250  Bl=2*PI*Deltalmm/Vlamsmm
9260  ! PRINT "----kkkk kDeltaL=";Bl;"kkkk"
9270  ! Deltalmmdhs=Deltalmm/Hmm/Vlamsmm
9280  ! PRINT "Deltalmm/h/lams=";Deltalmmdhs
9290  FIXED 2
9300  STOP
9310  !
9320 E: ! PRINT " Empirical determination of deltalmm"
9330  FIXED 3
9340  Betas=2*PI/Vlamsmm !mm,in substrate
9350  ! Deltalmm=54*(Hmm/Wmm)^2+.849
9360  Hds=Hmm/Vlamsmm
9370  IF Hds<.009 THEN GOTO 9420
9380  ! Deltalmm=(Wmm/Hmm*3.225E-4+.1421*LOG(111.11*(Hmm/Vlamsmm)))/Betas
9390  ! Deltalmm=(Wmm*3.225E-4/Hmm+.606+.128*LOG(Hmm/Vlamsmm))/Betas    !3/5/84
9400  C=.606+.128*LOG(Hmm/Vlamsmm)   !3/5/84
9410  GOTO 9430
9420  C=0
9430  Deltalmm=(Wmm*3.225E-4/Hmm+C)/Betas    !3/5/84                          (3.24)
9440  ! PRINT "C=";C,"h/lambdas=";Hmm/Vlamsmm,"W/h=";Wmm/Hmm
9450  Bd=Deltalmm*Betas
9460  Deltalmmdh=Deltalmm/Hmm
9470  ! PRINT
9480  ! PRINT "Dl=";Deltalmm,"Betas*Dl=";Bd,"Dl/h=";Deltalmmdh
9490  FIXED 2
9500  ! PRINT
9510  Focmhz=300/(2*(Vlengthmm/1000+2*Deltalmm/1000)*SQR(Effer))
9520  Error=(Focmhz-Fmhz)*100/Fmhz
9530  ! PRINT "MARTIN/h=";Deltalmmdh,"Freq=";Focmhz,"%e=";Error
9540  SUBEND
9550  !
9560  !
9570  !
9580 Msf: ! Microstrip feed point************************************************
9590  !
9600  SUB Msfp(Tlflag$,Freqmhz,Er,Effer,Wmm,Deltalmm,T,A,B,Xs)
9610  Freq=Freqmhz*1E6
9620  Vlengthmm=1000*(3E8-4*Freq*(Deltalmm/1000)*SQR(Effer))/(2*Freq*SQR(Effer))
 !Res half wave(m)
9630  Ar=Wmm/Vlengthmm  ! Patch aspect ratio
9640  Vlam=3E8/Freq
9650  Vlamomm=Vlam*1000
9660  Vlams=Vlam/SQR(Er) !m
9670  Vlamsmm=Vlams*1000
9680  ! PRINT "lamdas=";Vlamsmm;"mm"
9690  ! PRINT "h/lamdas=";T/Vlamsmm
9700  ! PRINT "d/lamdas=";A/Vlamsmm
9710  ! PRINT "r=";Ar
9720  IF Tlflag$="Sinusoidal" THEN GOTO 9810
9730  IF Tlflag$="Straight" THEN GOTO 10480
9740  IF Tlflag$="Carver" THEN GOTO 10560
9750  IF Tlflag$="Newman" THEN GOTO 10600
9760  IF Tlflag$="Sengupta" THEN GOTO 10640
9770  IF Tlflag$="Lier" THEN GOTO 10710
9780  IF Tlflag$="Griffin" THEN GOTO 10820
9790  PRINT "flag error Msf+10"
9800  PAUSE
9810  ! Sinusoidal equ-potential contour for the tapered coax TL
9820  ! that represents the walls of a tapered transmission line.
9830  !       INPUTS:Frequency(Freq).............MHz
9840  !              Dielectric Constant(Er)
9850  !              Substrate Height(T).........mm
9860  !              Radius of inner(A)..........mm
9870  !              Radius of outer(B)..........mm
9880  !              Patch aspect ratio(Ar)
9890  !
9900  !       OUTPUT:Series reactance.............Ohm
```

```
9910  F1=.5!                                                                T
9920  !
9930  !
9940  ! N:NUMBER OF SEGMENTS OVER T
9950  N=16!INITIAL NUMBER OF SEGMENTS ALONG T
9960  Zsiold=0!DUMMY FOR TESTING
9970  ! b:RADIUS OF OUTER CONDUCTOR
9980  Boxdiag=SQR(T^2+(B-A)^2)
9990  Break=1+(B-A)/20/A
10000 Rtoda=1.681*EXP(.153*Ar)*EXP(-4.369*(Boxdiag/Vlengthmm))  !5/4/84 :20 Mk2
10010 IF Rtoda>=Break THEN GOTO 10030
10020 Rtoda=Break !which will cause As to be zero.
10030 Aa=(B-A)/A
10040 F1=(Rtoda-1-Aa/20)/Aa
10050 F2=.9 !Shift factor:contour is started from the point a+(b-a)/20
10060 FIXED 3
10070 ! PRINT "Rto/A=";Rtoda;"L=";Vlengthmm;"Break=";Break;"A*Break(mm)";A*Break
10080 ! PRINT "T,A,Rto,As,F2,Boxdiag/Vlamsmm,Boxdiag/L" !                     P
10090 ! PRINT T;A;Rtoda*A;F1;F2;Boxdiag/Vlamsmm;Boxdiag/Vlengthmm !           P
10100 FIXED 2
10110 Zrr=0 !short circuit load
10120 Zri=0
10130 FOR K=0 TO N-1
10140 D=T/N !SEGMENT LENGTH
10150 Y=K*D
10160 Yy=F1*(B-A)*COS(PI/(2*T)*(T-Y))
10170 C=1.5*(B-A)-Yy-(1-F1)*(B-A)-F2*(B-A)/2
10180 Apc=A+C!A PLUS C
10190 Apcm=Apc/1000
10200 Am=A/1000
10210 CALL Zo(Apcm,Am,Er,Zor,Zoi)
10220 ! PRINT Zor!                                                           P
10230 Dm=D/1000
10240 CALL T11(Freq,Er,Dm,Zor,Zoi,Zrr,Zri,Zsr,Zsi)
10250 ! IF N=16THEN GOTO 4570!PRINT THE·PARAMETERS ONCE FOR THE CASE
10260 ! OF N=16
10270 ! PRINT "Freq,Er,T,D,Yy,Zor,Zrr,Zri,A,Apc,Zsi"
10280 ! PRINT Freq;Er;T;D;Yy;Zor;Zrr;Zri;A;Apc;Zsi
10290 Zri=Zsi
10300 Zrr=Zsr
10310 NEXT K
10320 ! PRINT N,Zor,Zsi,Zsi*50/Zor!                                          P
10330 IF N=16 THEN GOTO 10360
10340 Error=50*ABS(Zsi-Zsiold)/Zor
10350 IF Error<.5 THEN GOTO 10390
10360 Zsiold=Zsi
10370 N=N*2
10380 GOTO 10110
10390 Zsr=Zsr*50/Zor !re-normalisation
10400 Zsi=Zsi*50/Zor
10410 Xs=Zsi !series reactance
10420 ! PRINT "Zot@y=-h=";Zor
10430 ! PRINT "Xs=",Xs!                                                     T
10440 ! INPUT "As",F1!                                                      T
10450 ! GOTO 7332!                                                          T
10460 GOTO 10850
10470 !
10480 ! Straight sided coaxial transmission line
10490 !
10500 Zrr=0
10510 Zri=0
10520 Vlamsmm=3E5/(Freqmhz*SQR(Er))
10530 Xs=50*TAN(2*PI*T/Vlamsmm) !already normalised to 50 ohm
10540 GOTO 10850
10550 !
10560 ! Carver [34]
10570 Xs=376*TAN(2*PI*T/Vlamomm)/SQR(Er)!                          from (2.4)
10580 GOTO 10850
10590 !
10600 ! Newman Mexico pp9.3 [19]
```

```
10610 Xs=376*TAN(2*PI*T*SQR(Er)/Vlamomm)/SQR(Er)!                              (2.4)
10620 GOTO 10850
10630 !
10640 ! Sengupta APSIS '83 pp159 [45]
10650 Alpha=1+1.393*(T/Wmm)+.667*(T/Wmm)*LOG(Wmm/T+1.444)
10660 Beta=2*PI*SQR(Effer)/(Vlamomm/1000)
10670 Yc=Wmm*Alpha*SQR(Effer)/(377*T)!                                        (1.13)
10680 Xs=Beta*(Wmm/1000)*Alpha*LOG(2/(1.78107*Beta*(A/1000)))/(Yc*2*PI)!      (2.8)
10690 GOTO 10850
10700 !
10710 ! Lier IEE/H Aug '82 pp161-164 [46]
10720 Xq=4*PI/1E7*(T/1000)*(Freqmhz*1E6)
10730 Xq=Xq*LOG(6*1E8/(PI*1.781*(A/1000)*(Freqmhz*1E6)*SQR(Er)))!             (2.10)
10740 Elengthmm=Vlengthmm+2*Deltalmm
10750 CALL Zom(Vlengthmm,T,Zk) !Hammerstad
10760 RAD
10770 Xf=-Zk/(2*TAN(PI*(Wmm/2)/Elengthmm))!                                   (2.9)
10780 ! PRINT "Xq,Xf=";Xq,Xf
10790 Xs=Xq+Xf
10800 GOTO 10850
10810 !
10820 ! Griffin El Mar '82 pp266-269 [43]
10830 Zcoax=60*LOG(Vlengthmm/2/A)/SQR(Er) !approximation of a disc patch.  (2.6)
10840 Xs=Zcoax*TAN(2*PI*T/Vlamsmm) !ohm                                       (2.7)
10850 SUBEND
10860 !
10870 !
10880 !
10890 Mut:! Coupling between well separated patches*****************************
10900 !
10910 SUB Couplingfar(Dlamo,Freqmhz,Err,Ans$,Vlmm,Wmm,Hmm,Deltalmm)
10920 PRINT "-------------------------------------------------------------------"
10930 PRINT " MUTUAL COUPLING MODEL USING FAR FIELD RADIATION PATTERN"
10940 PRINT "       FORMULATIONS FOR APERTURE ANTENNAS"
10950 PRINT
10960 PRINT "          APERTURE ILLUMINATION METHOD"
10970 PRINT
10980 PRINT "-------------------------------------------------------------------"
10990 TRACE ALL VARIABLES
11000 FIXED 4
11010 RAD
11020 PRINTER IS 0
11030 OPTION BASE 0
11040 DIM Et(320),Eq(320),Eqs(320),Dden(320)
11050 DIM Er(320),Yff(320)
11060 DIM Prp(320),Theta(320),Thetar(320)
11070 DIM Rm(320),Ers(320),Xm(320),Betam(320)
11080 ! COM T(320),X(320),Y(320),Betam(320),Xm(320),Vlams!!
11090 ! Separation in free space wavelengths:Dlamo
11100 ! Freqmhz
11110 ! Separation terms of the wavelength in the dielectric:Dlams
11120 ! Dielectric constant:Err
11130 ! E or H plane coupling (E/H):Ans$
11140 ! Length(E-plane):Vlmm(mm)
11150 ! Width:Wmm(mm)
11160 ! Substrate height:Hmm(mm)
11170 ! Fringe length:Deltalmm(mm)
11180 ! PRINT "Patch dimensions:length,width,substrate height (mm)"
11190 ! PRINT "......where the length is that dimension in the E-plane ?"
11200 ! INPUT Vlmm,Wmm,Hmm
11210 !
11220 Printflag=1
11230 ! Dimensions of an equivalent air filled cavity
11240 Vlmme=(Vlmm+2*Deltalmm)*SQR(Err) !Electrical length
11250 Wmme=Wmm*SQR(Err)
11260 Hsubmme=Hmm*SQR(Err)
11270 ! Te:Effective aperture thickness for an air filled cavity
11280 Tmme=Hsubmme*2 !Ground plane removed
11290 Nmax=20
11300 Vlamo=3E2/Freqmhz !m
```

```
11310 Vlams=Vlamo/SQR(Err) !m(not used)
11320 Sepm=Dlamo*Vlamo !Separation in m
11330 Sepmm=Dlamo*Vlamo*1000 !Separation in mm
11340 Tme=Tmme/1000
11350 Wme=Wmme/1000
11360 Vlme=Vlmme/1000
11370 Beta=2*PI/Vlamo!in the equivalent cavity
11380 F=2*Tme/PI !Aperture thickness/PI ;same units as the separation(m).
11390 ! Note that the electrical aperture thickness is equal to twice that
11400 ! of the physical.
11410 Dlams=Sepm/Vlams !Separation in terms of dielectric wavelength
11420 IF Printflag=2 THEN GOTO 11530
11430 PRINT "Patch's physical dimensions:length,width,substrate height:"
11440 PRINT "             ";Vlmm;"mm by ";Wmm;"mm by ";Hmm;"mm"
11450 PRINT "Effective patch dimensions for an air filled patch"
11460 PRINT "using the effective electrical length:"
11470 PRINT "              ";Vlmme;"mm by ";Wmme;"mm by ";Hsubmme;"mm"
11480 PRINT "Frequency= ";Freqmhz;"Mhz"
11490 PRINT "Wavelength in the dielectric= ";Vlams;"m"
11500 PRINT "Wavelength in free space= ";Vlamo;"m"
11510 PRINT "Dielectric const.= ";Err
11520 PRINT "Coupling=";Ans$;"-PLANE"
11530 PRINT "Separation = ";Sepmm;"mm"
11540 PRINT "Separation in dielectric wavelengths= ";Dlams
11550 PRINT "Separation in free space wavelengths= ";Dlamo
11560 IF Ans$="E" THEN GOTO 11600
11570 IF Ans$="H" THEN GOTO 11620
11580 PRINT "E/H flag problem"
11590 STOP
11600 Slm=Wme !Sl=aperture length(in meter) for the calculations
11610 GOTO 11630
11620 Slm=Vlme !Sl=aperture length(in meter) for the calculations
11630 Ffd=2*SQR(Slm^2+Tme^2)^2/Vlamo*1000   !Distance to the far field(mm)
11640 PRINT "Distance to the far field= ";Ffd;"mm"
11650 IF Sepmm>Ffd THEN GOTO 11700
11660 PRINT
11670 PRINT "Separation is less than the far field distance and"
11680 PRINT "model is not valid !!!!!!!!!!!!!!!!!!!!!!!!!!!!!!!!!!!!!!!!"
11690 PRINT
11700    ! PRINT "N,Theta,X,R, in wavelengths"!                                P
11710 FOR N=0 TO Nmax
11720    Xm(N)=N*Slm/Nmax !m
11730    Theta(N)=PI/2+ATN((Slm/2-Xm(N))/Sepm) !rad
11740    Rm(N)=SQR((Slm/2-Xm(N))^2+Sepm^2) !m
11750    Thetad=Theta(N)*180/PI    !deg
11760    ! PRINT N;Thetad;Xm(N);Rm(N)!                                          P
11770 NEXT N
11780 ! ---Received power---
11790 IF Ans$="H" THEN GOTO 11850
11800 IF Ans$="E" THEN GOTO 11830
11810 PRINT "E/H flag problem"
11820 STOP
11830 CALL Eplane(Vlamo,Slm,Theta(*),Beta,Rm(*),F,Nmax,Er(*))
11840 GOTO 11860
11850 CALL Hplane(Vlamo,Slm,Theta(*),Beta,Rm(*),F,Nmax,Er(*))
11860 ! PRINT "N,Thetad,Er(N)"!                                                 P
11870 ! PRINT "       ILLUMINATED APERTURE FIELD DISTRIBUTION"!                  P
11880 FOR N=0 TO Nmax
11890 Thetad=Theta(N)*180/PI !deg
11900 IF Ans$="H" THEN GOTO 11930
11910 Tt=40+30*Er(N)/Er(Nmax/2)
11920 GOTO 11940
11930 Tt=30+10*Er(N)/Er(Nmax)
11940 ! PRINT N;Thetad;Er(N);TAB(Tt);"*"!                                       P
11950  Ers(N)=Er(N)^2
11960 NEXT N
11970 CALL Simp(Xm(*),Ers(*),Nmax,A)
11980 ! PRINT "Integral part of Pr";A!                                          P
11990 ! FOR N=0 TO Nmax
12000 ! PRINT "N,X,ER,ET";N,X(N),Er(N),Et(N)!                                  P
```

```
12010 ! NEXT N
12020 Pr=Tme*A*SQR(Err)/(120*PI)      !watt
12030 FLOAT 4
12040 PRINT "Received power =";Pr;"watt"
12050 ! ---transmitted power---
12060 FOR N=0 TO Nmax
12070 Theta(N)=N*PI/Nmax
12080 Rm(N)=SQR(Sepm^2+(Slm/2)^2)
12090 NEXT N
12100 IF Ans$="H" THEN GOTO 12130
12110 CALL Eplane(Vlamo,Slm,Theta(*),Beta,Rm(*),F,Nmax,Er(*))
12120 GOTO 12140
12130 CALL Hplane(Vlamo,Slm,Theta(*),Beta,Rm(*),F,Nmax,Er(*))
12140 Sepmm=Sepm*1000 !separation mm
12150 ! PRINT "        FAR FIELD RADIATION PATTERN"!                                P
12160 ! PRINT " Theta        Er at Distance = ";Sepmm;" mm"!                        P
12170 FOR N=0 TO Nmax
12180 Thetad=Theta(N)*180/PI !deg
12190 IF Ans$="H" THEN GOTO 12220
12200 Tt=30+30*Er(N)/Er(Nmax/2)
12210 GOTO 12230
12220 Tt=30+15*Er(N)/Er(Nmax)
12230 ! PRINT Thetad;Er(N);TAB(Tt);"*"!                                             P
12240 Ers(N)=Er(N)^2*SIN(Theta(N))!Er squared
12250 NEXT N
12260 CALL Simp(Theta(*),Ers(*),Nmax,A)
12270 Pt=PI*Sepm^2*A*SQR(Err)/(120*PI)    !watt
12280 PRINT "Transmitted power =";Pt;"watt"
12290 FIXED 4
12300 S21=10*LGT(Pr/Pt)-6 !Cavity transfer coefficient  [S21]^2
12310 IF Nmax=20 THEN GOTO 12340
12320 Error=ABS(S21-S21p)
12330 IF Error<.5 THEN GOTO 12370
12340 Nmax=Nmax*2
12350 S21p=S21
12360 GOTO 11710!8040
12370 Slmm=Slm*1000 !slot length in mm
12380 PRINT
12390 PRINT "****";Ans$;"-PLANE  COUPLING FOR ";Tmme;"mm by ";Slmm;" APERTURES**
*"
12400 PRINT "(...where the image beneath the ground plane is accounted for)"
12410 PRINT "Separation= ";Dlamo,"free space wavelengths    (";Sepmm;"mm    )"
12420 PRINT "              [S21]^2 =";S21;"dB","      (Nmax=";Nmax;")"
12430 PRINT LIN(3)
12440 ! IF Dlamo=2 THEN 12520
12450 ! Dlamo=Dlamo+.25
12460 ! Printflag=2 !Second pass
12470 ! GOTO 11280
12480 SUBEND
12490 !
12500 !
12510 !
12520 Epl:! E-plane coupling*****************************************************
12530 !
12540 SUB Eplane(Vlamo,Slm,Theta(*),Beta,Rm(*),F,Nmax,Er(*))
12550 FOR N=1 TO Nmax-1
12560 IF Theta(N)=PI/2 THEN 12660
12570 Ftheta=SIN(PI*(Slm/Vlamo)*COS(Theta(N)))*SIN(Theta(N))/COS(Theta(N))
12580 ! E=Slm/Vlams
12590 ! PRINT "E";E
12600 Reer=F*Ftheta*COS(Beta*Rm(N))/Rm(N)
12610 Imer=-1*F*Ftheta*SIN(Beta*Rm(N))/Rm(N)
12620 Er(N)=SQR(Reer^2+Imer^2)
12630 ! PRINT "Thetadeg,Theta(N),Ftheta(N),Er(N)"!                                 P
12640 ! Thetad=Theta(N)*180/PI
12650 ! PRINT Thetad;Theta(N);Ftheta;Er(N);Et(N)
12660 NEXT N
12670 Er(0)=2*Er(1)-Er(2)
12680 Er(Nmax)=Er(0)
12690 Er(Nmax/2)=Er(Nmax/2-1)+.3*ABS(Er(Nmax/2-2)-Er(Nmax/2-1)) !plus 30%
```

```
12700 ! of previous hop.
12710 SUBEND
12720 !
12730 !
12740 !
12750 Hpl:! H-plane coupling*************************************************
12760 !
12770 SUB Hplane(Vlamo,Slm,Theta(*),Beta,Rm(*),F,Nmax,Er(*))
12780 FOR N=1 TO Nmax-1
12790    IF N=Nmax/2 THEN 12850
12800    RAD
12810    Ftheta=COS(PI*(Slm/Vlamo)*COS(Theta(N)))/TAN(Theta(N))
12820    Reer=F*Ftheta*COS(Beta*Rm(N))/Rm(N)
12830    Imer=-1*F*Ftheta*SIN(Beta*Rm(N))/Rm(N)
12840    Er(N)=SQR(Reer^2+Imer^2)
12850 NEXT N
12860 Er(0)=2*Er(1)-Er(2)
12870 Er(Nmax)=Er(0)
12880 Er(Nmax/2)=0
12890 SUBEND
12900 !
12910 !
12920 !
12930 Sim:! Simpsons rule ***********************************************
12940 !
12950 SUB Simp(X(*),Y(*),Nmax,Result)
12960 ! Simpsons rule for a predetermined data array of Nmax elements.
12970 ! THOMOUS PP309
12980 ! Result=INTEGRAL
12990 ! (X(N),Y(N))=DATA POINTS
13000 ! N=0...NMAX WHERE NMAX IS EVEN
13010 ! FOR N=0 TO Nmax
13020 ! PRINT "Simp  X,Y=",,X(N);Y(N)
13030 ! NEXT N
13040 Sumo=0
13050 Sume=0
13060 FOR N=2 TO Nmax-2 STEP 2
13070    Sume=Sume+Y(N)
13080 NEXT N
13090 FOR N=1 TO Nmax-1 STEP 2
13100    Sumo=Sumo+Y(N)
13110 NEXT N
13120 H=(X(Nmax)-X(0))/Nmax
13130 Result=H/3*(Y(0)+Y(Nmax)+2*Sume+4*Sumo)
13140 ! PRINT "Integral for Nmax=";Nmax;"is";Result
13150 SUBEND
13160 !
13170 !
13180 !
13190 Tle:! Transmission Line Equation***************************************
13200 !
13210 SUB Tll(Freq,Er,D,Zor,Zoi,Zrr,Zri,Zsr,Zsi)
13220 ! All impedances are in ohm
13230 ! 27/5/82
13240 ! Freq(Hz)
13250 ! Distance(m)
13260 !    Zs:sending end impedance
13270 !    Zr:receiving end impedance
13280 Vlam=3E8/(Freq*SQR(Er))
13290 Beta=2*PI/Vlam
13300 T=TAN(Beta*D)
13310 Tr=0
13320 Ti=T
13330 CALL Cmult(Tr,Ti,Zor,Zoi,P5,P6)
13340 CALL Cmult(Tr,Ti,Zrr,Zri,P7,P8)
13350 P1=Zrr+P5
13360 P2=Zri+P6
13370 P3=Zor+P7
13380 P4=Zoi+P8
13390 CALL Cdiv(P1,P2,P3,P4,P9,P10)
```

```
13400 CALL Cmult(P9,P10,Zor,Zoi,Zsr,Zsi)
13410 GOTO 13500!                                                    P
13420 PRINT "----DEBUG:SUB TLL----"
13430 PRINT "Freq= ";Freq/1E6;"MHz"
13440 PRINT "Er= ";Er
13450 PRINT "D= ";D*1000;"mm"
13460 PRINT "Zo= ";Zor;Zoi
13470 PRINT "Zreceive= ";Zrr;Zri
13480 PRINT "Zsend= ";Zsr;Zsi
13490 PRINT "---------------------"
13500 SUBEND
13510 !
13520 !
13530 !
13540 Ptr:! Polar to rectangular*****************************************************
13550 !
13560 SUB Ptor(P1,P2,P3,P4)
13570 DEG
13580 P3=P1*COS(P2)
13590 P4=P1*SIN(P2)
13600 SUBEND
13610 !
13620 !
13630 !
13640 Rtp:! Rectangular to polar*****************************************************
13650 !
13660 SUB Rtop(P1,P2,P3,P4)
13670 DEG
13680 P3=SQR(P1*P1+P2*P2)
13690 DEFAULT ON
13700 P4=2*ATN(P2/(P1+P3))
13710 SUBEND
13720 !
13730 !
13740 !
13750 Cmu:! Complex multiply*********************************************************
13760 !
13770 SUB Cmult(P1,P2,P3,P4,P5,P6)
13780 P5=P1*P3-P2*P4
13790 P6=P1*P4+P2*P3
13800 SUBEND
13810 !
13820 !
13830 !
13840 Cdi:! Complex divide***********************************************************
13850 !
13860 SUB Cdiv(P1,P2,P3,P4,P5,P6)
13870 P7=P3*P3+P4*P4
13880 P5=(P1*P3+P2*P4)/P7
13890 P6=(P2*P3-P1*P4)/P7
13900 SUBEND
13910 !
13920 !
13930 !
13940 Csq:! Complex square-root*****************************************************
13950 !
13960 SUB Csqr(P1,P2,P3,P4)
13970 CALL Rtop(P1,P2,R,T)
13980 R=SQR(R)
13990 T=T/2
14000 CALL Ptor(R,T,P3,P4)
14010 SUBEND
14020 !
14030 !
14040 !
14050 Cre:! Complex reciprocal*******************************************************
14060 !
14070 SUB Crec(P1,P2,P3,P4)
14080 P3=P1/(P1^2+P2^2)
14090 P4=-1*P2/(P1^2+P2^2)
```

```
14100 SUBEND
14110 !
14120 !
14130 !
14140 Zoc:! Characteristic impedance of a coaxial transmission line**************
14150 !
14160 SUB Zo(B,A,Er,Zor,Zoi)
14170 !  USING JOHNSON PP87
14180 Zor=60*LOG(B/A)/SQR(Er)
14190 Zoi=0
14200 SUBEND
14210 !
14220 !
14230 !
14240 Cpp:! reactance of a parallel plate capacitor*****************************
14250 !
14260 SUB Cpp(Freq,Er,T,Area,Zrr,Zri)
14270 ! FREQ(Hz)
14280 ! Thickness(m)
14290 ! Area(m^2)
14300 Omega=2*PI*Freq
14310 Eo=1/(36*PI*1E9)
14320 Zrr=0
14330 Zri=-1*T/(Omega*Er*Eo*Area)
14340 SUBEND
14350 !
14360 !
14370 !
14380 Qan:! Quality factors and radiation conductance****************************
14390 !
14400 SUB Qandgrad(Focmhz,Hmm,Vlengthmm,Wmm,Grad,Qrad,Qdi,Qcu,Qo)
14410 DIM Th(300),Garg(300)
14420 Betao=2*PI*(Focmhz*1E6)/3E8 !free space
14430 RAD
14440 Nmax=20
14450 FOR N=0 TO Nmax
14460 Th(N)=N*PI/Nmax !rad
14470 Bessarg=Betao*(Vlengthmm/1000)*SIN(Th) !rad
14480 CALL Bessel(Bessarg,Bes)
14490 IF N=Nmax/2 THEN GOTO 14520
14500 Garg(N)=(1+Bes)*SIN(Betao*(Wmm/1000)*COS(Th(N))/2)^2*SIN(Th(N))^3/COS(Th(N
))^2
14510 ! PRINT "N,Th,Garg";N;Th(N);Garg(N)!                                    P
14520 NEXT N
14530 Nmaxd2=Nmax/2
14540 Garg(Nmaxd2)=Garg(Nmaxd2-1)
14550 CALL Simp(Th(*),Garg(*),Nmax,Result)
14560 Grad=Result/(60*PI^2)
14570 Uo=4*PI/1E7 !Permeability of free space
14580 O=1E7 !mho/m   Conductivity of copper
14590 Tandelta=.0018 !Typical loss tangent
14600 Qrad=PI*Wmm/(4*Grad*Uo*(Hmm/1000)*(Focmhz*1E6)*Vlengthmm)!          (3.16)
14610 Qdi=1/Tandelta!                                                    (3.37)
14620 Deltas=SQR(2/(2*PI*(Focmhz*1E6)*Uo*O)) !Skin depth!                (3.40)
14630 Qcu=Hmm/(1000*Deltas)!                                             (3.38)
14640 Qo=1/(1/Qrad+1/Qdi+1/Qcu)!                                         (3.35)
14650 SUBEND
14660 !
14670 !
14680 !
14690 Cav:! Cavity*************************************************************
14700 !
14710 SUB Cavity
14720 PRINTER IS 16
14730 PRINT "ANALYSIS OF A RECTANGULAR DIELECTRICALLY FILLED"
14740 PRINT " CAVITY TO OBTAIN ITS DIELECTRIC CONSTANT."
14750 PRINT " PROGRAM 1:RESONANT FREQUENCIES"
14760 PRINT "           INPUTS-CAVITY DIMENSIONS(A,B,D)"
14770 PRINT "                 -DIELECTRIC CONSTANT(Er)"
14780 PRINT "          OUTPUTS-RESONANT FREQUENCIES(F(n,m,l)Mhz)"
```

```
14790 PRINT "                                                    "
14800 PRINT " PROGRAM 2:Er BY INCREMENTAL CAVITIES"
14810 PRINT "           INPUTS-MODE DETAILS(n,l)"
14820 PRINT "                 -RESONANT FREQUENCIES"
14830 PRINT "                 -DIMENSIONS"
14840 PRINT "           OUTPUT-Er"
14850 PRINT "                                                    "
14860 INPUT "PROGRAM 1 OR 2?",N
14870 IF N=2 THEN GOTO 14930
14880 CALL Progone
14890 BEEP
14900 INPUT "PRESS 1 TO GO TO THE START OF PROG 1",N
14910 IF N=1 THEN GOTO 14880
14920 GOTO 14730
14930 CALL Progtwo
14940 BEEP
14950 INPUT "PRESS 2 TO GO TO THE START OF PROG 2",N
14960 IF N=2 THEN GOTO 14930
14970 GOTO 12240
14980 SUBEND
14990 !
15000 !
15010 !
15020 SUB Progone
15030 ! RESONANT FREQUENCIES OF A RECTANGULAR CAVITY
15040 ! FILLED WITH A DIELECTRIC FROM THE DIMENSIONS
15050 ! AND DIELECTRIC CONSTANT
15060 ! COLLIN PP322
15070 DIM F(10,10,10)
15080 PRINTER IS 0
15090 PRINT "A;WIDTH,B;HEIGHT,D;LENGTH(D>A) ?"
15100 INPUT A,B,D!mm
15110 PRINT "A=";A
15120 PRINT "B=";B
15130 PRINT "D=";D
15140 A=A/1000
15150 B=B/1000
15160 D=D/1000
15170 ! INPUT Er:DIELECTRIC CONSTANT
15180 PRINT "Er?"
15190 INPUT Er
15200 PRINT "Er=";Er
15210 PRINT LIN(2)
15220 PRINT "N       M       L       FREQ(Mhz)"
15230 PRINT LIN(2)
15240 C=300000000
15250 FOR N=0 TO 10
15260 FOR M=0 TO 10
15270 FOR L=0 TO 10
15280 F=(L/(2*D))^2
15290 G=(M/(2*B))^2
15300 H=(N/(2*A))^2
15310 F(N,M,L)=C*SQR(F+G+H)/SQR(Er)
15320 IF F(N,M,L)<1E9 THEN 15370!LOWER LIMIT
15330 IF F(N,M,L)>6E9 THEN 15370!UPPER LIMIT
15340 F(N,M,L)=F(N,M,L)/1E6
15350 FIXED 2
15360 PRINT N;M;L,F(N,M,L)
15370 NEXT L
15380 NEXT M
15390 NEXT N
15400 SUBEND
15410 !
15420 !
15430 !
15440 SUB Progtwo
15450 ! Er BY INCREMENTAL CAVITY METHOD
15460 ! R:ASPECT RATIO
15470 C=300000000
15480 PRINTER IS 0
```

```
15490 PRINT "A2>A1 where A is the length of the shorter sides of the"
15500 PRINT "two cavities,that is SMALL,LARGE"
15510 INPUT "DIMENSIONS:A1,A2(mm),ASPECT RATIO ?",A1,A2,R
15520 INPUT "MODE :n,l ? (in the directions: X,Z or W,L.And typically 0,1)",N,L
15530 INPUT "FREQUENCIES:F1,F2(MHz) where F1>F2 ?",F1,F2
15540 PRINT "A1,A2,ASPECT RATIO =";A1;A2;R
15550 PRINT "n,l=";N;L
15560 PRINT "F1,F2=";F1;F2
15570 A1=A1/1000!M
15580 A2=A2/1000!M
15590 F1=F1*1000000
15600 F2=F2*1000000
15610 Diff=A2^2-A1^2
15620 ! F=(N^2+L^2/R^2)*(B^2/M^2)
15630 ! Aa=1/(F1^2-F2^2)
15640 ! Bb=-1*((F2^2+F1^2)*Aa+F/Diff)
15650 ! Cc=F1^2*F2^2*Aa
15660 ! CALL Quadratic(Aa,Bb,Cc,Eplus,Eminus)
15670 ! PRINT Eplus,Eminus
15680 ! E=Eplus
15690 ! Er=C^2*M^2/(4*E*B^2)
15700 Er=C^2/(4*Diff)*(L^2/R^2+N^2)*(1/F2^2-1/F1^2)
15710 PRINT "Er=",Er
15720 SUBEND
15730 !
15740 !
15750 !
15760 Qua:! Quadratic equation*****************************************************
15770 !
15780 SUB Quadratic(A,B,C,Xplus,Xminus)
15790 Arg=B^2-4*A*C
15800 IF Arg>=0 THEN GOTO 15830
15810 PRINT "Argument negative @ Qua:"
15820 STOP
15830 Xplus=-1*B/(2*A)+SQR(Arg)/(2*A)
15840 Xminus=-1*B/(2*A)-SQR(Arg)/(2*A)
15850 SUBEND
15860 !
15870 !
15880 !
15890 Par:! Parallel combination of two impedances*******************************
15900 !
15910 SUB Parallel(Zin1r,Zin1i,Zin2r,Zin2i,Zinr,Zini)
15920 ! Paralleling Zin1 and Zin2
15930 CALL Cmult(Zin1r,Zin1i,Zin2r,Zin2i,D1,D2)
15940 Denr=Zin1r+Zin2r
15950 Deni=Zin1i+Zin2i
15960 CALL Cdiv(D1,D2,Denr,Deni,Zinr,Zini) !ohm
15970 SUBEND
15980 !
15990 !
16000 !
16010 Fac:! ***********************************************************************
16020 !
16030 SUB Factorial(I,Fac)
16040 P=I
16050 FOR N=1 TO I-1
16060 P=P*(I-N)
16070 NEXT N
16080 Fac=P
16090 SUBEND
16100 !
16110 !
16120 !
16130 Bes:! Bessel's function of order zero***************************************
16140 !
16150 SUB Bessel(X,Bes)
16160 DIM T(160),X(160),Y(160),Betam(160)
16170 Nmax=16
16180 FOR N=0 TO Nmax
```

```
16190 T(N)=N*PI/Nmax !radian
16200 Y(N)=COS(X*SIN(T(N)))
16210 NEXT N
16220 CALL Simp(T(*),Y(*),Nmax,A)
16230 Bes=A/PI
16240 GOTO 16310!                                                    T
16250 IF Nmax=16 THEN GOTO 16280
16260 Error=ABS(Besp-Bes)
16270 IF Error<.005 THEN GOTO 16310
16280 Besp=Bes
16290 Nmax=Nmax*2
16300 GOTO 16180
16310 ! PRINT "X,Bes,Nmax";X;Bes;Nmax
16320 SUBEND
16330 !
16340 !
16350 !
16360 Sci:! Sine and cosine integrals*****************************************
16370 !
16380 SUB Sici(Si,Ci,X)
16390 Z=ABS(X)
16400 IF Z>4 THEN 16480
16410 Y=Z*Z
16420 Si=X*((((((9.7942154E-12*Y-2.2232633E-9)*Y+3.0561233E-7)*Y-2.8341460E-5)*Y
+1.6666582E-3)*Y-5.5555547E-2)*Y+1)
16430 IF Z THEN 16460
16440 Ci=-1E75
16450 SUBEXIT
16460 Ci=.57721566+LOG(Z)-Y*(((((-1.3869851E-10*Y+2.6945842E-8)*Y-3.0952207E-6)*
Y+2.3146303E-4)*Y-1.0416642E-2)*Y+.24999999)
16470 SUBEXIT
16480 Si=SIN(Z)
16490 Y=COS(Z)
16500 Z=4/Z
16510 U=(((((((((4.0480690E-3*Z-.022791426)*Z+.055150700)*Z-.072616418)*Z+.049877
159)*Z-3.3325186E-3)*Z-.023146168)*Z-1.1349579E-5)*Z+.062500111)*Z+2.5839886E-10
16520 Vp=(((((((((-.0051086993*Z+.028191786)*Z-.065372834)*Z+.079020335)*Z-.04400
4155)*Z-.0079455563)*Z+.026012930)*Z-3.7640003E-4)*Z-.031224178)*Z-6.6464406E-7
16530 V=Vp*Z+.25000000
16540 Ci=Z*(Si*Y-Y*U)
16550 Si=-Z*(Si*U+Y*V)+PI/2
16560 IF X>=0 THEN 16470
16570 Si=-PI-Si
16580 SUBEXIT
16590 SUBEND
16600 PRINT "N,Thetad,Er(N)"
16610 !
16620 !
16630 !
16640 Rad:! radiation pattern*****************************************************
16650 !
16660 SUB Rad(Freqmhz,Er,Patchlengthmm,Wmm,Shmm,Deltalmm)
16670 PRINT
16680 PRINT "---------------- radiation pattern ------------------------------"
16690 PRINT
16700 ! INPUT "Tilt angle in degrees ?",Thitd
16710 ! INPUT "factor?",F
16720 Hmm=Deltalmm*SQR(Er)
16730 ! Hmm=Shmm
16740 Vlengthmm=Patchlengthmm+Hmm
16750 ! Vlengthmm=Patchlengthmm
16760 ! PRINT "Factor=";F
16770 PRINT
16780 PRINT "frequency=";Freqmhz;"Mhz"
16790 PRINT "aperture length=";Wmm;"mm"
16800 PRINT "effective aperture width=";Hmm;"mm"
16810 PRINT "aperture separation=";Vlengthmm;"mm"
16820 PRINT
16830 Thit=Thitd*PI/180!rad
16840 ! PRINT "Tilt angle=";Thitd,"H=";Hmm,"Lmm=";Vlengthmm
```

```
16850 DIM Thi(500),Thid(500),Theta(500),Thetad(500),Ee(500),Eh(500)
16860 Emaxe=.000001
16870 Emaxh=.000001
16880 RAD
16890 Vlamomm=3E5/Freqmhz
16900 Pl=PI*Vlengthmm/Vlamomm
16910 Pw=PI*Wmm/Vlamomm
16920 Ph=PI*Hmm/Vlamomm
16930 Nn=18!set to 36 for 5 degree increments
16940 FOR N=0 TO Nn
16950 Thid(N)=N*180/Nn!degrees
16960 Thetad(N)=N*180/Nn!degrees
16970 ! PRINT N;Thid(N)
16980 Thi(N)=N*180*PI/Nn/180!rad
16990 Theta(N)=N*180*PI/Nn/180!rad
17000 ! Pf=SIN(Pw*COS(Theta(N)))*TAN(Theta(N)) !Pattern factor
17010 S=Ph*COS(Thi(N)+Thit)
17020 D=Ph*COS(Thi(N)-Thit)
17030 ! Af=SQR((COS(Pl*D)+COS(Pl*S))^2+(SIN(Pl*D)-SIN(Pl*S))^2)!array factor
17040 ! E(N)=Pf*Af
17050 Cl=Pl*COS(Thi(N))
17060 Ch=Ph*COS(Thi(N))
17070 IF S=0 THEN GOTO 17110
17080 IF D=0 THEN GOTO 17110
17090 Ss=SIN(S)/S
17100 Sd=SIN(D)/D
17110 Ee(N)=SQR((COS(Cl)*(Ss+Sd))^2+(SIN(Cl)*(Sd-Ss))^2)! E-plane
17120 T=COS(Theta(N))
17130 IF T=0 THEN GOTO 17150
17140 Eh(N)=SIN(Theta(N))*SIN(Pw*COS(Theta(N))/(Pw*COS(Theta(N))))!H-plane
17150 ! PRINT "pattern of the left hand aperture"
17160 ! E(N)=SIN(Ch)/Ch!pattern of the left hand aperture...Bahl [61] pp2.45
17170 ! E(N)=SIN(Ch)/Ch*COS(Cl)! Bahl eq. 2.47 [61]
17180 ! E(N)=Ss!single slot
17190 IF Ee(N)<Emaxe THEN GOTO 17210
17200 Emaxe=Ee(N)
17210 IF Eh(N)<Emaxh THEN GOTO 17230
17220 Emaxh=Eh(N)
17230 NEXT N
17240 PRINT "Thi/Theta","20log(Ee/Emaxe)","20log(Eh/Emaxh)"
17250 FOR N=0 TO Nn STEP 1
17260 IF Ee(N)>0 THEN GOTO 17290
17270 Eelog=-9999
17280 GOTO 17300
17290 Eelog=20*LGT(Ee(N)/Emaxe)
17300 IF Eh(N)>0 THEN GOTO 17330
17310 Ehlog=-9999
17320 GOTO 17340
17330 Ehlog=20*LGT(Eh(N)/Emaxh)
17340 PRINT Thid(N),Eelog,Ehlog
17350 NEXT N
17360 GOTO 17420
17370 FOR N=0 TO Nn STEP 1
17380 PRINT
17390 PRINT Thid(N);TAB(10+50*En(N));"*"
17400 PRINT
17410 NEXT N
17420 SUBEND
17430 !
17440 !
17450 !
17460 Res:! Resonant frequency*****************************************************
17470 !
17480 SUB Fo(Foflag$,Feed$,Er,Effer,Vlengthmm,Radiusi,Radiuso,Wmm,Deltalmm,Hmm,X
series,Focmhzc)
17490 IF Foflag$="Martin" THEN GOTO Martin
17500 IF Foflag$="Sengupta" THEN GOTO Sen
17510 PRINT "flag error @ Pa+3"
17520 PAUSE
17530 !
```

```
17540 !
17550 !
17560 Martin:!     "Foc..RESONANT FREQUENCY FROM THE CAVITY MODEL"
17570 Focmhzc=300/(2*(Vlengthmm/1000+2*Deltalmm/1000)*SQR(Effer))
17580 PRINT "Resonant frequencies by the cavity and network models"
17590 PRINT "               (MARTIN)"
17600 PRINT "Calculated resonant frequency(Foc)=";Focmhzc;"Mhz"
17610 !     "Foz..RESONANT FREQUENCY FROM NETWORK MODEL"
17620 CALL Qandgrad(Focmhzc,Hmm,Vlengthmm,Wmm,Grad,Qrad,Qdi,Qcu,Qo)
17630 IF Feed$<>"TL" THEN GOTO 17660
17640 Fozmhzc=Focmhzc
17650 GOTO E
17660 ! Solving a quadratic equation in the frequency-tuning parameter
17670 !          Ftp=(woz-woc)/woz, usual symbol being delta                (3.32)
17680 Rr=1 !r=1 for critical coupling                                        (3.34)
17690 A=1
17700 B=-Rr/(2*Qo*(Xseries/50)) ! where r(=Rr) has been set equal to 1
17710 C=1/(4*Qo^2)
17720 ! PRINT A,B,C
17730 CALL Quadratic(A,B,C,Xplus,Xminus) !Ftp:Frequency tuning parameter
17740 Ftp=Xminus
17750 Fozmhzc=Focmhzc/(1-Ftp)
17760 E:PRINT "Calculated resonant frequency(Foz)=";Fozmhzc;"Mhz (assuming criti
cal coupling)"
17770 Rrad=1/Grad !ohm
17780 Re=Rrad/2 !Rrad=Rslot,Re:resistance at the end=Rslot//Rslot
17790 Gradmm=Grad*1000
17800 PRINT "Radiation conductance =";Gradmm;"mmho"
17810 PRINT "Radiation resistance =";Rrad;"ohm"
17820 PRINT "(Rrad//Rrad)/50=";Rrad*Rrad/(50*(Rrad+Rrad))
17830 PRINT "Q radiation =";Qrad
17840 PRINT "Q dielectric=";Qdi
17850 PRINT "Q copper =";Qcu
17860 PRINT "Q unloaded=";Qo
17870 GOTO 18070
17880 !
17890 !
17900 !
17910 Sen:PRINT "Resonant frequencies by Sengupta's model"
17920 Effer=(Er+1)/2+(Er-1)/(2*SQR(1+10*Hmm/Wmm))
17930 PRINT "...using Hammerstad's model for the effective dielectric const."
17940 Alpha=1+1.393+(Hmm/Wmm)+.667*(Hmm/Wmm)*LOG(Wmm/Hmm+1.444)!           (1.14)
17950 Ar=2*Hmm/(Effer*Vlengthmm*PI*Alpha)
17960 Fo=3E5/(2*Vlengthmm*SQR(Effer)) !Mhz
17970 Fozc=Fo*(1-Ar)/(1+Ar*LOG(2*Vlengthmm*SQR(Effer)/(1.78107*Hmm)))!     (3.18)
17980 Deltaf=PI/2*(Hmm/Vlengthmm)^2*(Wmm/Vlengthmm)*(Fozc/(Alpha*Effer^2)) !Mhz
17990 !
18000 Deltaf=Deltaf*LOG(2/(1.78107*PI*(Radius1/1000)))!                     (3.20)
18010 Focc=Fozc-Deltaf !Mhz
18020 PRINT "Calculated Foc=";Focc;"Mhz"
18030 PRINT "Calculated Foz=";Fozc;"Mhz"
18040 PRINT "Freq. shift=";Deltaf;"Mhz"
18050 ! Error=100*(Focc-Focmhz)/Focmhz
18060 ! PRINT "%e when compared with measurement=";Error
18070 SUBEND
18080 End:! !!!!!!!!!!!!!!!!!!END OF PROGRAM!!!!!!!!!!!!!!!!!!!!!!!!!!!!!!!!
```

APPENDIX D

LIST OF SCHOLARLY PUBLICATIONS RELATED TO THIS THESIS

[D.1] N.M.Martin, "Techniques for overcoming the bandwidth limitations of microstrip patch antennas," IREE Symposium on problems in Radio Communications, Adelaide, August 1980.

[D.2] N.M.Martin, D.W.Griffin, "A novel hexagonally shaped microstrip patch antenna," IREE, 18th International Electronics Convention Digest Melbourne, August 1981.

[D.3] N.M.Martin, D.W.Griffin, "A new approach to microstrip antenna bandwidth determination and its application to a novel hexagonally shaped patch," IEEE/ Antennas and Propagation Society International Symposium, Albuquerque, May 24th-28th, 1982.

[D.4] N.M.Martin, D.W.Griffin, "A tapered transmission line model for the feed probe of a microstrip patch antenna," IEEE/Antennas and Propagation Society International Symposium, Houston May 23rd-26th, 1983.

[D.5] N.M.Martin, D.W.Griffin, "New empirically determined parameters for modelling rectangular microstrip antennas," IEEE/Antennas and Propagation Society International Symposium, Houston, May 23rd-26th, 1983.

[D.6] N.M.Martin, D.W.Griffin, "Mutual coupling between well separated rectangular microstrip antennas using an aperture illumination method," IREE, 19th International Electronics Convention Digest, Sydney, September, 1983.

[D.7] N.M.Martin, D.W.Griffin, "Modelling the feed point of microstrip antennas," IREE, 19th International Electronics Convention Digest, Sydney, September, 1983.